Surface Shaped Synthetic Polymer Fibers and Fiber-based Adsorbents as Stationary Phases for the Preparative Purification of Biopharmaceuticals

Packing characterization, Modeling, Screening and Application

zur Erlangung des akademischen Grades eines
DOKTORS DER INGENIEURWISSENSCHAFTEN (Dr.-Ing.)

von der KIT-Fakultät für Chemieingenieurwesen und Verfahrenstechnik des
Karlsruher Instituts für Technologie (KIT)
genehmigte

DISSERTATION

von
Dipl.-Wi.-Ing. Johannes Winderl
aus Mallersdorf-Pfaffenberg

Tag der mündlichen Prüfung: 14.12.2020
Erstgutachter: Prof. Dr. Jürgen Hubbuch
Zweitgutachter: PD Dr. Egbert Müller

Danksagung

Auf dem Weg zu dieser Arbeit haben mich viele Menschen begleitet und unterstützt. Meinen besonderen Dank möchte ich folgenden Personen ausdrücken:

Prof. Dr. Jürgen Hubbuch danke ich für die Möglichkeit meine Arbeit in seiner Arbeitsgruppe im Rahmen eines spannenden und vielseitigen Industrieprojekts durchzuführen, die wissenschaftlichen Freiheiten dabei und das entgegengebrachte Vertrauen. Bei PD Dr. Egbert Müller möchte ich mich für die Übernahme des Korreferats und das Interesse an meiner Arbeit bedanken.

Dem Bundesministerium für Bildung und Forschung und dem VDI als Projektträger danke ich für die finanzielle Unterstützung meiner Arbeit. Gleichzeitig möchte ich mich bei allen Projektpartnern des PurMAb Projekts für die Bereitstellung von Materialien und die fachliche Unterstützung bedanken.

Besonders bedanken möchte ich mich bei den Studenten, die tatkräftig und mit großer Motivation zu verschiedenen Projekten im Rahmen dieser Arbeit beigetragen haben: Tamara Spies, Eva Donner, David Saleh, Roxana Disela, Philipp Holz, Dominik Reith, Patrick Endres, Lara Wehrle, Eric Neumann, Stephan Bürkle und Leon Clemenz.

Allen Mitarbeitern des Instituts möchte ich für die herzliche Aufnahme in die Gruppe und die gemeinsame Zeit danken. Margret Meixner, Marion Krenz, Iris Perner-Nochta und Michael Wörner danke ich für die administrative Unterstützung. Unserem Ingenieurteam bestehend aus Susanna Suhm, Cathrin Dürr, Nicolai Bluthardt, Stefanie Limbrunner, Kristina Schleining und Birgit Roser danke ich für die hervorragende Laborganisation. Meinen Kooperationspartnern Thiemo Huuk, Gang Wang, Tobias Hahn und Christopher Ladd-Effio danke ich für die gemeinsamen Projekte. Meinen Bürokollegen Gang Wang und Matthias Rüdt danke ich für die super Arbeitsatmosphäre, die spannenden fachlichen und außerfachlichen Diskussionen, und gemeinsame sportliche Unternehmungen außerhalb der Arbeit.

Ganz besonders bedanken möchte ich mich bei meinen Eltern und bei meiner Schwester, die mich immer und in jeder Lage unterstützt haben. Zum Schluss möchte ich mich bei Ashley bedanken, für ihre Liebe, ihre unermüdliche Unterstützung aus Nah und Fern, und ihre Toleranz gegenüber der Zeit, die in diese Arbeit geflossen ist.

"All things are difficult before they are easy."

Dr. Thomas Fuller

Abstract

The present thesis contributes to the development of alternative stationary phases for the preparative purification of biopharmaceuticals, and addresses important challenges that are related to the use of polymer fibers and fiber-based adsorbents for this purpose.

Biopharmaceuticals are used for the prevention, diagnosis and treatment of serious and potentially life threatening diseases. Many are essential medicines, such as vaccines which are used for the prevention of infectious diseases, insulins which are used for the treatment of metabolic disorders, and monoclonal antibodies which are used for the treatment of inflammatory diseases and cancer. Biopharmaceuticals are very complex, however, as they often are large macromolecules or macromolecular assemblies such as proteins. They have a complex structure which is dependent on environmental conditions, and many possibilities for chemical and structural modifications exist which can affect their function. Therefore, the manufacturing and development of biopharmaceuticals is very complex and requires significant time and resources. The development of new biopharmaceuticals is associated with high risks, as approximately 90% of all biopharmaceutical development projects fail during development. Consequently, the development and manufacturing costs of biopharmaceuticals are relatively high, and the supply of such medicines in a timely manner with the right quality and at reasonable costs is challenging.

Due to population growth and aging societies, the worldwide demand for biopharmaceuticals is expected to grow in the future. At the same time, novel types of biopharmaceuticals will have to be developed, which can be used in order to treat diseases which only affect few patients, or which show better efficacy in certain patient populations which currently do not benefit from the treatment with biopharmaceuticals. Thus, more biopharmaceuticals and a wider variety of biopharmaceuticals in potentially much smaller quantities will have to be manufactured and developed in the future. In addition, the development and manufacturing costs for biopharmaceuticals will have to be reduced in order to improve the access to such medicines in low-income countries, and in order to provide such medicines at less cost to society.

As a consequence of these developments there is a need for more flexible and more efficient development strategies and manufacturing processes for biopharmaceuticals which lead to higher productivity and/or lower costs. An essential part of the manufacturing of

biopharmaceuticals is downstream processing (DSP), which contributes significantly to the productivity and manufacturing costs of biopharmaceuticals and requires a high development effort. During DSP the target molecule is purified from an appropriate feedstream such as harvested cell culture fluid or fermentation broth, concentrated, and formulated. The purification is thereby mainly carried out with liquid chromatographic separation methods using solid and spherical stationary phases. These stationary phases are characterized by high binding capacities, high resolution, and good scalability. In recent years, high throughput tools and mechanistic models have been developed for such stationary phases, which can be used in order to expedite the process development with such stationary phases. The productivities of these stationary phases are comparatively low, however, as most binding sites are only accessible via slow diffusion processes, and high pressure drops limit the operating windows in terms of feasible bed heights and flow rates. In addition, the costs of such stationary phases can be quite high, because of high base material costs, high ligand costs, and elaborate manufacturing processes. Therefore the stationary phases are often reused, which requires a development of appropriate cleaning and storage protocols, and an evaluation of the performance after continued use.

For these reasons there is great interest in the development of alternative stationary phases for the preparative purification of biopharmaceuticals with improved characteristics in terms of productivity and/or costs. A promising class of such alternative stationary phases are polymer fibers and fiber-based adsorbents. Fibers have several unique features which could translate into potential advantages of such stationary phases in comparison to conventional stationary phases. Polymer fibers are mass produced for the textile industry and are therefore exceptionally cost-effective. The costs of synthetic polymer fibers are estimated to be up to 50 times lower than the costs of conventional support materials. Therefore the use of such materials as disposables could be feasible. In addition, most fibers are nonporous, such that most of the binding sites are located on the external fiber surface. This reduces diffusional limitations and can lead to very fast mass transfer rates. Furthermore, fibers are characterized by a relatively low resistance to flow, and correspondingly a high bed permeability for typical fiber diameters and bed porosities. This enables large operating windows. When taken together, these properties can lead to operations with high throughput, and if binding capacities are sufficiently high, also with high productivity. Moreover, there is a variety of surface modification techniques and packing arrangements for fibers.

The potential of fibers for high-throughput and cost-efficient analytical separations of macromolecules has been demonstrated for different types of conventional microfiber supports with different model protein and other model compounds in the past. For the preparative purification of biopharmaceuticals, however, there are several challenges that make it difficult to use polymer fibers and fiber-based adsorbents for this purpose. These consist of the low surface area of conventional microfiber supports and hence low binding capacities of fiber-based adsorbents which are an obstacle for preparative applications, and the packing of such adsorbents which requires packing optimization. Moreover, there is a

lack of high throughput microscale tools and mechanistic models for fiber-based adsorbents, which makes efficient material development and process development challenging, and there is a lack of knowledge whether and under which conditions the use of such adsorbents for industrial process applications is feasible.

These challenges were addressed in the present thesis by examining novel types of fiber-based adsorbents which were prepared from area enhanced surface shaped fibers via surface grafting with uncontrolled and controlled grafting techniques. First, the packing characteristics of such adsorbents were investigated in order to determine packing conditions under which such adsorbents can best be used. Subsequently, it was examined whether mechanistic models and high throughput microscale tools can be developed for such adsorbents. Finally, it was explored whether and under which conditions the use of such adsorbents for industrial process applications such as monoclonal antibody aggregate removal during antibody purification is feasible.

Initially, different types of surface shaped area enhanced microfibers were sourced for this thesis. Winged shaped microfibers had the highest surface area of all available surface shaped materials and were therefore examined in detail in this thesis. Both native winged shaped fibers and hydrogel grafted winged shaped fiber based adsorbents with hydrogels that were grafted either via free radical polymerization (FRP) or surface initiated atom-transfer radical polymerization (SI-ATRP) by a project partner were investigated. The grafted fibers were functionalized to either cation exchange or anion exchange fiber-based adsorbents. Other functional groups would be possible, but were not considered in this thesis. For the evaluation of the fibers and fiber-based adsorbents, tracer substances, model proteins and model nucleic acids, and feed streams from industrial antibody purification processes were used.

In the first part of this thesis, packing studies were performed in order to investigate the packing characteristics of native and grafted winged shaped fibers. For this purpose a suspension based packing technique was developed for the packing of short cut winged shaped fibers. With the use of this technique the fibers could be packed reproducibly into small laboratory scale columns, with a packing reproducibility that was comparable to packing reproducibilities that have been reported for other materials and other packing techniques at similar scale. The packing quality of the winged shaped fiber beds was found to be sufficient for preparative applications. Peak asymmetries and plate heights were within typical ranges of preparative columns, and plate heights were at the lower end of those reported for other fiber supports. Multivariate packing studies revealed that both packing density and bed height impact column performance. Lower packing densities resulted in lower plate heights, while increases in bed height resulted in more symmetric peak shapes. Packing density also affected the performance of grafted fibers. Dynamic binding capacity increased with increasing packing density, while capacity utilization and resolution decreased. The results from the multivariate studies could be used in order to optimize the packing of grafted winged shaped fibers, and it could be shown that for optimized packing conditions and fast mobile phase velocities, grafted winged shaped fibers can achieve

a better resolution than conventional adsorbents. Overall, the first part of this thesis provides information about the packing behavior and the packing characteristics of winged shaped fibers supports. The results indicated that the use of such area enhanced fibers for preparative applications is feasible. The results from the study enable a comparison to other fiber supports and other packing techniques, and it identifies packing conditions under which winged shaped fibers can be used most efficiently.

In the second part of this thesis, it was examined whether a mechanistic model can be developed for fiber-based adsorbents. This was assessed with the use of winged shaped anion-exchange fiber-based adsorbents. Characterization and efficiency experiments were performed and used in conjunction with criteria for model selection in order to develop a column model for the fiber-based adsorbents. The developed model accounted well for the dispersion of non-retained molecules inside the column, and it could accurately describe the binding, breakthrough, and elution of three differently sized proteins, with molecular sizes ranging from 6 to 160 kDa. The model parameters could be identified reliably from a few experimental column runs. Model comparisons showed that both binding kinetics and lumped film and pore diffusion are relevant mechanisms on the grafted winged shaped fibers. In conclusion, the second part of this thesis demonstrated that fiber-based adsorbents can be modeled mechanistically, using grafted winged shaped fibers as an example. It showed how the required model parameters can be determined, and it could demonstrate that modeling is possible for a range of molecular sizes that would be relevant for the purification of biopharmaceuticals. The results from this study contribute to a better understanding of mass transfer properties of grafted winged shaped fibers, and the presented model enables mechanistic comparisons to other types of stationary phases. Moreover, the presented model enables model based process development and optimization on fiber-based adsorbents.

In the third part of this thesis it was examined whether high-throughput microscale tools can be developed for fiber-based adsorbents. This was again assessed with the use of native and grafted short cut winged shaped microfibers. For these fibers an automated high throughput screening was established on a robotic liquid handling station in 96 well filter plates. Two techniques were identified that enabled accurate and reproducible portioning of the fibers. The impact of several screening parameters was examined and optimized. It could be shown that the data that is obtained from the HTS correlates with data from packed fiber columns. The usefulness of the developed HTS for material and process development was demonstrated in two case studies, which showed that the developed HTS can be used to optimize the hydrogel structure of controlled grafted fiber based adsorbents, and that it can be used for the development of step elution conditions for the purification of a monoclonal antibody from product- and process-related impurities. Overall, the study that is presented in the third part of this thesis showed that it is possible to develop high-throughput microscale tools for fiber-based adsorbents that can be utilized for material optimization and process development. The tool enables a faster and more complete characterization of fiber-based adsorbents, and it can be used for material and time efficient process development. The tool makes it easier to evaluate fiber-based

adsorbents alongside other materials, and thus could make it easier to integrate fiber-based adsorbents into industrial purification processes.

In the last part of this thesis, it was evaluated if and under which conditions fiber-based adsorbents can be used for industrial purification process applications. Here, the use of cation exchange fiber-based adsorbents for monoclonal antibody removal during antibody purification was explored. Two types of strong cation exchange fiber-based adsorbents with uncontrolled and controlled grafted hydrogel layers were examined and evaluated with respect to permeability, dynamic antibody binding capacity, resolution capabilities of mAb monomer and aggregates, and the performance in different operating modes. The study showed that due to high permeabilities, high dynamic binding capacities at fast mobile phase velocities, and good resolution capabilities of monomer and aggregates, the use of fiber-based adsorbents for mAb aggregate removal is feasible up to very high mobile phase velocities. The overall performance of the fiber-based adsorbents was found to be comparable to performance of an existing resin material, Poros 50 HS. In comparison of the two types of fiber-based adsorbents, the performance of grafted fiber-based adsorbents was found to be superior to the performance of uncontrolled grafted fiber-based adsorbents due to higher productivity and lower buffer consumption. In summary, the study that is presented in the last section shows that the use of fiber-based adsorbents for process applications during industrial antibody manufacturing is feasible and it identifies appropriate operating conditions.

In conclusion, the present thesis contributes to a better understanding of the properties and the performance of area enhanced winged shaped fibers and fiber-based adsorbents for preparative chromatography applications. It provides information about the packing characteristics of such adsorbents, mechanistic model parameters, relevant mass transfer and binding mechanisms, and the performance for monoclonal antibody aggregate removal. This data can be used for comparisons to existing materials and other types of fiber-based adsorbents. Moreover, the present thesis provides information about how the structure of fiber-based adsorbents with respect to the packing structure and the polymer nanolayer architecture affects the performance of such adsorbents, which helps to use such adsorbents efficiently and tailor them for specific applications. In addition, this thesis presents mechanistic models and high throughput screenings for fiber-based adsorbents. These models and tools will be valuable for the future design and evaluation of fiber-based adsorbents, as they enable an easier, material and time efficient, evaluation of such materials. This could make it easier to integrate such alternative adsorbents into process development workflows and processes. With respect to process applications, it could be shown that the use of fiber-based adsorbents for monoclonal antibody removal is feasible and the study provides relevant processing windows for this purpose. Overall, the information that is presented in this thesis could make it easier to use fiber-based adsorbents for preparative applications, and to make use of their benefits in order to address some of the current challenges in the field of downstream processing.

Zusammenfassung

Die vorliegende Arbeit leistet einen Beitrag zur Entwicklung alternativer stationärer Phasen für die präparative Aufreinigung von Biopharmazeutika und befasst sich mit wichtigen Herausforderungen, die mit der Verwendung von Polymerfasern und Adsorbern auf Faserbasis für diesen Zweck verbunden sind.

Biopharmazeutika sind wichtige Arzneimittel, die zur Vorbeugung, Diagnose und Behandlung schwerer und möglicherweise lebensbedrohlicher Krankheiten eingesetzt werden. Viele Biopharmazeutika sind essentielle Arzneimittel, z.B. Impfstoffe zur Vorbeugung von Infektionskrankheiten, Insuline zur Behandlung von Stoffwechselstörungen und monoklonale Antikörper zur Behandlung von chronisch-entzündlichen Erkrankungen und Krebs. Biopharmazeutika sind jedoch sehr komplex, da es sich häufig um große Makromoleküle oder makromolekulare Anordnungen wie z.B. Proteine mit einer komplexen Struktur handelt. Diese hängt von den Umgebungsbedingungen ab, und es existieren viele Möglichkeiten für chemische und strukturelle Modifikationen die ihre Funktion beeinflussen. Daher ist die Herstellung und Entwicklung von Biopharmazeutika sehr komplex und erfordert viel Zeit und Ressourcen. Die Entwicklung neuer Biopharmazeutika ist mit hohen Risiken verbunden, da etwa 90% aller biopharmazeutischen Entwicklungsprojekte während der Entwicklung scheitern. Unter anderem aus diesen Gründen sind die Entwicklungs- und Herstellungskosten von Biopharmazeutika relativ hoch, und die rechtzeitige Versorgung mit solchen Arzneimitteln mit der richtigen Qualität und zu angemessenen Kosten ist eine Herausforderung.

Aufgrund des Bevölkerungswachstums und alternder Gesellschaften wird erwartet, dass die weltweite Nachfrage nach Biopharmazeutika in Zukunft steigen wird. Gleichzeitig müssen neuartige Arten von Biopharmazeutika entwickelt werden, die zur Behandlung von Krankheiten eingesetzt werden können, von denen nur wenige Patienten betroffen sind oder die bei bestimmten Patientengruppen, die derzeit nicht von der Behandlung mit Biopharmazeutika profitieren, eine bessere Wirksamkeit zeigen. Insgesamt müssen also in Zukunft mehr Biopharmazeutika und eine größere Vielfalt von Biopharmazeutika in möglicherweise viel geringeren Mengen hergestellt und entwickelt werden. Darüber hinaus müssen die Entwicklungs- und Herstellungskosten für Biopharmazeutika gesenkt werden, um den Zugang zu solchen Arzneimitteln in Ländern mit niedrigem Einkommen zu verbessern und solche Arzneimittel zu geringeren Kosten für die Gesellschaft zur Verfügung zu stellen.

Infolge dieser Entwicklungen besteht ein Bedarf an flexibleren und effizienteren Entwicklungsstrategien und Herstellungsverfahren für Biopharmazeutika, die zu einer höheren Produktivität und / oder niedrigeren Kosten führen. Ein wesentlicher Bestandteil der Herstellung von Biopharmazeutika ist die Aufreining (engl. *Downstream Processing (DSP)*), die erheblich zur Produktivität und zu den Herstellungskosten von Biopharmazeutika beiträgt und einen hohen Entwicklungsaufwand erfordert. Während des DSP wird das Zielmolekül aus einem geeigneten Ausgangsmaterial wie geernteter Zellkulturflüssigkeit oder Fermentationsbrühe aufgereinigt, konzentriert und formuliert. Die Reinigung erfolgt dabei hauptsächlich mit flüssigchromatographischen Trennverfahren unter Verwendung fester und kugelförmiger stationärer Phasen. Diese stationären Phasen zeichnen sich durch hohe Bindekapazitäten, hohe Auflösung und gute Skalierbarkeit aus. In den letzten Jahren wurden Hochdurchsatzwerkzeuge und mechanistische Modelle für solche stationären Phasen entwickelt, die verwendet werden können, um die Prozessentwicklung mit solchen stationären Phasen zu beschleunigen. Die Produktivität dieser stationären Phasen ist jedoch vergleichsweise gering, da die meisten Bindungsstellen nur über langsame Diffusionsprozesse zugänglich sind und hohe Druckabfälle die Betriebsfenster hinsichtlich realisierbarer Betthöhen und Durchflussraten begrenzen. Darüber hinaus können die Kosten solcher stationären Phasen aufgrund der hohen Grundmaterialkosten und Ligandenkosten sowie der aufwändigen Herstellungsverfahren recht hoch sein. Daher werden die stationären Phasen häufig wiederverwendet, was die Entwicklung geeigneter Reinigungs- und Lagerungsprotokolle und eine Untersuchung der Lebensdauer bei wiederholter Verwendung erfordert.

Aus diesen Gründen besteht ein großes Interesse an der Entwicklung alternativer stationärer Phasen zur präparativen Aufreinigung von Biopharmazeutika mit verbesserten Eigenschaften hinsichtlich Produktivität und / oder Kosten. Eine vielversprechende Klasse solcher alternativen stationären Phasen sind Polymerfasern und Adsorber auf Faserbasis. Fasern weisen mehrere besondere Merkmale auf, die sich in potenziellen Vorteilen solcher stationären Phasen im Vergleich zu herkömmlichen stationären Phasen niederschlagen könnten. Polymerfasern werden in Massenproduktion für die Textilindustrie hergestellt und sind daher außerordentlich kostengünstig. Die Kosten für synthetische Polymerfasern werden auf bis zu 50-mal niedriger geschätzt als die Kosten für herkömmliche Trägermaterialien. Daher könnte die Verwendung solcher Materialien als Einwegartikel möglich sein. Außerdem sind die meisten Fasern nicht porös, so dass sich der überwiegende Teil der Bindungsstellen auf der äußeren Faseroberfläche befinden. Dies reduziert Diffusionsbeschränkungen und kann zu sehr schnellen Stoffübergangsraten führen. Weiterhin zeichnen sich Fasern durch einen relativ geringen Fließwiderstand und entsprechend eine hohe Bettpermeabilität für typische Faserdurchmesser und Bettporositäten aus. Dies ermöglicht große Betriebsfenster. Zusammengenommen können diese Eigenschaften zu Prozessen mit hohem Durchsatz führen, und wenn die Bindekapazitäten ausreichend hoch sind, auch mit hoher Produktivität. Darüber hinaus gibt es eine Vielzahl von Oberflächenmodifikationstechniken und Packungsanordnungen für Fasern.

Das Potenzial von Fasern für Hochdurchsatz- und kosteneffiziente analytische Trennungen von Makromolekülen wurde in der Vergangenheit für verschiedene Arten herkömmlicher Mikrofasern mit verschiedenen Modellproteinen und anderen Modellverbindungen bereits gezeigt. Für die präparative Aufreinigung von Biopharmazeutika gibt es jedoch mehrere Herausforderungen, die es schwierig machen, Polymerfasern und Adsorber auf Faserbasis für diesen Zweck zu verwenden. Diese bestehen in der geringen Oberfläche herkömmlicher textiler Mikrofasern und damit in geringen Bindekapazitäten von Adsorbern auf Faserbasis, die ein Hindernis für präparative Anwendungen darstellen, und in der Packung solcher Adsorber, die eine Packoptimierung erfordert. Darüber hinaus fehlt es an Hochdurchsatzwerkzeugen und mechanistischen Modellen für Adsorber auf Faserbasis, was eine effiziente Materialentwicklung und Prozessentwicklung schwierig macht. Außerdem fehlt es an Wissen, ob und unter welchen Bedingungen eine Anwendung solcher Adsorber für industrielle Prozessanwendungen durchführbar ist.

Diese Herausforderungen wurden in der vorliegenden Arbeit durch die Untersuchung neuartiger Arten von Adsorbern auf Faserbasis angegangen, die aus oberflächenstrukturierten Fasern durch Pfropfung mit unkontrollierten und kontrollierten Pfropftechniken hergestellt wurden. Zunächst wurden die Packeigenschaften solcher Adsorber untersucht, um die Packungsbedingungen zu bestimmen, unter denen solche Adsorber am besten verwendet werden können. Anschließend wurde untersucht, ob für solche Adsorber mechanistische Modelle und Hochdurchsatzverfahren entwickelt werden können. Schließlich wurde untersucht, ob und unter welchen Bedingungen die Verwendung solcher Adsorber für industrielle Prozessanwendungen wie für die Entfernung monoklonaler Antikörperaggregate während der Antikörperreinigung möglich ist.

Für diese Arbeit wurden zunächst verschiedene Arten von oberflächenstrukturierten Fasern untersucht. Winged Fasern hatten die höchste Oberfläche aller verfügbaren oberflächenstrukturierten Materialien und wurden daher in dieser Arbeit eingehender untersucht. Es wurden sowohl native Winged Fasern als auch hydrogelgepfropfte Adsorber untersucht mit Hydrogelen, die von einem Projektpartner entweder durch freie radikalische Polymerisation (engl. *free radical polymerization (FRP)*) oder oberflächeninitiierte Atomtransfer-Radikalpolymerisation (engl. *surface iniatiated atom transfer radical polymerization (SI-ATRP)*) gepfropft wurden. Die gepfropften Fasern wurden entweder zu Kationenaustauschern der Anionenaustauschern funktionalisiert. Andere funktionelle Gruppen wären möglich, wurden aber in dieser Arbeit nicht berücksichtigt. Zur Bewertung der Fasern und der Adsorber auf Faserbasis wurden Tracersubstanzen, Modellproteine und Modellnukleinsäuren sowie Prozesslöungen aus industriellen Antikörperreinigungsprozessen verwendet.

Im ersten Teil dieser Arbeit wurden Packstudien durchgeführt, um die Packseigenschaften von nativen und gepfropften Winged Fasern zu untersuchen. Zu diesem Zweck wurde eine suspensionsbasierte Packtechnik zum Packen von Kurzschnitt Winged Fasern entwickelt. Mit dieser Technik konnten die Fasern reproduzierbar in kleine Säulen im Labormaßstab gepackt werden. Dabei war die Reproduzierbarkeit der Packung mit der Reproduzier-

barkeit der Packung vergleichbar, die für andere Materialien und andere Packtechniken in ähnlichem Maßstab in der Literatur angegeben wurde. Die Packqualität erwies sich für präparative Anwendungen als ausreichend. Peakasymmetrien und Trennstufenhöhen lagen innerhalb typischer Bereiche von präparativen Säulen, und die Trennstufenhöhen lagen am unteren Ende der für andere Fasern angegebenene Bereiche. Multivariate Packstudien zeigten, dass sowohl die Packdichte als auch die Betthöhe die Säulenleistung beeinflussen. Niedrigere Packdichten führten zu niedrigeren Trennstufenhöhen, während eine Erhöhung der Betthöhe zu symmetrischeren Peakformen führte. Die Packdichte beeinflusste auch die Leistungseigenschaften von gepfropften Fasern. Die dynamische Bindekapazität nahm mit zunehmender Packdichte zu, während die Kapazitätsauslastung und die Auflösung abnahmen. Die Ergebnisse der multivariaten Studien konnten verwendet werden, um die Packung von gepfropften Winged Fasern zu optimieren, und es konnte gezeigt werden, dass gepfropfte Winged Fasern unter optimierten Packbedingungen und schnellen linearen Flussgeschwindigkeiten eine bessere Auflösung erzielen können als herkömmliche Adsorber. Insgesamt liefert der erste Teil dieser Arbeit Informationen über das Packverhalten und die Packeigenschaften von Winged Fasern. Die Ergebnisse zeigten, dass die Verwendung solcher oberflächenstrukturierter Fasern für präparative Anwendungen möglich ist. Die Ergebnisse der Studie ermöglichen einen Vergleich mit anderen Fasern und anderen Packtechniken und identifizieren Packbedingungen, unter denen Winged Fasern am effizientesten eingesetzt werden können.

Im zweiten Teil dieser Arbeit wurde untersucht, ob ein mechanistisches Modell für Adsorber auf Faserbasis entwickelt werden kann. Dies wurde unter Verwendung von Anionenaustauscherfasern bewertet. Charakterisierungs- und Effizienzversuche wurden durchgeführt und in Verbindung mit Kriterien für die Modellauswahl verwendet, um ein Säulenmodell für Faseradsorber zu entwickeln. Das entwickelte Modell konnte die Dispersion nicht-bindender Moleküle in der Säule gut beschreiben und konnte die Bindung, den Durchbruch und die Elution von drei unterschiedlich großen Proteinen mit Molekülgrößen im Bereich von 6 bis 160 kDa genau beschreiben. Die Modellparameter konnten anhand einiger experimenteller Säulenläufe zuverlässig identifiziert werden. Modellvergleiche zeigten, dass sowohl die Bindungskinetik als auch die Film- und Porendiffusion relevante Mechanismen auf den gepfropften Winged Fasern sind. Zusammenfassend zeigte der zweite Teil dieser Arbeit am Beispiel von gepfropften Winged Fasern, dass Adsorber auf Faserbasis mechanistisch modelliert werden können. Es wurde gezeigt, wie die erforderlichen Modellparameter bestimmt werden können, und es konnte ferner gezeigt werden, dass die Modellierung für eine Reihe von Molekülgrößen möglich ist, die für die Aufreinigung von Biopharmazeutika relevant wären. Die Ergebnisse dieser Studie tragen zu einem besseren Verständnis der Stoffübergangseigenschaften gepfropfter Winged Fasern bei, und das vorgestellte Modell ermöglicht mechanistische Vergleiche mit anderen Arten stationärer Phasen. Darüber hinaus ermöglicht das entwickelte Modell die modellbasierte Prozessentwicklung und -optimierung für Adsorber auf Faserbasis.

Im dritten Teil dieser Arbeit wurde untersucht, ob mikroskalige Hochdurchsatzwerkzeuge für Adsorber auf Faserbasis entwickelt werden können. Dies wurde erneut unter Verwendung

von nativen und gepfropften Winged Kurzschnittfasern bewertet. Für diese Fasern wurde ein automatisiertes Hochdurchsatz-Screening (engl. *High throughput screening (HTS)*) auf einer Roboterpipettierstation in Filterplatten mit 96 Wells etabliert. Es konnten zwei Techniken identifiziert werden, die eine genaue und reproduzierbare Portionierung der Fasern ermöglichen. Der Einfluss mehrerer Screening-Parameter wurde untersucht und optimiert. Es konnte gezeigt werden, dass die vom HTS erhaltenen Daten mit Daten von gepackten Fasersäulen korrelieren. Die Nützlichkeit des entwickelten HTS für die Material- und Prozessentwicklung wurde in zwei Fallstudien untersucht, die zeigten, dass das entwickelte HTS zur Optimierung der Hydrogelstruktur von Adsorbern auf Basis von kontrollierten gepfropften Fasern verwendet werden kann und, dass es zur Entwicklung von Stufenelutionsbedingungen für die Aufreinigung eines monoklonalen Antikörpers aus produkt- und prozessbedingten Verunreinigungen eingesetzt werden kann. Insgesamt hat die im dritten Teil dieser Arbeit vorgestellte Studie gezeigt, dass es möglich ist, mikroskalige Hochdurchsatzwerkzeuge für Adsorber auf Faserbasis zu entwickeln, die zur Materialoptimierung und Prozessentwicklung verwendet werden können. Das entwickelte Tool ermöglicht eine schnellere und vollständigere Charakterisierung von Adsorbern auf Faserbasis, und es kann für die material- und zeiteffiziente Prozessentwicklung verwendet werden. Das Tool erleichtert den Vergleich von Adsorbern auf Faserbasis mit anderen Materialien und könnte somit die Integration von Adsorbern auf Faserbasis in industrielle Aufreinigungsprozesse erleichtern.

Im letzten Teil dieser Arbeit wurde untersucht, ob und unter welchen Bedingungen Adsorber auf Faserbasis für industrielle Aufreinigungsverfahren verwendet werden können. Hier wurde die Verwendung von Kationenaustauscherfasern zur Entfernung monoklonaler Antikörperaggregate während der Antikörperreinigung untersucht. Zwei Arten von starken Kationenaustauschern auf Faserbasis mit unkontrollierten und kontrollierten gepfropften Hydrogelschichten wurden untersucht und hinsichtlich Permeabilität, dynamischer Antikörperbindekapazität, Auflösungsvermögen von mAb-Monomer und -Aggregaten und ihrer Performance in verschiedenen Betriebsmodi bewertet. Die Studie zeigte, dass aufgrund hoher Permeabilitäten, hoher dynamischer Bindekapazitäten bei schnellen Flussgeschwindigkeiten und guter Auflösungsfähigkeiten von Monomer und Aggregaten die Verwendung von Adsorbern auf Faserbasis zur Entfernung von mAb-Aggregaten bis zu sehr hohen Flussgeschwindigkeiten möglich ist. Es wurde festgestellt, dass die Gesamtleistung der Adsorber auf Faserbasis mit der Leistung eines vorhandenen Gelmaterials, Poros 50 HS, vergleichbar ist. Im Vergleich der beiden Arten von Fasern wurde festgestellt, dass die Leistung von kontrolliert gepfropften Adsorbern der Leistung von unkontrollierten gepfropften Adsorbern auf Faserbasis aufgrund höherer Produktivität und geringerem Pufferverbrauch überlegen ist. Zusammenfassend zeigt die im letzten Teil dieser Arbeit vorgestellte Studie, dass die Verwendung von Adsorbern auf Faserbasis für Prozessanwendungen während der Herstellung von industriellen Antikörpern machbar ist und beschreibt geeignete Betriebsbedingungen dafür.

Zusammenfassend trägt die vorliegende Arbeit zu einem besseren Verständnis der Eigenschaften und der Leistung von oberflächenstrukturierten Winged Fasern und Adsorbern

auf Faserbasis für präparative Chromatographieanwendungen bei. Die Arbeit liefert Informationen über die Packeigenschaften solcher Adsorber, mechanistische Modellparameter, relevante Stoffübergangs- und Bindungsmechanismen und die Leistungswerte bei der Entfernung von monoklonalen Antikörperaggregaten. Diese Daten können für Vergleiche mit vorhandenen Materialien und anderen Arten von Adsorbern auf Faserbasis verwendet werden. Darüber hinaus liefert die vorliegende Arbeit Informationen darüber, wie die Struktur von Adsorbern auf Faserbasis in Bezug auf die Packstruktur und die Polymer-Nanoschichtarchitektur die Leistung solcher Adsorber beeinflusst. Das trägt dazu bei, solche Adsorber effizienter zu verwenden und sie für bestimmte Anwendungen maßzuschneidern. Darüber hinaus werden in dieser Arbeit mechanistische Modelle und Hochdurchsatz-Screenings für Adsorber auf Faserbasis vorgestellt. Diese Modelle und Werkzeuge können für die zukünftige Entwicklung und Bewertung von Adsorbern auf Faserbasis von Nutzen sein, da sie eine material- und zeiteffiziente Bewertung solcher Materialien ermöglichen und erleichtern. Dies könnte es einfacher machen, solche alternativen Adsorber in Prozessentwicklungsworkflows und Aufreinigungsprozesse zu integrieren. In Bezug auf Prozessanwendungen konnte gezeigt werden, dass die Verwendung von Adsorbern auf Faserbasis zur Entfernung monoklonaler Antikörper möglich ist und diese Arbeit liefert relevante Betriebsfenster für diesen Zweck. Insgesamt könnten die erzielten Ergebnisse die Verwendung von Adsorbern auf Faserbasis erleichtern, um deren Vorteile zu nutzen, und damit einigen der aktuellen Herausforderungen im Bereich der präpartiven Aufreinigung von Biopharmazeutika zu begegnen.

Contents

List of Figures

List of Tables

1 Introduction

1.1 Biopharmaceuticals

1.1.1 Definition and Importance of Biopharmaceuticals

Biopharmaceuticals can be defined as pharmaceuticals that are "inherently biological in nature and manufactured using biotechnology" [1]. They are produced by or extracted from biological sources, in contrast to chemical-based pharmaceuticals or drugs, which are manufactured using chemical methods [1].

Biopharmaceuticals are used in the field of medicine for therapeutic, prophylactic or diagnostic purposes. Initially biopharmaceuticals were extracted from natural, i.e. non-engineered, biological sources such as microorganisms, animals, or humans [2, 3]. While this method is still being used, for instance for the preparation of blood plasma and blood plasma derived biopharmaceuticals such as serum albumin or clotting factors, most biopharmaceuticals are nowadays produced by modern biotechnological means [4, 5]. This means that recombinant DNA, and techniques such as genetic engineering or hybridoma technology are used [2, 3].

In terms of chemistry most biopharmaceuticals are organic macromolecules, in particular proteins, but they can also consist of nucleic acids, polysaccharide components or combinations of proteins and polysaccharides. Moreover combinations with organic molecules such as conjugated proteins or antibody drug conjugates are possible, and the range of biopharmaceuticals also includes macromolecular assemblies such as viruses and virus-like particles, or even microorganisms and whole cells. The major product classes of biopharmaceuticals are blood factors and other blood related products, hormones, growth factors, interferons/interleukins and tumor necrosis factor, vaccines, monoclonal antibodies (mAbs), and other products such as enzymes, nucleic acids, and cell based products [4]. In recent years monoclonal antibodies have accounted for more than 50% of newly approved biopharmaceuticals, and in 2017 they accounted for 66% of global biopharmaceutical sales [5, 6].

Biopharmaceuticals have had and continue to have a profound impact on the treatment of many diseases, such as cancer, inflammation-related conditions such as autoimmune diseases, hemophilia, and metabolic disorders such as diabetes [4]. Biopharmaceuticals are highly effective, as they are typically very specific for certain targets inside the body [3]. This, and the fact that most biopharmaceuticals are identical or nearly identical to naturally occurring substances inside the body often also leads to comparatively small side effects [3]. The recombinant production of biopharmaceuticals has made it possible to manufacture biopharmaceuticals in quantities that are independent of quantities that can be found in biological sources, and it avoids the extraction from dangerous biological sources or source materials which are infected with transmissible diseases [3]. In addition, it allows for modifications of the naturally occuring substances that can lead to improved characteristics, such as changes to the amino acid sequence of proteins which affect the duration of action [3].

All these factors have contributed to a strong increase in the number of biopharmaceutical approvals over the last 30 years [5]. In 2018 there were 316 individual biopharmaceutical products with active licenses [5], and in 2017 the global sales of all biopharmaceuticals amounted to $188 billion [5]. In addition, estimates suggest that there are currently about 2,400 biopharmaceuticals in development [5].

The development and manufacturing of biopharmaceuticals, however, is not easy. As outlined above, most biopharmaceuticals are large macromolecules, and are therefore structurally much more complex than chemical-based pharmaceuticals [7]. While most chemical-based pharmaceuticals are small molecules with molecular weights less than 500 Da, biopharmaceuticals can be orders of magnitude larger, such as mAbs with a molecular weight of 150 kDa. Biopharmaceuticals possess complex higher order structures [2], which are subject to environmental conditions, and which are essential for their function. Due to their size, there are a lot of possibilities for structural variations and posttranslational modifications [7]. During the production of biopharmaceuticals in living cells, a variety of side products such as aggregates can be generated. These may be very similar to the main product in terms of physicochemical properties, such that their removal can be challenging.

Overall, these characteristics have resulted in complex development and manufacturing processes for biopharmaceuticals. The development of a single biopharmaceutical can take up to 12 years and requires significant resources [8]. It is also associated with high risks, as approximately 90% of all biopharmaceutical development projects fail during development [8]. Partly because of these reasons, the development and manufacturing costs for biopharmaceuticals are relatively high.

This can make it difficult to provide biopharmaceuticals at low costs. Low costs are particulary important for prophylactics such as vaccines, which need to be as cost-effective as possible if large populations are to be treated, or treatments for chronic diseases which need to be used repeatedly over long periods of time. The high development and

manufacturing costs also make it difficult to provide biopharmaceuticals at affordable prices to patients in low-income countries, which is one of the reasons why the access to such medicines in low-income countries has been limited. In high-income countries patent-protected biopharmaceuticals have been and are often priced at prices which are independent of manufacturing costs, and which reflect the perceived value of the biopharmaceuticals by the biopharmaceutical companies in comparison to other existing treatments [8]. This has resulted in very high sales prices of biopharmaceuticals, which can lead to very high annual treatment costs in the range of 20,000 EUR up to 200,000 EUR [8]. These high prices have created a burden to healthcare budgets and have resulted in an increasing cost-awareness of healthcare providers and regulators.

Due to population growth and aging societies it is expected that the demand for biopharmaceuticals will be increasing in the future [8]. At the same time novel types of biopharmaceuticals will have to developed, which can be used in order to treat diseases which only affect few patients, or which show better efficacy in certain patient populations which currently do not benefit from the treatment with biopharmaceuticals. Thus, overall more biopharmaceuticals, but a wider variety of biopharmaceuticals in potentially much smaller quantities will have to be manufactured and developed in the future. This could make the treatment with biopharmaceuticals at current price levels unsustainable. The development and manufacturing costs of biopharmaceuticals will have to be reduced in order provide such medicines at less cost to society, and in order to improve the access to such medicines in low-income countries. In recent years, the first generic versions of biopharmaceuticals, so-called biosimilars, have been introduced into the market with average price reductions of 30% and in some cases even by up to 80% [8]. In order to provide biopharmaceuticals with such price reductions, low development and manufacturing costs are also essential.

As a consequence of these developments, for the future more flexible and more efficient development and manufacturing strategies and processes are needed for biopharmaceuticals which result in higher productivity and/or lower costs.

1.1.2 Development and Manufacturing of Biopharmaceuticals

The discovery and development of biopharmaceuticals is carried out in several distinct stages [8]. The first stage involves the identification of disease mechanisms that can be targeted with a biopharmaceutical. Thereafter, appropriate candidate biopharmaceuticals need to be developed and selected which can interfere with the identified disease mechanism. Subsequently, the safety and efficacy of the biopharmaceutical are evaluated in pre-clinical as well as several stages of clinical studies. As part of these activities an appropriate manufacturing process must be developed for the biopharmaceutical that enables the manufacturing of the biopharmaceutical with the right quality, safety, and efficacy, and in the right quantity. Process development activities for manufacturing in larger quantities typically start during

pre-clinical development [8]. During the course of clinical development, the processes are then optimized, scaled up, validated and transferred to commercial manufacturing. As part of these activities an understanding of the impact of process parameters on product quality must be established and critical process parameters (CPPs) which affect critical quality attributes (CQAs) must be identified [9].

Manufacturing occurs during all stages of discovery and development, however manufacturing at larger scales typically only starts during pre-clinical development, when material for toxicology studies needs to be produced [8]. For pre-clinical studies typically about 10 g-1 kg of material is required, while for early stages of clinical studies (Phase 1 and 2) 0.5-5 kg, and for Phase 3 clinical studies 10-30 kg may need to be produced [8]. Production quantities for commercial biopharmaceuticals can range from several 100 grams to several tons per year [8]. Therefore the manufacturing of biopharmaceuticals occurs at different scales, which increase in size from clinical scale manufacturing to commercial scale manufacturing.

The recombinant manufacturing itself consists of three steps [8]. During upstream processing (USP) a production host that has been genetically modified to express the biopharmaceutical is cultivated in a bioreactor under conditions that favor the expression of the biopharmaceutical. Subsequently, during downstream processing (DSP), the target molecule is recovered from the cultivation mixture, purified from other components that are also produced by the production host, for instance process-related impurities such as host cell proteins (HCPs) and DNA, or product-related impurities such as aggregates, and concentrated. Finally, during formulation the purified target molecule is transferred into an appropriate buffer such that it can be administered to the patient at the right dose, and remains stable over the intended shelf life. During or after formulation the biopharmaceutical is filled into appropriate devices or containers for later administration to patients and packaged.

Currently most manufacturing processes are carried out in batch mode [8], although semi-continuous and continuous processing is also possible [10]. USP typically accounts for the longest period of time during manufacturing, in particular if mammalian cells are used for production, where USP can take up to 14 days. DSP is shorter and typically takes about 2-5 days. However, DSP now typically accounts for the majority of the manufacturing costs [11]. In recent years titers in USP have increased. This has resulted in an overall reduction of manufacturing costs, but has also led to the situation that DSP now often accounts for the majority of manufacturing costs. Therefore currently a focus is being placed on improving DSP operations, in order to match the improvements in USP, and further bring down manufacturing costs.

Due to the developments that were outlined in the previous subsection, there is currently a strong interest in shortening and simplifying the development of new biopharmaceuticals, for instance via using prior knowledge and data, template processes and process sequences [12], or appropriate scale-down and in silico tools, and process automation [8]. In addition,

because future biopharmaceuticals may require smaller amounts of a wider variety of products might be required, there is an interest in smaller and more flexible manufacturing operations, and single use technologies that reduce fixed capital investments and enable quick product changeovers. In addition, in order to bring down manufacturing costs, there is an interest in increasing the productivity of manufacturing operations, for instance via process intensification through the use of semi-continuous or continuous processes, or through the use of novel materials.

1.1.3 Downstream Processing of Biopharmaceuticals

Biopharmaceutical downstream processing typically consists of several stages [8, 13, 14]. In the first stage the target product is recovered from the cultivation mixture, which involves cell disruption and/or cell separation as well as clarification steps. In the subsequent stage, the capture stage, the product is isolated from the harvested cell culture fluid and concentrated. In the following purification stage the main impurities such as product variants are removed, and finally during the polishing stage any remaining trace impurities such as host cell DNA are removed. Most downstream processes follow this sequence of stages, however, in many cases there are also additional reaction stages, for instance for unfolding or refolding, conjugation, or viral inactivation. The number of processing steps that are used in a downstream process should be kept to the minimum that is required in order to achieve purity targets, as any additional processing step leads to a reduction of product yield [13].

A variety of different unit operations can be used throughout these processing stages, however in most cases centrifugation, filtration, and in particular chromatography are being used. This is often done in order to simplify process sequences and process development efforts, and is particularly helpful if a number of biopharmaceuticals of the same class have to be purified. The prime example for this are monoclonal antibodies, for which template process sequences, so-called platform processes have been developed, which are nowadays being used in most companies [12]. The platform processes are based on the conserved Fc region which is shared between most monoclonal antibodies, and enables purification via Protein A affinity chromatography. A typical downstream process sequence for mAbs [15] consists of centrifugation and depth filtration operations for cell separation and clarification, which is followed by Protein A chromatography for product capture, concentration and removal of host cell impurities. The subsequent process sequence typically consists of two additional chromatography steps for the removal of product variants such as mAb aggregates and the further removal of HCP and trace impurities, as well as a low pH hold step for viral inactivation, and a nanofiltration step for virus removal. Finally the mAb is concentrated and buffer exchanged into the formulation buffer via ultrafiltration and diafiltration (UF/DF).

Therefore most of the separation tasks in mAb purification are carried out with the use of chromatography. This prevalence of chromatography can be found in other downstream processes of biopharmaceuticals. Due to the prevalence of chromatographic steps, which also account for most of the duration of the downstream process [16], the chromatographic steps have a big impact on the productivity of downstream processes. Moreover they contribute strongly to the overall costs of the downstream processes [17], which is a consequence of the associated buffer and stationary phase costs. Therefore focusing on chromatography can be a key factor in the context of improving productivity and reducing manufacturing and downstream processing costs.

1.2 Chromatography

There are several reasons for the prevalence of chromatography in biopharmaceutical downstream processing [18]. First, chromatography is a very versatile unit operation, as there are a number of different separation techniques and operating modes that can be used for chromatography. With most chromatographic techniques, separations can be performed under mild operating conditions in which the product remains stable and in its native configuration. In addition, chromatography features a high separation efficiency. Finally, the widespread application of chromatography means that there is a lot of experience, appropriate equipment for all manufacturing scales, and a lot of theoretical and practical guidelines, which facilitate the development of chromatographic processes.

1.2.1 Fundamentals

Chromatography can be defined as "a physical method of separation in which the components to be separated are distributed between two phases, one of which is stationary (stationary phase) while the other (the mobile phase) moves in a definite direction" [19]. Both phases can have different states of matter. For the preparative purification of biopharmaceuticals solid-liquid chromatography is the method of choice, in which the stationary phase is solid, and the mobile phase is liquid.

A number of different separation mechanisms and operating modes can be used for chromatography [20, 21]. Based on the mechanism of separation one can distinguish between partition chromatography which is based on differences in the solubilities of the sample components in the mobile and stationary phases, and adsorption chromatography, which is the main separation mechanism that is used for biopharmaceuticals, and which is based on differences between the adsorption affinities of the sample components for the surface of an active solid [19]. For ion-exchange chromatography (IEX) differences in the ion

exchange affinities of the sample components are exploited, while in hydrophobic interaction chromatography (HIC) the separation is based on differences in hydrophobicity. In affinity chromatography (AC), the separation is based on a specific interaction between the sample components and a ligand on the adsorbent surface, while in size exclusion chromatography (SEC) the separation is based on differences in molecular size or shape, which lead to a differential access to pores within the stationary phase.

In terms of operating mode, one can distinguish between frontal chromatography, displacement chromatography, and elution chromatography [20]. In frontal chromatography the sample is fed continuously into the chromatographic bed and the sample components emerge from the column exit in bands in order of increasing interaction strength. In displacement chromatography and elution chromatography the sample is fed into the bed in a finite slug. In displacement chromatography the sample or the mobile phase contain a displacer which is more strongly retained than the other components of the sample and displaces the other sample components. In elution chromatography the mobile phase contains a modifier such as salt, which reduces the affinity of the solute to the stationary phases and leads to elution. Elution chromatography and frontal chromatography are the main techniques that are used for the purification of biopharmaceuticals. Another operating mode that is frequently used for biopharmaceuticals is flowthrough chromatography. It is similar to frontal chromatography, because the sample is fed continuously into the column. The mobile phase conditions, however, are selected such that the product of interest does not interact with the column and flows through the columns, while impurities that are to be removed bind to the stationary phase.

Another distinction can be made between analytical and preparative chromatography [21]. The main difference is that analytical chromatography is carried out in order to obtain information about the composition of a sample, while preparative chromatography aims at purifying a single or few components of a sample in larger quantities. As a consequence, sample and column sizes often differ between these two modes of chromatography. Analytical chromatography is typically carried out with µg to mg amounts of sample in columns with inner diameters smaller than 1 mm, with the goal to separate and quantify the components of a sample. In preparative chromatography the goal is to purify a single component in larger quantities which can range from mg to tons. Therefore larger columns and larger equipment are utilized. While for analytical chromatography selectivity and speed are very important, for preparative chromatography purity, yield, productivity, and process economics are the main optimization parameters.

The separation inside a chromatography column is a result of the interplay of fluid dynamics, mass transfer, and thermodynamics [20–22]. All of these effects contribute to band broadening within a chromatography column. Fluid dynamic effects act on microscopic, mesoscopic, and macroscopic levels [21]. The main fluid dynamic effects that play a role for liquid chromatography are molecular diffusion, eddy diffusion, and nonuniformities in fluid velocity across the packed bed [21]. These can be caused by insufficient fluid distribution at the column inlet and outlet for large diameter columns,

packing bridges, or wall effects for small diameter columns. The different effects are often summarized into a single axial dispersion coefficient. Mass transfer occurs in the form of convective and diffusive transport of molecules in the interstitial liquid towards the adsorbent particles, film diffusion through the stagnant film surrounding the adsorbent particles, pore diffusion and/or surface diffusion inside the particles, and adsorption and desorption processes which can follow different reaction kinetics [20–22]. Thermodynamics define the solid liquid phase equilibria on the adsorbent surface. These effects are commonly described with isotherms. Depending on the isotherm shape the band profile can be affected in different ways.

The separation performance of a chromatographic column can be described with a number of parameters [20–22]. These parameters can often be related to properties of the stationary or the mobile phase, the solutes to be separated, as well as the underlying physical processes. In the following paragraphs essential parameters that were used and discussed in this thesis will be briefly described.

Porosity The porosity describes the ratio of the volume of voids to the total adsorbent volume. Depending on the stationary phase structure different porosities can be defined. The external or interstitial porosity ε describes the ratio of the interstitial fluid volume V_{int} to the total geometric bed volume V:

$$\varepsilon = \frac{V_{int}}{V} \tag{1.1}$$

For stationary phases with additional voids within the stationary phase due to additional pores within the stationary phase, an additional internal porosity can be defined. For particulate stationary phases this internal porosity or intra-particle porosity ε_p is defined as

$$\varepsilon_p = \frac{V_{pore}}{V_{pore} + V_{solid}} \tag{1.2}$$

where V_{pore} is the volume of the pore system within the stationary phase, and V_{solid} is the volume of the solid stationary phase skeleton. For stationary phases with a multimodal pore structure or superficially porous particles this internal particle porosity can be broken down further. The different porosities can be summarized into a total porosity ε_t, which describes the ratio of the total fluid volume V_{fluid} to the total geometric bed volume. For particulate stationary phases it can be calculated according to:

$$\varepsilon_t = \varepsilon + (1 - \varepsilon)\varepsilon_p \tag{1.3}$$

Mobile phase velocity The mobile phase velocity u, which is sometimes also called superficial velocity or velocity of the empty column, is the linear flow velocity of the mobile

phase. It is obtained from the volumetric flow rate of the mobile phase $\dot{V}$ and the cross-sectional area of the chromatographic bed A_c according to:

$$u = \frac{\dot{V}}{A_c} \tag{1.4}$$

Within the chromatographic bed the mobile phase moves at a faster velocity since a part of the chromatographic bed is occupied by the stationary phase. The interstitial velocity u_{int}, i.e. the velocity at which the mobile phase moves through the interstitial liquid within the chromatographic bed is defined as:

$$u_{int} = \frac{u}{\varepsilon} \tag{1.5}$$

Retention time If a finite slug of a solute component i is injected into a chromatography column it emerges from the column outlet after a certain residence time, the retention time $t_{R,i}$. The retention time can also be specified as a retention volume $V_{R,i}$, if the retention time $t_{R,i}$ is multiplied with the volumetric flow rate $\dot{V}$. The retention time depends on the dead time t_0 of the column, i.e. the time the component needs to travel through the voids of the column, and on the interaction of the component with the stationary phase. For symmetrical peak shapes such as Gaussian peaks, the retention time can be determined from the peak maximum of the chromatograpic peak. For asymmetrical peak shapes the retention time can be calculated from the first absolute moment of the peak $\mu_{t,i}$, i.e.

$$t_{R,i} = \mu_{t,i} = \frac{\int_0^\infty t c_i(t) dt}{\int_0^\infty c_i(t) dt} \tag{1.6}$$

where $c_i(t)$ stands for the concentration of the solute at the column outlet at time t.

Peak variance and peak width In addition to the retention time, the peak shape of a chromatographic peak can also be described by the peak variance and the peak width. The peak variance $\sigma_{t,i}^2$ can be determined from the second central moment according to:

$$\sigma_{t,i}^2 = \frac{\int_0^\infty (t - \mu_{t,i})^2 c_i(t) dt}{\int_0^\infty c_i(t) dt} \tag{1.7}$$

The peak width can be determined at different peak heights. Frequently used peak widths are the baseline width w_i and the width at half-height $w_{1/2,i}$. For Gaussian peaks these peak widths can be directly related to the peak variance:

$$w_{1/2,i} \approx 2.354 \cdot \sigma_i \tag{1.8}$$

$$w_i = 4 \cdot \sigma_i \tag{1.9}$$

Peak asymmetry The peak asymmetry A_s describes the amount of fronting or tailing of a chromatographic peak. Similar to the peak width it can be determined at different peak heights. Frequently it is determined at 10% peak height according to

$$A_s = \frac{b_{0.1}}{a_{0.1}} \tag{1.10}$$

where $b_{0.1}$ and $a_{0.1}$ stand for the right and left peak half at 10% peak height in relation to the peak maximum.

Retention factor The retention factor k'_i, which is also called capacity factor, is used to normalize the retention time of a component i in relation to the dead time t_0:

$$k'_i = \frac{t_{R,i} - t_0}{t_0} \tag{1.11}$$

It is equivalent to the mole ratio of component i in the stationary phase and mobile phase:

$$k'_i = \frac{n_{i,stat}}{n_{i,mob}} \tag{1.12}$$

Partition coefficient The partition coefficient $K_{P,i}$ describes the ratio between the stationary phase concentration $c_{stat,i}$ and mobile phase concentration $c_{mob,i}$ of component i. It is related to the retention factor k'_i via the phase ratio according to

$$K_{P,i} = \frac{c_{stat,i}}{c_{mob,i}} = k'_i \cdot \frac{V_{mob}}{V_{stat}} \tag{1.13}$$

where V_{mob} and V_{stat} stand for the volumes of mobile and stationary phase.

Separation factor The separation factor α, which is also called selectivity, describes the ratio of the retention factors or partition coefficient of two components

i and j, where i typically stands for the component that elutes first from the column:

$$\alpha = \frac{k'_j}{k'_i} = \frac{K_{P,j}}{K_{P,i}} \tag{1.14}$$

Column efficiency The column efficiency N_i, which is also called plate number, is a measure for the degree to which ideal chromatography conditions are achieved within a chromatographic bed. It can be determined according to:

$$N_i = \left(\frac{t_{R,i}}{\sigma_{t,i}}\right)^2 = \frac{\mu_{t,i}^2}{\sigma_{t,i}^2} \tag{1.15}$$

Plate height The height equivalent of a theoretical plate (HETP) H is used to normalize the plate number with the respective column length L:

$$H_i = \frac{L}{N_i} \tag{1.16}$$

The plate height can be related to the underlying fluid dynamic, mass transfer, and thermodynamic effects. An equation that is frequently used for this purpose is the Van Deemter equation [23]:

$$H_i = A_i + \frac{B_i}{u_{int}} + C_i \cdot u_{int} \tag{1.17}$$

The A-term describes the impact of eddy diffusion and axial mixing, while the B-term describes the impact of axial diffusion, and the C-term describes the impact from mass transfer and thermodynamic effects. Under typical operating conditions for preparative liquid chromatography (LC) of biopharmaceuticals the A-term and C-term are relevant, while the B-term contribution is often negligible.

Resolution In addition to the separation factor, the separation of two components i and j can also be described by the resolution R_s. The resolution accounts not only for the difference in retention, but also takes the respective peak widths into account:

$$R_s = \frac{t_{R,j} - t_{R,i}}{\frac{1}{2}(w_i + w_j)} = \frac{\mu_{t,j} - \mu_{t,i}}{2(\sigma_{t,i} + \sigma_{t,j})} \tag{1.18}$$

For equivalent peaks with equal peak width R_s can be described as a function of the separation factor, the retention factor, and the efficiency, which illustrates the parameters

that can be altered to affect resolution:

$$R_s = \left(\frac{\alpha}{\alpha - 1}\right)\left(\frac{k'_j}{k'_j + 1}\right)\frac{\sqrt{N_j}}{4} = (\alpha - 1)\left(\frac{k'_i}{k'_i + 1}\right)\frac{\sqrt{N_i}}{4} \tag{1.19}$$

The aforementioned parameters are relevant for analytical as well as preparative chromatography. For preparative chromatography there are additional parameters that are often used as performance criteria for the evaluation of preparative chromatography operations. The main parameters that were used in this thesis will be briefly defined in the following paragraphs.

Bed permeability The bed permeability B measures the ability of a mobile phase to flow through the chromatographic bed. For laminar flow conditions and incompressible stationary phases it can be determined from Darcy's law

$$\Delta p = \frac{1}{B}\eta u L \tag{1.20}$$

where η stands for the dynamic viscosity of the mobile phase. The bed permeability can be used in order to define the operating window in terms of bed height and mobile phase velocity for a stationary phase for a defined maximum column pressure drop Δp. In general, it is related to the interstitial porosity and the particle size and shape. There are a number of equations that can be used in order to determine the permeability from the porosity and the size and shape of the stationary phase particles, such as the Blake-Kozeny relationship [20–22] which is frequently used for particulate stationary phases.

Equilibrium binding capacity The equilibrium binding capacity (EBC), q is the amount of a substance that is bound to the stationary phase at equilibrium with the mobile phase. In general it depends on the mobile phase conditions, the feed concentration, and the isotherm shape, i.e. on thermodynamics. The EBC can be specified per packed bed volume, per stationary phase volume or by stationary phase skeleton volume or also the respective masses.

Static and dynamic binding capacity The static binding capacity (SBC) is typically measured via batch binding experiments. It describes the amount of a substance that is bound to the stationary phase for specific starting conditions after a certain period of time. If the batch binding experiment is carried out long enough to achieve equilibrium, then it is identical to the EBC. The dynamic binding capacity, DBC, describes the binding capacity that is obtained under flow conditions. Due to the dispersion and diffusion phenomena described above the DBC is typically only a fraction of the EBC. The

DBC is typically determined via breakthrough curves and specified for a certain level of breakthrough, e.g. 10% or 5%. The DBC is used in order to determine the load volume of a preparative column. To avoid product loss and to account for column aging the load volume is typically only set to a certain percentage of the DBC.

Capacity utilization The capacity utilization describes the ratio between the DBC at a certain level of breakthrough and the respective EBC.

Purity The purity Pu_i of a component describes the ratio of the component in a sample in relation to all components. In chromatography the purity is often based on the relative peak area:

$$Pu_i = \frac{Area_i}{Area_{total}} \tag{1.21}$$

Yield The yield Y_i of a component i describes the relative amount of the component that is recovered after a chromatographic step in comparison to the amount that is loaded:

$$Y_i = \frac{m_{recovered}}{m_{loaded}} \tag{1.22}$$

Productivity The productivity P describes the amount of product that can be processed per unit of bed volume and unit of time. It is related to the geometric bed volume V and the cycle time t_{cycle}:

$$P = \frac{m_{Product,recovered}}{V \cdot t_{cycle}} \tag{1.23}$$

In the cycle time all phases of the chromatographic cycle are included as well as potential lag times.

Throughput The throughput describes the amount of product that is processed per unit of time. It is defined by the productivity P and the bed volume V that is used. It can be increased via increasing the productivity or increasing the bed volume, for instance via using larger beds or beds that are run in parallel.

Buffer consumption The buffer consumption describes the volume of buffer that is consumed per mass of product that is processed. It contains the volumes of all cycles of the chromatographic process except for the loading phase.

1.2.2 Development of chromatographic processes

During the development of chromatographic processes a number of parameters need to be defined. If a downstream process contains several chromatography steps then the number of steps, the sequence of the steps, and the interaction mode and operating mode for each step must be defined. For each step an appropriate stationary phase must be selected, and for each phase of the chromatography cycle the operating conditions such as the mobile phase composition, sample concentration, flow rate, or the phase duration must be defined. For this purpose different process development approaches can be used [24–27], which encompass heuristic or knowledge-based approaches, experimental approaches, and model-based approaches as well as combinations of these different approaches.

1.2.2.1 Heuristic or knowledge-based process development approaches

Heuristic or knowledge-based process development approaches [28] are based on expert knowledge and prior experience [27]. This knowledge is described in the form of rules of thumb, development guidelines, or expert systems [29] which can be used for the design of process sequences or specific unit operations. Some of these guidelines are very general and independent of the molecules that are to be separated, while others require a knowledge of certain physicochemical properties of the molecules that are to be purified.

General guidelines for the design of chromatography sequences for instance suggest to use orthogonal chromatography techniques between different steps or to position chromatography steps in an order such that conditioning operations between the steps can be avoided [30]. For single process steps there are, for instance, guidelines on which salt should be used in HIC or how the mobile phase pH should be selected in IEC [8]. Another example of knowledge-based process development approaches are platform processes [12]. These are fixed series of unit operations which are used as templates for the purification of closely related molecules such as monoclonal antibodies. Here, only individual unit operations or phases of the unit operations have to be optimized.

The advantage of these approaches is that they are easy to use and fast as no or only minimal experimentation is required. They reduce the complexity of process development and can reduce the time until a working process exists that can be used for the production

of material for clinical trials. Platform processes make process transfers easier, and the knowledge and process understanding that is generated in previous processes can be reused. However, not all possible process combinations are explored with these approaches, and the suggested or selected process sequence may not be optimal. With no prior data or only limited information on the properties of the components, only qualitative process development recommendations can be made.

1.2.2.2 Experimental process development approaches

Therefore the development of chromatography processes and process sequences is often based on experiments. Even with platform processes and expert systems a certain number of experiments are performed in order to assess the performance of the recommended process sequence and, if necessary, optimize the process conditions. Typical experiments that are being performed focus on the selection of suitable stationary phase materials and mobile phase conditions that offer sufficient selectivity for the desired separation, and the optimization of individual phases of the chromatographic cycle such as the loading, wash, or elution phases [8].

Traditionally such experiments have been performed in laboratory scale columns. These experiments require significant amounts of material and time, and therefore the impact of only a single factor or a few factors can be studied at a time. While such experiments are still being used for the development of chromatography processes, nowadays many experiments are performed in a more systematic manner using structured experiments based on design of experiment (DoE) approaches and high throughput experimentation (HTE).

With HTE the experiments are miniaturized, and performed in an automated and parallelized fashion [31–33]. Process development that is performed with such experiments has been termed high-throughput process development (HTPD) [34]. Automation and parallelization of the experiments is typically achieved via performing the experiments on robotic liquid handling stations (LHS). Different formats can be used [32, 33] such as microtiter filter plates which are filled with small amounts of stationary phase, prepacked miniature columns, prepacked pipette tips, and lately also microfluidic devices microfluidic devices [35–37]. Such formats are well established for stationary phases such as resins [32, 33] or membranes [38], and various application examples have been presented [32].

HTE enables faster process development with less material requirements. Therefore a wider range of process options can be explored, and the chances to find good processing conditions become higher [33]. Structured experimentation with design of experiments has the advantage that processes can be optimized with fewer experiments and without an understanding of the underlying physical processes. However both of these experimental

approaches also have drawbacks. HTE results in a high amount of samples which need to be analyzed and large experimental datasets which need to be handled and analyzed efficiently [39]. DoE reduces the number of experiments, however as with HTE, it is not certain, that the optimal process conditions are included in the experiments. Both approaches in general do not allow for extrapolation beyond the experimental parameter ranges.

1.2.2.3 Model-based process development approaches

The third approach for the development of chromatographic processes is based on models that describe the relationship between process parameters and process outputs. These models are used to optimize the process parameters with respect to one or several objectives. They can be broadly classified into empirical models and mechanistic models, but combinations of these two model types, so-called hybrid models, also exist [27].

Empirical models Empirical models are based on experiments which are performed within a defined parameter space. The measured process outputs are then described mathematically as a function of the experimental input parameters. The input parameters can be different process conditions such as pH, buffer molarity, protein concentration etc., but they can also be molecule properties that are determined from the molecular sequence or structure or sensor data such as absorption spectra [27]. Frequently used empirical models are response surface models which are based on linear or quadratic regression functions, and multivariate calibration models which can be based on e.g. principal component analysis (PCA), partial least squares (PLS) regression or support vector machines (SVMs) [27]. The models do not describe the underlying physical mechanisms, and are therefore considered black box models. This can be an advantage, if the underlying physical phenomena are complex or not fully understood. Therefore such models are broadly applied during all stages of chromatographic process development. However, in general, they cannot be extrapolated beyond the calibrated parameter range, and need to be recalibrated if the inputs or input ranges change. In addition, it is not certain, that the regression functions can accurately describe the relationship between input and output parameters, in particular if wider parameter ranges are surveyed. Due to the empirical nature such models require relatively large datasets for calibration and validation.

Mechanistic models The other type of chromatography models are mechanistic models. Mechanistic chromatography models explicitly describe the physical phenomena that occur inside a chromatography column such as convection, diffusion, or adsorption processes with a set of coupled differential equations. These equations contain several parameters

that describe the underlying physical phenomena, such as structural parameters of the chromatography column, dispersion coefficients, diffusion coefficients, or isotherm parameters. The system of equations is solved numerically in space and time in order to simulate and optimize the separation process. There are different mechanistic chromatography models which differ in the number of physical phenomena that are described, and the level of detail with which the physical phenomena are described. They can be classified into stage models and plug flow models. The plug flow models can be further subdivided on the basis of the column model, the pore model, and the adsorption model that are being used. A detailed overview of all models can be found in [21, 22]. The models which were used in this thesis will be briefly outlined in the following subparagraphs.

Column and pore models The most basic plug flow model is the ideal model (IDM) which only accounts for the effects of convection, phase distribution, and phase equilibrium. The IDM is given in Eq. 1.24

$$\frac{\partial c_i}{\partial t}(x,t) = -u_m(t)\frac{\partial c_i}{\partial x}(x,t) - \frac{1-\varepsilon_t}{\varepsilon_t}\frac{\partial q_i(x,t)}{\partial t} \quad \forall i \tag{1.24}$$

where $c_i(x,t)$ stands for the mobile phase concentration and $q_i(x,t)$ stands for the stationary phase concentration of component i at position x in a column with length L. The first term in Eq. 1.24 accounts for the change in concentration due to convective mass transport, while the second term describes the change in concentration due to adsorption. The ideal model does not distinguish between interstitial and pore liquid. Therefore u_m is used as velocity within the column, where $u_m = \frac{\varepsilon}{\varepsilon_t} u_{int}$.

The equilibrium dispersive model (EDM) accounts for band broadening due to axial dispersion and mass transfer by means of an apparent dispersion coefficient D_{app} according to Eq. 1.25

$$\frac{\partial c_i}{\partial t}(x,t) = -u_m(t)\frac{\partial c_i}{\partial x}(x,t) + D_{app}\frac{\partial^2 c_i}{\partial x^2}(x,t) - \frac{1-\varepsilon_t}{\varepsilon_t}\frac{\partial q_i(x,t)}{\partial t} \quad \forall i \tag{1.25}$$

Transport models account for the effects of mass transfer and/or reaction kinetics through the inclusion of transport rates. The lumped rate transport dispersive model (TDM) accounts for the effect of film and pore diffusion by means of an effective mass transfer coefficient $k_{eff,i}$ which describes the mass transfer rate in relation the the specific surface area a_p:

$$\begin{aligned}\frac{\partial c_i}{\partial t}(x,t) = &-u_{int}(t)\frac{\partial c_i}{\partial x}(x,t) + D_{ax}\frac{\partial^2 c_i}{\partial x^2}(x,t) \\ &-\frac{1-\varepsilon}{\varepsilon}k_{eff,i}a(c_i(x,t) - c_{p,i}(x,t)) \quad \forall i\end{aligned} \tag{1.26}$$

$$\frac{\partial c_{p,i}}{\partial t}(x,t) = \frac{k_{eff,i}a_p}{\varepsilon_p}(c_i(x,t) - c_{p,i}(x,t)) - \frac{1-\varepsilon_p}{\varepsilon_p}\frac{\partial q_i}{\partial t}(x,t) \quad \forall i \tag{1.27}$$

In this case the concentration of a component i in the mobile phase distributes into an interstitial concentration $c_i(x,t)$, and a pore concentration $c_{p,i}(x,t)$, and two coupled mass balances. Instead of D_{app}, D_{ax} is used which describes the axial dispersion within the interstitial mobile phase.

For numerical simulations boundary conditions need to be specified. Frequently Danckwerts boundary conditions are used, as shown in Eq. 1.28, where $c_{in,i}(t)$ is the injected concentration of component i at the column inlet at time t:

$$\frac{\partial c_i}{\partial x}(0,t) = \frac{u_{int}(t)}{D_{ax}}(c_i(0,t) - c_{in,i}(t)) \quad \forall i \tag{1.28}$$

$$\frac{\partial c_i}{\partial x}(L,t) = 0 \quad \forall i \tag{1.29}$$

Adsorption models The adsorption process is typically described with an isotherm equation. The most general isotherm equation is the Langmuir isotherm [21]. The single component equilibrium Langmuir isotherm for a component i is given by the following equation:

$$q_i(x,t) = \frac{q_{i,max}(x,t)c_{p,i}(x,t)}{K_{d,i} + c_{p,i}} \tag{1.30}$$

Here $q_{i,max}$ describes the maximum binding capacity of component i, and $K_{d,i}$ describes the binding affinity.

The Langmuir isotherm is only valid for a single set of mobile phase conditions. For practical separation problems often multicomponent systems need to be described with variable mobile phase conditions. A frequently used isotherm equation for ion-exchange is the steric mass action (SMA) isotherm [40]. The kinetic version of the SMA isotherm is given by Eqs. 1.31-1.32:

$$\frac{1}{k_{des,i}}\frac{\partial q_i(x,t)}{\partial t} = k_{eq,i}\left(\Lambda - \sum_{j=1}^{k}(\nu_j + \sigma_j)q_j(x,t)\right)^{\nu_i} c_{p,i}(x,t) - c_{p,salt}^{\nu_i}(x,t)q_i(x,t) \qquad \forall i \neq salt \tag{1.31}$$

$$q_{salt}(x,t) = \Lambda - \sum_{j=1}^{k}\nu_j q_j(x,t) \tag{1.32}$$

Here, j is a loop variable that loops over all k protein components of $i = 1, ..., N$ components. $q_i(x,t)$ describes the concentration of protein adsorbed to the stationary phase and $c_{p,salt}(x,t)$ is the pore salt concentration. $k_{eq,i} = k_{ads,i}/k_{des,i}$ is an equilibrium constant and is defined as the ratio between the rates of adsorption $k_{ads,i}$ and desorption $k_{des,i}$, whereas $k_{kin} = 1/k_{des}$. $q_{salt}(x,t)$ describes the salt concentration in the stationary phase, which is obtained as the difference between the ionic capacity Λ and the number of binding sites taken up by electrostatic adsorption. This is equivalent to the assumption that shielded binding sites are still occupied with counter-ions.

Hybrid models Hybrid models can be created via combining empirical and mechanistic models. For instance, quantitative structure-activity relationship (QSAR) models or artificial neural network (ANN) models can be combined with mechanistic models in order to predict model parameters of the mechanistic model such as isotherm parameters directly from a QSAR model [41] or an ANN [42]. Another type of hybrid models are metamodels, which are models of other models. For instance, ANN or PLS models can be built on top of a mechanistic model in order to describe an underlying mechanistic model [43]. Hybrid models have the advantage that they can reduce the amount of experimentation that is needed in order to calibrate a mechanistic model, and reduce the computational time that might be required in order to evaluate a mechanistic model. This can speed up model calibration and model evaluation. This can be advantageous if the evaluation of the underlying mechanistic model is too complex or too time consuming. Such approaches however require careful model training and validation, and the propagation of model errors has to be considered adequately.

1.2.2.4 Combinatorial process development approaches

Combinatorial process development approaches consist of combinations of heuristic, experimental, and model based process development approaches [27]. Such combinations can be used for the optimization of process sequences or for single process steps. For instance, physicochemical characterization experiments or computational approaches can be combined with expert systems in order to determine process sequences. Another example are combinations of HTE with mechanistic modeling, which enable efficient experimentation to determine parameters for mechanistic models, but also enable explicitly accounting for scale differences between HTE and laboratory scale experiments. Such approaches can be valuable, but aspects such as error propagation and data quality need to be considered.

1.2.3 Stationary phases for chromatography

1.2.3.1 General requirements and classification

The performance of a chromatographic process is strongly impacted by the properties of the stationary phase. Therefore the selection of a suitable stationary phase is very important. There are a number of features which are desirable for stationary phases that are used in the preparative purification of biopharmaceuticals [18, 21, 44]. To some extent these are application and use case dependent. In general features such as high selectivity, good mass transfer properties with high dynamic binding capacities, good recovery with low unspecific adsorption, mechanical and chemical stability, reusability with long shelf life and cleanability, as well as reasonable costs are viewed as essential requirements [20, 44].

A number of different types of chromatographic stationary phases have been developed for the purification of biopharmaceuticals. These fulfill the general requirements to different degrees. They can be classified based on their chemical composition or based on their physical properties [8, 20, 44].

1.2.3.2 Chemical composition

In terms of chemical composition one can distinguish between stationary phases that are composed of natural polymers, synthetic polymers, inorganic materials, or composite materials [8, 44]. Many modern chromatographic stationary phases are not composed of a single material, but instead consist of a base matrix with a surface that is altered via coatings, spacer arms, or different types of surface extenders such as polymer brushes [45, 46]. Natural polymers that are used to make up chromatographic stationary phases are for instance cellulose, agarose, and dextran. These materials are generally very hydrophilic, and hence show very low non-specific binding, and can be easily functionalized. Stationary phases that are made of natural polymers are characterized by smaller pores, low solid densities, and limited mechanical strength [20]. Frequently used synthetic polymers are polymethacrylate, polyacrylamide, or polystrene. These materials are more hydrophobic than natural polymers, which can result in higher non-specific binding, and may make functionalization more difficult [20]. With these materials large pores are possible, with higher solid densities and greater mechanical strength. Inorganic media and composite media are less frequently used nowadays. Inorganic media comprise materials such as hydroxyapatite, controlled porous glass or silica, while composite media can for instance be gel in a shell particles which consist of a soft hydrogel that is polymerized into a porous particle shell [44].

1.2.3.3 Physical properties

In terms of physical properties one can distinguish between discrete stationary phases which are made up of particles with a specific form and defined characteristic size, and continuous stationary phases such as monoliths, membranes or continuous fiber stationary phases [8]. Continuous stationary phases can be formed in situ inside a column as is done with monoliths [47], or outside a column and later packed into a suitable device as is done with membranes [48, 49]. For continuous fiber stationary phases both techniques can be used. Discrete stationary phases can be further classified based on the shape of the particles. In most cases spherical particles are used, but the particles can also be cylindrically such as fibers or irregularly shaped.

Additional physical properties that are used in order to characterize stationary phases are particle size, surface area, pore size, degree of grafting, ligand density, and permeability [8, 18, 20, 44]. Depending on the type of stationary phase these properties are either bulk properties or properties of the packed stationary phase. Many of these physical properties are interrelated and therefore cannot be optimized independently of each other.

Discrete particles can be characterized by an average particle size and a particle size distribution [50]. These can be determined by various different techniques, such as coulter counting or microscopic techniques such as light microscopy or scanning electron microscopy (SEM). For stationary phases whose structure depends on the surrounding environment, special techniques such as environmental scanning electron microscopy (ESEM) or confocal laser scanning microscopy (CLSM) may be required in order to determine the particle size under relevant process conditions. Particle sizes for chromatographic stationary phases can range from < 2 µm to 300 µm [18, 44]. For preparative applications particle sizes are typically in the range of 30 µm-100 µm with a relative standard deviation (RSD) of up to 30% [21]. Smaller particle sizes are advantageous because they reduce diffusional path lengths and hence lead to higher efficiency and higher dynamic binding capacity. However smaller particles are more difficult to manufacture and pack and lead to higher pressure drops.

Another important physical property is the specific surface area. It can be measured by techniques such as nitrogen adsorption, mercury intrusion, inverse size exclusion chromatography (iSEC) or permeation with liquids. Typical values for discrete stationary phases range from 5-400 m^2/cm^3 [18, 44]. The specific surface area depends on the porosity, the pore size, and in the case of discrete particles also on particle size and shape. Higher porosities lead to higher specific surface area, however they may also result in lower mechanical strength. Typical particle porosities range from 0.25 in the case of superficially porous particles to 0.9 for soft particles made from natural polymers [44]. However, what matters more than porosity is the pore size and the pore structure. Pores can be classified into micropores with a diameter < 2 nm, mesopores with pore diameters ranging from 2 nm

- 50 nm, and macropores with pore diameters > 50 nm [51]. The pore size needs to be large enough in comparison to the molecule size in order to enable unhindered diffusion [20]. Conventional particle stationary phases therefore consist mostly of mesopores and macropores with pore sizes of 10 nm - 100 nm. Some modern particle stationary phases also have larger pores, which are known as gigapores or perfusive pores, and feature a bimodal pore structure [18]. Continuous stationary phases in general have larger pore sizes on the order of 1-10 µm. Larger pores are advantageous for fast mass transfer, however they provide less surface area. The specific surface area is important, because it defines the area that is available for adsorption and hence the binding capacity. On the other hand the pore size on continuous stationary phases also impacts the permeability and hence the pressure drop.

For polymer functionalized stationary phases the degree of grafting can be defined. It is a measure for the mass of grafted polymer in comparison to the mass of the support matrix. Higher grafting degrees are advantageous because they increase the area that is available for protein binding, however, higher DGs can also lead to pore filling and can strongly reduce permeability.

The ligand density is a measure for the density of functional groups on the stationary phase. It can be expressed as a density per mass, per volume or per surface area of the stationary phase. The volume definition can be based on either the pore volume or the adsorber skeleton volume. Suppliers often provide ligand densities such as ion exchange capacities per volume of packed bed. The ligand density can be determined by different techniques, for instance via acid-base titration in the case of ionic ligands. Ligand densities are typically in the range of 1-100 µm/cm^3 per volume of packed bed [18].

1.2.3.4 Limitations of current stationary phases

Currently, spherical and porous resin particle stationary phases are mainly used for the preparative purification of biopharmaceuticals. Continuous stationary phases are employed for special applications [8], e.g. MAs for the polishing of mAbs in flowthrough mode [52], MAs and monoliths for the purification of large biomolecules such as plasmid DNA or viruses [49, 53, 54], and monoliths for analytical applications [55].

Resins are frequently used because they are characterized by high binding capacities for most biopharmaceuticals, high resolution, and good scalability. However, most of the binding sites on resins are located within the adsorbent particles, and are therefore only accessible via slow diffusion processes [56]. Therefore long column residence times and low mobile phase velocities have to be used with resins, and the productivities are low. For small resin particles with high binding capacities and efficiency, the pressure drop is comparatively high, and therefore the range of mobile phase velocities and bed heights is limited. In addition, due to base material costs, elaborate manufacturing processes, and

ligand costs, the costs of resins can be quite high. Therefore, resins are typically reused, which requires an evaluation of the cleaning and storage protocols, and the performance after continued use. In summary, with resins current limitations are related to productivity and material costs.

Membrane adsorbers and monoliths are characterized by faster mass transfer and higher productivity than resins. However the binding capacities for most biopharmaceuticals are low and column sizes are limited [48]. The permeability of stacked membrane layers is low. Therefore the bed heights on membrane adsorbers are generally low, typically $<$ 1 cm. On monoliths the bed volume is currently limited to 8 L [47]. Therefore, even though the productivities of membrane adsorbers and monolith are high, current size limitations can make it difficult to achieve the throughputs that are required for certain applications.

Therefore in light of the current challenges in downstream processing and chromatography, which call for higher productivity and lower costs, there is an interest in developing new stationary phase materials that address the limitations of current stationary phases.

1.3 Fiber stationary phases

1.3.1 Classification and properties of fibers

One class of such alternative stationary phase materials are fibers. Similar to conventional stationary phase materials fiber stationary phases can be classified according to their chemical composition and their physical properties [57, 58]. In terms of chemistry one can distinguish between natural fibers such as cotton or wool, semi-synthetic fibers such as regenerated cellulose, inorganic fibers consisting of silica and glass, and synthetic polymer fibers as well as composite fibers. The majority of fibers are synthetic polymer fibers which are mass produced, in particular for applications in textiles. In 2018 synthetic fibers accounted for 63% of the worldwide fiber consumption of 106 million tons [59]. Due to the large consumption and production volumes, synthetic fibers are very cheap to manufacture. Base polymers that are frequently used for synthetic fibers are polypropylene (PP), polyethylene terephthalate (PET), and polyamides such as nylon (PA6) [60]. Fibers consisting of such base polymers are typically manufactured via melt extrusion processes [60]. As fibers are frequently modified for textile applications e.g. for fiber dyeing, a variety of chemistries for surface derivatization have been developed [57].

In terms of physical properties one can distinguish between discrete fiber stationary phases and continuous fiber stationary phases. Continuous fiber stationary phases consist of

discrete fibers or yarns that are arrranged into a two-dimensional or three-dimensional textile, such as non-wovens e.g. sheets or felts, knits, braids or wovens [60]. In terms of morphology fibers (and yarns) can be classified based on their length, diameter and cross-sectional shape [60]. Based on fiber length fibers can be classified into short fibers, so called staple fibers, and technically endless fibers, which are known as filaments [60]. Staple fiber lengths are typically in the range of 6 mm-40 mm, but long staple fibers with lengths $>$ 40 mm and short (3-6 mm) and ultra short cut or flock fibers ($>$ 0.25-0.5 mm) are also possible [60]. Textile fiber diameters are typically in the micrometer range. Fibers with diameters $<$ 2 µm can only be produced by special technologies such as electrospinning [61]. Cross-sectional shapes are typically round, however recently techniques have been developed to manufacture various types of surface shaped fibers with high productivity [62]. In terms of porosity most polymeric fibers are very dense structures and contain mostly micropores [63]. As most biopharmaceuticals cannot penetrate such pores due to their size, fibers are often considered to be nonporous in the context of biopharmaceutical separations [57]. The specific surface area of fibers is thus essentially defined by the external surface area. In the case of round fibers, the surface area is directly related to the fiber diameter. For typical microfibers the specific surface area is $<$ 2 m^2/cm^3. With surface shaped fibers [62] or nanofibers [64] higher specific surface areas are possible.

1.3.2 Potential advantages of fibers

Due to these properties, fibers, in particular synthetic polymer fibers, are considered to be potential alternatives to conventional stationary phase materials. There are a number of reasons why fibers could be suitable alternatives to conventional stationary phase materials [57, 65]. The polymers that are used to manufacture polymeric fibers are chemically very resistant and can tolerate many mobile phases that are used for LC [57]. In addition, a number of surface chemistries exist that can be used to alter the surface properties and attach ligand to polymer fiber surfaces. Since most binding sites are located on the adsorbent surface, size exclusion effects are avoided and diffusional limitations are reduced, which can lead to very fast mass transfer rates [57]. For typical fiber diameters and bed porosities fibers have a relatively low resistance to flow and a high permeability [57]. Thus, operation at high flow rates could be possible. When taken together, these properties can enable operations with high throughput, and in case of high enough binding capacities also with high productivity. In addition, due to the mass production of fibers for textiles, the material costs for fibers are very low. Estimates suggest that synthetic fiber supports may cost up to 50 times less than conventional support materials such as agarose [66] or silica [57]. Therefore the use of fiber stationary phases in a disposable format might be economically viable. In summary these characteristics suggest that fibers could be suitable alternatives to conventional stationary phases, and help address the current challenges in DSP which call for lower costs and more productivity.

Owing to these potential advantages, a number of studies have been carried out with different types of fiber stationary phases in the past. Detailed summaries of the studies in the context of LC can be found in the reviews of Marcus [57, 65], and Ladisch and Zhang [58]. Apart from LC, fiber stationary phases have also been investigated in the fields of gas chromatography, capillary electrochromatography [65], and water purification [67]. In LC most studies have been performed under high-pressure conditions with a focus on analytical or preparative separations with high throughput [57, 58]. Chemically, fibers made from natural polymers, inorganic materials, semisynthetic polymers, and in particular synthetic polymers have been investigated. In terms of physical structure discrete fiber stationary phases such as randomly packed short fibers (RPSFs) [68] as well as continuous fiber stationary phases consisting of aligned fibers or woven fabrics such as rolled continuous stationary phases (RSPs) [69] have been examined. Fiber diameters were typically in the micrometer range, and fiber shapes were typically round. Recently surface shaped fibers, so-called capillary-channeled fibers (C-CP) have also been investigated [70]. In these studies the properties of different base polymers [71], the impact of fiber morphology and packing conditions on permeability and separation performance [71, 72], mass transfer properties [73], static and dynamic binding capacities, and the performance for different applications such as SEC [74] or high throughput separations of model proteins were investigated. The studies enabled the optimization of packing and separation conditions, and could demonstrate that high throughput separations are possible with fiber stationary phases [74, 75]. The use of such adsorbents for the preparative purification of biopharmaceuticals has however hardly been explored. With respect to such applications, the previous studies also pointed at some important limitations of current polymer fiber stationary phases [65].

1.3.3 Limitations of fibers for preparative applications

The most prominent limitations of the current polymer fiber stationary phases which were also highlighted in the review of Marcus [65] are the much lower specific surface areas and the packing of fiber stationary phases. Due to the low specific surface area, comparatively low binding capacities are obtained with conventional round microfiber supports. Binding capacity is however very important for preparative applications as it has a strong impact on the productivity, buffer consumption and process economics. Previous packing studies showed that the packing efficiency on fibers depends on the packing structure [72]. Therefore optimization of the packing structure is required. For conventional round microfibers comparatively low packing efficiencies have been reported, even under optimized conditions [71, 74]. Apart from these limitations there is currently also a lack of microscale tools and mechanistic models which could be used for material characterization and process development on fiber stationary phases. In addition, while the performance of fiber stationary phases has been compared with the performance of conventional adsorbents with the use of model systems, very limited data is available that evaluates the performance of such adsorbents for actual process applications such as the

removal of product variants or other impurities. Therefore, it is currently not known if and under which conditions the use of fiber stationary phases for process applications is feasible.

In recent years advances have been made in the manufacturing of polymer fibers with high specific surface areas. A number of different techniques have been described which can be used for such purposes. These are electrospinning to prepare nanofiber discs [64], the preparation of fibers with internal hydrogel structures [76], or the preparation of surface shaped microfibers via bi-component extrusion with a dissolvable sheat [62]. In addition, a number of different techniques have been described for the surface modification of conventional stationary phases in order to graft polymer layers onto the pore surface in order to increase binding capacities. These techniques are based on uncontrolled grating schemes such as free radical polymerization (FRP) or controlled grafting techniques such as atom transfer radical polymerization (ATRP) [77]. Such techniques might enable additional means for increasing the binding capacity on polymer fiber stationary phases, however, they have hardly been used or transferred to the surface modification of area enhanced fibers.

1.4 Research Proposal

As described in the previous sections, biopharmaceuticals are on the one hand very important pharmaceuticals, but on the other hand also very complex molecules with elaborate development and manufacturing processes which require significant time and resources (cf. section 1.1.1). Due to several developments, which were outlined in section 1.1.1, there is currently a need for more flexible and more efficient development strategies and manufacturing processes for biopharmaceuticals which result in higher productivity and/or lower costs.

An essential part of the manufacturing of biopharmaceuticals (cf. section 1.1.2) is the downstream processing (cf. section 1.1.3), which contributes significantly to the productivity and manufacturing costs of biopharmaceuticals and requires a high development effort. DSP aims at isolating the target biopharmaceutical from an appropriate feedstream. The purification is thereby mainly carried out with liquid chromatographic separation methods (cf. section 1.2.1) using solid and spherical stationary phases. As most downstream processes contain several chromatography steps, the productivity and the costs of downstream processes depend strongly on chromatographic unit operations.

The performance and the costs of chromatographic processes in turn are strongly impacted by the properties of the stationary phase (cf. section 1.2.3). Conventional spherical stationary phases are characterized by high binding capacities, high resolution, and good scalability. In recent years high throughput tools and mechanistic models have been developed for such stationary phases, which can be used in order to expedite the process development (cf. section 1.2.2) with such stationary phases. However, conventional spherical stationary phases also have limitations in terms of low productivities, limited operating windows, and high material costs (cf. section 1.2.3.4).

For these reasons there is an interest in the development of alternative stationary phases for the preparative purification of biopharmaceuticals with improved characteristics in terms of productivity and/or costs. A promising class of such alternative stationary phases are polymer fibers and fiber-based adsorbents (cf. section 1.3). As described in section 1.3.2 fibers have several unique features, which could translate into potential advantages of such materials in comparison to conventional adsorbents. The potential of fibers for high-throughput and cost efficient analytical separations of macromolecules has been demonstrated for different types of conventional microfibers with different model proteins and other model compounds in the past (c.f. section 1.3.2). The use of fiber-based adsorbents for the preparative purification of biopharmaceuticals has, however, hardly been explored.

There are several limitations that make the use of such adsorbents for this purpose challenging (cf. section 1.3.3). A main limitation lies in the low specific surface area of

conventional textile fibers with typical diameters on the order of several micrometers. These give rise to fibers and fiber-based adsorbents with comparatively low binding capacities. Binding capacity is, however, very important for preparative applications as it has a strong impact on productivity, buffer consumption, and process economics. Another challenge lies in the packing of fiber-based adsorbents. In previous studies it has been observed that the packing efficiency of fibers depends on the packing structure. Therefore, optimization of the packing structure is required. For conventional round fibers comparatively low packing efficiencies have been reported, even under optimized conditions. In addition, while different high throughput microscale tools and mechanistic models have been developed for conventional stationary phases, such tools and models are currently not available for fiber-based adsorbents. This makes characterization, material optimization, and process development for fiber-based adsorbents challenging. Finally, while the performance of fiber-based adsorbents has been compared with the performance of conventional adsorbents with the use of model systems, very limited data is available that evaluates the performance of such adsorbents for actual process applications such as the removal of product variants or other impurities. It is currently not known if and under which conditions the use of fiber-based adsorbents for process applications is feasible.

In order to address these challenges the present thesis proposes to investigate novel types of synthetic polymer fibers and fiber-based adsorbents which are prepared from area enhanced surface shaped fibers via surface grafting with uncontrolled and controlled grafting techniques. Such fiber-based adsorbents could be better suited for the preparative purification of biopharmaceuticals due to higher binding capacities and better packing efficiencies.

There were four main objectives of this research project. The first goal was to investigate the packing characteristics of such fibers. The second goal was to assess if mechanistic models can be developed for such materials. The third goal was to assess if high throughput process development tools can be developed for such adsorbents, and the fourth objective was to investigate the feasibility of using these novel types of adsorbents for process applications in biopharmaceutical downstream processing.

1.5 Overview of manuscripts

The following paragraphs give an overview of the manuscripts that were written in the scope of this thesis. Each manuscript addressed one of the four research objectives that have been described in the research proposal above (cf. section 1.4). Each of the following paragraph describes the respective research question of the study, the methods that were used, the key results, and the current publication status of the respective manuscript.

Chapter 2: Packing characteristics of winged shaped polymer fiber supports for preparative chromatography

Johannes Winderl, Tamara Spies, Jürgen Hubbuch

Journal of Chromatography A (1553), 2018, 67-80

In this study the packing characteristics of native and grafted short-cut winged shaped polymer fiber supports were investigated. These fiber supports were selected from a collection of surface shaped microfibers due to their particularly high surface area and potentially low manufacturing costs. A suspension based packing technique was established for the packing of the fibers into small laboratory scale columns, and packing studies were performed in order to assess the packing reproducibility, the packing characteristics, and the impact of packing parameters such as packing density and bed height, and grafting parameters such as degree of grafting on column performance parameters such as peak asymmetry, column efficiency, dynamic binding capacity, and resolving power. It was observed that the winged fibers can be packed reproducibly. Column performance was found to depend both on packing density as well as bed height, with lower packing densities resulting in lower plate heights and increases in bed height being associated with more symmetrical peak shapes. On grafted fibers the DBC increased with increasing packing density, while capacity utilization and resolving power decreased. A comparison to conventional perfusive and diffusive adsorbents revealed that under optimized packing conditions grafted winged shaped fibers can achieve a better resolution than conventional adsorbents at high mobile phase velocities. Overall this study indicated that winged shaped fibers can be packed reproducibly with good packing characteristics, and the study identified packing conditions for which these fibers can be used most efficiently for preparative applications.

Chapter 3: A mechanistic model of ion-exchange chromatography on polymer fiber stationary phases

Johannes Winderl, Tobias Hahn, Jürgen Hubbuch

Journal of Chromatography A (1475), 2016, 18-30

In this study a mechanistic model for grafted ion exchange fiber-based adsorbents was developed. For this purpose, characterization and efficiency experiments were performed on a randomly packed fiber column, and the data was used in conjunction with criteria for model selection in order to develop a column model. Subsequently, it was tested whether the developed mechanistic model could accurately describe the convection and dispersion of non-retained molecules, and the binding, breakthrough, and elution of differently sized proteins. In addition, it was assessed whether the model parameters can be identified reliably, and the model was compared to alternative models in order to identify relevant transport phenomena. The developed model accurately accounted for the convection and dispersion of non-retained tracers, and the breakthrough and elution behavior of proteins with sizes from 6-160 kDa were accurately modeled. The model parameters were plausible, and could be identified reliably with small confidence estimates. Through model comparison, film and pore mass transfer and binding kinetics were identified as the relevant transport and binding mechanisms on the fiber-based adsorbents. The developed model enables a better understanding of the relevant transport mechanisms on the fiber-based adsorbents, allows for mechanistic comparisons to other types of adsorbents, and can be used for the development and optimization of processes that use fiber-based adsorbents.

Chapter 4: High throughput screening of fiber-based adsorbents for material and process development

Johannes Winderl, Stephan Bürkle, Jürgen Hubbuch

Manuscript in preparation

This chapter describes the development of an automated high throughput screening (HTS) for fiber based adsorbents which was established on a robotic liquid handling station in 96 well filter plates. The study covers the selection of a screening format, the development of techniques for adsorbent portioning, and the optimization of several screening parameters such as phase ratio, shaking frequencies and incubation times for different types of fiber-based adsorbents. A comparison between HTS experiments and lab scale column experiments was conducted in order to investigate the comparability between different scales. The comparison showed that the data from the developed HTS correlate with data from packed fiber columns. The applicability

of the developed HTS for material and process development was demonstrated in two case studies. The developed HTS allows for a faster and more complete characterization of fiber-based adsorbents with a significant reduction of material and time requirements, and enables an easier evaluation of fiber-based adsorbents alongside existing materials.

Chapter 5: Exploration of fiber-based cation exchange adsorbents for the removal of monoclonal antibody aggregates

Johannes Winderl, Eric Neumann, Jürgen Hubbuch

Manuscript in preparation

In this study it was evaluated if and under which conditions the use of fiber-based cation exchange adsorbents for monoclonal antibody removal, a typical processing step during industrial antibody purification, is feasible. Two types of fiber-based adsorbents, with an uncontrolled and a controlled grafted hydrogel layer, were examined, and evaluated with respect to permeability, dynamic antibody binding capacity, resolution capabilities of mAb monomer and aggregates, and the performance in different operating modes with respect to typical performance indicators, productivity, and buffer consumption. The study showed that the use of fiber-based adsorbent for mAb aggregate removal is feasible, and identifies appropriate operating conditions. The overall performance of the fiber-based adsorbents was found to be comparable to the performance of an existing resin material, Poros 50 HS. The performance of controlled grafted fibers was found to be superior to the performance of uncontrolled grafted fiber-based adsorbents due to higher productivity and lower buffer consumption.

2 Packing characteristics of winged shaped polymer fiber supports for preparative chromatography

Johannes Winderl[1], Tamara Spies[1], Jürgen Hubbuch[1]

[1] Institute of Engineering in Life Sciences, Section IV: Biomolecular Separation Engineering, Karlsruhe Institute of Technology (KIT), Karlsruhe, Germany

Abstract

Polymer fibers have been identified as a promising alternative support material for liquid chromatography. Area enhanced fibers may overcome the shortcomings of conventional fiber supports with respect to binding capacity and packing efficiency. One type of area enhanced fiber supports are winged shaped microfibers, which have a more than tenfold higher surface area than round fibers, and can be manufactured via inexpensive, conventional extrusion techniques.

In the present study, the packing characteristics of native and grafted winged shaped fiber supports have been investigated. A suspension based packing technique was used to pack short winged shaped polyamide 6 (PA6) fibers into small laboratory scale columns. Low column-to-column variabilities in porosities, plate heights, axial dispersion coefficients, and peak asymmetries were observed. Peak asymmetries were within typical ranges of preparative columns, and plate heights were at the lower end of those reported for other fiber supports. Packing density was found to be the

main parameter that affected column performance. Lower packing densities were associated with lower plate heights, while increases in bed height resulted in more symmetric peak shapes. Packing density was also found to have a strong impact on the performance of poly (glycidyl methacrylate) (PGMA) grafted and sulfonated (SO_3^-) winged shaped PA6 fibers. Higher packing densities resulted in higher dynamic binding capacities (DBCs), but led to a decrease in capacity utilization and resolution. A comparison to conventional perfusive and diffusive adsorbents revealed that under optimized packing conditions such adsorbents can achieve a better resolution than conventional adsorbents at high mobile phase velocities.

Overall, these results suggest, that winged shaped fibers have strong potential as supports for preparative chromatography. Further improvements may be possible via adjustments in the fiber dimensions.

2.1 Introduction

Chromatographic unit operations account for a large fraction of the manufacturing costs of biotherapeutics. One of the main reasons for this is the high cost of chromatography adsorbents, which make up a significant portion of the material costs for chromatography steps [52]. This is due to both the cost of the support materials, and the costs for modification and functionalization of the support materials. While a wide range of modification and functionalization schemes have been developed [45], and applied to different supports, only certain types of supports have been found to be suitable for preparative protein chromatography [44]. At present the majority of chromatographic processes are performed in packed beds filled with adsorbents that are prepared from spherical, porous supports. Typically, these are reused for multiple cycles, which necessitates a costly, thorough evaluation of both the cleaning and storage protocols, and the performance degradation after continued use.

Polymeric fibers have been identified as alternative chromatography supports [78] with several possible advantages over conventional supports [57, 65]. Most of these materials are non-porous or have a very limited porosity such that the majority of binding sites are accessible via convection. This reduces diffusional limitations for large biomolecules and favors fast mass transfer. This characteristic is also accompanied by low resistance to flow, which allows for operations at higher flow rates, together with faster mass transfer rates that can enable higher overall productivity. As fibers originate from the textile industry, technologies for mass production exist, which lead to very low costs of these materials. The costs of synthetic fibers are

estimated to be up to 50 times lower than the costs of conventional support materials such as agarose [66] or silica [57]. Consequently, fibers are good candidates for use as low-cost disposables and could be suitable materials for high productivity and cost-efficient bioseparations. This may help to meet current challenges in downstream processing, which call for more productivity and lower costs of downstream operations.

Despite the many possible benefits of fibers, research into fibers and fiber-based adsorbents has mostly been restricted to analytical applications. A main reason for this lies in the low specific surface area of conventional non-porous textile fibers with typical diameters on the order of several micrometers [61]. These give rise to fibers and fiber-based adsorbents with rather low binding capacities. Recently, several studies have investigated how this problem might be solved. One approach lies in the use of porous fibers with internal hydrogel structures [76, 79]. While this increases the specific surface area for protein binding, it may also increase mass transfer resistances. An alternative approach is to use nanofibers [64, 80], which can be produced in the form of non-woven discs via techniques such as electrospinning [61]. Challenges with this approach are the limited mechanical stability of the non-woven fiber discs, which may require further treatment [81] and the low speed of electrospinning in comparison to conventional mechanical fiber-spinning techniques [61]. A third approach is the use of surface shaped fibers. These can be produced by conventional techniques and possess significantly increased cross-sectional areas compared to conventional fibers with equivalent diameters and circular cross-sections. Different cross-sections have been developed, such as capillary-channeled polymer (C-CP) fibers [70] or winged shaped fibers [62]. In recent studies it has been demonstrated that with appropriate surface modification techniques, fiber-based adsorbents with high dynamic binding capacities at short residence times can be prepared from such fibers [66, 82, 83].

The second challenge for the use of fibers is the packing of such materials. Suitable packing techniques must ensure a good efficiency of the packed bed, and must be reproducible and scalable. To make use of the cost benefit of fibers, they should be combinable with surface modification steps and be easy to integrate into current packing equipment. For preparative applications pressure drop constraints (typically less than 2-3 bars) also have to be satisfied. In addition, the packing conditions, for instance packing density and bed height, have to be optimized in order to achieve the best column performance. The choice of a suitable packing technique for fibers is influenced by various factors, but depends predominantly on the fiber manufacturing process, the resulting fiber structure and the techniques that are used for fiber modification and functionalization. Both suspension based packing techniques [68] and dry packing techniques [69, 84] have been described in the literature. For conventional round fibers, however, comparatively low

packing efficiencies have been reported [74], even under optimized packing conditions [71].

Area enhanced shaped fibers may have better packing characteristics due to their different structure. However, there are only a few studies that have reported on the packing of area enhanced shaped fibers. Only C-CP fibers have been investigated in detail. Marcus et al used filaments of capillary channeled fibers and aligned them in a colinear fashion to prepare C-CP fiber columns [70]. The packing reproducibility [85] and the impact of packing conditions such as column diameter, column length and fiber packing density on packing efficiency [63, 73, 75, 86] and on the dynamic binding capacity of proteins [72] on different types of native C-CP fibers have been evaluated. The packing technique was reproducible [85]. Plate heights of 6 mm for thyroglobulin [63] and 0.9 mm for uracil [75] have been reported. However these studies focused on HPLC applications and high packing densities were used, which may not be feasible for preparative operations with low pressure drop requirements.

The packing characteristics of other types of area enhanced shaped fibers such as winged shaped microfibers have hardly been explored. These fibers have a more than tenfold higher surface area than round fibers and a higher surface area than C-CP fibers, and they can be manufactured via inexpensive, conventional extrusion techniques [62]. Schwellenbach et al recently prepared strong cation-exchange fiber based adsorbents from short-cut winged shaped polyethylene terephthalate (PET) fibers [83]. A dry packing technique was used to pack the fiber-based adsorbents. Plate heights of 0.1 cm and peak asymmetries of 1.8 were reported for acetone on a reference fiber-based adsorbent with optimized grafting parameters. However only the fiber-based adsorbent was investigated, and the packing characteristics of native winged fibers or the impact of different packing conditions and grafting on packing efficiency were not explored. Other packing techniques, such as suspension based packing techniques, which could be performed with conventional packing equipment directly after suspension based surface modification, still have to be evaluated.

In the present study the packing characteristics of native winged shaped polyamide 6 (PA6) fibers were investigated. We evaluated if slurry based packing can be performed with such fibers and if this is reproducible. We characterized the resulting fiber beds and studied the impact of packing density and bed height on the column performance in terms of porosities, plate heights, axial dispersion coefficients and peak asymmetries. In addition, we assessed if and how this impacts the column performance, both in terms of column efficiency, but also in terms of dynamic binding capacity and resolving power.

2.2 Experimental

2.2.1 Materials

2.2.1.1 Chemicals, buffers and proteins

Sodium dihydrogen phosphate, sodium chloride (NaCl), hydrogen chloride (HCl), sodium hydroxide (NaOH), ethanol (EtOH), methanol (MeOH), isopropanol (IPA) and acetone were purchased from Merck (Darmstadt, Germany). Ammonium sulfate was from AppliChem (Darmstadt, Germany). Sodium phosphate, lysozyme from chicken egg white (Lys, no. L6876), cytochrome c from bovine heart (Cyt c, no. 30398), and dextran with an average molecular mass of 2000 kDa (D2000) from *Leuconostoc spp.* were obtained from Sigma-Aldrich (St. Louis, MO, USA). The monoclonal antibody (mAb) was a CHO-derived IgG from a known industrial manufacturer. All buffers were prepared with ultra-pure (UP) water (Purelab Ultra, Elga LabWater, High Wycombe, UK). The pH was adjusted with HCl or NaOH as needed. Prior to usage the buffers were filtered through 0.2 μm cellulose acetate (CA) membrane filters (Sartorius, Göttingen, Germany) and degassed via sonication. All proteins and tracers were dissolved in the appropriate buffers as needed and filtered through 0.2 μm CA syringe filters (Sartorius, Göttingen, Germany). Buffer exchange for the mAb was performed with PD-10 desalting columns (GE Healthcare, Little Chalfont, UK). The protein concentration of protein solutions was verified photometrically with a NanoDrop2000c UV-Vis spectrophotometer (Thermo Fisher Scientific, Waltham, MA, USA).

2.2.1.2 Stationary phases

Area enhanced shaped polymer fibers with different cross-sectional shapes were obtained for this study. Each fiber type was sourced in the smallest available linear density and characterized with respect to morphology and specific surface area (SSA). Winged shaped fibers (3 deniers per filament (dpf)) were selected for this study due to their high specific surface area (SSA) in comparison to round fibers, but also in comparison to other types of area enhanced shaped polymer fibers. The fibers were acquired from Allasso Industries (Raleigh, NC, USA) and were made from polyamide 6 (PA6). Fig. 2.1 shows the morphology of the winged fibers (cf. Fig. 2.1A) in comparison to the one of deep-grooved 4DG fibers (cf. Fig. 2.1B). The 4DG fibers (6 dpf) were from Fiber Innovation Technology (Johnson City, TN, USA) and also consisted of PA6. The structure of these fibers is identical to the

structure of the capillary channeled fibers which have previously been investigated by the group of Marcus et al [72, 73, 75, 85, 87]. Apart from size, the main difference between winged fibers and 4DG fibers is the number of projections. 4DG fibers have 8 grooves which create 8 channels along the longitudinal axis of the fibers, while winged fibers have an approximately elliptical cross section with a thin backbone along the major axis and a plurality of projections that extend from both sides of the backbone. This is also reflected in the SSAs which were determined by BET nitrogen adsorption experiments as described in [83]. The SSA of the winged fibers was 2 m^2/g, while an SSA of 0.3 m^2/g was measured for the 4DG fibers. For this study either native or grafted and functionalized (cf. section 2.2.3) winged fibers were used. For performance comparisons with the grafted and functionalized fibers, SP Sepharose Fast Flow (SPFF) (GE Healthcare, Little Chalfont, UK) and Poros 50 HS (Thermo Fisher Scientific, Dreieich, Germany) resins were used. The ion-exchange capacities of these resins have been determined in [88] via acid-base titration. For SPFF an ion-exchange capacity of 0.213 M per geometric column volume was reported, and for Poros 50 HS an ion-exchange capacity of 0.08 M was measured. This corresponds to values of 3.929 M and 0.276 M per resin skeleton.

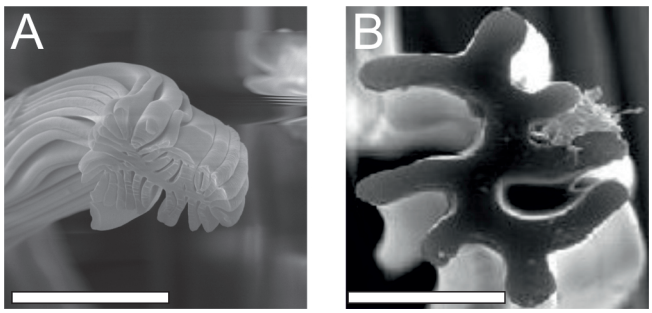

Figure 2.1: Scanning electron microscopy (SEM) images of area enhanced surface shaped fibers. (A) Winged fibers, (B) 4DG fibers. The scale bars indicate 20 μm.

2.2.1.3 Chromatographic instrumentation

The chromatographic experiments were carried out on two liquid chromatography systems. An ÄKTA purifier 10 system equipped with Pump P-903, UV Monitor UV-900 with a 10 mm UV flow cell, pH, conductivity and temperature monitor pH/C-900, autosampler A-905, fraction collector Frac-950, and flow restrictor FR-902 was used for all experiments except for the determination of dynamic binding capacities. The instrument was controlled with UNICORN 5.31. For the determination of dynamic binding capacities an ÄKTA start system was used, and the instrument was controlled with UNICORN start 1.0 (all GE Healthcare). For both systems the setups and tubing connections were kept constant in between experiments.

2.2.1.4 Software and data analysis

Data processing was performed with Matlab R2017a (Mathworks, Natick, MA, USA), Microsoft Excel 2013 (Microsoft, Redmond, WA, USA) and OriginPro 2017 (OriginLab, Northampton, MA, USA). The design of experiment (DoE) studies were designed and analyzed with MODDE 10.1 (Sartorius Stedim Biotech, Umea, Sweden).

2.2.2 Methods

2.2.2.1 Column packing and storage

For packing of the fibers Omnifit BenchMark columns (Diba Industries, Danbury, CT, USA) with an I.D. of 6.6 mm and two adjustable endpieces were used. The fibers, which were received in a dry form, were placed in a Büchner flask, in which the side arm had been sealed off with a fine filter frit. Then the fibers were deagglomerated via purging with pressurized air from the top. Subsequently the fibers were placed in an appropriate packing solution at a ratio of 1 g of fibers per 500 mL solution. The resulting suspension was agitated overnight at 120 rpm on an orbital shaker (MaxQ 6000, Thermo Scientific, Marietta, OH, USA) to allow for proper homogenization. Afterwards, the suspension was transferred into the column, excess solution was removed with a peristaltic pump (Gilson, Middleton, WI, USA) connected to the column outlet at a flow rate of 6 mL/min, and the bed was compressed to the final target bed height with the adjustable column endpieces. Prior to usage the columns were flushed with 20 vol% isopropanol in 50 mM NaPi at pH 7 to remove any remaining air bubbles, and the columns were equilibrated with 50 mM NaPi at pH 7. To verify that the fiber beds were stable over the intended range of mobile phase velocities (up to 1500 cm/h), pressure-flow profiles were recorded. For these the mobile phase velocity was increased from 100 cm/h to 1500 cm/h and back in 200 cm/h increments and the system pressure for each flow velocity was monitored. Bed stability was determined via examining if the pressure flow curves were linear. SP Sepharose Fast Flow and Poros 50 HS were flow packed into the same column hardware as the fibers according to the respective manufacturer's instructions. In between experiments all columns were stored in aqueous solutions containing 20 vol% EtOH and 150 mM NaCl. After the characterization experiments the fiber columns were unpacked and the fibers were dried. For comparison experiments all stationary phases were packed to the same bed height of 4 cm.

2.2.2.2 Determination of column performance characteristics

Upon packing the fiber columns were subjected to a series of characterization experiments to determine different column performance characteristics. Two sets of experiments were performed. In the first set of experiments the reproducibility of the slurry based packing technique was assessed. In the second set of experiments the packing density and bed height were varied in a multivariate study to determine the impact of these parameters on the column performance. In both sets of experiments the same column performance parameters were considered. The parameters that were varied and the performance characteristics that were considered in the multivariate study are summarized in Table 2.1.

Table 2.1: Packing parameters and measured column performance parameters for the multivariate study of the native PA6 winged fibers examined in this study.

Packing Parameter	Range	Unit	Column Performance Parameter
Fiber packing density	0.2-0.4	g fiber/mL CV	Porosity, ε
Bed height, L	1-4	cm	Peak asymmetry, A_s
			HETP, H
			Axial dispersion coefficient, D_{ax}

Porosity The porosity of the fiber columns was determined via pulse injections with 1 M NaCl in 50 mM sodium phosphate (NaPi) buffer at pH 7. The injection volume was set to 100 μL. All injections were performed in triplicate at a mobile phase velocity of 100 cm/h. The injections were also carried out at 800 cm/h to assess bed stability and repeated with 10 g/L D2000 to investigate if there are any differences in the accessible volume fractions of NaCl and larger sized molecules. The injections were repeated with an empty column with the plungers pushed together to account for the delay and dispersion introduced by the chromatography system and the column plungers. The resulting peaks were analyzed by the moment method. The first and second moments, $\mu_{c,i}$ and $\sigma^2_{c,i}$, for the columns were determined via subtracting the moments μ_{sys} and σ^2_{sys} attributed to the system and the column plungers from the moments $\mu_{c+sys,i}$and $\sigma^2_{c+sys,i}$ for the system with column:

$$\mu_{c,i} = \mu_{c+sys,i} - \mu_{sys} \tag{2.1}$$

$$\sigma^2_{c,i} = \sigma^2_{c+sys,i} - \sigma^2_{sys} \tag{2.2}$$

The porosity ε was calculated from the first moment of the NaCl pulse injections and the geometric column volume V as follows:

$$\varepsilon = \frac{\mu_{c,i}}{V} \tag{2.3}$$

Peak asymmetry The asymmetry factor, A_s, was determined from the peak of the NaCl pulse injections at 100 cm/h, and was evaluated at 10% peak height.

Column efficiency and plate height Column efficiencies, N, and heights equivalent to a theoretical plate (HETPs), H, were calculated from the first and second moments of the NaCl peak and the bed height L:

$$N = \frac{\mu_{c,NaCl}^2}{\sigma_{c,NaCl}^2} \tag{2.4}$$

$$H = \frac{N}{L} \tag{2.5}$$

Axial dispersion coefficient The axial dispersion coefficient D_{ax} was determined from the moments of the NaCl peaks, using a connection between the moments and the axial dispersion coefficient [21]:

$$D_{ax} = \frac{1}{2} \cdot L \cdot u_{int} \cdot \left(\frac{\sigma_{c,NaCl}}{\mu_{c,NaCl}} \right)^2 \tag{2.6}$$

2.2.2.3 Preparation of fiber-based strong cation exchange adsorbents

Strong cation exchange fibers with different degrees of grafting were prepared from native winged shaped PA6 fibers via two reaction steps. First the fiber surface was modified via ammonium cerium(IV) nitrate (ACN) initiated grafting polymerization [89] of glycidyl methacrylate (GMA). In a typical experiment 20 g of fibers were added to an aqueous solution of GMA, N,N'-methylenbisacrylamide, ACN and HNO_3, and the resulting suspension was agitated for 1 h at 35°C. Afterwards the fibers were filtered and washed with copious amounts of UP water and ethanol before being dried and weighed. The degree of grafting was controlled via adjusting the amount of GMA in the polymerization solution. In the second reaction step the residual epoxy groups in the poly(GMA) layer were reacted with sodium sulfite to anchor sulfonic acid groups within the hydrogel layer. For this purpose tetrabutylammonium hydrogensulfate (TBABS) was used as a phase-transfer catalyst [90]. In a typical experiment the fibers from the first reaction step were placed in a solution containing 18wt% sodium sulfite, 5wt% TBABS, 2wt% dipotassium hydrogen phosphate and 75wt% UP water, which had been adjusted to pH 8 with sodium hydroxide and heated to 85°C. The resulting suspension was agitated for 45 min before the fibers were filtered and washed with UP water. Subsequently the functionalized fibers were dried at 60°C for 24 h.

2.2.2.4 Characterization of fiber-based strong cation exchange adsorbents

Degree of grafting The degree of grafting (DG) of the fiber-based adsorbents was determined gravimetrically via measuring the weight of the fibers before and after grafting

$$DG = \frac{m_g - m}{m} \tag{2.7}$$

where m is the mass of the unmodified fibers and m_g is the mass of the dried grafted fibers.

Determination of equilibrium binding capacity Equilibrium binding capacities of the fibers for lys were determined via batch binding experiments in 50 mM NaPi buffer at pH 7. 10 mg of the fibers were placed in 1.5 mL reaction tubes (Eppendorf, Haburg, Germany) and incubated with 750 µL of different stock solutions for predetermined amounts of time on an orbital shaker at 1000 rpm. Two equilibration steps in 50 mM NaPi were carried out at 10 mins each, followed by a 24 hour binding step with lys solution in 50 mM NaPi. The initial lys concentration was set to achieve a loading density of 100 mg lys/g fiber. After the binding step the lys concentration in the supernatant was measured, and additional protein solution was added to achieve a supernatant concentration of 2 g/L , followed by another 24 hour binding step. This procedure was repeated until no further change in the supernatant concentration was observed. The amount of bound protein was determined via mass balance from the final protein concentration after incubation and the initial protein concentrations of the added protein solutions.

Determination of ion-exchange capacity The ion-exchange capacity of the native fibers and the fiber-based adsorbents was determined via acid-base titration experiments on packed columns of known packing density as described in [88].

2.2.2.5 Determination of column performance characteristics of modified fibers

The column performance of the modified fibers was examined in a second study. The degree of grafting and the packing density were chosen as input variables and the dynamic binding capacity and capacity utilization for lys as well as the resolution of a

3 component protein mixture were studied as additional performance characteristics. The input variables and the measured performance characteristics are summarized in Table 2.2.

Table 2.2: Packing parameters and measured column performance parameters for the multivariate study of the grafted PA6 winged fibers examined in this study.

Packing Parameter	Range	Unit	Column Performance Parameter
Fiber packing density	0.2-0.4	g fiber/mL CV	Porosity, ε
Degree of grafting, DG	low, medium, high	-	HETP, H Dynamic binding capacity, $DBC_{10\%}$ Capacity utilization, $DBC_{10\%}/EBC$ Resolution, R_s

Determination of dynamic binding capacity The dynamic binding capacity (DBC) of the modified fibers was determined at a low (100 cm/h) and a high mobile phase velocity (800 cm/h) by overloading the packed fiber columns with lys solution. 50 mM NaPi was used as low salt buffer for equilibration and wash steps, and 50 mM NaPi + 1 M NaCl was used as high salt buffer for elution, all at pH 7. The method consisted of a 4 CV equilibration step in low salt buffer, and a 20 mL loading step with 2 g/L lys in low salt buffer. Unbound and weakly bound protein was removed with a 15 CV wash step in low salt buffer and bound protein was eluted with a linear salt gradient over 20 CV from 0-100% high salt buffer followed by a post gradient step at 100% over 5 CVs. The DBC was evaluated from the volume $V_{10\%}$ corresponding to 10% breakthrough. The retention volume of acetone $V_{ret,acetone}$ was subtracted to account for system and column dead volumes:

$$DBC_{10\%} = \frac{V_{10\%} - V_{ret,acetone}}{V} \tag{2.8}$$

Determination of capacity utilization Capacity utilization was determined from the ratio of the DBCs at 10% breakthrough and the respective equilibrium binding capacities.

Determination of chromatographic resolution The chromatographic resolution was determined via linear gradient elution experiments (LGE) with a 3

component model protein mixture. The mixture consisted of lys, cyt c and a mAb at a concentration of 1 g/L of each component in 10 mM NaPi at pH 7. The method was composed of a 5 CV equilibration step with 10 mM NaPi pH 7, followed by injection of 100 µL of the protein mixture with a sample loop, a 3 CV wash step with 10 mM NaPi pH 7, a linear salt gradient over 15 CV from 0-50% high salt buffer (10 mM NaPi + 1 M NaCl pH 7) and two 5 CV salt steps at 50% and 100% high salt buffer. The mobile phase velocity was 800 cm/h. For the comparison experiments of the different stationary phases the salt gradient was run from 0-100% high salt buffer over 30 CV to ensure complete elution of all proteins during the linear gradient. The resolution of adjacent peaks was calculated from the chromatograms via UV peak deconvolution and calculation of the statistical moments according to

$$R_s = \frac{\mu_j - \mu_i}{2(\sigma_i + \sigma_j)} \tag{2.9}$$

where i and j stand for the compounds that elute in the peaks, and i denotes the compound that elutes first.

2.3 Results and Discussion

2.3.1 Suspension based packing of winged shaped fibers

A key requirement for column packing techniques is that particle agglomeration has to be avoided. However, most synthetic fibers are prone to agglomerate due to a buildup of static charges. This is a consequence of the hydrophobic and non-conductive nature of the resins that are used to manufacture such fibers [91]. While this can be controlled in part via the addition of antistatic agents during fiber manufacture, the supplied winged fibers, which were composed of PA6, still tended to agglomerate. Thus we tested different packing buffers for their ability to deagglomerate the fibers and create homogeneous slurries. The buffers were selected on the basis of chemical compatibility, wetting behavior, gas solubility, and viscosity. We included buffers that have commonly been used for wash steps in polymerization protocols, and for the packing of hydrophobic interaction chromatography (HIC) media, as well as organic solvents that have been suggested by other authors for the packing of short cut fibers such as methanol [92] or isopropanol [66]. Placing the fibers in purely organic or purely salt containing solutions resulted in the formation of fiber clouds. The most homogeneous slurries were obtained when the fibers were placed in solutions containing organic solvents and low amounts of salt. A solution containing 20 vol.%

ethanol in 50 mM sodium phosphate with 0.4 M NaCl showed the best results and was selected for suspension based packing of the fibers.

2.3.2 Reproducibility of suspension based packing of winged shaped fibers

As a first step we evaluated the reproducibility of the suspension based column packing technique. For this purpose columns were repeatedly packed under identical conditions (4 cm bed height, 0.25 g/mL packing density) and characterized with respect to a set of key column performance parameters (cf. Table 2.3). The reproducibility of the suspension based column packing technique was determined via calculating the standard deviations (SD) and relative standard deviations (RSD) of the performance parameters as suggested by Li et al [71] and Nelson et al [85]. To account for possible variations in column hardware, a single column and columns of the same type were packed repeatedly. The respective performance parameters for both scenarios are given in Table 2.3. The RSDs of the performance characteristics considered spanned a range of 0.83% to 10.55%. This indicates that the suspension based packing technique is reproducible. The study of Li et al [71], who used a wet rolling technique to pack columns with 10 different fabrics, reported inter-column RSDs in the range of 0.5-8.9% and 2.2-15.1% for porosity and HETP. For the present fibers and packing technique the inter-column RSDs for porosity and HETP were within this range. Nelson et al [85] developed a packing technique to pack capillary-channeled fibers in a colinear fashion and reported inter-column RSDs of 0.7-1.8%, 9.0-18.9%, 3.6-34.6% and 9.9-18.2% for the retention time, peak width, peak height and peak area of lysozyme, respectively, which was eluted under reversed-phase gradient conditions from PP and PET fibers. For the tracer injections on the winged fibers the respective inter-column RSDs were 1.2%, 8.9%, 4.3% and 0.7%. Taken together, these data suggest that the reproducibility of the suspension based packing

Table 2.3: Measured column performance parameters and inter- and intra-column reproducibilities for suspension based packing of the native PA6 winged fibers examined in this study.

	Intra-column (n=3)			Inter-column (n=3)		
	Mean	SD	RSD (%)	Mean	SD	RSD (%)
Porosity, ε (-)	0.766	0.006	0.83	0.781	0.018	2.31
Peak asymmetry, A_s (-)	1.670	0.027	1.62	1.567	0.059	3.79
HETP, H_{NaCl} (cm)	0.097	0.010	9.80	0.085	0.009	10.30
Axial dispersion coefficient, D_{ax} (mm^2/s)	0.176	0.009	9.83	0.152	0.009	10.55

technique of the present fibers is similar to the one that was reported for the other two packing techniques, although care has to be taken when comparing the different data sets, as different conditions were used in the studies. Unfortunately no column-to-column variabilities of performance or peak characteristics have been reported for other fibers or fiber packing techniques. Studies of slurry packed resins that had been packed into preparative columns of similar ID, including a recent study with 30,000 prepacked columns, reported relative standard deviations in HETP or reduced HETP of 10-30% [93, 94]. This suggests that the column-to-column variability for suspension based packing of the present fiber materials is not worse than the one for the packing of resins into preparative columns of similar scale.

2.3.3 Packing characteristics of winged shaped fibers

For the selected packing conditions, we determined porosities of 0.766 ± 0.006 and 0.781 ± 0.018 for the fiber columns from the NaCl pulse injections (cf. Table 2.3). Control measurements with D2000 revealed almost identical porosities of 0.770 ± 0.019 and 0.761 ± 0.012. This suggests that both molecules could access the same voids and that NaCl could not access any additional intrafiber pores. The determined porosities agree well with the packing density of 0.25 g/mL and the density of PA6 of 1.14 g/cm^3 [95], and indicate that little to no swelling occurred for the present fiber material upon exposure to the suspending liquids. The peaks of the pulse injections showed some degree of peak tailing with an average peak asymmetry factor of 1.57. Although at the higher end of the range, this falls within typically observed and accepted ranges for preparative columns filled with beads (A_s = 0.8-1.8) and also would meet regulatory recommendations for the tailing factor (<2) [96]. The observed tailing may be a consequence of insufficient radial distribution at the column inlet, which is often observed for low pressure drop media [21]. The tailing may also be a consequence of the fiber geometry. For higher packing densities, individual fibers or fiber channels may interdigitate during packing and create stagnant flow paths. Such effects have been reported for capillary channeled fibers in colinear arrangement [73] with 8 projections, and thus are likely to occur for the short and flexible winged shaped fibers which possess 32 projections. Tailing has been reported for both the capillary channeled fibers and the porous fibers of Gavara et al, when these fibers were packed into columns with similar I.D.s as the one used in the present study. Gavara et al reported peak asymmetry factors of ≤ 1.6 for dry packing of short modified cotton fibers into 5 mm ID columns [79]. Stanelle et al reported peak asymmetry values of 1.6 and 2.5-3 when different capillary channeled fibers were packed into 7.7 mm I.D. columns [73]. These values could be lowered down to 1.5 with the addition of a flow distributor and a low porosity frit to the column inlet. This highlights the importance of proper fluid distribution for fiber stationary phases and may provide avenues for improvement.

Apart from the peak asymmetry, the HETP and the axial dispersion coefficient are two other key measures of column packing quality. The observed HETP of 0.085-0.097 cm for an excluded and non retained tracer at an interstitial velocity of 0.28 mm/s is high when comparing to current analytical scale columns, but is within ranges that are typical of preparative and process-scale chromatography [74]. The lowest plate heights that have been reported for excluded and non-retained molecules on aligned fiber stationary phases range from 1 mm for BSA on cotton [71], 7 mm for dextran 506,000 on cellulose/PET [74], and 2 mm for PEG 20,000 on DEAE cellulose/PET [74] for rolled continuous stationary phases to 6 mm for thyroglobulin on PP capillary channeled fibers [63]. For aligned, porous silica fibers, lower plate heights of 0.7 mm have been reported for polystyrene 900,000 and 1,860,000 [84]. For smaller tracers such as uracil or acetone, lower plate heights or A-terms have been reported, with 0.9 mm for radially compressed microbore capillary channeled fibers [75] and 0.5 mm for randomly packed porous cellulose fibers [79]. This suggests that higher plate heights are common for fiber stationary phases, with the plate height of the present fibers being at the lower end of the reported range. For a non-retained and excluded tracer both molecular diffusion and axial mixing may affect the HETP. For an estimated diffusion coefficient of NaCl of $7.0 \cdot 10^{-6} cm^2/s$ [97] and a typical value of the tortuosity of $\gamma = 0.7$ [21], the contribution of molecular diffusion to the HETP is $4.9 \cdot 10^{-6}$ cm. This is insignificant in comparison to the measured HETP, and suggests that axial mixing is the dominant mechanism. This effect has been shown to be related to the particle diameter. Correlations for packed beds predict eddy dispersion terms on the order of the measured axial dispersion coefficient for spherical particles with diameters of 0.2 mm [98, 99] to 0.8 mm [100, 101]. For fibers, no correlation has been suggested that relates the fiber dimension to the resulting dispersion. For aligned fibers, low packing densities and intermediate fiber diameters have been found to give rise to the lowest HETPs, as these conditions enable the best interdigitation and most uniform flow paths. In addition, porosity has been found to be advantageous to even out differences between parallel flow channels [84]. The present fibers have a smaller cross-sectional diameter than the aforementioned particles, but are much longer. Depending on the orientation of the fibers in relation to the direction of flow, solutes will either flow in the direction of the fibers or perpendicular to the fibers. This may explain the relatively large dispersion despite the narrow cross sectional dimensions of the fibers. Gavara et al used fibers with 1-20 µm in diameter, which were homogenized into fibers with length < 1 cm and reported HETP on a similar order as the present fibers, which supports this conclusion.

2.3.4 Impact of packing density and bed height on column performance

Based on the packing performance of the fibers, the use for preparative applications seems most promising. Additionally, fibers may be used for high throughput HPLC applications as well. High throughput HPLC has been demonstrated for capillary-channeled fibers, where flat HETP profiles and high permeabilities enabled operation at high flow rates with little sacrifices in column efficiency.

For both areas of application, preparative or analytical, sufficient bed homogeneity must be ensured, (as evidenced by low peak asymmetries and high column efficiencies). Packing density and bed height have been shown to be two key parameters that affect asymmetry and column efficiency on fiber columns [71, 73, 75]. In the context of preparative applications, there is a tradeoff for both packing density and bed height, as increased packing densities and bed heights are advantageous in terms of loadability and resolution, but detrimental in terms of column pressure drop and consequently the attainable flow rates.

A multivariate study was conducted in order to investigate the impact of bed height and packing density on bed homogeneity. The bed height was varied within a range of 1-4 cm and the packing density was adjusted from 0.2-0.4 g/mL according to a face-centered central composite design with three center-point replicates. These conditions were selected in order to enable operation of the columns at mobile phase velocities of up to at least 1500 cm/h with column pressure drops below 2 bars, while ensuring sufficient bed stability without compression of the fiber beds. A central composite design was chosen in order to account for possible interaction effects or quadratic effects, as such effects were reported in the study of Li et al [71].

Eleven columns in total were packed for the study and characterized with respect to the performance parameters that are listed in Table 2.1. Fig. 2.2 shows the retention volumes and plate heights of NaCl for the 11 columns as a function of column dry fiber mass, grouped by bed height. Retention volumes increased with increasing bed height, and decreased with increasing fiber mass for each bed height (cf. Fig. 2.2A). This is in line with an increase in column volume, and hence fluid volume, with increasing bed height, and a decrease in fluid volume with increasing fiber mass. For each packing density, the retention volumes scaled with bed height. The retention volumes for the three center-point replicates were close to each other, with a RSD of 2.9%. When taken together, this suggests that the bed heights and packing densities of the columns in the study were set correctly and reproducibly. Plate heights increased gradually with increasing fiber mass for each bed height (cf. Fig. 2.2B). The percentage change from the lowest to the highest packing density ranged from +50% to +160%. In contrast to this, no clear trend was observed for bed height.

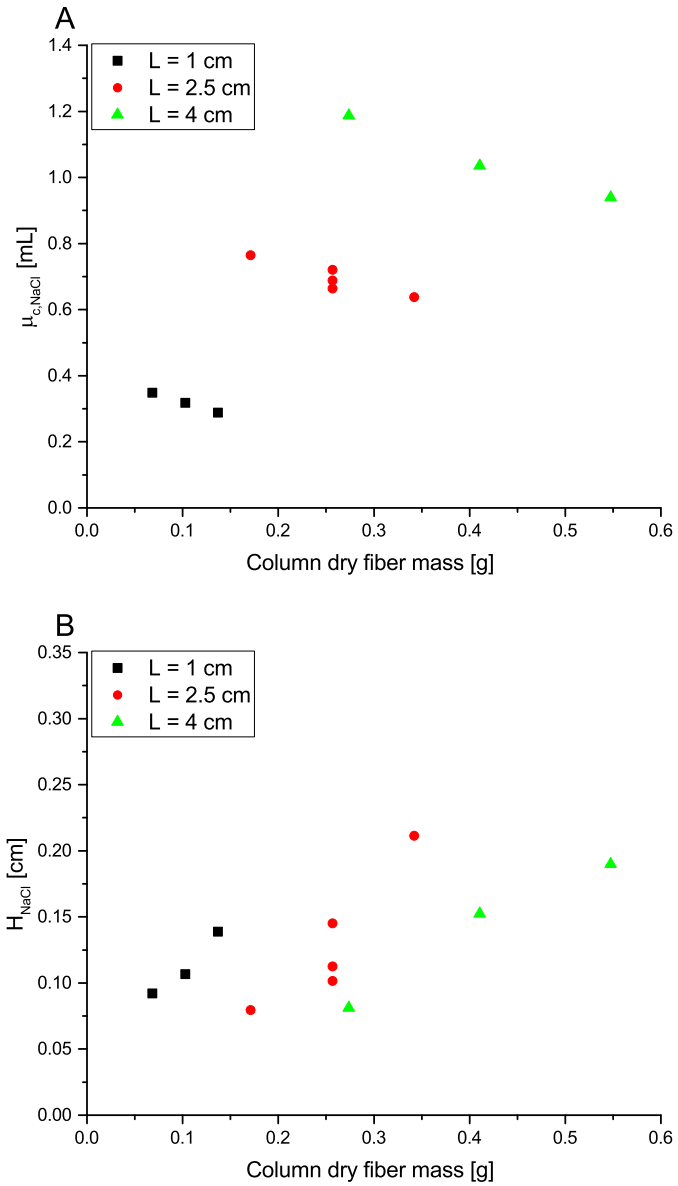

Figure 2.2: Influence of column fiber mass on (A) net retention volumes, and (B) plate heights of NaCl. Data points were obtained at a mobile phase velocity of 100 cm/h from 11 suspension packed fiber columns with variable bed height (1-4 cm) and packing density (0.2-0.4 g/mL). Columns were prepared using native PA6 winged fibers, and bed height and packing density were set according to a face-centered central composite design.

Increases in bed height from 1 cm to 4 cm resulted in either a decrease or an increase in plate heights. The percentage changes were smaller than those for packing density and ranged from -10% to +40%. The plate heights for the center-point replicates were also close to each other with a RSD of 14.1 %.

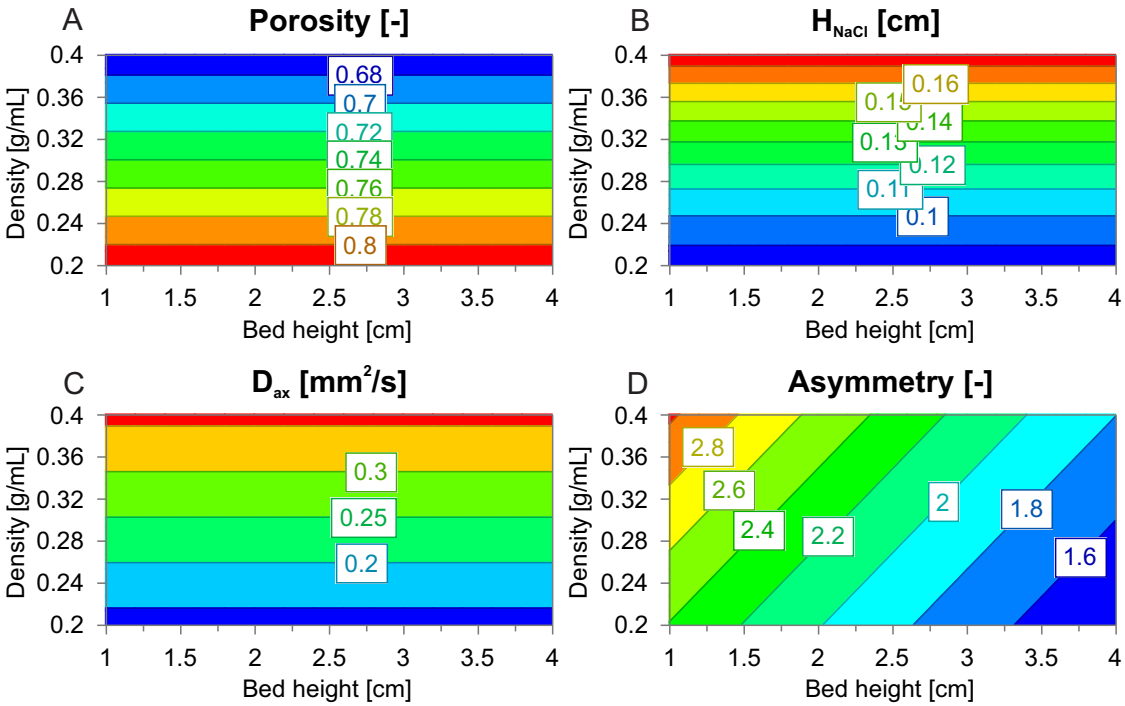

Figure 2.3: Contour plots of the response surface models for the influence of bed height (BH) and packing density (PD) on (A) porosity, (B) plate heights, (C) axial dispersion, and (D) peak asymmetry. The models are based on the 11 experiments from the face-centered central composite design. Contour lines show the predicted values for the respective column performance parameters.

For each performance parameter, response surface models were fitted to the experimental data in order to determine which parameters or parameter combinations had a significant effect on the respective response. Fig. 2.3 shows the contour plots that were obtained after response surface regression of the packing parameters (bed height, packing density) to the measured column performance parameters, porosity (cf. Fig. 2.3A), HETP (cf. Fig. 2.3B), axial dispersion (cf. Fig. 2.3C), and peak asymmetry (cf. Fig. 2.3D). Each model is based on all 11 experiments in the design. Non-significant model terms (p-value > 0.05) were removed from the models and the models with the highest R^2 and Q^2 were chosen, which are displayed in Fig. 2.3. Table 2.4 summarizes key statistical parameters for the fitted models, while Fig. 2.4 displays the scaled and centered coefficients for the model terms.

Interaction terms or quadratic terms were not found to be statistically significant (all with p-values > 0.1). For the responses porosity, HETP, and axial dispersion, only a

Table 2.4: Key model statistics for the response surface models for the packing study of the native PA6 winged fibers.

Response	R^2	Q^2	N	Model Validity	Reproducibility
Porosity, ε (-)	0.90	0.89	11	0.98	0.75
HETP, H_{NaCl} (cm)	0.77	0.73	11	0.90	0.69
Axial dispersion coefficient, D_{ax} (mm^2/s)	0.77	0.71	11	0.82	0.90
Peak asymmetry, A_s (-)	0.72	0.58	11	0.89	0.60

single linear model term was found to be statistically significant (cf. Fig. 2.3A-C and Fig. 2.4A-C, p-values < 0.001). This term accounted for 77-90% of the variability in the experimental data with Q^2 values that were in a similar range (cf. Table 2.4). R^2 and Q^2 values for the response peak asymmetry were slightly lower (cf. Table 2.4). An additional linear model term for the parameter packing density was kept for this response (cf. Fig. 2.3D and Fig. 2.4D), as its removal resulted in a decrease of both R^2 and Q^2. This parameter was only significant for a 90% confidence level (p-value=0.096). For all responses, model validity and model reproducibility were high and exceeded recommended values of 0.25 and 0.5 [102], respectively. This indicates that no statistically significant model problems were present, and that the variation of the replicates was small compared to overall variability.

Impact on porosity Packing density was the only parameter that had an effect on porosity (cf. Fig. 2.3A and Fig. 2.4A). Increases in packing density were associated with a reduction in porosity. This can also be seen in the negative sign of the regression coefficient in Fig. 2.4A. This trend is in line with the analysis of the retention times described above. For the packing density levels in the study of 0.2, 0.3, and 0.4 g/mL, the model predicted total porosities of 0.814 ± 0.023, 0.740 ± 0.013, and 0.665 ± 0.023. This matches with values of 0.824, 0.737, and 0.650, that are obtained when using the density of PA6 to calculate the theoretical porosity. For the packing density of 0.25 g/mL that had been used in the reproducibility experiments, which were not used for response surface modeling, the model predicted a porosity of 0.777 ± 0.016. This matches with the experimentally determined porosities of the reproducibility experiments, which are listed in Table 2.3. Overall these data indicate that no swelling or compression of the fibers occured within the range of packing densities and buffer conditions that were investigated in the study. This suggests that the decrease in porosity with increasing packing density is the consequence of a tighter packing of the fibers and not the result of a change in fiber dimensions.

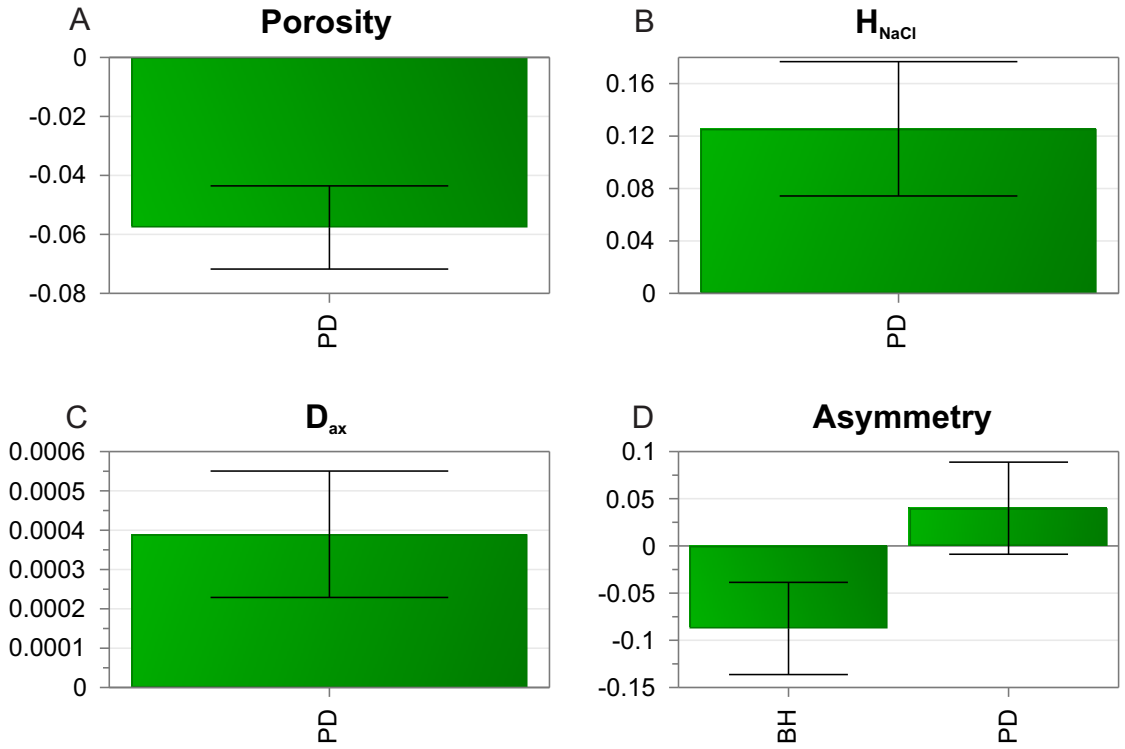

Figure 2.4: Regression coefficient plot of the response surface models for the influence of bed height (BH) and packing density (PD) on (A) porosity, (B) plate height, (C) axial dispersion, and (D) peak asymmetry. Error bars represent 95% confidence intervals.

Impact on plate heights Packing density was also the only parameter which was found to have an effect on plate heights (cf. Fig. 2.3B and Fig. 2.4B). Plate heights increased with increasing packing density, while bed height did not have a significant effect on plate height. This is in agreement with the analysis on the basis of fiber mass which was described above (cf. Fig. 2.2B). For the conditions of the reproducibility experiments, model predictions also coincided with the experimental measurements (cf. Table 2.3). These results suggest that for a fixed packing density the overall mass transfer characteristics inside the columns did not change when bed height was increased. The lowest plate heights were obtained for low packing densities. Similar results for the impact of packing density on plate heights have been reported by Li et al for rolled, continuous stationary phases [71], and Stanelle et al for capillary-channeled fibers [73]. As different packing techniques and different fibers where used in each study, including the present one, this effect seems to be independent of packing technique and fiber type. From an analysis of the van Deemter equation the B-term contribution to HETP is expected to decrease with increasing packing density, while the C-term contribution is expected to increase. For the porosities in the present study, the B-term contribution is expected to decrease by 18%, while the C-term contribution is expected to increase by 22% when

increasing the packing density from 0.2 g/mL to 0.4 g/mL. However, as explained above, the HETP for NaCl was mostly defined by the A-term. B-term contributions were determined to be negligible for the chosen experimental conditions. NaCl and dextran 2000 eluted at very similar retention times in the reproducibility experiments, which suggests that there were no major C-term contributions either. This leads to the assumption that the observed strong increase in plate heights by 111% is mostly due to an increase in A-terms. It is likely that with increasing packing density there are more restrictions to flow, in particular for a randomly packed fiber bed, where individual fibers can have various different orientations with respect to the direction of flow. Thus the chances of flow splitting and the creation of zones with differing flow velocities become higher with increasing packing density. Both effects result in an increase in van Deemter A-terms.

Impact on axial dispersion The axial dispersion coefficient was correlated with the packing density as well (cf. Fig. 2.3C and Fig. 2.4C). Increases in the packing density resulted in increases in the axial dispersion coefficient. Model predictions matched with the data from the reproducibility experiments (cf. Table 2.3). The model predicted an increase in the axial dispersion coefficient by a factor of 2.75 from the lowest to the highest packing density. This agrees with calculations on the basis of the models for porosity and HETP. These predict a change in HETP by a factor of 2.11 and a change in porosity by a factor of 0.82. This leads to a change of the interstitial flow velocity by a factor of 1.22 and an expected change in the axial dispersion coefficient by a factor of 2.57, which is in reasonable agreement with the predictions by the model for the axial dispersion coefficient. As explained earlier, axial mixing and flow nonuniformities can be considered to be the main sources of axial dispersion for the chosen experimental conditions. From the correlations for the axial mixing term that were cited above (cf. section 3.3), the axial mixing term is expected to increase in proportion to the interstitial velocity. Although these correlations are only valid for packed beds of spheres or cylinders, they lend support to the hypothesis that flow nonuniformities are the main reason for the observed increases in the axial dispersion coefficient.

Impact on peak asymmetry This hypothesis is supported by the model for peak asymmetry (cf. Fig. 2.3D and Fig. 2.4D). Peak asymmetry was affected by both packing density and bed height. Bed height had the strongest impact on peak asymmetry, while the effect of packing density was less pronounced (cf. Fig. 2.4D). The model predicted the lowest peak asymmetry for the highest bed height and the lowest packing density (cf. Fig. 2.3D). For the set-point in the reproducibility experiments a peak asymmetry of 1.51 with a confidence interval of 1.24 to 1.84 was predicted. This agrees well with the data in Table 2.3. The deterioration of

peak symmetry with increasing packing density could be due to the aforementioned creation of flow nonuniformities. The same effect for packing density has been reported in the study of Stanelle et. al [73] for capillary channeled fibers. The small regression coefficient for the effect in our study is assumed to be due to the narrow range of packing densities that was investigated. As explained above, this range was selected on the basis of pressure drop considerations for preparative applications. To maximize productivity, a range of short bed heights was investigated. For this range of bed heights peak asymmetry improved with increasing bed height. Two effects may contribute to this. Due to the length of the fibers a completely random distribution of the fibers along the column may not be achieved for very short bed heights. Thus, flow may be largely unrestricted at some radial positions inside the column, such as in the fiber channels, while in other positions there may be considerable restrictions to the flow. This leads to a decrease in uniformity of the flow profile and results in an increase in peak asymmetry. When bed height is increased, a more random distribution of the orientation of fibers with respect to the direction of flow can be achieved. In this way, differences between different flow paths are evened out and more symmetric peak profiles are obtained. In addition, the ratio between extracolumn volume and column volume becomes smaller with increasing bed height, thereby also decreasing any extracolumn volume contributions to peak asymmetry.

2.3.5 Impact of grafting on column performance

The model for peak asymmetry (cf. Fig. 2.3D) implies that a minimum bed height of 2.7 cm is required in order to achieve a peak asymmetry ≤ 1.8. At the minimum bed height, this value is only reached for the lowest packing density. For the longest bed height, i.e. 4 cm, this target is achieved over the entire range of packing densities, thereby making it possible to leverage the benefits of a higher packing density while still satisfying peak asymmetry requirements. As a consequence of this, higher volumetric binding capacities might be achieved, as higher packing densities lead to a higher number of fibers per geometric volume, and hence higher fiber surface areas. The model for plate height (cf. Fig. 2.3B), on the other hand, implies that increases in packing density lead to an increase in plate height and accordingly to a decrease in column efficiency. Thus capacity utilization, which is a function of column efficiency [20], and describes the ratio between the dynamic binding capacity (DBC) at a certain level of breakthrough (BT) and the equilibrium binding capacity (EBC), should change accordingly.

In order to test this hypothesis, we determined the EBCs of lysozyme on native PA6 winged fibers, and three types of poly (glycidyl methacrylate) (PGMA) grafted and SO_3^--functionalized PA6 winged fibers. Grafting was performed in order to

increase the binding capacity of the fibers, as this is a key performance parameter for preparative applications. Native PA6 fiber surfaces can be used for protein separations [87], but relatively low protein binding capacities have been reported [72]. Grafting was performed via a simple one step reaction with the use of a cross-linking agent (cf. section 2.2.3), giving rise to fibers with densely cross-linked PGMA layers and low degrees of grafting. Functionalization was performed in order to anchor sulfonic acid groups within the PGMA layer (cf. section 2.2.3). Three types of modified fibers with different DG were prepared. Table 2.5 summarizes the DG, the ionic capacities, and EBCs of the different types of fibers. Low binding capacities on the order of a few mg/g were measured for the native fibers. This is in agreement with earlier data for protein binding capacities on native PA6 fibers [72]. It is likely a consequence of the specific surface area (SSA) of the nonporous fibers and the low ionic capacity of PA6. The SSA of the winged fibers is higher than the SSA of other types of microfibers, but low when comparing to other types of support materials [44]. A theoretical binding capacity of 3-6 mg/g can be calculated from the dimensions of lysozyme [103], when assuming full monolayer coverage of the fiber surface. The binding capacities for the grafted fibers exceeded this value by up to more than one order of magnitude and increased with increasing DG. This, and the increasing ionic capacities, confirm that surface modification was successful. The increase in binding capacity is a consequence of the formation of a hydrogel layer which contains additional ligands for protein binding. The relatively low binding capacity of the fibers with the lowest DG can be explained by the low DG and the chosen experimental conditions. Hydrogel formation only occurs if a certain DG is exceeded [45]. Buffers were selected to match the conditions of the packing experiments and contained 50 mM sodium phosphate. For a lower buffer concentration of 10 mM, an increase in the EBC of the fibers with lowest DG was observed, while the EBCs of the other fibers only changed slightly (data not shown).

In the next step the fibers were packed into columns at different packing densities in order to determine the impact of packing density on DBCs and capacity utilization. Due to the low binding capacity of the native fibers, which makes accurate determination of DBC for higher protein load concentrations challenging [72], only grafted fibers were investigated. Bed height was set to 4 cm and packing densities

Table 2.5: Grafting degrees and equilibrium binding capacities for lysozyme for the grafted PA6 winged fibers examined in this study.

Adsorbent name	DG (%)	Ionic capacity (mol/g)	EBC (mg/g)
Winged PA6 native	-	0.002	1.9
Winged PA6 PGMA low graft SO_3^-	6.8	0.013	3.2
Winged PA6 PGMA medium graft SO_3^-	13.1	0.149	50.5
Winged PA6 PGMA high graft SO_3^-	15.1	0.153	79.2

were varied within a range of 0.2-0.4 g/mL (cf. Table 2.2). One column of each fiber type was packed for each packing density. For the medium graft fibers 4 columns were packed in order to assess column-to-column variability. This resulted in a total set of 12 columns.

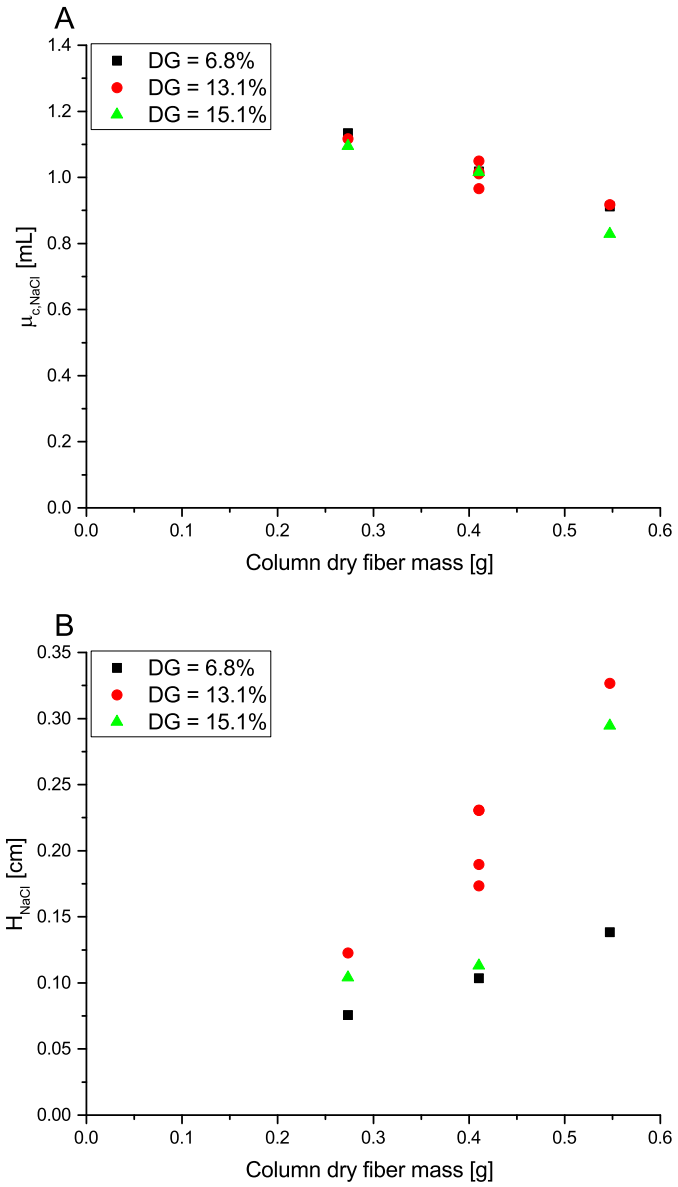

Figure 2.5: Influence of column fiber mass on (A) net retention volumes, and (B) plate heights of NaCl. Data points were obtained at a mobile phase velocity of 100 cm/h from 12 suspension packed fiber columns. Columns were prepared using PGMA-grafted and SO_3^--functionalized PA6 winged fibers with 3 different degrees of grafting (DG, 6.8-15.1%). Columns were packed at 3 variable packing densities (0.2-0.4 g/mL) to a bed height of 4 cm.

Prior to dynamic loading experiments, the columns were characterized via tracer injections. Fig. 2.5 shows the retention volumes and plate heights of NaCl for the 12 columns as a function of column dry fiber mass, grouped by DG. For each fiber type retention volumes decreased with increasing fiber mass (cf. Fig. 2.5A). The retention volumes of the 4 replicate columns were close to each other, with a RSD of 2.9%. Only small differences were observed between the retention volumes of different fiber types. The retention volumes for the grafted fibers were very similar to the retention volumes for the native PA6 fibers at the same bed height (cf. Fig. 2.2A and Fig. 2.5A). This indicates that fluid volume and hence total porosity decreased with increasing fiber mass for all fiber types. Plate heights increased gradually with increasing fiber mass for each fiber type (cf. Fig. 2.5B). This matches with the trends that were observed for the native fibers (cf. Fig. 2.2B). The percentage changes were in a similar range as for the unmodified fibers and ranged from +80% to +180%. The smallest and the largest changes were observed for the fibers with the lowest and the highest DGs, respectively. This could be the consequence of stronger diffusional resistances for the fibers with the higher DG, however, additional columns would have to be packed to clearly distinguish between the HETPs of the different types of fibers, which was not intended here. In summary, it can be concluded that fiber mass had the same effect on retention volumes and plate heights on the grafted fibers as on the native fibers.

Impact on dynamic binding capacity and capacity utilization Fig. 2.6A shows the DBCs of lysozyme for the different columns in comparison to their respective EBCs. The data is grouped by DG and packing density. DBCs were evaluated at 10% BT and volumetric EBCs were calculated via multiplying the EBCs on the basis of fiber mass (cf. Table 2.5) with the respective fiber packing density. DBCs were measured at a low (100 cm/h) and a high (800 cm/h) flow velocity (equivalent to volumetric flow rates of 0.6 mL/min and 4.6 mL/min) in order to study how mobile phase velocity affects the DBCs of the different fiber types under different packing densities. For each fiber type DBCs increased with increasing fiber packing density. However, this increase was not directly proportional to the increase in EBC. DBCs correlated with the DG and the EBCs. For each packing density the highest DBC was measured for the fibers with the highest DG and EBC. Flow velocity had a constant but small effect on DBCs. For the 7-fold increase in flow velocities the DBCs of the medium graft fibers decreased by an average of 16.0 ± 1.0%, while the DBCs of the high graft fibers decreased by 19.0 ± 1.2%. This is consistent with the low DG and the difference in DG between the two fiber types. The opposing trend for the low graft fibers can be explained by the very low recoveries of bound lysozyme from the low graft fibers (< 10%). As the fast flow velocity experiments were run first, lysozyme was still bound to the low graft fibers and affected the DBC measurements for the low flow velocity. For the other fibers almost complete recovery

of the bound protein was observed (> 95%) in the salt gradient that was employed for elution. It is likely that the low recovery from the low graft fibers is due to hydrophobic interactions with the PA6 backbone, as such effects have been reported for this specific protein on PA6 C-CP fibers [87].

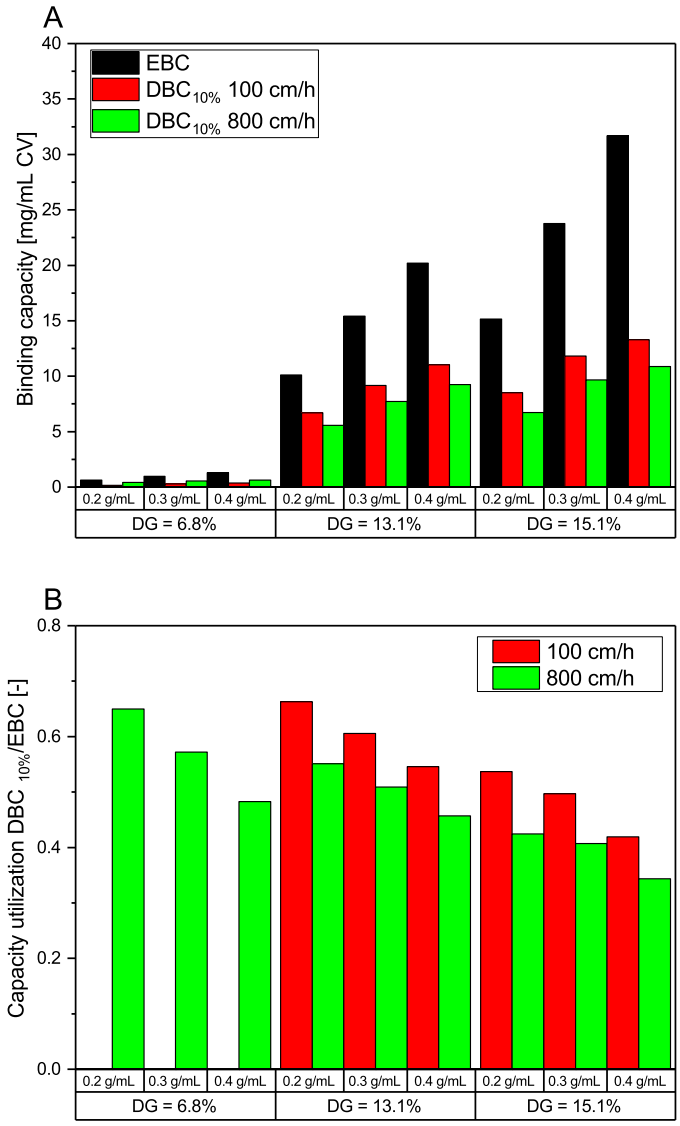

Figure 2.6: Impact of degree of grafting (DG), packing density, and mobile phase velocity on (A) binding capacity of lysozyme and (B) capacity utilization on PGMA-grafted and SO_3^--functionalized PA6 winged fibers. Protein concentration: 2 g/L. Buffer conditions: 50 mM NaPi, pH 7.

From the measured DBCs capacity utilization was calculated as the ratio between the $DBCs_{10\%}$ and the EBCs. The capacity utilization for each fiber type, packing density and flow velocity is displayed in Fig. 2.6B. For the low graft fibers the capacity

utilization was only calculated for the high flow velocity. Capacity utilization for the lowest packing density and the low flow velocity ranged from 54% to 66%. Capacity utilization decreased with increasing fiber packing density, increasing DG, and increasing flow velocity. From the lowest to the highest fiber packing densities the capacity utilization decreased by 19% to 26%. From the porosities, the increase in interstitial flow velocity from the lowest to the highest packing density can be estimated to be approximately 27%. This change in velocity does not explain the change in capacity utilization, as the 7-fold increase in interstitial velocity with increasing mobile phase velocity leads to a similar decrease in capacity utilization as seen from the lowest to the highest packing density. This suggests that the decrease in capacity utilization with increasing fiber packing density is not the result of kinetic effects alone. With increasing fiber packing density, fibers are packed more tightly; it is likely that this leads to the creation of stagnant flow zones or zones in the fiber bed which are not reached via convection. Both effects would lead to a reduction in capacity utilization. The latter effects have been reported by Wang et al for native PA6 C-CP fibers [63]. The difference in capacity utilization between the different fiber types for a given fiber packing density, can be explained by the different DG, and consequently the different extent of mass transfer limitations. With increasing DG the thickness of the grafted hydrogel layer increases, leading to stronger diffusional limitations. It may also be possible that parts of the channels between the fiber projections get filled as the DG increases, which would lead to longer diffusion paths.

Impact on resolution Apart from the DBC, the resolution is another key column performance parameter. Under linear chromatography conditions it depends essentially on the retention factor, the selectivity, and on the efficiency [21]. Packing density and DG should both impact these parameters. An increase in packing density should result in higher retention factors, but may decrease efficiency as it results in higher interstitial flow velocities. Grafting can have an impact on selectivity, but may also decrease efficiency. Whether these effects lead to a change in resolution will depend on which of these effects dominates.

In order to study how resolution of the fibers changes with packing density and DG, we performed linear gradient elution (LGE) experiments for the 12 columns at the high flow velocity with a 3-component protein mixture consisting of a monoclonal antibody (IgG), cytochrome c (cyt c), and lysozyme (lys). Fig. 2.7A shows the chromatograms for the 4 replicate columns with the same fiber type and packing density. The three proteins could be separated in the gradient, and eluted in the order of increasing pIs, i.e. IgG was followed by cyt c and lys. Peak shapes, peak heights, and peak widths were very similar between the different columns, which indicates a high column-to-column reproducibility. Fig 2.7B compares the

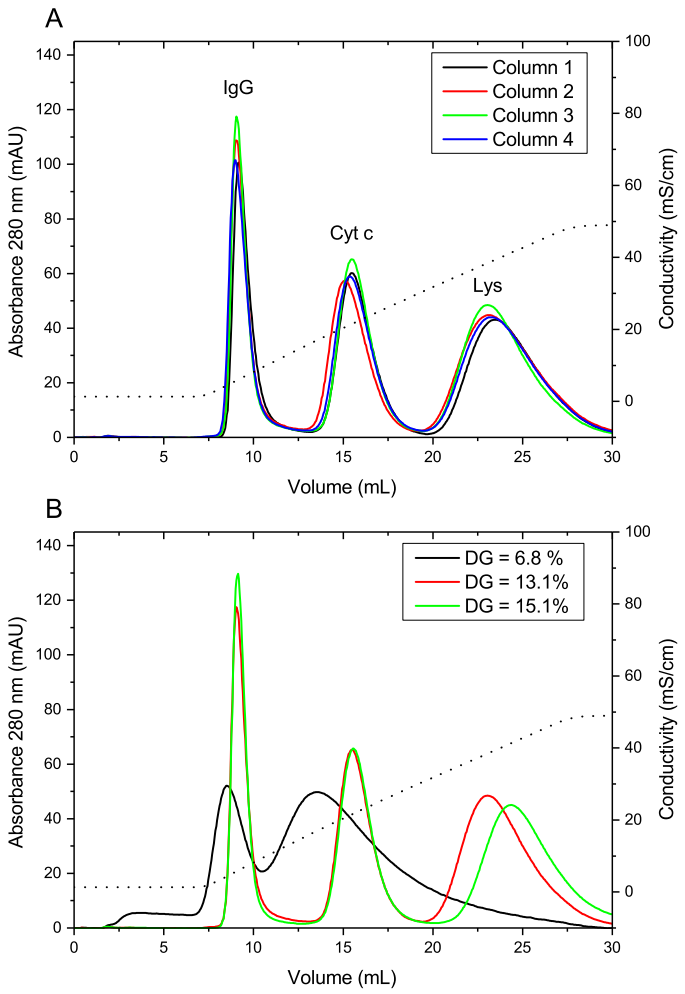

Figure 2.7: Chromatograms for the separation of IgG, cytochrome c, and lysozyme on PGMA-grafted and SO_3^--functionalized PA6 winged fibers via linear salt gradient elution. (A) Comparison of elution profiles for 4 columns with the same fiber type (DG = 13.1%) and packing density (0.3 g/mL). (B) Comparison of elution profiles for fibers with different degrees of grafting at the same packing density (0.3 g/mL). Load buffer: 10 mM NaPi, pH 7. Elution buffer: 10 mM NaPi + 1 M NaCl, pH 7. Gradient: 0-50% elution buffer over 15 CV. Mobile phase velocity: 800 cm/h.

chromatograms of the replicate columns, which contained fibers with a medium DG, with the chromatograms of the columns that contained fibers with the other two DG, in order to illustrate the differences in the elution profiles. The chromatograms for the fibers with the higher DG (DG = 15.1%) were similar to the ones for the fibers with the medium DG (DG = 13.1%). However, the retention volumes and the distances between adjacent peaks increased, which is particulary evident for the last eluting compound lys. This indicates that the selectivity of the fibers with the higher DG is higher than the selectivity of the fibers with the medium DG. This is

consistent with the higher DG, which results in a higher ionic capacity. A higher ionic capacity will particularly affect the retention volumes of later eluting compounds, i.e. compounds with higher characteristic charges. For the fibers with the low DG a different elution profile was observed. Cyt c eluted isocratically during the wash step and at the beginning of the salt gradient, while IgG and lys eluted later during the gradient and could not be resolved. This suggests that additional interactions, such as the previously mentioned hydrophobic interactions, had an impact on the retention on the low graft fibers. The extent of such interactions will differ between different proteins, as has been observed by Stanelle et al on native PA-6 C-CP fibers [73]. With increasing salt concentration, the extent of hydrophobic interactions will increase, while electrostatic interactions will be strongly reduced. The retention of each protein has to be understood as the combined result of the hydrophobic and electrostatic interactions under isocratic conditions and the change in both of these effects with increasing salt concentration.

The resolution between adjacent peaks was calculated from the chromatograms of the different columns via UV peak deconvolution and calculation of the statistical moments. For the low graft fibers no resolution could be calculated, as cyt c eluted both isocratically and during the gradient, and the peak for IgG and lysozyme could not be deconvoluted from the available UV measurements. The calculated resolutions for the medium and high graft fibers are displayed in Fig. 2.8, and are grouped by DG and packing density. The resolution was higher for the fibers with the higher DG. For both types of fibers the resolution decreased with increasing packing density. Resolutions decreased by 9-12% for the medium graft fibers and 16-18% for the high

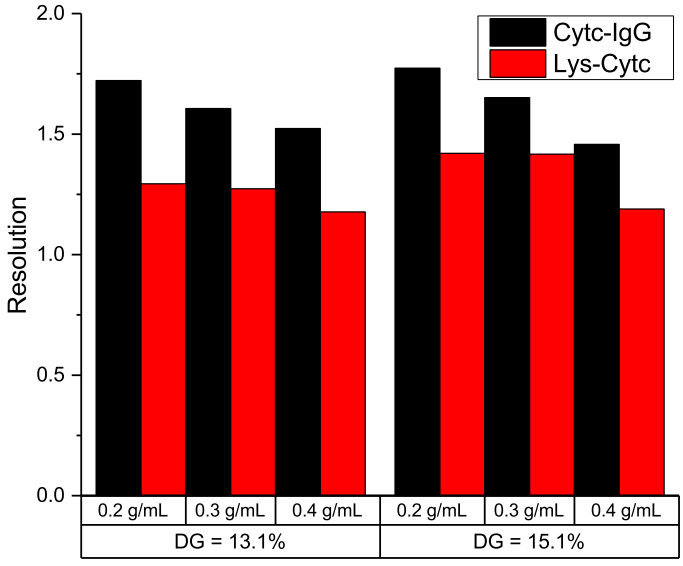

Figure 2.8: Influence of degree of grafting and packing density on the resolution of cytochrome c and IgG, and lysozyme and cytochrome c in the linear salt gradient elution experiments.

graft fibers when the packing density was increased from 0.2 g/mL to 0.4 g/mL. The main reason for this change was that for all proteins the peak widths increased more strongly with increasing packing density than the retention time difference. This suggests that the reduction in efficiency is stronger than the increase in capacity factors that lead to an increase in the retention time difference. For each fiber type the peak widths of different proteins increased by a similar percentage, i.e. 25 ± 2% for the medium graft fiber and 39 ± 1% for the high graft fiber. This suggests that the increase in peak widths with increasing packing density is mostly a consequence of the different packing structure.

Comparison to other stationary phases Overall these results indicate that both the resolution and the DBC of the fibers may be affected via the packing density and the DG. The selection of the best set-point for these two parameters will depend on the intended use. When trying to balance volumetric binding capacity and resolution, a medium packing density offers the best compromise for the present fiber material. In the present study the highest resolution was achieved for the fibers with the highest DG. In order to illustrate how the resolution of such a fiber column compares to the resolution of other types of strong CEX stationary phases, we repeated the gradient elution experiments with a diffusive, and a perfusive resin at different mobile phase velocities. Fig. 2.9 shows the chromatograms for the fibers with the highest DG at a medium packing density, the diffusive resin SP Sepharose Fast Flow, and the perfusive resin Poros 50 HS. At the lowest flow velocity, cyt c and lys eluted close to each other on SPFF and were hardly separated, while on the fibers and on Poros 50 HS all three proteins eluted at distinct volumes and were well separated. Peak heights were higher, and peak widths were smaller on Poros 50 HS than on SPFF and on the fibers. With increasing flow velocity peak heights decreased and the peak widths increased strongly on Poros 50 HS and on SPFF. This resulted in an overlap of the peaks of cyt c and lys on SPFF and in a reduction of the resolution of the two proteins on Poros 50 HS. Peak heights also decreased on the fibers, but this decrease was less pronounced than on the resins, such that the resolution between cyt c and lys was hardly affected.

This comparison shows that the grafted fibers can achieve a higher resolution separation than other adsorbents, in particular at high mobile phase velocities. The differences in the chromatograms of the three adsorbents reflect the different extent of contributions from hydrodynamic and thermodynamic mechanisms. The different distances between adjacent peaks point at different selectivities of the three adsorbents. The resins have a higher selectivity for the separation of IgG and cyt c, while the grafted fibers have a higher selectivity for the separation of cyt c and lys. This is most likely a consequence of the different chemistry of the three stationary phases, for instance the different ionic capacities. These range from 0.043 M per

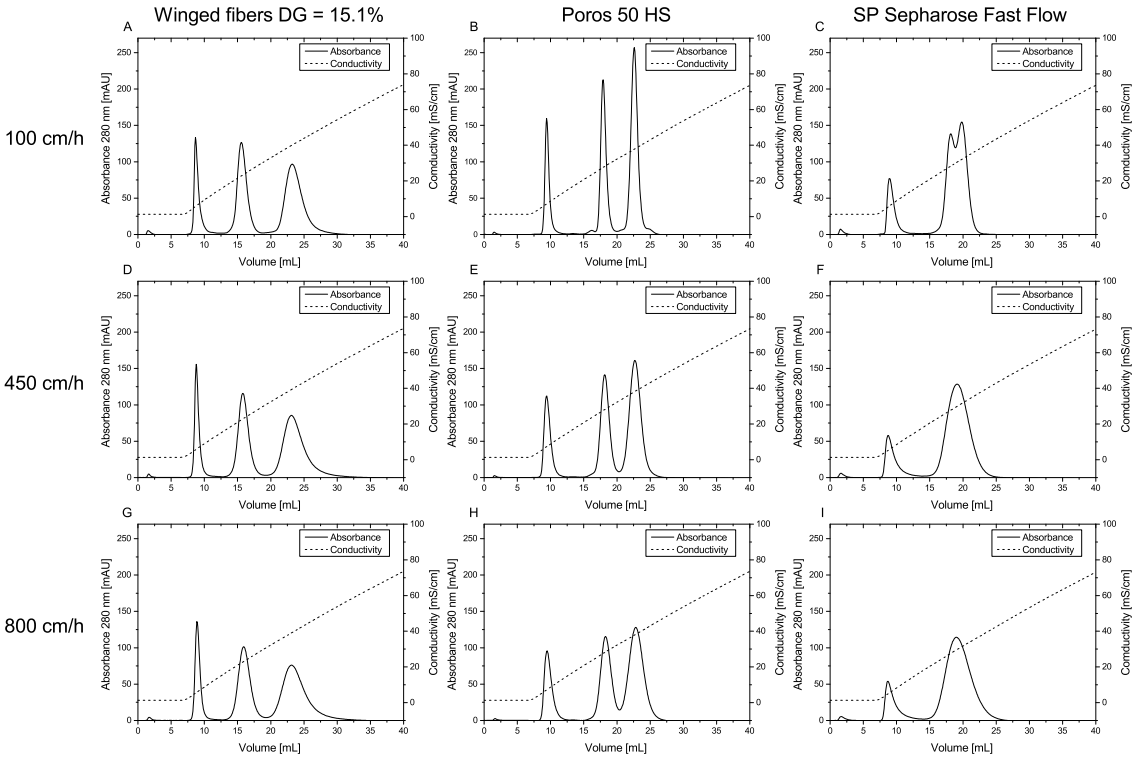

Figure 2.9: Comparison of chromatograms for the separation of IgG, cytochrome c, and lysozyme on PGMA-grafted and SO_3^--functionalized PA6 winged fibers, Poros 50 HS, and SP Sepharose Fast Flow in linear salt gradient elution experiments at different mobile phase velocities. Load buffer: 10 mM NaPi, pH 7. Elution buffer: 10 mM NaPi + 1 M NaCl, pH 7. Gradient: 0-100% elution buffer over 30 CV.

CV for the fibers and 0.08 M per CV for Poros to 0.213 M for SPFF. Based on the entire skeleton the respective ionic capacities are 0.175 M, 0.273 M and 3.929 M. Within the grafted hydrogel layer, where most of the functional groups on the grated fibers are located, the ionic capacity will be even higher than 0.175 M. The volume of the hydrogel layer can be estimated from the difference in the excluded volume fractions of D2000 and NaCl. This leads to an ionic capacity of 0.311 M within the hydrogel layer. The different peak widths at the lowest mobile phase velocity are a consequence of the different degrees of axial dispersion as well as differences in mass transfer resistances. Eddy dispersion increases with particle diameter, which explains the increase in peak widths from Poros to SPFF and the grafted fibers. The peak width of each protein further depend on the extent of mass transfer resistances which increase with increasing flow velocity. Due to the thin hydrogel layer this effect is smaller for the fibers than for the porous resins, which explains the smaller decrease of the peak widths of the fibers with increasing flow rate. From this discussion it becomes evident that the grafted fibers have particular advantages at faster mobile

phase velocities, where the comparatively low mass transfer resistance outweighs the comparatively larger axial dispersion.

2.4 Conclusions

In the present study we investigated the packing characteristics of winged shaped polymer fibers as potential low-cost support materials for preparative chromatography adsorbents. A suspension based packing technique was used to pack short cut fibers into laboratory scale columns with an inner diameter of 6.6 mm. The packing procedure was reproducible, as evidenced by a low column-to-column variability in key column performance parameters such as peak asymmetry, plate height, and the axial dispersion coefficient. Packing reproducibility was comparable to reproducibilities that have been reported for other packing techniques at similar scale. Peak asymmetries were within typical ranges of preparative columns. Plate heights of the present fibers were on the order of 0.09 cm. Packing density and bed height both affected column performance. The lowest plate heights and the most symmetric peak shapes were observed for lower packing densities and longer bed heights. Packing density also affected the performance of modified fibers. Dynamic binding capacity increased with increasing packing density, while capacity utilization and resolution decreased. For optimized packing conditions and fast mobile phase velocities, the modified winged fibers achieved a better resolution than conventional adsorbents.

In conclusion, the short winged shaped fibers showed good packing characteristics in terms of peak asymmetry, plate heights, and axial dispersion coefficients. Packing density was found to impact the column performance in a similar way as on other fiber supports, while plate heights were at the lower end of plate heights that have been reported so far. This lends support to the idea of using the present fibers for preparative applications.

The present study identifies packing conditions under which these fibers can be used most efficiently. This will be valuable for the future evaluation of these fibers. Further improvements in the packing characteristics of the present fibers may be possible via adjustments in the fiber dimensions. Future work will be directed at assessing the scale up performance of the present fibers.

Acknowledgments

The authors gratefully acknowledge material supply by Sartorius Stedim Biotech. We would like to thank Sartorius for providing SEM images of the different fiber types and performing BET measurements. In addition we would like to thank David Saleh for assistance in the lab. This study has been funded by the German Federal Ministry of Education and Research (BMBF) under the reference number 13N13322.

3 A mechanistic model of ion-exchange chromatography on polymer fiber stationary phases

Johannes Winderl[1], Tobias Hahn[2], Jürgen Hubbuch[1]

[1] Institute of Engineering in Life Sciences, Section IV: Biomolecular Separation Engineering, Karlsruhe Institute of Technology (KIT), Karlsruhe, Germany
[2] GoSilico GmbH, Karlsruhe, Germany

Abstract

Fibers are prominent among novel stationary phase supports for preparative chromatography. Several recent studies have highlighted the potential of fiber-based adsorbents for high productivity downstream processing in both batch and continuous mode, but so far the development of these materials and of processes employing these materials has solely been based on experimental data. In this study we assessed whether mechanistic modeling can be performed on fiber-based adsorbents. With a column randomly filled with short cut hydrogel grafted anion exchange fibers, we tested whether tracer, linear gradient elution, and breakthrough data could be reproduced by mechanistic models. Successful modeling was achieved for all of the considered experiments, for both non-retained and retained molecules. For the fibers used in this study the best results were obtained with a transport-dispersive model in combination with a steric mass action isotherm. This approach accurately accounted for the convection and dispersion of non-retained tracers, and the breakthrough

and elution behaviors of three different proteins with sizes ranging from from 6 to 160 kDa were accurately modeled, with simulation results closely resembling the experimental data. The estimated model parameters were plausible both from their physical meaning, and from an analysis of the underlying model assumptions. Parameters were determined within good confidence levels; the average confidence estimate was below 7% for confidence levels of 95%. This shows that fiber-based adsorbents can be modeled mechanistically, which will be valuable for the future design and evaluation of these novel materials and for the development of processes employing such materials.

3.1 Introduction

Chromatography is the main unit operation for the purification of biological products at preparative scale. At present, the majority of such unit operations are performed in packed beds filled with porous and spherical adsorbent particles. These are prepared from inorganic base materials or natural or synthetic polymers such as agarose and dextran or polystyrene and polymethacrylate [44]. While these stationary phase materials offer high binding capacities and high separation efficiencies, there are several disadvantages [104] with respect to preparative scale bioseparations. As most binding sites in these materials are located within the adsorbent particles, they are only accessible via diffusion. This results in diffusional limitations, particularly for larger molecules with low diffusivity, such as proteins. Packed beds filled with such stationary phase materials feature high packing densities and high pressure drops. When taken together, these properties limit the range of feasible operational flow rates and bed heights, and thus also limit the throughput of processes involving these materials.

Higher titers in upstream processing, overall increasing demand for biopharmaceuticals, and tightening cost constraints necessitate increasing both the throughput and the productivity of downstream processes. At the same time, regulatory requirements call for a better process and quality understanding. To overcome the limitations of conventional adsorbents, several alternative stationary phases with improved flow and/or mass transfer properties have been developed and commercialized, such as pellicular or gigaporous beads, monoliths and membrane adsorbers.

Another approach, which has been proposed early on [78] and has regained interest recently [57, 65, 76, 79, 80, 83, 105], lies in the use of polymeric fibers as chromatographic supports. They can be prepared from various base polymers, including natural and synthetic ones, and are available in different formats, i.e. different

shapes, lengths, and structures. They can be arranged in different ways for use as a chromatography matrix [57], ranging from randomly packed short fibers [68, 76, 92] to aligned fibers [70, 84] to non-woven fiber mats [80], and woven fabrics [69]. Fibers are major intermediate products of the textile industry, and various technologies for mass production and surface modification exist. This results in very low manufacturing costs for fibers, which are potentially much lower than the costs for other stationary phases [57]. Recent advances in the fabrication of high surface area fibers and in surface modification protocols have made it possible to prepare fiber-based adsorbents with high capacities and low pressure drops at high flow rates. Several experimental studies have highlighted the potential of such materials for high throughput and high productivity downstream processing in both batch [76, 79, 80] and continuous mode [105].

Despite these promising reports, all studies on fibers as chromatographic supports have been based on experimental data only. To the best of our knowledge, no attempts have been made to model chromatographic processes on fiber stationary phases. For other types of stationary phases a wide variety of mechanistic models have been developed [22, 106]. Different models have been compared and criteria for selecting the appropriate modeling depth [107] and work flows for the determination of model parameters have been put forward [106]. Mechanistic modeling has been shown to be valuable for process optimization [108], process characterization [109, 110] and process scale up [111, 112], as well as the optimization of the adsorbent structure itself [113, 114]. A validated mechanistic model for fiber-based adsorbents would therefore be of great use; it would generate an understanding of the relevant transport and binding mechanisms, and thereby support the ongoing development and evaluation of these novel materials.

In this study we assessed whether mechanistic modeling can be performed on fiber-based adsorbents. First, we performed characterization and efficiency experiments on hydrogel grafted anion-exchange fibers in order to develop a mechanistic model. Then, we tested whether the proposed model can accurately describe the convection and dispersion of non-retained molecules. Next, the applicability of the model towards simulating the binding, breakthrough, and elution of differently sized proteins was evaluated. Finally, we assessed whether the model parameters can be identified with good confidence and compared the proposed model with alternative models.

3.2 Theory

In this study an experimental investigation was conducted in order to determine the porosities and transport properties of a column filled with randomly-packed fibers (cf. Sections 3.4.1 and 3.4.2). The fibers were short cut, shaped, hydrogel grafted strong anion exchange fibers (cf. Section 3.3.1). Based on the results of these experiments, the following mechanistic model was developed for a column that is randomly packed with fibers.

3.2.1 Model Assumptions

In order to define the model parameters, a few assumptions needed to be made. When the column was randomly packed with fibers as described in Section 3.3.2, no peak fronting or major peak tailing was observed during efficiency testing. Because of this, the column was assumed to be radially homogeneous, without major cavities and with no influence from wall effects. As the column inlet pressure was typically below 4 bars, the compressibility of the mobile phase was neglected and the mobile phase velocity was considered to be constant. The fibers were assumed to be porous and uniform in size. We assumed that both the grafted hydrogel layer and the support phase can contribute to the porosity of the fibers. The pores between the fibers were considered to be uniform in size. The axial dispersion coefficient was considered to be independent of the axial position inside the column or the solute concentration. Finally, we made the general assumptions that the partial molar volumes of the sample components are the same in the mobile and the stationary phase, that the solvent is not adsorbed, that no thermal effects are present, and that the column is operated under constant conditions [22].

3.2.2 Transport Dispersive Model

A transport-dispersive model (TDM) was used to describe the macroscopic mass transport through the fiber column. The mobile phase was divided into the interstitial volume between the fibers with concentration c_i of component i and the pore volume within the fibers with concentration $c_{p,i}$ of component i, with respect to $i = 1, ..., N$ components. The fraction of the interstitial volume V_{int} with respect to the total column volume V is represented by the interstitial porosity ε, and the fraction of the pore volume within the fibers with respect to the total fiber volume is represented by the fiber porosity ε_f. The overall column porosity results from the sum of the

interstitial volume between the fibers and the pore volume within the fibers, as depicted in Eq. (3.1):

$$\varepsilon_t = \varepsilon + \varepsilon_f(1-\varepsilon) \tag{3.1}$$

The rate of change of the interstitial concentration $c_i(x,t)$ of component i at position x in a column with length L is described by Eq. (3.2):

$$\begin{aligned}\frac{\partial c_i}{\partial t}(x,t) &= -u_{int}(t)\frac{\partial c_i}{\partial x}(x,t) + D_{ax}\frac{\partial^2 c_i}{\partial x^2}(x,t) \\ &\quad -\frac{1-\varepsilon}{\varepsilon}k_{eff,i}a_f(c_i(x,t)-c_{p,i}(x,t)) \quad \forall i\end{aligned} \tag{3.2}$$

The first term in Eq. (3.2) accounts for the change in concentration due to convective mass transport along the column with an average interstitial velocity u_{int}. Peak broadening effects due to axial diffusion and hydrodynamic dispersion are modeled as dispersion in space with an axial dispersion coefficient D_{ax}. The last term in Eq. (3.2) describes the concentration exchange between the interstitial volume and the volume of the fibers. It considers the differences in concentrations and volumes and depends on the specific surface area (SSA) of the fibers a_f and a component-specific effective mass transfer coefficient $k_{eff,i}$, which lumps contributions of external film and internal pore diffusion processes. For the column inlet and outlet Danckwerts boundary conditions were used, as shown in Eq. (3.3) and (3.4), where $c_{in,i}(t)$ is the injected concentration of component i at the column inlet at time t:

$$\frac{\partial c_i}{\partial x}(0,t) = \frac{u_{int}(t)}{D_{ax}}(c_i(0,t)-c_{in,i}(t)) \quad \forall i \tag{3.3}$$

$$\frac{\partial c_i}{\partial x}(L,t) = 0 \quad \forall i \tag{3.4}$$

The concentration of component i within the fiber pores $c_{p,i}$ depends on the fiber porosity ε_f, and its rate of change is influenced by exchange with the interstitial phase and stationary phase, as depicted in Eq. (3.5):

$$\frac{\partial c_{p,i}}{\partial t}(x,t) = \frac{k_{eff,i}a_f}{\varepsilon_f}(c_i(x,t)-c_{p,i}(x,t)) - \frac{1-\varepsilon_f}{\varepsilon_f}\frac{\partial q_i}{\partial t}(x,t) \quad \forall i \tag{3.5}$$

3.2.3 Steric Mass Action Isotherm

The concentration exchange with the stationary phase was described with the steric mass action (SMA) isotherm [40]. The SMA isotherm is a commonly used semimechanistic isotherm for ion-exchange chromatography, and its applicability for adsorbents with grafted hydrogel layers has already been demonstrated [53,

115]. It considers the concentration of binding sites on the adsorbent, which is represented by the total ionic capacity Λ, and the competition between proteins and salt counter-ions for these binding sites. The number of binding sites a protein interacts with is described by the characteristic charge ν_i. Binding of a protein i leads to stoichiometric displacement of a number of salt counter-ions equivalent to its characteristic charge, but also results in steric shielding of additional binding sites without electrostatic interactions, which are included as a factor σ_i. The kinetic form of the SMA isotherm is given in Eq. (3.6) and (3.7):

$$\begin{aligned} \frac{1}{k_{des,i}}\frac{\partial q_i(x,t)}{\partial t} &= k_{eq,i}\left(\Lambda - \sum_{j=1}^{k}(\nu_j+\sigma_j)q_j(x,t)\right)^{\nu_i} c_{p,i}(x,t) \\ &\quad - c_{p,salt}^{\nu_i}(x,t)q_i(x,t) \qquad \forall i \neq salt \end{aligned} \tag{3.6}$$

$$q_{salt}(x,t) = \Lambda - \sum_{j=1}^{k}\nu_j q_j(x,t) \tag{3.7}$$

Here, j is a loop variable that loops over all k protein components of $i = 1, ..., N$ components. $q_i(x,t)$ describes the concentration of protein adsorbed to the stationary phase and $c_{p,salt}(x,t)$ is the pore salt concentration. $k_{eq,i} = k_{ads,i}/k_{des,i}$ is an equilibrium constant and is defined as the ratio between the rates of adsorption $k_{ads,i}$ and desorption $k_{des,i}$. Instead of k_{des}, a kinetic rate constant $k_{kin} = 1/k_{des}$ was used for parameter estimation, for reasons previously explained in [116]. $q_{salt}(x,t)$ describes the salt concentration in the stationary phase, which is obtained as the difference between Λ and the number of binding sites taken up by electrostatic adsorption. This is equivalent to the assumption that shielded binding sites are still occupied with counter-ions.

3.2.4 Model alternatives for model discrimination

For model discrimination we compared the presented model to two alternative models that have been used for grafted ion-exchange membranes [117]. A TDM without binding kinetics is obtained from the presented model if k_{kin} is set to 0. This is equivalent to the assumption that the rates of adsorption and desorption are infinitely fast and that the binding can be modeled as a reaction at equilibrium. Some authors have used this assumption, as the kinetics of ion exchange are considered to be very fast. Another model that has frequently been used for grafted ion-exchange membranes is the equilibrium-dispersive model (EDM) [115, 118]. It is obtained from a TDM if film mass transfer effects are neglected and the interstitial phase is considered to be in equilibrium with the pore phase. Since in this case c_i and $c_{p,i}$ are identical, it is not necessary to distinguish between the the two phases, such that

the EDM is usually denoted on the basis of ε_t:

$$\frac{\partial c_i}{\partial t}(x,t) = -u_m(t)\frac{\partial c_i}{\partial x}(x,t) + D_{app}\frac{\partial^2 c_i}{\partial x^2}(x,t) - \frac{1-\varepsilon_t}{\varepsilon_t}\frac{\partial q_i(x,t)}{\partial t} \quad \forall i \tag{3.8}$$

This leads to a new mobile phase velocity u_m and a new dispersion coefficient D_{app}, where $u_m = \frac{\varepsilon}{\varepsilon_t}u_{int}$ and $D_{app} = \frac{\varepsilon}{\varepsilon_t}D_{ax}$. The D_{app} of the EDM differs from the D_{ax} of the TDM as it based on ε_t and can thus potentially contain mass transfer effects.

3.2.5 Computational Methods

3.2.5.1 Numerical solution

The numerical solution of the system of model equations was performed with the software package ChromX, as reported previously [119]. Briefly, for discretization in space, a linear finite element method (FEM) was used with $30 - 50$ axial cells. For discretization in time, a fractional step θ-scheme was used because of its superior stability. Typical time steps were on the order of $0.5 - 2$ s. Non-linear equation systems were solved with fixed point iteration and linear equation systems were solved with a direct LU factorization method.

3.2.5.2 Parameter estimation

For estimation of unknown parameter sets $\bar{p}_{opt}$ the following least squares objective function was used

$$\bar{p}_{opt} = \arg\min_{\bar{p}} \sum_j \left(m(t_j) - \sum_{i \geq 1} c_i(L,t_j;\bar{p}) \cdot a_i \right)^2 \tag{3.9}$$

where $m(t_j)$ is the measured chromatogram value for the detector of interest at point in time t_j, c_i is the simulated molar concentration of component i at the column outlet at time t_j, and a_i is a component-specific calibration factor that scales from molar concentrations to the detector output of interest. The resulting optimization problem was solved with a combination of heuristic and deterministic optimization methods. Heuristic methods based on a genetic algorithm [120] and adaptive simulated annealing [121] were used to identify suitable starting points for subsequent parameter refinement with a deterministic algorithm. An implementation of the Levenberg-Marquardt algorithm was used for the deterministic method [122].

3.2.5.3 Estimation of parameter certainty

Confidence intervals for the model parameters within a confidence of 95% were calculated based on an estimate of the covariance matrix, as reported previously in [123].

3.3 Experimental

3.3.1 Materials

3.3.1.1 Chemicals, Buffers and Proteins

Tris, sodium chloride (NaCl), hydrogen chloride (HCl), sodium hydroxide (NaOH), potassium phosphate, potassium dihydrogen phosphate, ethanol (EtOH), and acetone were purchased from Merck (Darmstadt, Germany). EDTA was from Dojindo (Kumamoto, Japan). All other chemicals and proteins were obtained from Sigma-Aldrich (St. Louis, MO, USA) except for recombinant human insulin (no. FCP003), which was obtained from Kerafast (Boston, MA, USA). All chromatography experiments were conducted in 20 mM Tris buffers at pH 7.5 with 0 M (low salt buffer) or 1 M NaCl (high salt buffer). Ultra-pure water (Purelab Ultra, Elga LabWater, High Wycombe, UK) was used for buffer preparation and the pH was adjusted with HCl. Prior to usage all buffers were filtered through 0.2 μm cellulose acetate (CA) membrane filters (Sartorius, Göttingen, Germany) and dissolved gases were removed via sonification. NaCl, acetone, and dextrans with average molecular masses of 1, 12, 25, 670 and 2000 kDa were used for the determination of column porosities. The total ionic capacity of the anion exchange fibers was measured via acid-base titration with 0.5 M NaOH and 0.01 M HCl. Three proteins with different molecular weights (MWs) were used for this study.

The physical properties of the proteins are listed in Table 3.1 together with estimates for the bulk diffusivity and stokes radius, calculated from [97] and the Stokes-Einstein

Table 3.1: Physical properties of the three proteins used in this study.

Protein	MW (kDa)	pI	Bulk diffusivity (cm^2/s)	Stokes radius (nm)
Insulin	5.8	5.7	$1.5 \cdot 10^{-6}$	1.4
BSA	66	4.7	$6.7 \cdot 10^{-7}$	3.2
GO	160	4.2	$5.0 \cdot 10^{-7}$	4.3

equation. Insulin was dissolved in low salt buffer containing 1 M EDTA and dialyzed against low salt buffer with 0.1 M EDTA and low salt buffer to prepare zinc-free monomeric insulin. This was carried out in Slide-A-Lyzer dialysis cassettes (Thermo Fisher Scientific, Waltham, MA, USA) with a molecular weight cut-off (MWCO) of 2 kDa. Bovine serum albumin (BSA, no. A3294) and glucose oxidase from *Aspergillus niger* (GO, no. G7141) were dissolved directly in low or high salt buffers as needed. All protein solutions were filtered through 0.2 μm CA syringe filters (Sartorius, Göttingen, Germany). Buffer exchange was performed with PD-10 desalting columns (GE Healthcare, Little Chalfont, UK) and protein concentration was carried out in Vivaspin centrifugal concentrators (Sartorius) with PES membranes and MWCOs of 3 kDa.

3.3.1.2 Chromatography media

Table 3.2: Chemical and structural properties of the anion exchange fibers used in this study.

Property	Value
Fiber base material	Polyamide 6
Cross-sectional shape	Elliptical
Cross-sectional dimensions ($\mu m \times \mu m$)	10×20
Length (mm)	6
Specific surface area (m^2/g)	2
Degree of grafting (g/g)	15%
Functional group	$R - CH_2 - N^+(CH_3)_3$

The polymer fiber stationary phase investigated in this study consisted of short cut hydrogel grafted strong anion exchange fibers, which had been kindly provided by Sartorius. The fibers had been prepared from short cut, winged shaped nylon fibers (Allasso Industries, Raleigh, NC, USA) via ammonium cerium(IV) nitrate (CAN) initiated grafting polymerization of glycidyl methacrylate (GMA). Subsequently, the residual epoxide groups in the poly(GMA) layer had been functionalized with trimethylamine, in order to introduce quarternary trimethlyalkylammonium cations for strong anion exchange functionality. The key chemical and structural properties of the resulting fiber material as supplied by the manufacturer are summarized in Table 3.2. Fig. 3.1 shows a schematic drawing of the proposed cross-sectional structure of the modified fibers. The outer cross-section of the fibers can be approximated by an ellipse. The fibers consist of a backbone along the major axis and 32 projections that extend from both sides of the backbone [62]. The channels between the fibers have a width of 500-600 nm in the native fibers. A thin hydrogel layer has been anchored to the surface of the fibers. Depending on the degree of grafting this may alter the shape of the fibers, but as the degree of grafting was low in the present study, we assumed that the shape of the fibers is preserved. The spherical, perfusive

resin Poros 50HQ (Applied Biosystems, Waltham, MA, USA) served as a reference for efficiency experiments (cf. Section 3.4.2).

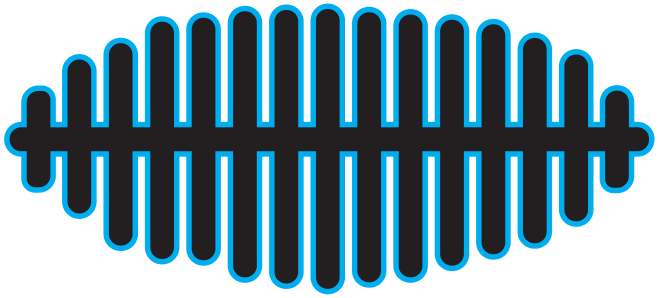

Figure 3.1: Proposed cross-sectional structure of the anion exchange fibers used in this study. Winged shaped PA6 support (black) with grafted hydrogel layer (blue).

3.3.1.3 Chromatographic instrumentation

The chromatographic experiments were carried out on two liquid chromatography systems. An ÄKTApurifier 10 system equipped with Pump P-903, UV Monitor UV-900 with a 10 mm UV flow cell, pH, conductivity and temperature monitor pH/C-900, autosampler A-905, fraction collector Frac-950, and flow restrictor FR-902 was used for plate height determinations. An ÄKTAmicro system equipped with Pump P-905, UV Monitor UV-900 with a 3 mm UV flow cell, pH, conductivity and temperature monitor pH/C-900, autosampler A-905, fraction collector Frac-950, and flow restrictor FR-902 was used for all other experiments. Both instruments were controlled with UNICORN 5.31 (all GE Healthcare).

3.3.1.4 Software

Data processing was performed with Microsoft Excel 2013 (Microsoft, Redmond, WA, USA) and Matlab R2016a (Mathworks, Natick, MA, USA). Figures were prepared with OriginPro 9.1.0 G (OriginLab, Northampton, MA, USA). Simulations and parameter estimations were carried out with ChromX (GoSilico, Karlsruhe, Germany).

3.3.2 Methods

3.3.2.1 Column packing and storage

The anion exchange fibers were slurry-packed into Omnifit BenchMark columns (Diba Industries, Danbury, CT, USA) with an I.D. of 6.6 mm. The appropriate amount of fibers required to achieve a final packing density of 0.3 g fiber per mL column volume (CV) was placed in a buffered solution containing 10 mM potassium phosphate at pH 7, at a ratio of 1 g of fiber per 500 mL of solution. The resulting suspension was slowly agitated overnight to allow for proper homogenization. Afterwards, the suspension was transferred into the column, excess solution was removed with a peristaltic pump (Gilson, Middleton, WI, USA) connected to the column outlet at a flow rate of 6 mL/min, and the bed was compressed to a final bed height of 40 mm with an adjustable column endpiece. For Poros 50HQ pre-packed 5 x 50 mm columns from Atoll (Weingarten, Germany) were used. For both media the quality of the packed columns was assessed via pulse injections of 1 M NaCl at a mobile phase velocity of 100 cm/h and evaluation of the HETP and the peak asymmetry measured at 10% peak height. Columns were deemed acceptable if the HETP was below 0.1 cm and the peak asymmetry was within the range of 0.8-1.4. Upon packing and in between experiments the columns were stored in aqueous solutions containing 20 vol% EtOH and 150 mM NaCl.

3.3.2.2 Measurement of column permeabilty

The permeability of the anion exchange fiber column for low salt buffer was determined from measurements of the system pressure drop with and without the column at mobile phase velocities in the range of 100-1500 cm/h (0.57-8.55 mL/min). From these measurements column pressure drops Δp were calculated and the permeability was obtained from a linear regression of $\eta \cdot u \cdot L$ against Δp, where η is the dynamic viscosity of the buffer, u is the mobile phase velocity, and L is the length of the column.

3.3.2.3 Isocratic elution experiments

Isocratic pulse response experiments were used for the study of plate heights as a function of mobile phase velocity, and performed under non-binding conditions in high salt buffer. Mobile phase velocities were varied between 100 and 1500 cm/h. This corresponds to interstitial velocities of 140-2140 cm/h for the anion exchange

fibers and 200-3000 cm/h for Poros 50HQ. Insulin, BSA, and GO were all dissolved in high salt buffer at a concentration of 1 g/L. NaCl was dissolved in low salt buffer at a concentration of 1.5 M and the pH was adjusted to 7.5 with HCl. For all experiments the columns were equilibrated with 2 CVs of buffer, followed by an automatic 20 μL injection of the respective test molecule and a 5 CV elution under isocratic conditions. The experiments were performed in triplicate for both columns and for the ÄKTA system without a column.

3.3.2.4 Linear gradient elution experiments

Linear gradient elution (LGE) experiments were used for the determination of the SMA isotherm parameters of insulin, BSA, and GO. For these experiments a constant mobile phase velocity of 175 cm/h was used. The method consisted of a 6 CV equilibration step with low salt buffer, followed by injection of 100 μL of protein with a sample loop, a 3 CV wash step with low salt buffer to remove unbound protein, a linear salt gradient of variable length from 0-100% high salt buffer, and a 5 CV post gradient step at 100% high salt buffer. In between runs the column was cleaned with 2 CVs of 0.1 M NaOH and regenerated with 5 CVs of high salt buffer followed by 5 CVs of low salt buffer. All proteins were applied in low salt buffer at a concentration of 2 g/L.

3.3.2.5 Breakthrough experiments

Frontal analysis experiments were used for the determination of the shielding parameter of the SMA isotherm. These experiments were performed at a constant mobile phase velocity of 175 cm/h. The column was equilibrated with 4 CVs of low salt buffer. Subsequently, protein was loaded onto the column with a 50 mL Superloop (GE Healthcare) until complete breakthrough was observed. Then, column loading was terminated and unbound protein was removed with a 5 CV wash step with low salt buffer. Bound protein was eluted with a linear salt gradient over 5 CVs from 0-100% high salt buffer followed by a post gradient step at 100% over 10 CVs. In between runs the columns were cleaned with 2 CVs of 0.1 M NaOH and regenerated with 5 CVs of high salt buffer followed by 5 CVs of low salt buffer. Buffers and protein concentrations were the same as in the LGE experiments.

3.3.2.6 Determination of model parameters

The hydrodynamic and thermodynamic model parameters were determined in a stepwise manner as described by Michel et al. [106]. 100 μL pulse injections of 1%

v/v acetone, 10 g/L dextran 2000, and 1 M NaCl without a column were performed to determine the extra column volumes from the injection valve to the UV and conductivity detectors. Known amounts of insulin, BSA, and GO were injected for the calibration of the ÄKTA UV detector. The calibration of the UV detector was performed at a wavelength of 280 nm as well 260 and 300 nms to avoid detector saturation. 5 mL salt steps with 10% increments from 0-100% B were performed with the fiber column, and the recorded conductivities at each plateau were used for calibration of the conductivity detector. The pulse injections with acetone, dextran 2000, and 1 M NaCl were repeated with the column for the determination of the column and fiber porosities. It has been shown that dextran 2000 is excluded from hydrogel layers similar to the one grafted onto the fibers [124]. Therefore, dextran 2000 was used for the determination of the interstitial volume and the column porosity. The ligand density of the anion exchange fibers was measured via titration with 0.5 M NaOH and 0.01 M HCl, according to standard protocols. An initial value for the axial dispersion coefficient was obtained from moment analysis of the dextran 2000 pulse injections, and parameter estimation was used for parameter refinement. The effective mass transfer coefficient of NaCl $k_{eff,NaCl}$ was determined via parameter estimation from the salt step transition experiments. The $k_{eff}s$ of insulin, BSA, and GO and the SMA isotherm parameters k_{eq}, k_{kin}, ν, and σ were determined via chromatogram fitting. First, the linear isotherm parameters ν and k_{eq} were determined from the LGE experiments. This also resulted in initial estimates for k_{kin} and k_{eff}. Then, the breakthrough experiments were added and σ, k_{kin}, and k_{eff} were estimated from the combined data set. With these parameters as starting points, a final round of parameter estimation for all 5 parameters was performed on the combined data set.

3.4 Results

In this study, short hydrogel grafted anion exchange fibers were randomly packed into chromatography columns, and the resulting columns were characterized experimentally in order to determine the relevant mass transfer phenomena for inclusion in a column model. The results of these experiments will be presented first in Sections 3.4.1 and 3.4.2. On this basis, different models were evaluated and a final model was selected and developed for the grafted anion exchange fibers. Model evaluation was performed by testing whether the model could accurately describe the experimental band profiles of non-retained and retained molecules. This is demonstrated in Sections 3.4.3 and 3.4.4. Finally, the proposed mechanistic model was compared with alternative models and the results of this comparison are given in Section 3.4.5.

3.4.1 System and column characterization

Table 3.3: Measured and calculated system and column parameters for the anion exchange fiber column used in this study.

Parameter	Symbol	Value	Unit	Source
Diameter	d	6.6	mm	From manufacturer
Length	L	40	mm	Manually controlled
Extra column volume	V_d	0.50	mL	Acetone pulse injection without column
Retention volume acetone	V_{RetAc}	1.61	mL	Pulse injection with column
Retention volume dextran	V_{RetDex}	1.46	mL	Pulse injection with column
Retention volume NaCl	$V_{RetNaCl}$	1.54	mL	Pulse injection with column
SD of dextran	σ_{Dex}	0.32	mL	Unicorn peak integration
Volume of HCl	V_{HCl}	18.52	mL	Acid-base titration
Molarity of HCl	c_{HCl}	0.01	M	Manually controlled
Mobile phase velocity	u	0.49	mm/s	Manually controlled
Column permeability	B	2.86	Darcy	Pressure drop measurements
Column volume	V	1.37	mL	$\frac{1}{4} \cdot \pi \cdot d^2 \cdot L$
Fluid volume	V_f	1.11	mL	$V_{RetAc} - V_d$
Interstitial volume	V_{int}	0.96	mL	$V_{RetDex} - V_d$
Total column porosity	ε_t	0.81		$\frac{V_f}{V}$
Interstitial porosity	ε	0.70		$\frac{V_{int}}{V}$
Fiber porosity	ε_f	0.37		$\frac{V_f - V_{int}}{V - V_{int}}$
Interstitial velocity	u_{int}	0.70	mm/s	$\frac{u}{\varepsilon}$
Axial dispersion	D_{ax}	1.57	mm^2/s	$\frac{1}{2} \cdot L \cdot u_{int} \cdot \left(\frac{\sigma_{Dex}}{V_{int}}\right)^2$
Ionic capacity	Λ	0.69	M	$\frac{c_{HCl} \cdot (V_{HCl} - V_{RetNaCl})}{V(1-\varepsilon)(1-\varepsilon_f)}$

As a first step towards modeling of the grafted anion exchange fibers, a column was randomly packed with short anion exchange fibers and characterized experimentally with respect to porosity, permeability, axial dispersion, and total ionic capacity. For the porosity experiments, acetone was used as a non-interacting, pore-penetrating tracer. Dextran with an average molecular weight (MW) of 2000 kDa was used as a non-interacting, non-pore-penetrating tracer that should be excluded from the pores of grafted hydrogel layers, as has been shown by earlier studies on grafted anion exchange membranes [124]. Based on the retention volume of acetone, a value of 0.81 for the total column porosity ε_t was obtained. The majority of the porosity was contained within the interstitial volume in between the fibers. Based on the retention volume of dextran, the interstitial porosity ε was determined to be 0.70. This was accompanied by a high column permeability of 2.86 Darcy with a maximum backpressure of 0.52 bar at 1500 cm/h. The porosity of the grafted fibers ε_p was determined to be 0.37, indicating that only a limited volume fraction of the fibers is accessible for small molecules such as acetone. Additional analysis via

inverse size exclusion experiments with dextrans of known MWs revealed that the accessible volume fraction decreased gradually with increasing MW. For dextrans greater than 670 kDa no further change was observed (data not shown). Based on these observations, an initial estimate for the axial dispersion coefficient D_{ax} was calculated from the second moment σ_{Dex} of the dextran 2000 kDa peak and found to be 1.57 mm^2/s. For the total ionic capacity Λ, a value of 0.69 M was obtained via acid-base titration. All measured and calculated system and column parameters are summarized in Table 3.3.

3.4.2 Transport properties of the grafted anion exchange fibers

In the next step, we studied the efficiency of the fiber column as a function of the mobile phase velocity, to asses whether mass transfer limitations exist that need to be accounted for in a mechanistic column model. These experiments were performed under non-binding conditions with NaCl and three proteins with different MWs, i.e. insulin, bovine serum albumin (BSA), and glucose oxidase (GO). The same set of experiments was carried out on a Poros 50HQ column. Poros 50HQ is a perfusive resin, and was chosen for comparison as it can be operated in the same flow rate range as the fibers. Fig. 3.2 shows the obtained HETP profiles for the resin (cf. Fig. 3.2A) and the fibers (cf. Fig. 3.2B). For Poros, distinct plate height levels were observed for each molecule with NaCl having the lowest HETPs and GO having the highest HETPs. For all molecules, plate heights increased with increasing mobile phase velocity, indicating reduced column efficiency at higher velocities. This increase was strongest for the largest molecule GO and weakest for the smallest molecule NaCl,

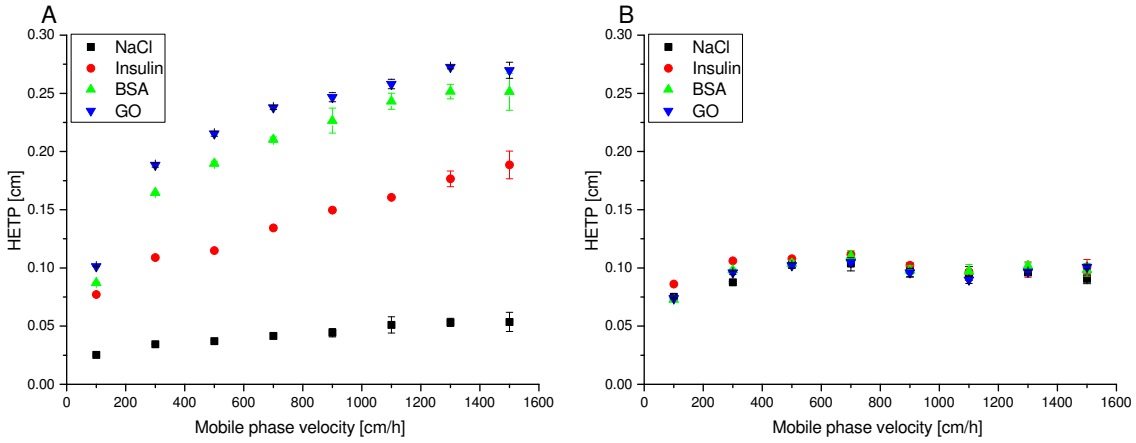

Figure 3.2: Effect of mobile phase velocity on the HETPs for NaCl, Insulin, BSA, and GO under non-binding conditions evaluated on (A) a Poros 50HQ column and (B) a column randomly filled with the hydrogel grafted anion exchange fibers used in this study.

suggesting different extents of mass transfer limitations. While plate heights increased nearly linearly for NaCl an increasing curvature in the HETP profiles was observed for the larger molecules, in particular GO. In contrast to Poros no strong differences in plate heights for different molecules were observed for the fibers. At most velocities plate heights for NaCl were the lowest, but those were generally always higher than for Poros, which points at a better efficiency of Poros for smaller molecules. With increasing flow velocity plate heights increased initially up to 500 cm/h and remained nearly constant thereafter at about 0.1 cm.

3.4.3 Modeling of column hydrodynamics

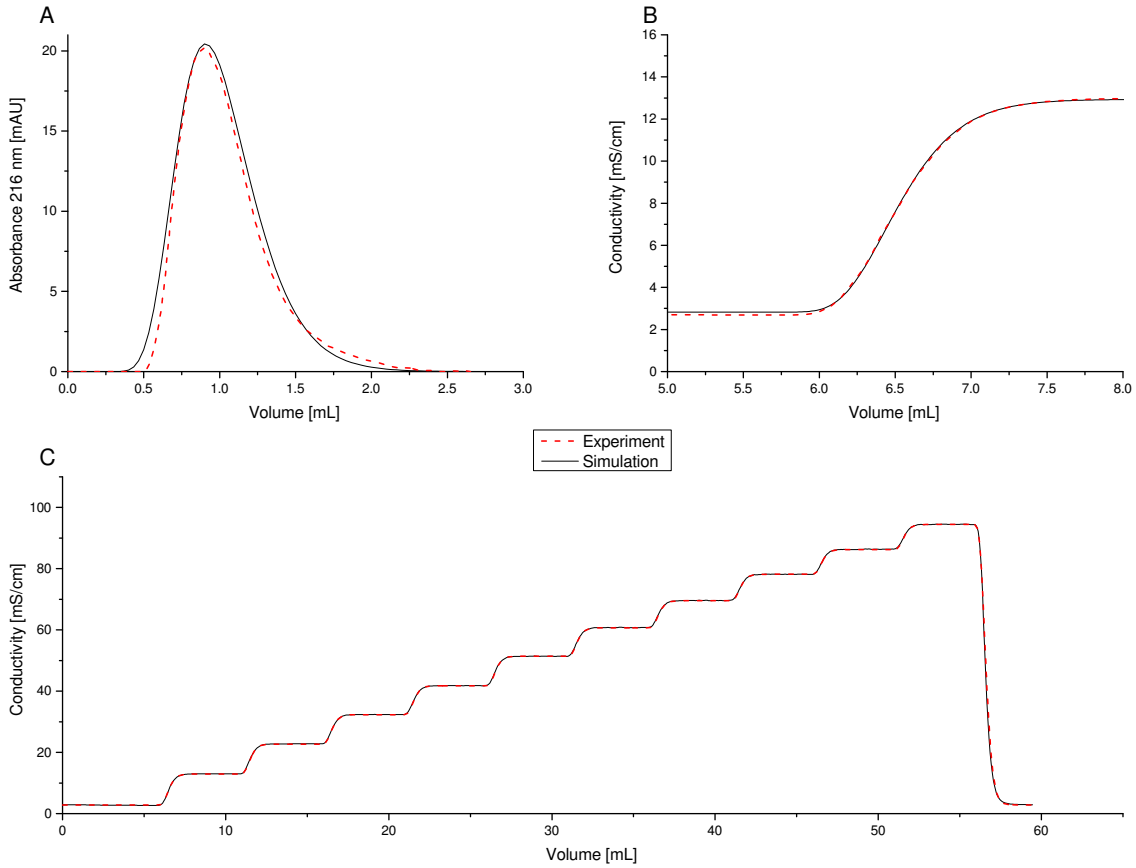

Figure 3.3: Comparison of experimental (dashed lines) and simulated (solid lines) chromatograms for the fiber column for (A) pulse experiments with dextran 2000 kDa, (B) a 100 mM salt step, and (C) a series of salt step transitions from low salt buffer to high salt buffer. (B) is a close-up of the first salt step of (C).

In summary, the characterization and efficiency experiments revealed a limited intra-fiber porosity and a limited but comparatively small impact of mass transfer resistances. Based on these observations we evaluated different mechanistic models

and developed a model for the grafted anion exchange fibers, which accounts for the fiber porosity and mass transfer resistances. Details of the model can be found in Section 3.2. To evaluate the model it was tested whether it can accurately account for experimental band profiles of non-retained molecules. First, we tested whether the model can capture the axial dispersion in the fiber column. Values for D_{ax} from moment analysis typically only provide limited accuracy [106]. Therefore, the dextran pulse injection data was used to determine D_{ax} via chromatogram fitting. The results are displayed in Fig. 3.3A. Using the estimated D_{ax} of $1.19 \pm 0.07\ mm^2/s$, good agreement was found between the simulated UV signal and the measured UV signal. Peak retention volume, peak width and peak tailing were matched. Next, it was tested whether salt transitions, involving exchange with the fiber pores, can be accurately described with the model. For this purpose a series of step transitions from low salt buffer to high salt buffer was performed and used to determine the effective mass transfer coefficient of NaCl via chromatogram fitting (cf. Fig. 3.3B-C). Fig. 3.3B shows the comparison between the measured and simulated conductivity traces for the 100 mM salt step. The simulation was performed with the D_{ax} value obtained from the dextran peak, and the estimated $k_{eff,NaCl}$ of $1.34 \cdot 10^{-3}\ mm/s$. The simulated conductivity trace closely resembled the measured one and peak start, peak end, and curvature were matched. This was observed for the entire series of step transitions, which is displayed in Fig. 3.3C.

3.4.4 Modeling of protein binding and elution

To investigate whether protein binding to, and elution from the grafted anion exchange fibers can be modeled, breakthrough experiments and linear gradient elution (LGE) experiments were performed with the three proteins that had been used in the efficiency experiments. Insulin, BSA, and GO were used because their MWs cover the range of MWs of the majority of current biotherapeutics. For the binding model, the SMA isotherm was chosen as it takes the influence of counter ions into account.

Table 3.4: Estimated mass transfer coefficients and isotherm parameters with 95% confidence intervals for the three proteins and the anion exchange fibers used in this study.

	Insulin	BSA	GO
k_{eff} (mm/s)	$1.13 \cdot 10^{-3} \pm 6.23 \cdot 10^{-5}$	$9.81 \cdot 10^{-4} \pm 5.82 \cdot 10^{-5}$	$8.93 \cdot 10^{-4} \pm 4.71 \cdot 10^{-5}$
k_{kin} (sM^{ν})	$7.75 \cdot 10^{-4} \pm 3.70 \cdot 10^{-5}$	$1.15 \cdot 10^{-7} \pm 2.60 \cdot 10^{-8}$	$1.36 \cdot 10^{-7} \pm 2.61 \cdot 10^{-8}$
k_{eq} $(-)$	$2.19 \cdot 10^{-2} \pm 5.26 \cdot 10^{-4}$	$1.57 \cdot 10^{-4} \pm 1.80 \cdot 10^{-5}$	$1.21 \cdot 10^{-4} \pm 1.63 \cdot 10^{-5}$
ν $(-)$	3.79 ± 0.01	6.33 ± 0.07	6.44 ± 0.04
σ $(-)$	36.79 ± 0.04	353.55 ± 1.08	1312.66 ± 1.75

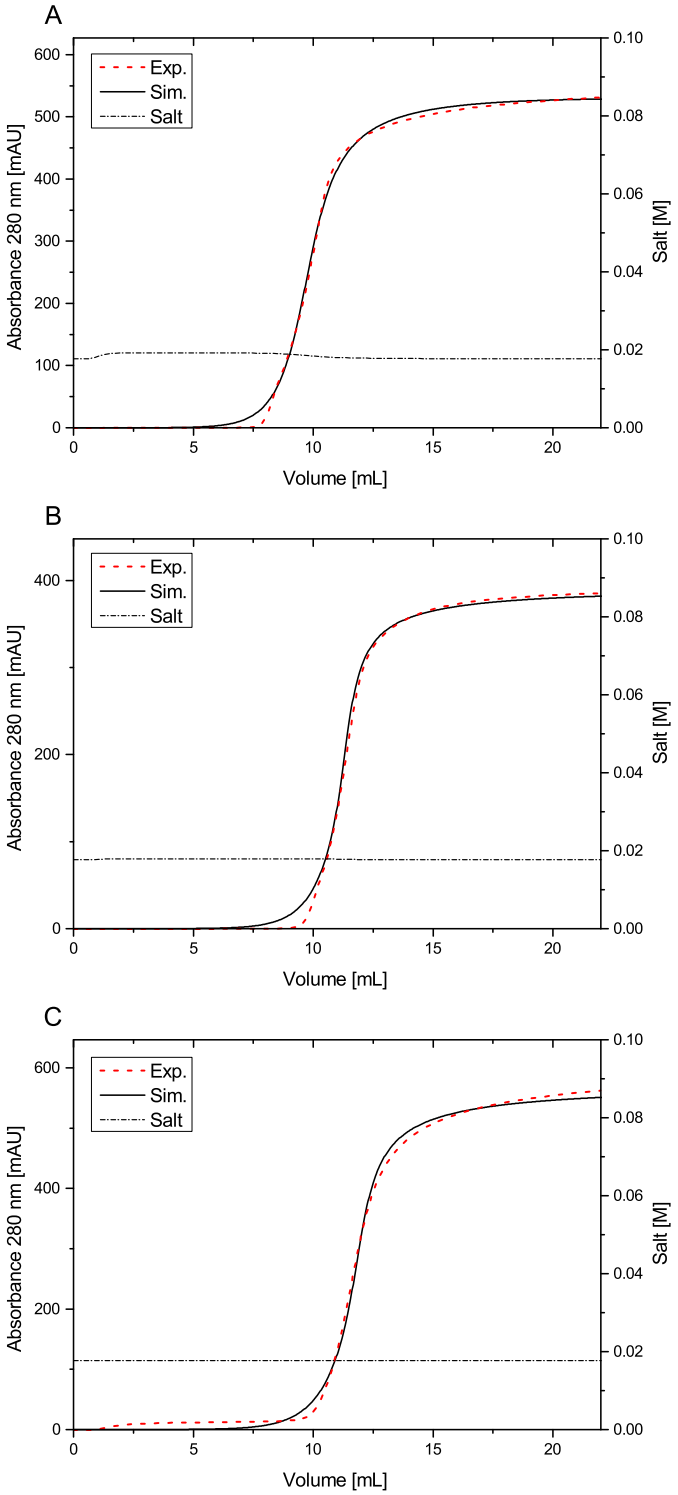

Figure 3.4: Comparison of experimental (dashed lines) and simulated (solid lines) chromatograms for breakthrough experiments on the fiber column with (A) insulin, (B) BSA, and (C) GO. Dotted lines represent the simulated salt profiles at the column outlet. Flow rate: 1 ml min^{-1}. Protein concentrations: 2 g/L.

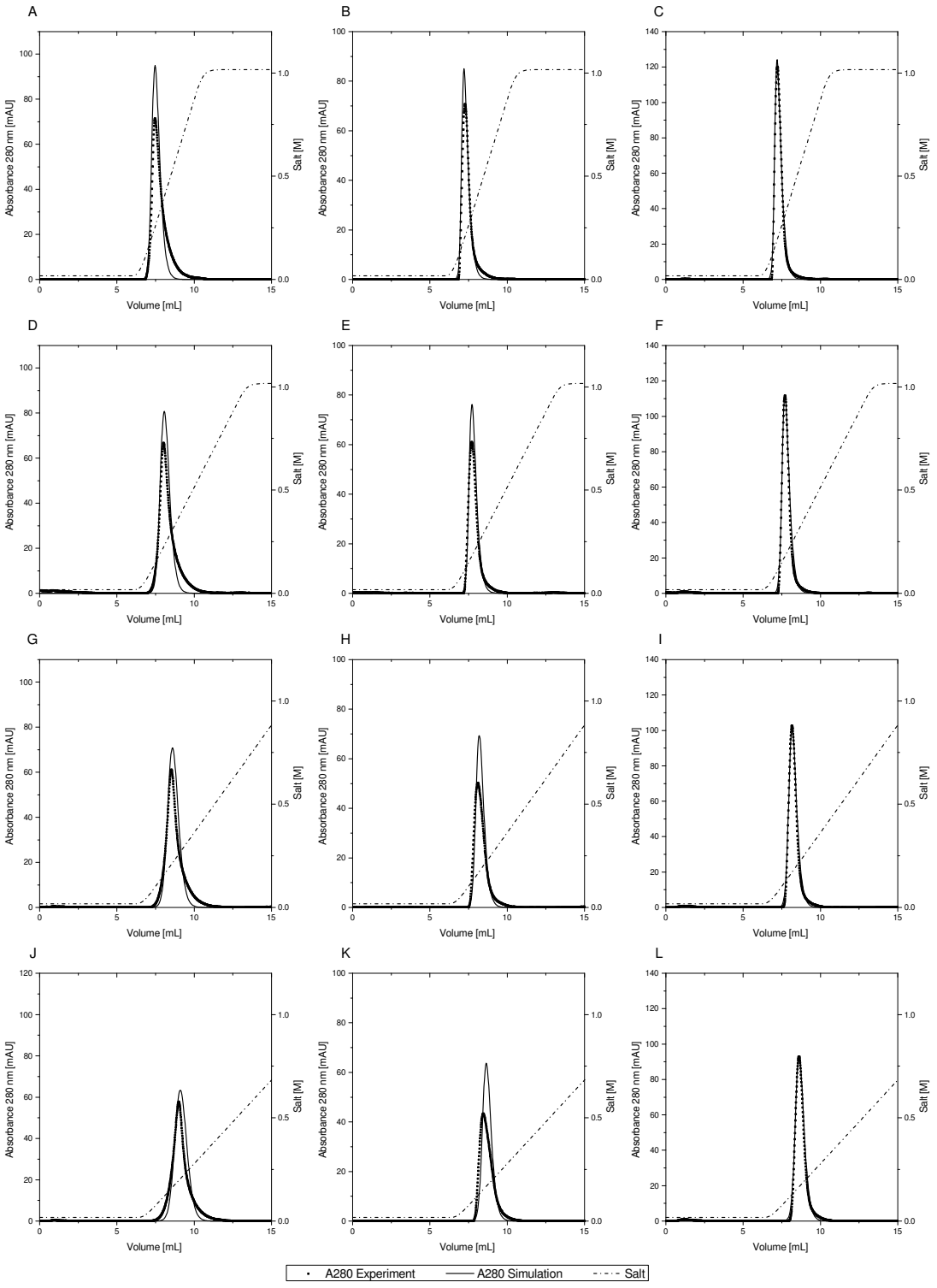

Figure 3.5: Comparison of experimental (squares) and simulated (solid lines) chromatograms for linear gradient elution experiments on the fiber column for (A-C) 3CV, (D-F) 5 CV, (G-I) 7 CV, and (J-L) 9 CV gradients from 0-1 M NaCl for (A,D,G,J) insulin, (B,E,H,K) BSA, and (C,F,I,L) GO. Dot chain lines represent the simulated salt profiles at the column outlet. Flow rate: 1 ml min^{-1}. Protein concentrations: 2 g/L.

The applicability of this isotherm for adsorbents with grafted hydrogel layers has already been demonstrated for membrane adsorbers [53, 115]. The SMA isotherm parameters for each protein were estimated from the breakthrough and LGE data, via chromatogram fitting.

All estimated parameters and estimates for their confidence intervals are summarized in Table 3.4. The characteristic charges increased with increasing protein net charge. The equilibrium constants increased with increasing elution volume in the LGE experiments. Shielding parameters were correlated with the proteins' molecular weights. The estimated effective mass transfer coefficients were on the same order of magnitude and smaller than the k_{eff} obtained for NaCl. Values for k_{eff} decreased with increasing molecular weight and radius. All model parameters were well defined with average confidence estimates of 2.6%, 8.3% and 7.7% for Insulin, BSA and GO.

The experimental and simulated breakthrough curves for the three proteins are shown in Fig. 3.4. The model accurately accounted for the breakthrough behavior of all three proteins, and the overall slopes of the breakthrough curves were well-matched. Volumes typically considered for the analysis of breakthrough curves and column hardware design, such as the volumes corresponding to 10%, 50%, or 80% breakthrough were closely matched. The relative offsets for the volumes at 10% breakthrough were 0.6% for insulin, 2.2% for BSA, and 2.1% for GO.

The fits for the LGE experiments for insulin, BSA and GO are displayed in Fig. 3.5. In all cases, a good agreement was found between the measured and simulated retention volumes and peak widths. The conformity between measurements and simulations was highest for GO and the model accounted well for the peak heights in all gradients. The model slightly overestimated the peak heights of BSA and insulin for the longest respectively shortest gradients, but for the other gradients peak heights were reflected.

3.4.5 Model discrimination

The developed model for the grafted anion exchange fibers accounted for both binding kinetics and mass transfer effects. This choice was based on the characterization and efficiency data, and will be discussed in Section 3.5.3. To confirm this approach and to verify if both of these mechanisms are required for modeling of the grafted anion exchange fibers, we assessed whether the experimental data could be fitted to models that neglect mass transfer effects or binding kinetics. Such models have been used for hydrogel grafted membrane adsorbers (cf. Section 3.2.4).

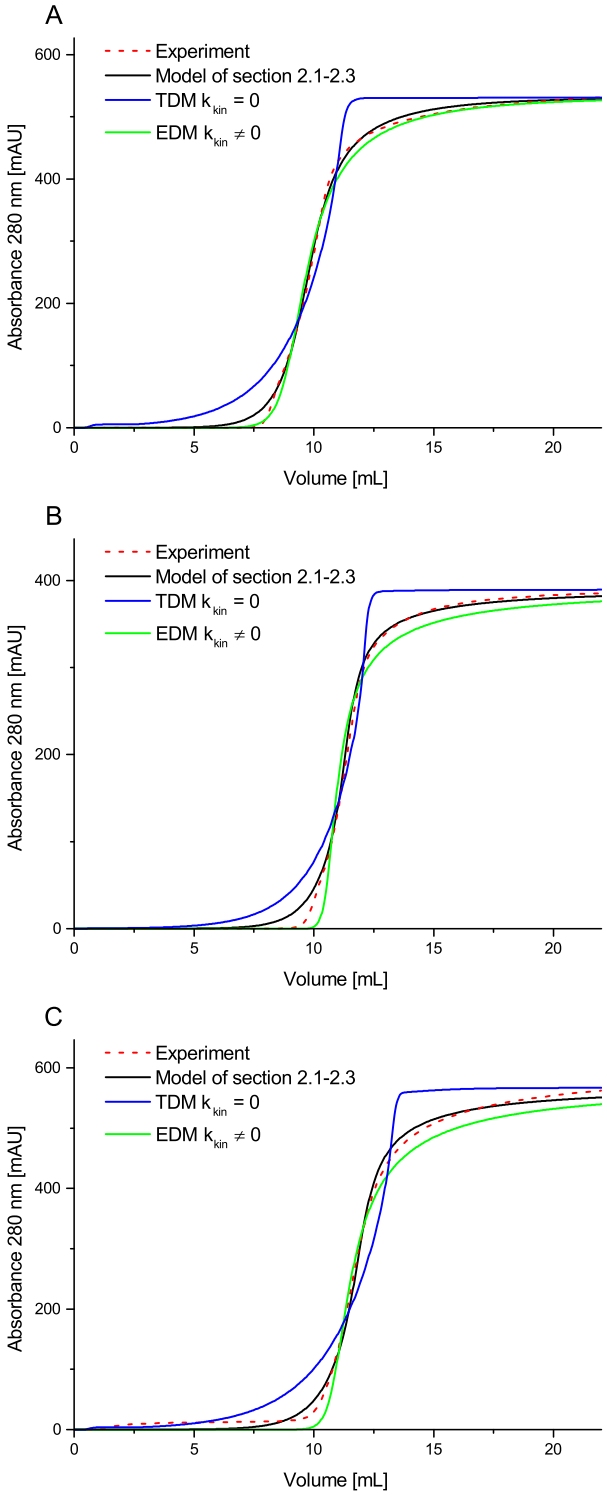

Figure 3.6: Comparison of experimental (dashed lines) and simulated (solid lines) breakthrough curves for different models of the anion exchange fiber column. Proteins: (A) insulin, (B) BSA, and (C) GO . Flow rate: 1 ml min^{-1}. Protein concentrations: 2 g/L.

Table 3.5: Sum of squared residuals for the mechanistic model of the anion exchange fibers developed in this study and alternative mechanistic models.

	Insulin	BSA	GO
Model of Section 2.1-2.3	0.32	0.35	0.13
TDM $k_{kin} = 0$	1.91	1.81	2.03
EDM $k_{kin} \neq 0$	0.44	0.83	0.42

Fig. 3.6 display both the experimental breakthrough curves, and the simulated breakthrough curves for the different models considered. The sums of the squared residuals that were obtained when the different models were fitted to the experimental data are summarized in Table 3.5. The residuals are normalized to the absorption of the load material to account for the different extinction coefficients and molar inlet concentrations of the three proteins. The best representation of the experimental data was achieved with the model that has been described above, which accounts for mass transfer effects and binding kinetics. Models with infinitely fast binding kinetics (TDM $k_{kin} = 0$) predicted breakthrough curves with shallower initial ascents and steeper final transitions towards the inlet concentrations than in the experimental breakthrough curves. This could not be compensated via refitting of the remaining isotherm or mass transfer parameters. The summed residuals for these models were 5.2-15.6 times larger than for the models with binding kinetics. When mass transfer effects were neglected and the experimental data was fitted to an equilibrium dispersive model with binding kinetics (EDM $k_{kin} \neq 0$), breakthrough curves with very steep initial breakthroughs were obtained. This could not be resolved by adjustment of the isotherm parameters. The summed residuals for these models were smaller than for the models without binding kinetics, but 1.4-3.2 times larger than the ones for the model with mass transfer effects.

3.5 Discussion

First the results of the characterization and efficiency experiments will be discussed with respect to available data on fiber stationary phases. This discussion will serve to evaluate whether the presented model might be applicable to other fiber stationary phases. Next, the model choice will be addressed and possible alternatives will be discussed. Finally, the estimated model parameters will be discussed with respect to the characterization and literature data, and possible reasons for deviations between simulations and experiments will be addressed.

3.5.1 System and column characterization

The determined porosities for the grafted fibers are in line with the fiber packing density and the degree of grafting (DG). The packing density of 0.3 g dry fibers per mL CV and the DG of 15% correspond to a packing density of the polyamide 6 (PA6) support fibers of 0.26 g/mL CV. With the density of PA6 of 1.14 g/cm^3 [95], a theoretical void fraction of 0.77 can be calculated. This is close to the experimentally determined ε_t of 0.81. The minor difference might be due to a limited degree of porosity of PA6. This has been reported by others for another type of PA6 fibers [72] and was also observed by us when we performed experiments with the unmodified support fibers, which revealed a fiber porosity ε_f of 0.16. Another possible explanation of the difference could be swelling of the PA6 fibers in buffer, yet the moisture absorption of PA6 is very low and only on the order of a few percent [95]. The limited porosity of the grafted fibers of $\varepsilon_f = 0.37$ is consistent with the DG and a limited degree of internal porosity. The observed size dependent accessibility of the grafted hydrogel layer with exclusion of large dextrans matches with the reports of others for grafted membrane adsorbers [124] and grafted fibers [83].

When comparing to other types of stationary phase materials it can be stated that the bed structure of the grafted fiber column is similar to the bed structures that have been reported for membranes [124] and monoliths [125]. All are characterized by higher interstitial porosities and smaller particle porosities than conventional resins. The particle porosity of the grafted anion exchange fibers is higher than the intrafiber porosities of 0.2 that have been determined for non-functionalized fibers [71] or directly functionalized anion exchange fibers [74]. While this depends on polymer and probe molecule, a much higher value of 0.94 has recently been reported with acetone for porous GMA-grafted anion exchange fibers [79]. The interstitial fraction ε of 0.70 is at the high end of the range of values of 0.4-0.7 that have been reported in the literature. In general this parameter strongly depends on the fiber packing density. The majority of studies on fibers have focused on analytical applications, where packing densities greater than 0.3 g/m CV have been used. For preparative applications, lower packing densities are preferred as this results in lower pressure drops. This is supported by the high permeability of the grafted fiber column. In summary, the determined porosities and the determined bed structure seem plausible from the available literature. This also holds for the TIC of 0.69 M per L skeleton which corresponds to a TIC of 0.14 M per L CV. This is in the range of ionic capacities of 0.08-0.3 M reported for anion exchange resins [126].

3.5.2 Transport properties of hydrogel grafted anion exchange fibers

The efficiency experiments were conducted in order to assess the relative impact of mass transfer resistances. This was used to develop a suitable mechanistic model for the grafted fibers. Poros 50HQ was chosen for comparison as detailed efficiency data is available for this resin [127] and the corresponding cation exchanger [128]. The efficiency trends observed for Poros 50HQ in this study are in line with the data presented by Staby et al. [127] and Wu et al. [128]. Both studies reported increasing plate heights with increasing molecule size. When plotted in reduced form, the data for insulin yields a straight line as has been reported for the small proteins aprotinin [127] and lysozyme [128]. In contrast to this, we observed some curvature in the efficiency plots for the larger molecules, in particular GO. This matches with the data for IgGs in the aforementioned studies. The authors attributed this to a shift from diffusion-limited transport within micropores to convection-limited transport within flowthrough-pores [128]. This was particularly evident for even larger molecules such as thyroglobulin or virus-like particles. For these molecules distinct plateaus with HETPs on the order of 1 cm were reported for interstitial flow rates greater than 1800 and 500 cm/h respectively. For the grafted fibers a flattening of the HETP plots was observed for the molecules tested at interstitial flow rates of about 700 cm/h with HETPs in the range of 0.09-0.11 cm. This indicates that mass transfer resistances exist for the grafted anion exchange fibers, but that the overall impact on efficiency is limited. This fits with the efficiency data that has been reported for fiber stationary phases [74, 79, 86]. When comparing the different datasets, the change in efficiency with flow rate observed in this study is larger than what has been observed for fibers with very limited porosity, but smaller than what has been observed for porous fibers. This suggests that the grafting of the fibers results in slightly increased mass transfer resistance.

3.5.3 Model choice

The development of our model was based on the characterization and efficiency experiments and an evaluation of criteria that have been used in the literature for model selection. As the experiments pointed at limited, but non-negligible mass transfer resistances, we chose to use a transport-dispersive model, which includes the specific surface area (SSA) available for transfer and a lumped effective mass transfer coefficient. The advantage of this approach is that it takes the fiber composition into account and can be used to determine the rate of exchange between the interstitial phase and the fibers, while not requiring a description of the fiber geometry. It can be used even if no information on the SSA of the fibers is available if $k_{eff}a_f$ is combined into a single factor. Alternatively, a_f can also be factored out to represent

different fiber geometries. The model might thus be be useful if fibers with different geometries or different SSAs are to be compared or if fibers of the same type with different hydrogels, prepared e.g. via controlled grafting techniques [83], are to be analyzed.

A limitation of using lumped rate mass transfer coefficients is that film and pore diffusion effects are not separated. If this was of interest, a general rate model (GRM) [106] would have to be used. This would require to define the relevant characteristic lengths for film diffusion and pore diffusion. This would also be necessary if an appropriate mechanistic model was to be selected on the basis of comparisons between the characteristic times of different transport phenomena. In both cases the random, irregular structure of the fiber bed and the complex structure of the fibers would have to be approximated. As pointed out by Detobel and Desmet for monoliths [129], which also possess a random irregular bed structure, different possibilities exist for the geometrical distribution of interstitial and particle volumes. The interstitial volume could be partitioned into cylindrical through-pores with an SSA equal to the SSA of the fibers. This results in a pore diameter of 5.4 μm. Alternatively an equivalent pore diameter could be calculated from the permeability of the fiber bed, which would require a measurement or an estimate for the tortuosity. If a tortuosity value for membranes is used [124] a pore diameter of 14.6 μm can be calculated. Similar possibilities exist for the fibers. Effective particle diameters could be calculated from the permeability data, which results in diameters of $7.7 - 15.4$ μm [130], or the elliptical cross-section of the fibers with channels could be converted to a cylinder with equivalent SSA. This leads to a diameter of 2.3 μm. Alternatively the average thickness of the projections could be used, as suggested for monoliths [129], or the thickness of the hydrogel layer. The thickness of the hydrogel layer could be approximated from the accessible volume fraction of excluded and fully penetrating tracers [83]. This results in a thickness of 140-211 nm, depending on whether the porosity of the PA6 support is taken into account or not. This supports the assumption that the channel structure of the fibers is maintained.

Depending on which of these conventions is adopted, different effective lengths for mass transfer result. These can be used in conjunction with literature correlations for mass transfer, to determine the characteristic times for different transport phenomena and exclude certain processes. On this basis film diffusion has often been neglected in models of grafted membrane adsorbers. With the through-pore diameters calculated above, this would also be justified for the grafted fibers, as film diffusion would be much faster than convection. However, for fast binding kinetics as in ion exchange chromatography, film diffusion and pore diffusion could still limit the rate of binding [117]. This was observed by Gebauer et al. [131], who reported that a pore diffusion model could best describe the breakthrough curves on an ion-exchange membrane

grafted with a hydrogel layer similar to the one in our study. Thus, we chose to use an effective mass transfer coefficient and a model with binding kinetics, as it could not be ruled out that the kinetics of binding are faster than the kinetics of film diffusion for the range of possible through-pore diameters.

3.5.4 Modeling of column hydrodynamics

One of the key questions related to modeling of the grafted fiber stationary phase was whether the convection through and the dispersion inside a randomly packed bed of fibers can be accurately described with typical approaches for a 1D rate model of chromatography. The results presented for the combination of a plug flow reactor to account for system hold-up volumes and an axial dispersion coefficient to account for dispersion inside the fiber bed, suggest that this is possible. The estimated D_{ax} of 1.19 mm^2/s is relatively large, but in line with axial dispersion coefficients that can be calculated from the plate height data of other fiber stationary phases. From the data of Yang et al. [69] and Hamaker et al. [74] axial dispersion coefficients of 16.5 mm^2/s and 0.7 mm^2/s can be calculated for the excluded molecules PEG 20000 and BSA. From the data of Wang et al. an axial dispersion coefficient of 1.57 mm^2/s can be calculated for thyroglobulin [63]. This suggests that larger dispersion coefficients are a common feature of fiber stationary phases. The large value for the grafted fibers might be due to the irregular shape of the fibers with a very large ratio of length to cross-section. This is supported by general studies on the impact of particle shape on dispersion in packed beds, which found that dispersion decreases with increasing particle sphericity [132]. The random packing of the fibers might also lead to more axial dispersion, as it results in different orientations of the fibers with respect to the direction of flow, which favors different flow paths.

Improvements in the presented model could be made if a system dispersion model would be added. This was considered, since system dispersion contributes to the estimated D_{ax}. In general, system dispersion models have been used for large column diameter-to-length ratios and situations where the hold-up volume is on the order of the bed volume. This was not the case here. The contribution of system dispersion to overall dispersion was below 5% as judged by a comparison of the σ^2 with and without column. As the determined D_{ax} was in the range of values that have been reported for fiber stationary phases and retention time, peak width, and tailing of the dextran peak were accounted for by the presented model, no additional dispersion elements were included. This is supported by the data for the NaCl step transitions, which could be well described with the determined D_{ax} over the entire concentration range that was considered.

3.5.5 Modeling of protein binding and elution

The TDM captured the binding, breakthrough and elution of the three proteins considered when it was combined with a kinetic SMA isotherm. The estimated isotherm parameters are reasonable and agree with the underlying assumptions of the SMA isotherm and the proteins' physical data. Larger proteins are expected to shield more binding sites, and characteristic charges are expected to increase with distance to the protein's pI. This was the case for all three proteins. The desorption rate constant k_{des} is exponentially correlated with a proteins characteristic charge, so that for smaller characteristic charges smaller k_{des} and hence larger k_{kin} values should be expected. This was also observed in this study. The lack of fit for the models that neglect binding kinetics, suggest that finite binding kinetics are required in order to describe the binding of proteins onto the hydrogel grafted fibers. This has been observed for other types of hydrogel grafted ion-exchange adsorbents. As the binding in such material is mostly confined to the dense and highly charged hydrogel layer, both electrostatic effects and steric factors play a role and affect the accessibility of ligands and consequently the rate of adsorption [46]. Initially electrostatics may favor fast adsorption rates, while with increasing protein binding, electrostatic repulsion [46] and steric crowding may limit the access to binding sites [133]. Despite being finite, the determined kinetic parameters still indicate fast binding kinetics as the effect only becomes rate-limiting for the breakthrough curves at high stationary phase loadings.

With the estimated parameters the adsorption rates are initially faster than the effective mass transfer rates. This supports the initial considerations for model selection and explains why later and steep breakthrough curves have been observed when mass transfer effects were neglected. The lack of fit for these models suggests that mass transfer effects cannot be neglected for the grafted anion exchange fibers. The estimated effective mass transfer coefficients were finite with confidence estimates in the range of 5.3-9.6% and trended with molecular size. Since lumped mass transfer coefficients were used, both external film and internal pore diffusion processes contribute to the estimated mass transfer coefficients. If pore diffusion effects are neglected and the determined k_{eff}s are considered to be only comprised of external film diffusion, literature correlations for external mass transfer [134] would predict film mass transfer coefficients k_f as the ones estimated for spheres with a diameter of 100 μm or cylinders with a diameter of 67 μm. This is outside of the range of particle diameters or through-pore diameters that were calculated above. For these diameters, correlations predict values for k_f that are one to two orders of magnitude larger than the estimated k_{eff}s. This suggests that internal mass transfer resistances define the estimated k_{eff}s. If this were to be taken into account and film and pore diffusion effects were to be separated in a general rate model, one could account for conditions were both processes are rate-limiting. This is likely to occur during initial

breakthrough, were both processes might be slower than the adsorption kinetics. Thus with a GRM the minor offsets in the initial phase of breakthrough ($< 5\%$ breakthrough) could be solved.

For insulin and BSA slight offsets in the peak heights in the LGE experiments were observed. This could be due to additional species that were present in the load material, as both proteins are known to dimerize in solution. These could be separated in longer gradients, resulting in lower peak heights. The opposing trend for insulin could be due to additional interactions with the matrix, as insulin is small and hydrophobic in nature and could interact with the polyamide matrix. Another reason might be structural changes in the grafted hydrogel layer as the ionic strength is increased. This would change the determined porosities and mass transfer coefficients.

3.6 Conclusions

Several recent experimental studies have highlighted the potential of fiber-based adsorbents for high-capacity and high-throughput bioseparations. In this study we developed a mechanistic model for these materials. For this purpose, short hydrogel grafted anion exchange fibers with extended surface were randomly packed into laboratory scale chromatography columns. Key structural model parameters of the resulting fiber bed were determined from standard column characterization experiments. Comparative efficiency experiments provided valuable insights into relevant mass transfer phenomena. This data was used in conjunction with criteria for model selection to develop a suitable mechanistic model. The developed model, a transport-dispersive model with lumped mass transfer coefficients, accounted well for the hydrodynamics inside the fiber column. When combined with a kinetic SMA isotherm, it accurately described the breakthrough and elution behavior of three proteins ranging from 6-160 kDa in size, and this resulted in finite and well-defined mass transfer and isotherm parameters. The developed model reproduced the experimental data better than models that neglect mass transfer effects or binding kinetics.

In conclusion, this study shows, for the first time, that fiber-based adsorbents can be modeled mechanistically and that the required model parameters can be determined reliably from a few experimental column runs. This was demonstrated for three proteins ranging from the size of insulin to the size of monoclonal antibodies, and should thus be applicable to a number of industrially relevant molecules. For the hydrogel grafted fibers used in this study, the best results were obtained with a

transport-dispersive model. Axial dispersion, film and pore mass transfer, and binding kinetics were identified as the relevant transport and binding mechanisms for this type of fiber stationary phase. The advantage of the presented TDM is that it is flexible and can be used with or without a description of the fiber geometry, while taking the mass transfer between the interstitial phase and the fibers into account. Thus, we think that the model should be applicable to a number of fiber-based adsorbents and could also be useful for the study of novel fiber formats such as area enhanced or hydrogel optimized fibers. Depending on the fiber structure, simpler models could be used, which have been described in the study, or the presented model could be extended towards a general rate model, which has been discussed as well.

Apart from being useful for the optimization of fiber-based adsorbents and fiber-based adsorbent bed structure, the immediate benefit of the presented model for fiber-based adsorbents is that it can be used for development and optimization of processes on fiber-based adsorbents, and thus can support the experimental efforts that are already ongoing. Future work will be directed at investigating the performance of the presented model under different operating conditions and applying the model towards separation problems that are typically encountered in industry.

Acknowledgments

The authors gratefully acknowledge material supply by Sartorius Stedim Biotech (Jan Schwellenbach, Florian Taft, Louis Villain) and the financial support from the German Federal Ministry of Education and Research (BMBF) under the reference number 13N13321. The authors bear the complete responsibility for the content of this publication. The authors declare no conflict of interest.

4 High throughput screening of fiber-based adsorbents for material and process development

Johannes Winderl[1], Stephan Bürkle[1], Jürgen Hubbuch[1]

[1] Institute of Engineering in Life Sciences, Section IV: Biomolecular Separation Engineering, Karlsruhe Institute of Technology (KIT), Karlsruhe, Germany

Abstract

There has been a growing interest in fibers and fiber-based adsorbents as alternative adsorbents for preparative chromatography. While the benefits of fiber-based adsorbents in terms of productivity have been highlighted in several recent studies, microscale tools that enable a fast characterization of these novel adsorbents, and an easy integration into process development workflows, are still lacking.

In the present study an automated high-throughput screening (HTS) for fiber-based adsorbents was established on a robotic liquid handling station in 96 well filter plates. Two techniques – punching and weighing – were identified as techniques that enabled accurate and reproducible portioning of short-cut fiber-based adsorbents. The impact of several screening parameters such as phase ratio, shaking frequency, and incubation time were investigated and optimized for different types of fiber-based adsorbents. The data from the developed HTS correlated with data from packed fiber columns,

and binding capacities from both scales matched closely. Subsequently, the developed HTS was utilized to optimize the hydrogel structure of anion exchange (AEX) fiber-based adsorbent prototypes. A novel AEX fiber-based adsorbent was developed that compared favorably with existing resin and membrane adsorbents in terms of productivity and DNA binding capacity. In addition, the developed HTS was also successfully employed in order to identify step elution conditions for the purification of a monoclonal antibody from product- and process-related impurities with a cation exchange (CEX) fiber-based adsorbent. Trends from the HTS were found to be in good agreement with trends from lab scale column runs.

The tool developed in this paper will enable a faster and more complete characterization of fiber-based adsorbents, easier tailoring of such adsorbents towards specific process applications, and an easier integration of such materials into processes. In comparison to previous lab scale experiments, material requirements are reduced by a factor of 3-40 and time requirements are reduced by a factor of 2-5.

4.1 Introduction

The field of biopharmaceutical downstream processing is currently faced with many challenges [8]. Increasing demand for biopharmaceuticals and increasing titers in upstream processing call for increases in productivity and throughput of downstream operations. Competition within major therapeutic areas and competition from biosimilars lead to a pressure to reduce process development times and processing costs. At the same time processes have to be optimized to meet quality and cost targets, while regulatory requirements also call for a better process and quality understanding.

These challenges apply in particular to chromatographic unit operations which form the core of most current downstream processes. Although alternatives to chromatography have been put forward [56, 135], the vast majority of downstream processes are composed of two to four chromatography steps. Typically these are executed in batch mode in a packed bed format with spherical, porous adsorbent particles. However this approach suffers from a limited throughput as high pressure drops and diffusional limitations that are associated with these adsorbents restrict the productivity . Thus, to meet the challenges in chromatography and downstream processing, improved or alternative adsorbents are required. To capitalize on the benefits of such adsorbents, a seamless integration into process development workflows and manufacturing must be ensured, and an understanding of the factors that affect their performance must be established.

Among alternative adsorbents, fiber-based adsorbents have recently attracted much attention [57, 76, 80, 83, 136, 137]. New techniques for the manufacture of high surface area fibers [62] and for the surface modification [76, 83] of such fibers have made it possible to develop high capacity and low pressure drop fiber-based adsorbents. Several fold increases in productivity have been reported for such adsorbents [80] for the purification of model proteins. The very low costs of fibers may enable the use as disposables. In addition, with controlled grafting schemes [83], fiber-based adsorbents could be tailored towards specific process applications, with possible further benefits in terms of process performance.

However, this has only been demonstrated for model proteins and artificial protein mixtures. No studies have been published which describe the integration of such materials into actual processes or process steps. Currently, both the development of these materials and of processes employing these materials rely on time-consuming and material-intensive laboratory-scale experiments which often involve many manual steps. In published studies [138] and patents [136, 139] fiber-based adsorbent properties such as static binding capacities have been determined via manual batch binding experiments with 14-200 mg of adsorbent in 5-15 mL of liquid or via frontal analysis experiments on packed fiber columns [76, 79] or cartridges [80]. Process development for model protein separations has also been carried out in laboratory-scale columns [76, 79, 87] or cartridges [80, 105, 137, 140] with geometric column volumes of up to a few mL. While such approaches may be feasible for initial characterization experiments and studies with model proteins, they are much less applicable to material development for and process development with real process feeds, where material and time are typically scarce, in particular during early stages of process development. With the higher capacities that new fiber-based adsorbents offer, more material is also required for realistic process challenges.

High-throughput (HT) microscale tools for the characterization of fiber-based adsorbents and for the development of processes that utilize fiber-based adsorbents are lacking. Such tools are well established for traditional chromatography adsorbents such as resins [32, 33] or membranes [38]. For these adsorbents HT formats which are based on microtiter filter plates, prepacked miniature columns, prepacked pipette tips, and lately also microfluidic devices [35–37] have been developed. Numerous examples for the application of such systems towards material and process development have been presented [32]. For instance, such systems have been used to screen different ligands [37, 141] and resins with respect to binding capacities, or to determine the impact of process conditions, such as buffer compositions, protein concentrations [142, 143], and flow rates [144] on process performance. While each of the four formats has its advantages and disadvantages they all have benefits over laboratory scale column experiments. The key benefits are lower material requirements and time savings, resulting in reduced development cost. Due to parallelization a larger parameter

space can be explored with higher chances to reach an optimal process. In addition the automation that these formats offer results in less error prone manual handling steps. Thus it is desirable to implement such methods for fiber-based adsorbents in order to enable a fast characterization of these materials and the integration into processes.

In this study an automated high throughput screening (HTS) for fiber-based adsorbents on a robotic liquid handling station was developed. The first part of this paper describes the setup and optimization of the screening system. Then a comparison of the HTS data with data from laboratory scale experiments is presented. Finally two case studies demonstrate the application of the HTS for material and process development.

4.2 Experimental

4.2.1 Materials

4.2.1.1 Chemicals, Buffers and Proteins

Potassium dihydrogen phosphate, tris(hydroxymethyl)aminomethane (Tris), potassium chloride (KCl), sodium chloride (NaCl), hydrogen chloride (HCl), acetic acid, citric acid monohydrate, sodium hydroxide (NaOH) and ethanol (EtOH) were purchased from Merck (Darmstadt, Germany). Dipotassium phosphate, and potassium phosphate were obtained from VWR International (Darmstadt, Germany). Sodium hydrogen phosphate, lysozyme from chicken egg white (Lys, no. L6876), and bovine serum albumin (BSA, no. A3294) were from Sigma-Aldrich (St. Louis, MO, USA). 3-morpholinopropane-1-sulfonic acid (MOPS) was from Carl-Roth (Karlsruhe, Germany), and succinic acid as well as 2-(N-morpholino)ethanesulfonic acid (MES) monohydrate were from AppliChem (Darmstadt, Germany). Hering sperm DNA (HS-DNA, no. D1815) was purchased from Promega (Madison, WI, USA). Harvested cell culture fluid (HCCF) and a protein A eluate from a monoclonal antibody (mAb) process were provided by an established industrial manufacturer. Both contained the same CHO-derived IgG. In the experiments three different buffers were used. For native fibers and for cation exchange adsorbents 10 mM potassium phosphate (KPi) pH 7, and 20 mM multicomponent buffers (MCBs) with pHs of 4.5-6.0 were used. The multicomponent buffers were mixed from low and high pH multicomponent buffers, which were composed of MOPS, MES, acetic acid and succinic acid. The buffer recipes for the MCBs were calculated according to Kröner and Hubbuch [145]

in order to obtain a linear pH gradient with constant buffering capacity from pH 4.5 to 6.0. The experiments with anion exchange adsorbents were conducted with 20 mM Tris buffers at pH 7.5. For analytical Protein A chromatography phosphate equilbration and elution buffers at pH 7.1 and pH 2.6 were used which were composed of sodium chloride (37.3 g/L), potassium chloride (0.2 g/L), potassium phopshate (0.2 g/L) and sodium hydrogen phosphate (1.15 g/L). Analytical size exclusion chromatography was carried out at pH 7 with a phosphate buffer that contained 250 mM dipotassium phosphate and 250 mM potassium chloride. All buffers were prepared with ultra-pure (UP) water (Purelab Ultra, Elga Lab-Water, High Wycombe, UK). The pH was adjusted with HCl or NaOH as needed. Prior to usage the buffers were filtered through 0.2 µm cellulose actetate (CA) membrane filters (Sartorius, Göttingen, Germany) and degassed via sonication. All proteins were dissolved in the appropriate buffers as needed and filtered through 0.2 µm CA syringe filters (Sartorius, Göttingen, Germany). HS-DNA was diluted in 20 mM tris buffer pH 7.5 to the desired concentration.

4.2.1.2 Disposables

For screenings on the liquid handling station (LHS) 1 mL AcroPrep Advance 96-Well Filter Plates with 0.45 µm Supor membranes (Pall, Dreieich, Germany) were used. Buffer and protein solutions were pipetted on the LHS into 1.2 mL round (Thermo Fisher Scientific, Waltham, MA, USA) or 2.2 mL square (VWR International, Radnor, USA) 96 well deep well polypropylene plates. The supernatants from the filter plates were collected in 96 well flat bottom UV-Star microplates or 96 well flat bottom polypropylene plates (both Greiner Bio-One, Kremsmünster, Austria).

4.2.1.3 Stationary phases

Different types of native fibers and fiber-based adsorbents were used in the experiments. For the assessment of possible fiber deposition techniques round microfibers with different diameters (14-100 µm) and lengths (0.25-6 mm) were obtained from Schwarzwälder Textil-Werke (Schenkenzell, Germany). For all other experiments winged shaped polyamide 6 (PA6) and polyethlenterephtalate (PET) fibers (Allasso Industries, Raleigh, NC, USA) and fiber-based adsorbents were used. The fiber-based adsorbents were provided by Sartorius Stedim Biotech (Göttingen, Germany) and were prepared via free radical polymerization (FRP) or surface- initiated atom transfer radical polmerization (SI-ATRP) as described in [83, 146, 147]. Two strong

CEX fiber-based adsorbents were used with hydrogel structures that had been pre-optimized by Sartorius Stedim Biotech. One was prepared via FRP (Fibers FRP S) and the other one (Fibers ATRP S) was prepared via SI-ATRP. In addition a library of 17 different strong anion exchange fiber-based adsorbent prototypes was examined. In these prototypes the chain density, the chain length and the ligand density in the hydrogel layer had been varied via SI-ATRP according to a face centered central composite design. For performance comparisons Q Sepharose Fast Flow resin (GE Healthcare, Uppsala, Sweden) and Sartobind Q membranes (Sartorius Stedim Biotech, Göttingen, Germany) were used.

4.2.1.4 Liquid handling station

The screening experiments were carried out on a Freedom EVO 200 liquid handling station (Tecan, Männedorf, Switzerland). The LHS was equipped with a liquid handling arm (Liquid LiHa) with eight tips, a 96-channel pipetting head (MCA 96), a robotic manipulator arm (RoMa), an orbital shaker (Te-Shake), two microplate stackers (Te-Stack), a centrifuge (Hettich Rotanta RSC 46, Tuttlingen, Germany) and a microplate reader (infinite M200). It was controlled with EVOware 2.5.

4.2.1.5 Chromatographic instrumentation

Lab scale chromatography runs were performed on three liquid chromatography systems. An ÄKTA purifier 10 system equipped with autosampler A-905, pump P-903, a 90 µL mixing chamber, UV monitor UV-900 with a 10 mm UV flow cell, pH, conductivity and temperature monitor pH/C-900, fraction collector Frac-950 and flow restrictor FR-902, and an ÄKTAmicro system equipped with pump P-905, a 90 µL mixing chamber, UV monitor UV-900 with a 3 mm flow cell, pH, conductivity and temperature monitor pH/C-900, autosampler A-905, fraction collector Frac-950, and a flow restrictor FR-902 were used for the majority of experiments. The instruments were controlled with UNICORN 5.31. For the determination of dynamic binding capacities and pressure-flow profiles an ÄKTA Pure 25 system was used. The system was equipped with sample pump S9, column valve kit V9-C, UV-monitor U9-M with 2 mm path length, conductivity monitor C9 and fraction collector F9-C. The ÄKTA Pure 25 was controlled with Unicorn 6.4.1 (all GE Healthcare).

4.2.1.6 Tangential flow filtration

For buffer exchange of the HCCF a KrosFlo Research 2i Tangential Flow Filtration System (Spectrum Laboratories, Rancho Dominguez, CA, USA) was used. Buffer exchange was performed with mPES MicroKros hollow fiber filters with a pore size of 10 kD and surface areas of 20-40 cm^2 depending on the amount of HCCF to be processed.

4.2.1.7 Analytical instruments

The protein and DNA concentrations of pure stock solutions were determined spectrophotometrically with a NanoDrop 2000c UV-Vis spectrophotometer (Thermo Fisher Scientific, Waltham, MA, USA). On the LHS UV absorptions were measured on the built-in plate reader in 96 well flat bottom UV-Star microplates and the concentrations were determined from predetermined calibration curves. For experiments with HCCF the mAb concentrations were determined via analytical protein A chromatography with a POROS A 20 µm column (2.1 x 30 mm) which was connected to a Dionex UltiMate 3000 RS UPLC system (both Thermo Fisher Scientific, Waltham, MA, USA). The system was controlled with Chromeleon 6.8.

4.2.1.8 Software and data analysis

Data processing and analysis was performed with Matlab R2017a (Mathworks, Natick, MA, USA), OriginPro 2017 (OriginLab, Northampton, MA, USA), and Microsoft Excel 2016 (Microsoft, Redmond, WA, USA). The design of experiment (DoE) studies were designed and analyzed with Modde 10.1 (Sartorius Stedim Biotech, Umea, Sweden).

4.2.2 Methods

4.2.2.1 Buffer exchange

Buffer exchange of the HCCF was performed via tangential flow filtration with a 10 kD membrane. The HCCF was first adjusted to the desired target pH with 1 M citric acid, and precipitated cell culture media components were removed via

centrifugation at 12000 g for 10 minutes. Afterwards the solution was concentrated tenfold and buffer exchanged into MCB via diafiltraton for five diavolumina. For buffer exchange of the Protein A purified mAb PD-10 desalting columns were used (GE Healthcare, Little Chalfont, UK).

4.2.2.2 High throughput screening

The high throughput screenings were carried out on the LHS in filter plates that were filled with fibers and fiber-based adsorbents. A custom Evoware script was developed in order to automate liquid handling, microplate handling, incubation, phase separation and UV measurements as well as data import and export. Buffer and load compositions were calculated in Excel and imported as worklists into Evoware. The script consisted of two equilibration phases, a load phase, a wash phase, and two elution phases. During each phase the filter plate was incubated on the orbital shaker. For all phases an incubation time of 20 min was used, except for the load phase for which the duration was adjusted according to the type of screening and molecule investigated. During the development of the screening method the impact of several screening conditions was investigated and optimized as described in the following paragraphs.

Fiber deposition Accurate and reproducible portioning of adsorbents is important for high throughput screenings. In addition the exact amount of adsorbents should be known, in particular if quantitative predictions of the behavior at larger scales are intended. For conventional chromatography adsorbents two techniques have been described for the portioning of adsorbents. Both techniques use resin particle suspensions. These are either homogenized via agitation and pipetted directly into filter plates [143] or they are distributed into forms with defined geometries in order to prepare plaques which are dried and subsequently transferred into filter plates [148]. For membrane adsorbers (MA) the filter in the filter plate is simply replaced with one to several layers of the MA, and the MA is cut and/or sealed to well size [38]. The main difference between fibers and the other adsorbents are the different dimensions. While the diameters of fibers are in the micrometer or sub-micrometer range, the lengths are typically $>$ 3-6 mm for short cut fibers and $>$ 0.25-0.5 mm for ultra short cut or flock fibers. This exceeds the diameters of conventional resins by far, and may require alternative techniques for adsorbent portioning. Three techniques were investigated: pipetting, weighing and cutting from fiber mats. For pipetting first the impact of fiber length on fiber pipettability was investigated. For this purpose suspensions of round microfibers with different fiber diameter and fiber lengths were prepared at a ratio of 50 mg fibers in 25 mL 20% EtOH. The suspensions were transferred into pre-weighed 2 mL reaction tubes with 1 or 5 mL pipette tips and

dried at 70 °C for 24-48 hours. Subsequently the amount of fiber per reaction tube was determined from the difference in the weight of filled and empty reaction tubes. In these experiments it was realized that accurate pipetting is only possible up to a certain fiber length. As the length of the fiber-based adsorbents exceeded this value, the fiber-based adsorbents were first cut to shorter lengths with a chopping-knife before being suspended and pipetted into 96 well filter plates. This technique was compared with weighing where pre-weighed amounts of fiber were placed directly in the wells of the 96 well filter plate, and cutting from fiber mats. For the preparation of the fiber mats an appropriate amount of fibers was suspended in solution at a ratio of 1.25 mg fiber per mL solution, and shaken overnight at 120 rpm on a rotary shaker to create a homogeneous suspension. The homogenized suspension was filtered over a vacuum filter to remove the suspending liquid and retain the fibers in a mesh filter to obtain a fiber mat. The fiber mat was pressed to improve uniformity and dried subsequently at 70 °C until complete dryness. A wad punch was used to cut out circular pellets from the fiber mat, which were placed into the wells of a 96 well filter plate. For comparison of the three techniques the filter plate was dried and the distribution of dry fiber weights was determined. In addition the binding capacity for lysozyme was determined and the means and the relative standard deviations for the different approaches were compared.

Selection of suitable phase ratios The phase ratio is defined as the ratio between the liquid volume and the stationary phase volume in each well. It affects the mixing behavior, material requirements, data quality and choice of possible analytical assays. A ratio of 30-60 µL liquid per mg fiber was found to be optimal in order to ensure coverage, suspending and mixing of full length fiber-based adsorbents. For lower phase ratios full coverage of the fibers could not be ensured and the fibers extended beyond the liquid level. Typically 300 µL liquid and 5-10 mg fibers were used in the experiments.

Determination of liquid hold-up volumes The liquid hold-up volume is defined as the liquid that remains in the filter plates after evacuation. It can be composed of interstitial liquid, liquid within the adsorbent pores and liquid that remains within the pores of the filter in the filter plate. It leads to a dilution of the solution added in each stage. Its exact amount should be known for correct mass balance calculations. The liquid hold-up volume was determined from the carryover volume of NaCl as suggested by Coffman et al [143] and Nfor et al [149]. The wells of a 96 well filter plate were filled with 2.5-10 mg of the different fibers and fiber-based adsorbents and incubated with 300 µL of 2 M NaCl for 10 min on an orbital shaker at 1100 rpm. Afterwards the filter plate was evacuated via centrifugation at 1200 g for 5 min. This process was repeated 3 times. Thereafter 300 µL of 10 mM NaCl was

added to each well and the filter plate was incubated on the orbital shaker for 20 min. The supernatant was collected via centrifugation and its conductivity was measured on an Äkta purifier via injecting 100 µL of each supernatant and determining the peak area of the conductivity curve. The salt concentration was calculated from a calibration curve which was prepared on the same instrument and the hold up volume was determined via mass balance.

Shaking frequency Sufficient agitation is important in high throughput screenings in order to ensure that adsorbent particles are fully suspended and protein uptake is not hindered due to sedimentation of the adsorbents [141, 144]. The shaking frequency was optimized via measuring protein uptake curves at different shaking frequencies ranging from 500 rpm to 1400 rpm. For slow shaking frequencies shallow uptake curves were observed with a high variability between replicate measurements. For shaking frequencies above 1100 rpm different uptake profiles were observed, where the protein concentration decreased exponentially over time and consistently between replicate measurements. Thus a shaking frequency of 1100 rpm was selected for all further experiments.

Evacuation of filter plates The evacuation of filter plates can be achieved via vacuum filtration or centrifugation. Removal of the majority of the supernatant is important as any remaining liquid will lead to a dilution in the subsequent step. Both techniques were compared in terms of consistency between different wells and overall amount of liquid recovered for both empty wells and wells filled with fibers. For vacuum filtration a pressure of 300 mbar was applied for 5 min and the robot was programmed to drop the filter plate onto the vacuum station from a low height to remove remaining liquid drops from the bottom of the filter plates. Centrifugation was carried out at 1200 g for 5 min. In both cases the liquid was recovered in UV plates and the liquid level was determined from the absorbance at 990 and 900 nm. In addition the mass of liquid recovered was measured. With centrifugation 99 % of the supernatant added was recovered, while only 96 % of the supernatant could be recovered via filtration. Liquid recovery was also more consistent for centrifugation, while for filtration some of the fibers sticked to well walls with liquid remaining there. Thus centrifugation was used for the evacuation of the filter plates.

Determination of stationary phase concentrations The stationary phase concentration q_i of a component in experimental step i was determined via mass

balance according to

$$c_{i-1}V_H + q_{i-1}m_{fiber} + c_{0,i}V_{sample} = c_i(V_{sample} + V_H) + q_i m_{fiber} \tag{4.1}$$

where c_{i-1} is the concentration in the liquid in step $i-1$, V_H is the liquid hold-up volume, q_{i-1} is the stationary phase concentration in step $i-1$, m_{fiber} is the fiber mass, $c_{0,i}$ is the concentration in the sample added, V_{sample} is the volume of sample added in step i and c_i is the final concentration after incubation in step i. For the first loading step with protein or DNA after equilibration $c_{i-1} = 0$ and $q_{i-1} = 0$, and q_i can be determined according to

$$q_i = \frac{c_{0,i}V_{sample} - c_i(V_{sample} + V_H)}{m_{fiber}} \tag{4.2}$$

Determination of adsorption kinetics For the determination of adsorption kinetics uptake curves were generated. The method was identical to the general high throughput method, except that protein was added sequentially to the columns within the filter plate, starting with the longest incubation time first as described in [141, 143, 144]. Twelve different incubation times were used, ranging from 1 min to 2 h, and two different protein concentrations for lys and the mAb, representing column load densities of 5 g/L and 30 g/L column volume (CV) on packed fiber columns with packing densities of 0.3 g fiber per mL CV.

Determination of static binding capacities and isotherms for lysozyme The static binding capacity (SBC) of the Fiber FRP S adsorbent for lysozyme was determined in 10 mM KPi at pH 7. A protein concentration of 2 g/L and an incubation time of 30 min was used. Isotherm screenings were carried out in 10 mM KPi at pH7 with different amounts of NaCl added. The protein concentration in the load was varied between 0.1 and 4 g/L and the incubation time was set to 120 min.

Screening of static binding capacities of anion exchange fiber prototypes for BSA and HS-DNA For the optimization of the hydrogel structure of the anion exchange fiber prototypes the static binding capacities for BSA and HS-DNA were determined. An incubation time of 1 h was chosen for both screenings. The screenings were carried out in 20 mM Tris-HCl at pH 7.5. The loading concentration was 10 g/L BSA and 1.01 g/L DNA, which is equivalent to a load challenge of 600 mg/g fiber respectively 60.8 mg/g fiber.

Screening of binding of antibody, high-molecular weight species and host-cell proteins For the determination of binding and step elution conditions for the purification of a monoclonal antibody (mAb) from product- and process-related impurities, two HTS were carried out on the LHS with the SI-ATRP S fiber-based adsorbent and the buffer exchanged HCCF. The screenings were performed in 20 mM MCB within a pH range of 4.5-6 at a low and a high load density. For the low load density screen the NaCl concentration was varied between 0-300 mM NaCl, and for the high load density screen it was varied from 0-250 mM NaCl. The data from the low load density screen was used in order to determine the partition coefficient of the antibody, while the data from the high load density screen was used in order determine the partition coefficients of the impurities. The amount of mAb and impurities bound was determined from the concentration in the elution fractions. The incubation time was set to 30 min for the low load density screen, and 60 min for the high load density screen. From the measured binding capacities partition coefficients, K_p and separation factors α as defined in [150] were calculated. For the calculations all stationary phase concentrations were based on the adsorbent skeleton volume.

4.2.2.3 Column packing and storage

For comparison experiments the fiber-based adsorbents were packed into laboratory scale Omnifit BenchMark columns (Diba Industries, Danbury, CT, USA) with an I.D. of 6.6 mm or MiniChrom columns (Repligen, Weingarten, Germany) with an I.D. of 8 mm. A fiber packing density of 0.3 g fiber per mL column volume (CV) was used, and bed heights ranged from 2-4 cm. A suspension based packing technique was used for PA6 fiber-based adsorbents as reported previously [146, 151]. For PET fiber-based adsorbents a dry packing technique was used as reported in [83]. Q Sepharose Fast Flow was flow packed into Omnifit colums according to the manufacturer's instructions. Sartobind Q was packed into a void volume optimized flat sheet membrane holder with a flow dispenser which was obtained from Sartorius Stedim Biotech (Göttingen, Germany). 3 layers of membrane with a diameter of 3 cm were packed into the holder. Within the holder 2.59 cm of the membrane are percolated. For three membrane layers a bed height of 0.825 mm is obtained, which results in membrane volume of 0.435 mL. In between experiments all columns and devices were stored in aqueous solutions containing 20 vol% EtOH and 150 mM NaCl.

4.2.2.4 Lab scale chromatography

Breakthrough experiments Breakthrough experiments were carried out with an Omnifit column that had been packed with the Fiber FRP S adsorbent (I.D. 6.6 mm, bed height 40 mm). The mobile phase velocity was adjusted to match the loading density and incubation time in the HTS isotherm screens. Lysozyme solutions in 10 mM KPi pH 7 with 0 and 250 mM NaCl with lys concentrations identical to the equilibrium concentrations of the HTS screen were loaded onto the column. The flowthrough was collected and the amount of protein bound to the fiber-based adsorbents q was determined via mass balance.

Bind and Elute experiments Bind and elute experiments were performed in order to compare the results from the binding conditions screen on the LHS for the mAb and the impurities with results from conventional lab scale experiments. For this purpose an Atoll Minichrom column was used that was filled with the Fiber ATRP S adsorbent (0.3 g/mL packing density, 8 mm I.D., 20 mm bed height). The load material was the same as in the HTS screens and consisted of HCCF that was buffer exchanged into 20 mM MCB at pH 4.5 with 50 mM NaCl added. A loading density of 25 g/L CV was used. The method was run at a mobile phase flow rate of 1 mL/min (119 cm/h) and consisted of a 5 CV equilibration step, followed by the load phase, a 5 CV wash step, and a step elution with the desired NaCl concentration over 30 CV. The runs were fractionated, fractions of the elution peaks were pooled up to optical densities at 280 nm of 2.2-0.2 for a path length of 2 mm, and load and elution pools were analyzed via analytical Protein A chromatography, analytical SEC, and HCP Elisa.

Determination of dynamic binding capacities For the determination of the dynamic binding capacities (DBCs) the columns and membrane devices were loaded with BSA or DNA solutions. The UV absorbance was monitored and loading was terminated once 10% of the maximum UV absorbance was reached. The DBC was calculated from the volume $V_{10\%}$ corresponding to 10% breakthrough, the system void volume V_0, and the geometric column or membrane volume V as follows:

$$DBC_{10\%} = \frac{V_{10\%} - V_0}{V} \tag{4.3}$$

Determination of permeability The permeability of the anion exchange adsorbents was determined from pressure flow experiments in 20 mM Tris buffers at pH

7.5 as previously described in [151]. Briefly, the mobile phase flow rate was varied from 0 to 25 mL/min and the resulting column pressure drop Δp was calculated from measurements of the system pressure drop with and without the column or membrane. The permeability was determined from a linear regression of $\eta \cdot u \cdot L$ against Δp, where η is the dynamic viscosity of the buffer, u is the mobile phase velocity, and L is the length of the column.

4.2.2.5 Analytical methods

UV/Vis spectroscopy Protein and DNA concentrations were determined from the absorbance at 280 nm and 260 nm. In each case a baseline correction was applied via subtracting the absorbance at 340 nm to account for the effect of light scattering particulates and instrument noise. For measurements in microtiter plates the path length was determined from the absorbance at 990 and 900 nm as described in [152] and the measurements were corrected to a path length of 10 mm.

Analytical Protein A chromatography The method for analytical Protein A chromatography was carried out on a POROS A 20 µm column (2.1 x 30 mm), and consisted of a 20 µL sample injection, a wash step with equilibration buffer for 0.8 min, elution over 0.6 min with elution buffer, and reequilibration over 2.4 min with equilibration buffer. The flow rate was set to 2 mL/min, which resulted in an analysis time of 3.8 min per sample. The mAb concentration was determined from the peak areas of the elution peaks, using a calibration curve that was determined from an external mAb standard with known concentration.

Analytical size exclusion chromatography The analytical size exclusion chromatography was carried out with a TSKgel SuperSW mAb HTP (4.5 mm I.D. x 15 cm L) column at a volumetric flow rate of 0.45 mL/min. 20 µL of each sample were injected. Samples with a concentration > 1 g/L were diluted accordingly with MCB.

Host cell protein analysis The host cell protein concentration of samples was determined with the Gyrolab CHO-HCP kit 1, which is a microfluidic CD-based ELISA assay, that was carried out on a Gyrolab XPlore station. The Gyrolab XPlore station was controlled by the Gyrolab software (all Gyros Protein Technologies AB, Upsalla, Sweden).

4.3 Results and Discussion

In order to setup an automated high-throughput screening for fiber-based adsorbents, first a suitable screening format had to be selected and several aspects of the screening needed to be characterized and optimized. The results of these experiments will be presented in section 4.3.1. On this basis a comparison between HTS experiments and lab scale experiments was conducted in order to investigate the comparability between different scales. These results will be presented in section 4.3.2. Finally, the developed HTS was employed for material development and process development. The results of these experiments will be presented in section 4.3.3.

4.3.1 Setup of the screening system

The goal of this study was to establish a HTS for short-cut fiber-based adsorbents. The key structural and chemical properties of these adsorbents are outlined in Table 4.1. First an appropriate screening format needed to be selected. Microtiter filter plates were chosen as the HTS format due to their flexibility, ease-of-use, and potential sample throughput. Microcolumns would be an alternative, however material requirements would be higher, and due to the length of the fibers the integration into standard microcolumns - in our case - proved to be difficult. The integration of single fibers into microfluidic devices has been demonstrated, however it is not straightforward and may require special analytics such as fluorescent imaging [35, 36]. As previous mechanistic modeling studies with the fiber-based adsorbents had demonstrated that both adsorption kinetics and mass transfer effects are relevant on the fiber-based adsorbents [151], the use of microtiter filter plates is also supported from an engineering standpoint [32].

Table 4.1: Structural and chemical properties of the fiber based adsorbents used in this study.

Property	Value
Fiber base material	PA6, PET
Cross-sectional shape	Elliptical
Cross-sectional dimensions µm x µm	10 x 20
Fiber length (mm)	6
Type of surface grafting	FRP, SI-ATRP
Functional groups	S, Q

4.3.1.1 Fiber deposition

The portioning of adsorbents is an important aspect of high throughput screenings. For conventional chromatography adsorbents 3 techniques have been described for the portioning into microtiter plates. Resin portioning has been achieved via resin particle suspensions which are either agitated and pipetted directly into filter plates [143] or distributed into forms with defined geometries in order to prepare particle plaques which are dried and subsequently transferred into filter plates [148]. For membrane adsorbers (MA) the filter in the filter plates has been replaced with one to several layers of the MA, and the MA has been cut and/or sealed to well size [38]. Portioning techniques for HTS should be accurate and reproducible, in particular if the amount of adsorbent in each well is not quantified after portioning and if qualitative comparisons between different wells or quantitative predictions of larger scales are intended. Alternatively the amount of adsorbent in each well can be quantified via methods that are based on for example light scattering [153] or the ionic capacity [154]. Nonetheless, even if quantification is used, deviations between different wells and between the scheduled and actual adsorbent amount should not bee too large, as this could for instance change the region of the isotherm that is examined or affect the applicability and precision of subsequent analytics.

So far fiber-based adsorbents have been prepared from two fiber structures. Endless fibers and staple fibers with lengths $\geq$ 5 mm or fiber mats. Fiber mats might be integrated into filter plates in a similar way as MAs. For this study we intended to screen fiber-based adsorbents which had been prepared from staple fibers with a length of 6 mm. Staple is the immediate end product of fiber manufacturing, while the preparation of ordered structures such as mats, felts or webs requires special processes such as electrospinning or additional manufacturing steps. Several techniques were tested for the portioning of the fiber-based adsorbents. The preparation of fiber plaques was not possible as some of the fibers extended beyond the cavities in the device. As these fibers entangeled other fibers in the plaque, the plaques were destroyed as the perforated plate of the plaque device was pulled out. Pipetting from fiber suspensions was examined for a fiber-based adsorbent and a set of short cut staple fibers with lengths of 0.25-6 mm. Accurate and reproducible pipetting was only possible for fibers with lengths $\leq$ 1 mm using cut 1 mL or 5 mL pipette tips, while longer fibers and the fiber-based adsorbent clogged the pipette tips. Cutting or homogenization of the fiber-based adsorbent improved pipettability and portioning, but this also changes the adsorbent structure, and was found to change adsorbent properties such as the measured protein binding capacities per fiber weight.

Two techniques were identified that enabled accurate and reproducible portioning of the fiber-based adsorbent. Weighing, and punching of fiber mats in combination with

Table 4.2: Well-to-well variability of different fiber deposition techniques.

	Weight (mg)			protein binding (%)			Binding capacity (mg/g)		
Portioning method	Mean	SD	RSD	Mean	SD	RSD	Mean	SD	RSD
Weighing	5.07	0.17	3.36	63.53	0.02	3.28	79.86	4.23	5.30
Punching	5.16	0.35	6.72	62.37	0.02	3.81	80.49	3.04	3.77

titration or weighing for adsorbent quantification. The fiber mats for punching were prepared via filtering fiber slurries with defined fiber densities over a mesh with a defined filter area in order to prepare fiber mats with defined fiber densities per area. With both techniques the exact amount of adsorbent in each well is known and can be accounted for in the setup and/or evaluation of the HTS. Punching, or cutting from fiber mats, which might also be used, offers the advantage that the material for several wells can be portioned at once and that in combination with automated titration scripts on the LHS slow weighing procedures can be avoided. The accuracy and precision of both techniques was investigated for a scheduled fiber mass of 5 mg per well. For this purpose the fiber weights and the binding capacities were evaluated for 32 wells that were prepared with each technique. Table 4.2 summarizes the measured weights, percentages of protein binding, and binding capacities together with the associated SDs and RSDs. The measured weights were 1.4% and 3.2% higher than the scheduled weight of 5 mg. This is within the 5% tolerance that was accepted during fiber weighing. The RSD in fiber weights was higher for the punching procedure than for the weighing procedure, which can be explained by variations in the thickness of the fiber mats. With both portioning techniques the variability in % protein binding were less than 4% which is comparable to the values that have been reported by Coffman et al [143] for resin pipetting. With both portioning techniques similar protein binding capacities of 79.86 ± 4.23 mg/g and 80.49 ± 3.04 mg/g fiber were measured. The difference in protein binding capacities was not found to be statistically significant (p=0.57). This suggests that the adsorbent structure is not altered via the punching procedure. Thus it was concluded that both techniques can be used for the portioning of fiber-based adsorbents.

4.3.1.2 Incubation times

Another important aspect of HTS in microplates is the selection of an appropriate incubation time. The incubation time in HTS should match with process contact times in packed columns [144]. If thermodynamic equilibrium parameters are to be measured even longer incubation times may be required. For a fixed phase ratio and mixing intensity, the time required in order to achieve equilibrium will depend on

the initial protein concentration, the size of the protein and its diffusivity, as well as the kinetic and thermodynamic effects that govern the adsorption process. Typical bed heights for columns with fiber-based adsorbents range from 3-5.5 cm, with residence times of 0.2-4.4 min [79, 83, 146]. Contact times for loading have been in the range of 1-134 mins. Thus batch uptake kinetics were measured for two proteins with different size, lysozyme (lys) and a monoclonal antibody (mAb), under strong binding conditions at two different protein concentrations, representing column load challenges of 5 g/L and 30 g/L column volume, with incubation times ranging from 1 min to 2 h. Two types of fiber-based strong cation exchange adsorbents were used with different hydrogel compositions. One with an uncontrolled grafted hydrogel that was prepared via free radical polymerization (Fiber FRP S), and one with a

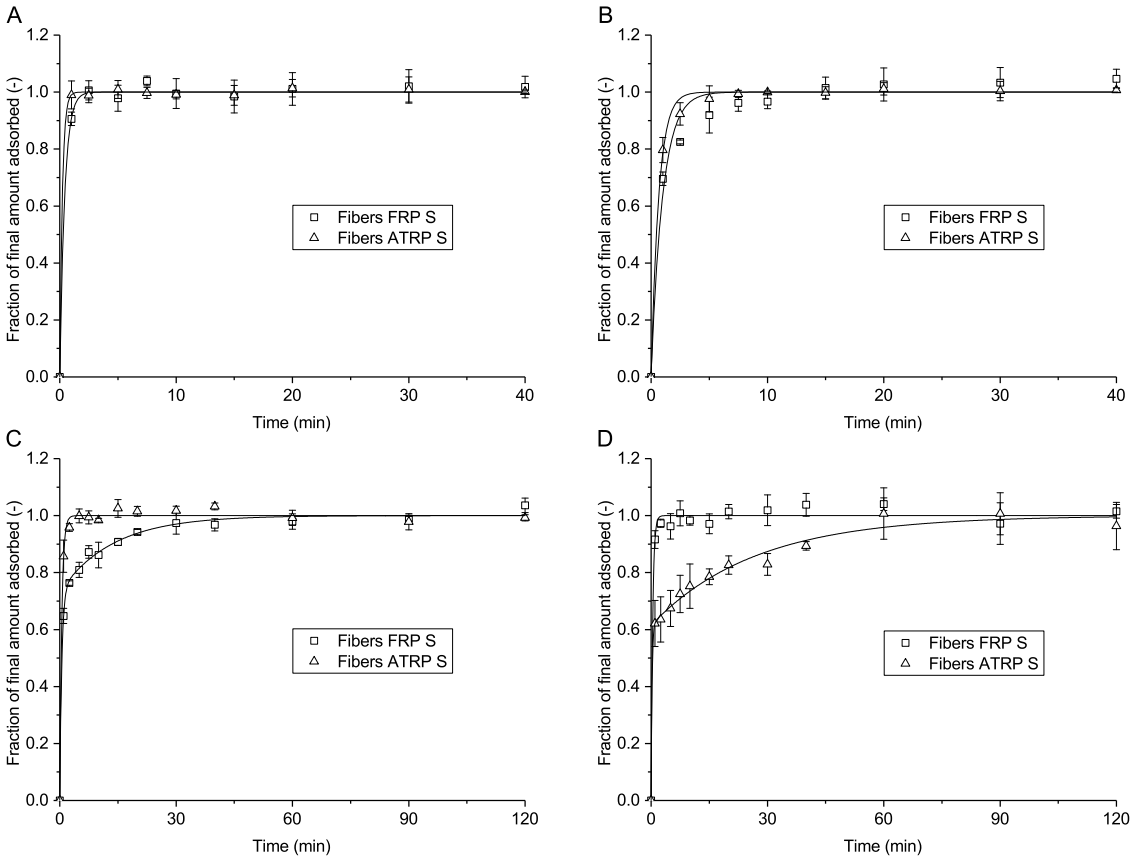

Figure 4.1: Uptake kinetics of (A,C) lysozyme, and (B,D) a monoclonal antibody on two different types of strong fiber-based cation exchange adsorbents in 96-well filter plates. Initial protein concentrations of (A,B) 0.3 g/L and (C,D) 1.8 g/L were used in the experiments, representing column load challenges of 5 g/L and 30 g/L in packed fiber columns. Mobile phase conditions: (A,C) 10 mM KPi, pH 7, (B,D) 20 mM MCB, pH 4.5. Error bars are ± 1 SD from 4 replicate wells for each time point. The lines show exponential and bi-exponential fits to the data with the parameters that are given in Table 3 and 4.

controlled grafted hydrogel that was prepared via surface initiated atom transfer radical polymerization (Fiber ATRP S).

Fig. 4.1 shows the uptake curves for lys (cf. Fig. 4.1A, C) and the mAb (cf. Fig. 4.1B, D) for the 5 g/L (cf. Fig. 4.1A, B) and 30 g/L (cf. Fig. 4.1C, D) load challenges. For the quantification of the incubation times exponential decay functions were fit to the data as suggested by Coffman et al. [143]. The respective parameters of the fits are listed in Table 4.3 and 4.4. The low load challenges equilibrated quickly for both molecules and both types of fibers (cf. Fig. 4.1A, B). The final binding capacity was reached after 10 mins in each. The uptake curves could be fit with single exponential decay functions (cf. Table 4.3). The time constants for the ATRP fibers were shorter than for the FRP fibers and on both adsorbents the time constants for the mAb were slightly longer. The longest time constant was $\tau_1 = 1$ min. Thus an incubation time of 10 min would be sufficient to achieve 100% of the final binding capacity for low load challenges. For the higher load challenge the incubation times were found to depend on the type of molecule and the type of fiber-based adsorbent. For some of the uptake curves bi-exponential fits were required, which suggests that the adsorption kinetics are more complex. This is consistent with internal mass transfer resistances and kinetic resistances that have been observed in previous modeling studies of such adsorbents [151]. For lys a quick uptake on the ATRP S fibers was observed, while the uptake on the FRP S fibers required a bi-exponential fit. For mAb it was the other way round and the uptake on the FRP S fibers could be described with a single exponential decay function, while the uptake on the ATRP S fibers required a bi-exponential fit. These differences can be explained by the different hydrogel composition and binding capacities of the two adsorbents. The FRP fibers have a low binding capacity and a cross-linked hydrogel, while the ATRP fibers have a higher binding capacity and a hydrogel that is not cross-lined. Thus the accessibility of lys and mAb on the two fiber types is different and the fibers are satured to a different level of the binding capacity. The longest time constant was 26.7 min for the mAb on the ATRP S fibers. Thus longer incubation times than 10 min are needed for higher load challenges.

Table 4.3: Parameters of the exponential fits of the uptake curves at 5 g/L load challenge.

	Lys		mAb	
	Fibers FRP S	Fibers ATRP S	Fibers FRP S	Fibers ATRP S
A_1 (-)	1.00 ± 0.02	1.00 ± 0.01	1.00 ± 0.03	1.00 ± 0.02
τ_1 (min)	0.42 ± 0.04	0.26 ± 0.06	1.00 ± 0.08	0.66 ± 0.03

Thus for the screening the incubation times were adjusted depending on the load challenge and the type of study. For low load challenges an incubation time of 30 min was used, while for higher load challenges an incubation time of 1 h was used, which is the maximum of typical loading times for these adsorbent in packed

columns. For isotherm studies the adsorption kinetics were first measured in order to set appropriate incubation times.

Table 4.4: Parameters of the exponential and bi-exponential fits of the uptake curves at 30 g/L load challenge.

	Lys		mAb	
	Fibers FRP S	Fibers ATRP S	Fibers FRP S	Fibers ATRP S
A_1 (-)	0.73 ± 0.02	1.00 ± 0.02	1.00 ± 0.02	0.62 ± 0.04
τ_1 (min)	0.52 ± 0.05	0.52 ± 0.03	0.41 ± 0.04	0.23 ± 0.26
A_2 (-)	0.27 ± 0.02	NA	NA	0.38 ± 0.03
τ_2 (min)	13.7 ± 1.96	NA	NA	26.88 ± 6.15

4.3.1.3 Hold-up volumes

The liquid hold-up volume was determined for the two types of fiber-based adsorbents and empty wells in the filter plate in order to account for the dilution that is caused by this volume. For empty wells a hold-up volume of 4.48 ± 0.28 µL was measured. This matches well with the manufacturer specified values of 3-5 µL. The hold-up volume of the fibers correlated with the fiber mass. The hold-up volume of the FRP S fibers was 0.57 ± 0.09 µL/mg. This corresponds to 0.43 ± 0.07 µL/µL fiber, when using data from previous porosity measurements in packed columns [146] in order to convert the fiber mass to a fiber volume. For the ATRP S fibers a hold-up volume of 0.58 ± 0.11 µL was measured, which corresponds to 0.44 ± 0.08 µL/µL fiber [83]. The volumetric hold up volumes for the fibers were lower than the hold up volumes that have been reported for resins [143, 149]. This is consistent with the lower particle porosity of the surface grafted fibers for which values of 0.37-0.48 have been reported [83, 146]. The determined hold up volumes of 0.43-0.44 fall within this range, which suggests that the hold up that is caused by the fibers is due to liquid that remains within the fiber pores / the hydrogel layer. For the fiber amounts and phase ratios that were typically used in the screenings, the hold up volume accounted for 2-3% of the total liquid in each stage, with 50-70% of the liquid volume being due to the hold up in the filter plate and the remaining portion being due to the hold-up within the fibers.

4.3.2 Scale comparison

HTS is typically used in order to identify conditions for larger scale operations in packed columns or devices. Therefore it is important, that the data from HTS correlate with data from larger scales.

To study this, we compared binding capacities that were measured with the developed HTS with binding capacities that were measured via breakthrough experiments on a packed fiber column. For this purpose a HTS with lys and the FRP S fibers was performed, and the binding capacities of lys were measured at two different salt concentrations over a range of initial protein concentrations. For the screening an incubation time of 2 h was used in order to ensure full equilibration. Subsequently three equilibrium protein concentrations from the HTS were selected, and the binding capacities for these protein concentrations were measured via breakthrough experiments on a packed fiber column. The protein load densities and the incubation times respectively the loading times were kept constant in between the two scales.

Fig. 4.2 compares the binding capacities that were measured at the two different scales. In the HTS, higher binding capacities were measured for the low salt concentration than for the high salt concentration. Binding capacities increased sharply with increasing protein concentration for the low salt concentration, and only gradually for the high salt concentration. Both curves could be described approximately with Langmuir isotherms, $q = q_{max}c/(K_d + c)$, with $q_{max} = 82.917 \pm 5.883$ mg/g and $K_d = 0.006 \pm 0.003$ mg/mL for 0 mM NaCl, and $q_{max} = 73.750 \pm 12.084$ mg/g and $K_d = 0.303 \pm 0.200$ mg/mL for 250 mM NaCl.

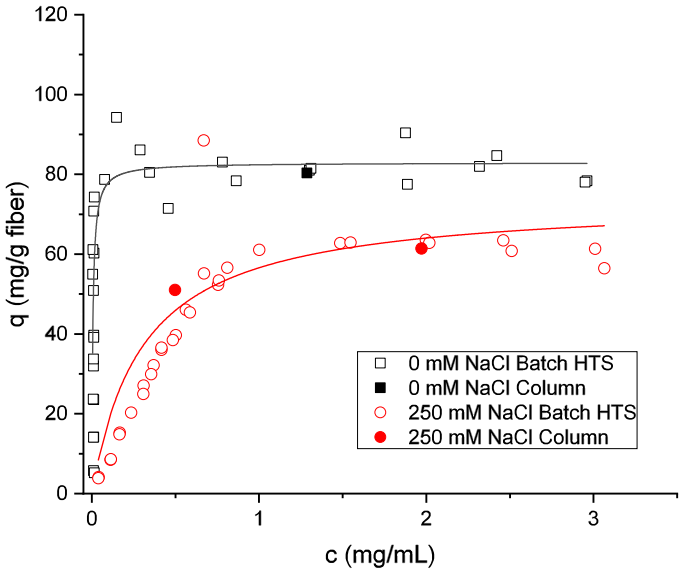

Figure 4.2: Comparison of the binding capacities of Fiber FRP S adsorbents for lysozyme determined via batch HTS experiments and breakthrough experiments on a packed fiber column. Buffer: 10 mM KPi, pH 7. Solid lines represent Langmuir isotherm fits to the respective batch HTS data.

Similar trend as in the HTS were observed for the column data. Higher binding capacities were measured for the low salt concentration than for the high salt concentration. For the high salt concentration binding capacities increased with increasing protein concentration. For all of the investigated conditions, the binding capacities from the column experiments agreed well with the experimental and fitted binding capacities of the HTS. The average deviation between the column binding capacities and fitted batch binding capacities was 1.7%.

This confirms that the data from the developed HTS correlates with data from packed fiber columns, and suggests that the developed HTS can be used in order to determine conditions for packed fiber columns.

4.3.3 Application examples

4.3.3.1 Material development

A key question in the development of fiber-based adsorbents with controlled grafted hydrogels is how the grafted hydrogel layer should be designed for specific applications. With controlled grafting techniques several structural parameters of the grafted hydrogel layer such as chain density or chain length can be adjusted via varying grafting parameters such as initiator density or polymerization time. This can be used to affect adsorbent properties such as protein binding capacities in a favorable way, as has been demonstrated in several recent studies [83, 147]. However, currently, no predictive approaches exist that could be used to pre-select an appropriate hydrogel architecture for a specific molecule at specific conditions or the corresponding grafting parameters in advance. Thus, the impact of grafting parameters on adsorbent properties has to be examined experimentally. This is usually done with lab scale experiments. Due to the large number of grafting parameters and the material and time requirements, such studies have typically been performed with single model proteins at set mobile phase conditions where only one grafting parameter is varied at a time. However, there may be interactions between different grafting parameters, the best hydrogel architecture may be different for different molecules and it can also depend on the mobile phase conditions.

HTS could facilitate the experimental characterization of fiber-based adsorbents with grafted hydrogel layers, as the impact of several parameters (grafting parameters, molecule type, mobile phase conditions) can be studied at the same time. While HTS has been used for resin screening and the screening of mixed-mode and affinity ligands, it has not been used for the optimization of adsorbents with grafted hydrogel layers. Thus we decided to use the developed HTS in order to optimize the hydrogel

structure of controlled grafted anion-exchange (AEX) fiber-based adsorbents. To this end, 17 AEX fiber prototypes with different hydrogel structures were prepared via SI-ATRP by methods that have been described previously [83]. To achieve the different hydrogel structures the grafting parameters aminolysis time, polymerization time and monomer composition were varied according to a face-centered central composite design. These parameters affect the chain density, the chain length and the ligand density in the grafted hydrogel layer. For the 17 prototypes the static binding capacities for BSA and HS-DNA were determined via HTS . The goal was to select grafting parameters/a hydrogel structure that provides a high binding capacity for BSA as well as HS-DNA for a potential application of the optimized adsorbent in antibody polishing processes where the complete removal of DNA is one of the key functions [155]. HS-DNA was used because it is a model DNA that has been used in several AEX polishing studies, and BSA was selected because it is a standard model protein for AEX adsorbents and thus enables comparisons to other adsorbents.

Fig. 4.3 shows the results from the HTS in the form of the contour plots that were obtained after response surface regression of the grafting parameters to the measured static binding capacities (SBCs) for BSA (cf. Fig. 4.3A) and HS-DNA (cf. Fig. 4.3B). The response surfaces are based on all 17 prototypes in the design (R^2=0.91 and Q^2=0.87 for BSA, R^2=0.96 and Q^2=0.89 for HS-DNA). For BSA the highest SBCs were measured for prototypes with low initiator/chain densities and long polymerization times/chain lengths, while the monomer composition/ligand density was not found to have an effect in the investigated factor range. For HS-DNA the polymerization time/chain length was also found to have the strongest impact on the SBCs. For the initiator density there was an interaction with polymerization time. At low polymerization times increases in initiator density resulted in a decrease in the SBC of HS-DNA, while at longer polymerization time increases in the initiator density resulted in an increase in the SBCs of HS-DNA. Furthermore the ligand density was found to have a slight positive effect on the SBCs of HS-DNA.

Based on the models a prototype with medium initiator density/chain density, long polymerization time/chain length and a high ligand density would be best in order to achieve a high binding capacity for both BSA and HS-DNA. The prototype in the design that matched these settings closest, was selected and characterized further in a packed column. First the dynamic binding capacity (DBC) for HS-DNA was determined via breakthrough experiments to provide a reference to other anion exchange adsorbents. At 10% breakthrough a DBC of 12.7 mg/mL CV (42 mg/g fiber) was measured which corresponds to 83 % of the SBC from the HTS (50.8 mg/g). This is a typical ratio that has been described in previous packing studies for winged fibers. The measured DBC is 40 % higher than the DBCs that have been

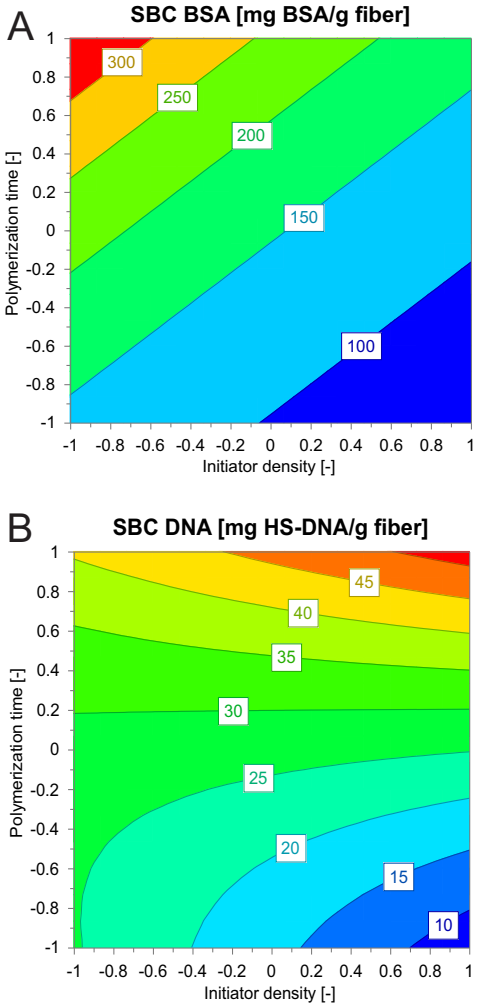

Figure 4.3: Contour plots of the response surface models for the influence of polymerization parameters/polymer nanolayer architecture on the static binding capacities of (A) BSA and (B) HS-DNA on controlled grafted fiber-based anion exchange adsorbents. The models are based on 17 prototypes from a face-centered central composite design. The SBCs were determined via HTS. Load challenges: (A) 600 mg BSA/g fiber, (B) 61 mg HS-DNA/g fiber. Buffer: 20 mM Tris-HCl, pH 7.5. Contour plots are displayed for a medium ligand density and show the predicted values for the respective SBCs.

reported for Sartobind Q membranes under similar conditions, and fall in the range of DBCs that have recently been reported for ATRP-grafted membrane adsorbers [77].

In the second step we compared the performance of the selected prototype with a Sartobind Q membrane adsorber and a Q Sepharose Fast Flow (QSFF) resin. For this purpose we determined the DBCs for BSA at different mobile phase velocities

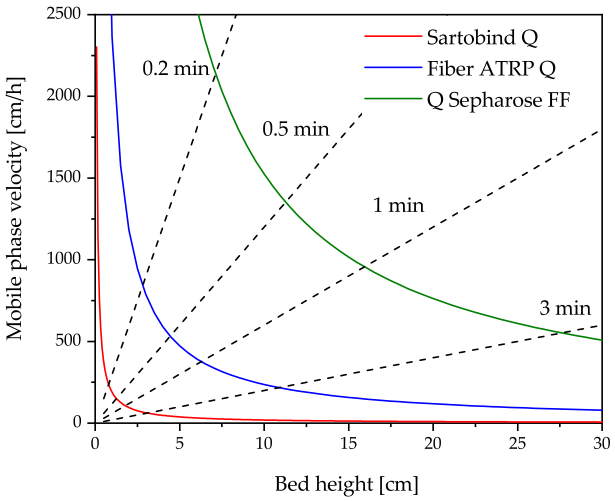

Figure 4.4: Comparison of the operating windows of the selected anion exchange fiber prototype and different commercially available adsorbents. The solid lines were calculated from the permeability of each adsorbent and display the limits up to which each adsorbent can be operated when assuming a maximum allowable pressure drop of 3 bar. Dashed lines show bed residence times. Buffer: 20 mM Tris, pH 7.5, Conductivity: 1.4 mS/cm.

(cf. Fig. 4.5) and the permeabilities of the different adsorbents in order to calculate potential operating windows (cf. Fig. 4.4). For QSFF the highest DBC was measured with 52.4 mg/mL at 100 cm/h, but this value decreased by 91% as the mobile phase velocity was increased to 600 cm/h. Sartobind Q showed a lower, but constant DBC of 26.0 mg/mL. The DBC of the selected fiber prototype was 16% lower than the DBC of QSFF at 100 cm/h, but 68% higher than the DBC of Sartobind Q. For an increase in the mobile phase velocity from 100 cm/h to 900 cm/h the DBC of the fiber prototype decreased by 23%. The permeabilities ranged from 15.92 $\pm$ 0.61 mD for Sartobind Q and 198.08 $\pm$ 5.73 mD for the selected fiber prototype to 1277.75 $\pm$ 14.41 mD for QSFF. Fig. 4.4 shows the bed heights and mobile phase velocities that would be feasible with each adsorbent when assuming a maximum allowable pressure drop of 3 bar. While the selected fiber prototype cannot not be operated with the same mobile phase velocity as resins at bed heights that are typical of resins, i.e. $>$ 20 cm, it can be operated with the same mobile phase velocity as membranes at larger bed heights than what is typical for current membrane adsorbers ($\leq$ 8 mm).

In previous studies it has been shown that a bed height of 3 cm is required in order to achieve a good packing performance for winged fibers [83, 146]. For resins a bed height of 5 cm is typically required in order to achieve a good packing performance and enable packing at larger scales [156]. Taking these constraints into account, we calculated

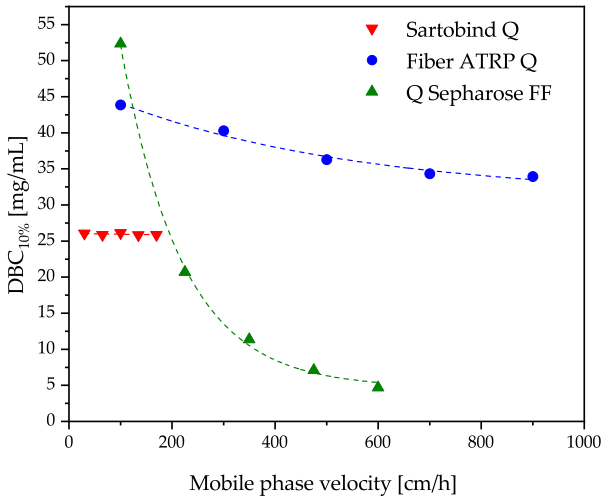

Figure 4.5: Comparison of the dynamic binding capacities (DBCs) for BSA of the selected anion exchange fiber prototype and different commercially available adsorbents. DBCs were evaluated at different mobile phase velocities at 10% breakthrough in 20 mM Tris buffer at pH 7.5 for a protein concentration in the load of 2 g/L. Dashed lines show asymptotic exponential (Fiber ATRP Q, Q Sepharose FF) and linear fits (Sartobind Q) to the respective data.

the productivity (cf. Fig. 4.6A), the required number of cycles (cf. Fig. 4.6B), and the buffer consumption (cf. Fig. 4.6C) for the three adsorbents for bed heights ranging from 8 mm to 5 cm. The calculations were based on the operating windows and the measured DBCs for BSA, and full chromatographic cycles with regeneration and cleaning in place (CIP) steps were assumed. The maximum productivity of the selected fiber prototype is 2-3 times as high as the maximum productivity of QSFF and in a similar range as the productivity of Sartobind Q at bed heights that are 4-6 times greater than the maximum bed height for Sartobind Q (0.8 cm). Less cycles are required with the selected fiber prototype than with Sartobind Q, while the number of cycles also remains constant over wide mobile phase velocity ranges. The buffer consumption of the selected fiber prototype is comparable to the buffer consumption of QSFF at the window of optimum productivity of QSFF, while for higher mobile phase velocities QSFF needs much more buffer. At the same productivity the buffer consumption for the selected fiber prototype is 24-38% lower than the buffer consumption for Sartobind Q. Overall these results show that the selected fiber prototype can compete with a resin and a membrane adsorber. Due to the longer bed heights that are possible with the fiber prototype than with the membrane adsorber, the use for an application where a moderate level of resolution is required might be attractive.

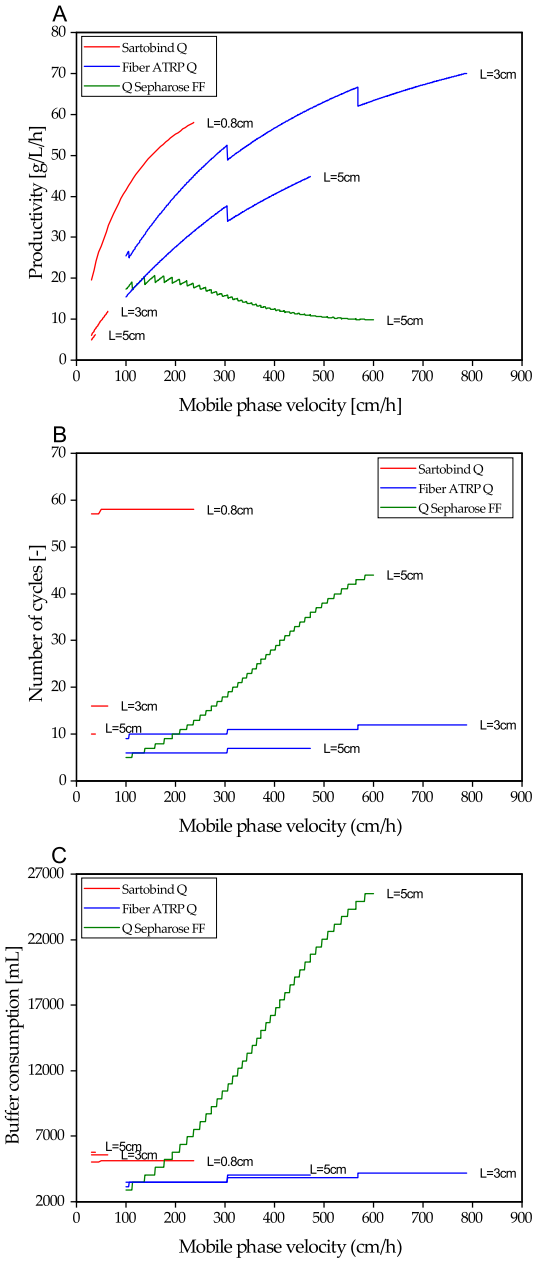

Figure 4.6: Comparison of the potential (A) productivity, (B) required number of cycles, and (C) buffer consumption of the selected anion exchange fiber prototype and different commercially available adsorbents at different bed heights L. For the calculations it was assumed that a volume of 2500 mL BSA solution with a protein concentration of 2 g/L needs to be purified with columns and membranes with diameter of 2.6 cm, which is equivalent to the diameter of flat sheet Sartobind capsules. For equilibration, wash, elution and regeneration a duration of 5 CV was assumed for each step. In addition a CIP step over 2 CV with a contact time of 15 min was included in the calculations. The calculations are based on the DBCs and operating windows that are displayed in Fig. 4.5 and Fig. 4.4.

4.3.3.2 Experimental process development

HTS is frequently used in order to identify appropriate process conditions for individual chromatography steps. To further assess the capabilities of the developed HTS, it was used in order to determine step elution conditions for the purification of a monoclonal antibody (mAb) from product- and process-related impurities. For this purpose the binding of antibody, high-molecular-weight species (HMWS), and host-cell proteins (HCPs) to controlled grafted CEX adsorbents was investigated with respect to pH and sodium concentration. Two HTS at different load densities were performed, and the data was used to calculate partition coefficients, K_ps for the antibody and the impurities, as suggested by McDonald2016 et al [157].

Fig. 4.7 displays the measured K_ps for the antibody (cf. Fig. 4.7A), HMWS (cf. Fig. 4.7B), and HCPs (cf. Fig. 4.7C). Antibody K_ps ranged from values typical of strong binding conditions to values typical of non-binding conditions, and decreased with increasing pH and increasing sodium concentration (cf. Fig. 4.7A). K_ps for the HMWS followed the same trends with respect to pH and sodium concentration, but for each pH the K_ps were shifted to higher sodium concentrations (cf. Fig. 4.7B). In contrast to this, for both the antibody as well as the HMWS, the K_ps at pH 5.0 and pH 4.5 increased or remained constant with increasing sodium concentration for concentrations up to 50-125 mM sodium. This can be explained by charge repulsion effects and steric hindrance effects, which have been observed previously on cation exchange adsorbents [158]. These effects are strongest under conditions of high net charge, i.e. low pH, and low ionic strength, i.e. low sodium concentration. In addition, with increasing ionic strength, a deswelling of the hydrogel layer on the fiber-based adsorbents occurs [83] which improves hydrogel accessibility, in particular for larger molecules. In principle, an insufficient incubation time could also explain these trends, but higher capacities with higher ionic strength have previously been observed on the same adsorbent even after prolonged equilibration for 16 h [83]. HCP K_ps followed the same general trends with respect to pH and sodium concentration as the antibody and the HMWS (cf. Fig. 4.7C). However, no increase in K_ps with increasing sodium concentration was observed for pH 4.5 and 5.0, and the differences between the different pH values were less pronounced. In addition, K_ps decreased only gradually with increasing sodium concentration, and binding continued up to the highest sodium concentration. These effects might be a consequence of the smaller size and isoelectric points of HCPs, as well as the heterogeneity of HCPs with respect to size and pI. Similar trends have been reported by McDonald2016 et al [157].

Based on the K_p data, separation factors were calculated in order to assess the selectivity of the fiber-based cation exchange adsorbents for the separation of antibody and impurities (cf. Fig. 4.8). At each pH level there was a maximum of

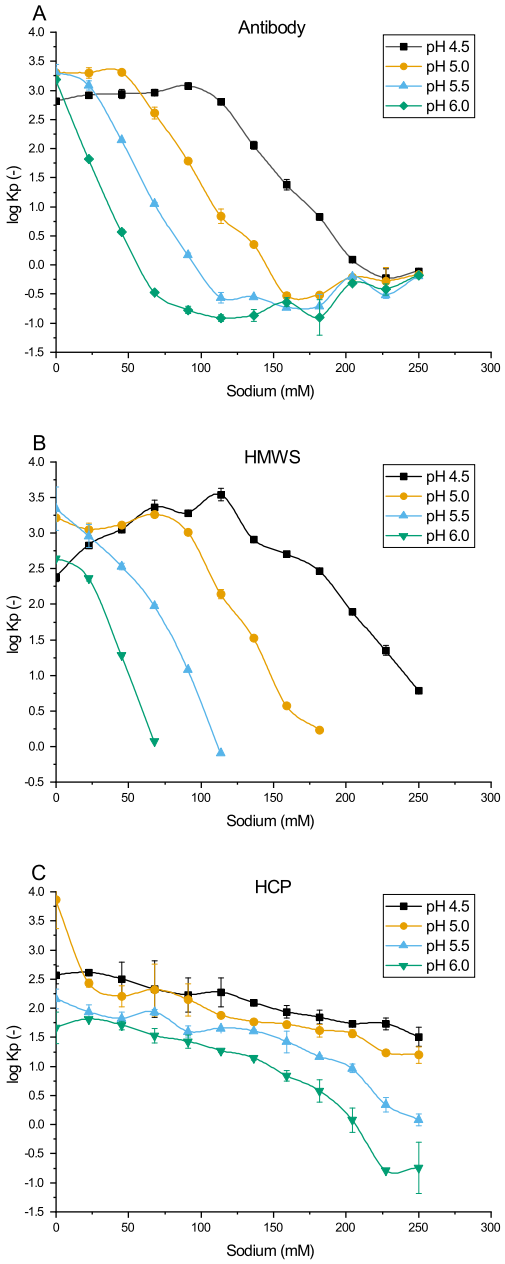

Figure 4.7: Partition coefficients of (A) antibody, (B) high-molecular weight species, and (C) host-cell proteins on Fiber ATRP S adsorbents determined with the HTS developed in this study. Buffer: 20 mM MCB, pH: 4.5-6.0, Na+: 0-250 mM. Error bars are ± 1 SD from 3 replicate wells for each condition.

the separation factors at distinct sodium concentrations. The maxima of the HCP-antibody separation factors were found to be at higher sodium concentrations than the maxima of the HMWS-antibody separation factors. This implies that a trade-off

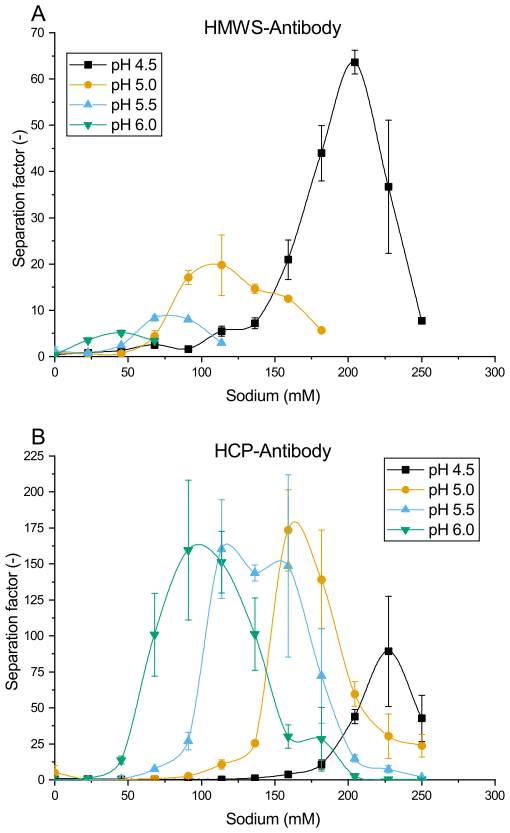

Figure 4.8: Separation factors of (A) HMWS and antibody, and (B) HCP and antibody on Fiber ATRP S adsorbents.

between HMWS removal and HCP removal has to be found when selecting elution conditions. Separation factors for the separation of HMWS and antibody were highest at the lowest pH level with a maximum at a sodium concentration of 205 mM (cf. Fig. 4.8A), while the maxima for the HCP-antibody separation factors were obtained for higher pH levels (cf. Fig. 4.8B). The maximum separation factors for the separation of HMWS and antibody were high when comparing with the data of McDonald2016 et al [157], while HCP-antibody separation factors where moderate. This implies that the fiber-based adsorbents have a high selectivity for the separation of HMWS-antibody and a moderate selectivity for the separation of HCPs and antibody.

For the step elution HMWS removal was considered to be more important than HCP removal. Thus conditions with the highest HMWS-antibody separation factors and low antibody K_ps were selected for verification runs on a 1 mL fiber column (bed height = 2 cm). The selection of small enough product K_ps is important in order to achieve a high product yield within a small pool volume. Three step elution runs at

pH 4.5 and sodium concentrations > 190 mM close to the concentrations in the HTS were performed in order to assess the comparability between the screening results and lab scale column runs.

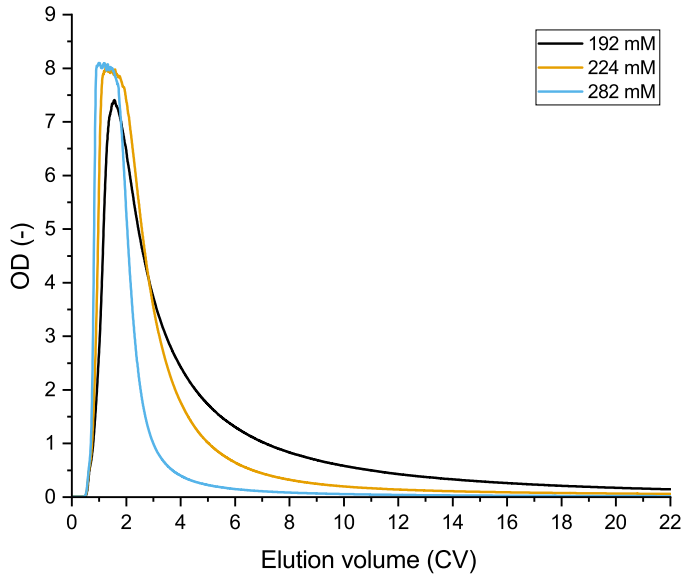

Figure 4.9: Elution profiles of step elution verification experiments on a packed 1 mL Fiber ATRP S column. Buffer: 20 mM MCB, pH 4.5. Sodium concentration: 192-282 mM.

Fig. 4.9 shows the elution profiles of the three step elutions, and Fig. 4.10 displays the respective pool volumes, monomer yields, and impurity levels for different pool end criteria. With increasing sodium concentration steeper elution profiles and narrower elution peaks were observed (cf. Fig. 4.9). This led to a decrease in pool volumes (cf. Fig. 4.10C), while yields increased with increasing sodium concentration (cf. Fig. 4.10D). The same trends were observed for all of the pool end criteria evaluated. This was also the case for the trends with respect to HMWS and HCP levels (cf. Fig. 4.10A and B). The load material contained 9.2% HMWS and 67 μg/mg HCP. For the lowest sodium concentration no HMWS could be detected in the elution pools (cf. Fig. 4.10A). With increasing sodium concentration HMWS levels increased up to 8.2% for the highest sodium concentration and lowest pool end criteria. HCP levels were reduced by 36-49% for the lowest sodium concentration (cf. Fig. 4.10B). With increasing sodium concentrations HCP levels followed a U shaped trend, and the lowest HCP levels were measured for the intermediate sodium concentration.

These trends in HCP and HMWS levels were consistent with the trends in the separation factors from the HTS experiments (cf. Fig. 4.8). HCP-antibody separation factors also followed a U shaped trend. At pH 4.5 the highest separation factor was measured for a sodium concentration of 225 mM, for which the lowest HCP level was

obtained in the column experiments (cf. Fig. 4.8B and Fig. 4.10B). The lowest HMWS levels in the column experiments were obtained for the highest HMWS-antibody separation factor in the HTS experiments (cf. Fig. 4.8A and Fig. 4.10A). HMWS levels increased with increasing sodium concentration, which is in line with the decrease in HMWS-antibody separation factors. This shows, that the trends from the HTS correlated with the trends in lab scale column runs, which suggests that the data from the developed HTS can be used to identify appropriate process conditions for lab scale column runs.

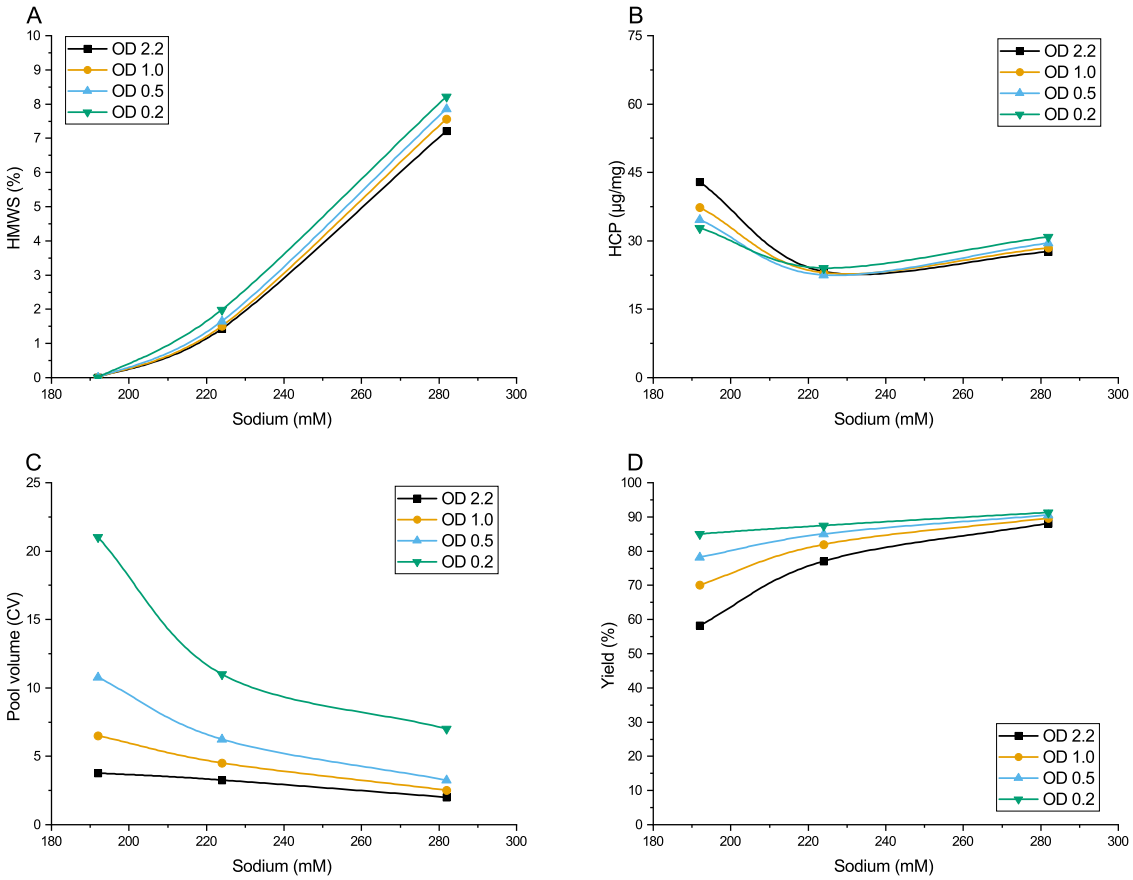

Figure 4.10: (A) HMWS levels, (B) HCP levels, (C) pool volumes, and (D) pool yields for the step elution verification experiments displayed in Fig. 4.9 for different pool end criteria.

4.4 Conclusions

Fiber-based adsorbents have recently attracted much attention as alternative adsorbents for preparative chromatography, however high-throughput microscale tools for such adsorbents are still lacking.

In the present study an automated high-throughput screening for fiber-based adsorbents was established on a robotic liquid handling station in 96 well filter plates. Two techniques were identified that enabled accurate and reproducible portioning of short cut fiber-based adsorbents. The impact of several screening parameters such as phase ratio, shaking frequency, and incubation time was investigated and optimized. The data from the developed HTS correlated with data from packed fiber columns, and binding capacities from both scales matched closely. The developed HTS could be utilized in order to optimize the hydrogel structure of anion exchange fiber-based adsorbents. A novel AEX fiber-based adsorbent was developed that compared favorably with existing resin and membrane adsorbents in terms of productivity and DNA binding capacity. In addition, the developed HTS was successfully employed in order to identify step elution conditions for the purification of a monoclonal antibody from product- and process-related impurities with a CEX fiber-based adsorbents. Trends from the HTS were found to be in good agreement with trends from lab scale column runs.

In summary, the present study describes the setup of an automated, microscale, high-throughput screening for fiber-based adsorbents, which provides data that correlate with data in packed fiber columns. This tool will enable a faster and more complete characterization of novel fiber-based adsorbents, and an easier tailoring of such adsorbents towards specific process applications. In addition, it enables material and time efficient process development for processes that use fiber-based adsorbents. When comparing with previous approaches for characterization of and process development with fiber-based adsorbents, material requirements are reduced by a factor of 3-40 and time requirements are reduced by a factor of 2-5. The availability of a HTS for fiber-based adsorbents will facilitate the evaluation of such materials alongside existing chromatography materials, and make it easier to integrate such materials into processes, for instance during early stages of process development, were material and time are typically scarce. Overall this will help to make better use of the benefits of fiber-based adsorbents in terms of productivity and costs in order to address some of the current challenges in downstream processing.

4.5 Acknowledgments

The authors gratefully acknowledge material supply by Sartorius Stedim Biotech (Jan Schwellenbach, Florian Taft, Louis Villain) and the financial support from the German Federal Ministry of Education and Research (BMBF) under the reference number 13N13322. The authors bear the complete responsibility for the content of this publication. The authors declare no conflict of interest.

5 Exploration of fiber-based cation exchange adsorbents for the removal of monoclonal antibody aggregates

Johannes Winderl[1], Eric Neumann[1], Jürgen Hubbuch[1]

[1] Institute of Engineering in Life Sciences, Section IV: Biomolecular Separation Engineering, Karlsruhe Institute of Technology (KIT), Karlsruhe, Germany

Abstract

Cation exchange chromatography (CEX) is a widely used technique for the removal of monoclonal antibody (mAb) aggregates. At present, diffusive or perfusive resins are mainly used for this purpose, as convective types of adsorbents such as membrane adsorbers (MAs) have often not demonstrated overall comparable performance for this particular application. Fiber-based adsorbents can overcome the current limitations of MAs with respect to permeability, binding capacity, and adsorbent cost. For this reason, fiber-based adsorbents have the potential to be a viable alternative to resins for the removal of mAb aggregates. It has not been evaluated, however, whether and under which conditions the use of such adsorbents is feasible for this purpose.

In the present study, the use of fiber-based CEX adsorbents for mAb aggregate removal was examined. Two types of fiber-based adsorbents, an uncontrolled grafted (Fiber FRP S) and a controlled grafted fiber-based adsorbent (Fiber SI-ATRP S), were

evaluated with respect to permeability, dynamic antibody binding capacity (DBC), resolution capabilities of mAb monomer and aggregates, and the performance in bind and elute and frontal chromatography mode with respect to typical performance indicators, productivity, and buffer consumption. The permeabilities of the fiber-based adsorbents ranged from 200-1700 mD, making it possible to use the fiber-based adsorbents at larger bed heights than membrane adsorbers with fast mobile phase velocities. Antibody DBCs ranged from 20-41 g/L at 150 cm/h, and at higher mobile phase velocities exceeded the DBC of an existing resin material, Poros 50 HS, which has frequently been used for aggregate removal. Both fiber types showed good resolution capabilities of monomer and aggregates, and provided better resolution per column length than Poros 50 HS. Typical purity and yield constraints were fulfilled for both fiber types in both bind and elute and frontal chromatography mode for mobile phase velocities ranging up to 480 cm/h and 1060 cm/h. The overall performance of the controlled grafted fibers was found to be superior to the performance of uncontrolled grafted fiber-based adsorbents due to higher productivity and lower buffer consumption. The overall performance of the fiber-based adsorbents was found to be comparable to the performance of Poros 50 HS at typical operating conditions.

The results in this study indicate that the use of fiber-based adsorbents for mAb aggregate removal is feasible with a performance that is comparable to the performance of an existing resin material. Depending on the cost of the fiber-based adsorbents and the use scenario, the usage of such adsorbents could be beneficial. Further improvements in performance might be possible via adjustments in the architecture of the polymer-nanolayer of the controlled grafted fiber-based adsorbents.

5.1 Introduction

Monoclonal antibodies (mAbs) represent the largest share of approved biopharmaceuticals [4] and recently approved protein therapeutics [7]. Several hundred mAbs are currently under development and/or in clinical trials. Due to the high degree of similarity between different mAbs, the purification of mAbs has been standardized via platform processes [12]. While these processes are well established, there is an interest in improving the productivity and reducing the cost and complexity of such processes, in order to meet the future demand for mAbs, and lower the manufacturing costs.

An essential part of the purification of therapeutic mAbs is the removal of antibody aggregates. Aggregates can form during different parts of mAb processing [159], and

need to be removed as they can have different biological activities as monomeric antibodies, and can trigger immune responses when administered to patients, which can affect both safety and efficacy [159, 160]. Due to the similarities in chemical and physical properties between aggregates and monomeric antibodies, the removal of antibody aggregates can be challenging.

A widely used technique for aggregate removal is cation exchange (CEX) chromatography. CEX chromatography makes use of the different number of surface charges between aggregates and monomers. It is typically operated in bind and elute mode, but alternatively it can also be performed in frontal chromatography mode [161–164]. In bind and elute mode the mAb feed is loaded onto the column, and monomer and aggregates are subsequently separated via isocratic elution or with a gradient in salt concentration and/or pH [165]. In frontal chromatography mode the column is loaded beyond breakthrough with mAb feed under conditions that favor aggregate binding, and the flowthrough is collected until a certain pool aggregate content is reached. The choice between these operating modes depends on the purities and yields that can be obtained, but also on factors that affect platform fit and process economics such as pool volumes, pool conductivities, productivities, and buffer consumption. Bind and elute mode is often selected for robustness reasons, however the load density in this operating mode has to be below the breakthrough capacity, which limits the productivity [163]. In industrial processes the load density is typically selected very conservatively and contains a certain safety margin in order to avoid any potential product loss, which further reduces the productivity. In frontal chromatography mode the column can be loaded to much higher load densities [162], which can result in higher productivities, however the operating window in terms of pH and conductivity is smaller [163], and clearance of other impurities under optimal conditions for aggregate removal can be limited.

At present, diffusive or perfusive resins are mainly used for aggregate removal via cation exchange chromatography. Convective adsorbents such as membrane adsorbers (MAs), which have advantages in terms of mass transfer properties and productivity, have been evaluated [155, 162], but have often not demonstrated overall comparable performance for this particular application. Limitations that have been identified in previous studies, were comparatively low binding capacities for antibodies and aggregates [155, 162], and the higher costs of such adsorbents per volume basis [155].

With the use of fiber-based adsorbents it is possible to address these shortcomings. They can be prepared from low cost polymeric fibers, which are estimated to cost only a fraction of what other support materials cost. Fiber-based adsorbents can be prepared with the use of uncontrolled grafting polymerization techniques or controlled polymerization techniques such as atom-transfer radical polymerization [83] which

allow for more control of the grafted polymer-nanolayer architecture with potential benefits in terms of process performance. Previous characterization studies with model proteins have shown that such adsorbents feature high permeabilites, and binding capacities that exceed the binding capacities of current MAs. Consequently such adsorbents could be a viable alternative for the removal of mAb aggregates. However, up to now, fiber-based adsorbents have only been characterized with model proteins, and it is not known, whether the use of such adsorbents for process applications such as mAb aggregate removal is feasible, and how different types of fiber-based adsorbents compare in this application.

The purpose of the present study was to investigate if, and under which conditions fiber-based adsorbents can be used for monoclonal antibody aggregate removal in bind and elute mode or frontal chromatography mode. Two types of fiber-based adsorbents, an uncontrolled and a controlled grafted fiber-based adsorbent, were evaluated with respect to permeabilities, dynamic antibody binding capacities, resolution capabilities of mAb monomer and aggregates, the performance in bind and elute and frontal chromatography mode, and the productivities and buffer consumption in these operating modes.

5.2 Experimental

5.2.1 Materials

5.2.1.1 Chemicals, buffers and proteins

Potassium chloride (KCl), sodium chloride (NaCl), hydrogen chloride (HCl), acetic acid, citric acid monohydrate, sodium hydroxide (NaOH), and ethanol (EtOH) were purchased from Merck (Darmstadt, Germany). Dipotassium phosphate was obtained from VWR International (Darmstadt, Germany). 3-morpholinopropane-1-sulfonic-acid (MOPS) was from Carl Roth (Karlsruhe, Germany), and succinic acid as well as 2-(N-morpholino)ethanesulfonic acid monohydrate (MES) were from AppliChem (Darmstadt, Germany). Dextran with an average molecular mass of 2000 kDa from *Leuconostoc* spp. was acquired from Sigma-Aldrich (St. Louis, MO, USA). The monoclonal antibody (mAb) was provided by an established industrial manufacturer. It was a CHO-derived IgG which had been purified via Protein A chromatography. The composition was 93.97% monomer, 4.87% high molecular weight HMW1 species (dimer) and 1.16% HMW2 species (predominantly trimer) as determined by analytical size exclusion chromatography (SEC). For the experiments

a 10 mM multicomponent buffer (MCB) was used, which was composed of 14.14 mM MOPS, 4.96 mM MES, 6.45 mM acetic acid, and 9.10 mM succinic acid. The buffer composition was calculated according to [145] in order to obtain a constant buffering capacity within the pH range of 4.5-6.0. Analytical size exclusion chromatography was carried out at pH 7 with a phosphate buffer that contained 250 mM dipotassium phosphate and 250 mM potassium chloride. All buffers were prepared with ultra-pure (UP) water (Purelab Ultra, Elga Lab-Water, High Wycombe, UK). The pH of pure buffer solutions was adjusted with NaOH or HCl as needed. Prior to usage all buffers were filtered through 0.2 μm cellulose acetate (CA) membrane filters (Sartorius, Göttingen, Germany).

5.2.1.2 Stationary phases

Two types of fiber-based strong cation exchange adsorbent prototypes were evaluated in this study. Both prototypes were SO_3^--functionalized, and grafted with poly(glycidyl methacrylate). One of the prototypes (Fiber FRP S) was prepared from winged shaped polyamide 6 fibers (Allasso Industries, Raleigh, NC, USA) via free radical polymerization as previously described in [146], while the other prototype (Fiber SI-ATRP S) was prepared from winged shaped polyethylenterephtalate fibers via surface-initiated atom transfer radical polymerization as detailed in [83]. Both prototypes were provided to us by Sartorius Stedim Biotech (Göttingen, Germany). The fiber-based adsorbents were compared with the commercially available perfusive resin Poros 50 HS (Thermo Fisher Scientific, Dreieich, Germany), and the membrane Sartobind S (Sartorius Stedim Biotech, Göttingen, Germany). The ion-exchange capacity of all adsorbents was determined via acid-base titration. The following ion-exchange capacities per skeleton volume were measured: 0.273 M (Fiber FRP S), 0.310 M (Fiber SI-ATRPS S), 0.276 M (Poros 50 HS) and 0.312 M (Sartobind S).

5.2.1.3 Chromatographic instrumentation

The chromatography experiments were carried out on an ÄKTAmicro, two ÄKTA-purifier 10, and an ÄKTA pure 25 system. The ÄKTAmicro system was equipped with pump P-905, UV monitor UV-900 with a 3 mm UV flow cell, pH, conductivity and temperature monitor pH/C-900, autosampler A-905, fraction collector Frac-950, and a flow restrictor FR-902. The ÄKTA purifier systems were equipped with pump P-903, UV monitor UV-900 with 10 mm UV flow cell, pH, conductivity and temperature monitor pH/C-900, autosampler A-905, fraction collector Frac-950, and flow restrictor FR-902. Depending on flow rate, 90 μL or 200 μL mixing chambers

were used. All of the three instruments were controlled with Unicorn 5.31. The ÄKTA pure system consisted of a sample pump S9, column valve kit V9-C, UV monitor U9-M with 2 mm path length, conductivity monitor C9 and fraction collector F9-C. It was controlled with Unicorn 6.4.1 (all GE Healthcare, Little Chalfont, UK).

5.2.1.4 Analytical instruments

The protein concentrations of antibody stock solutions were determined spectrophotometrically with a NanoDrop 2000c UV-VIS spectrophotometer (Thermo Fisher Scientific, Waltham, MA, USA), using the antibody extinction coefficient E1% of 15.28 $(g/100\ mL)^{-1}cm^{-1}$. Analytical size exclusion chromatography was performed with a TSKgel SuperSW mAb HTP column (4.6 mm I.D. x 15 cm L) (Tosoh Bioscience, Griesheim, Germany) which was connected to a Dionex UltiMate 3000 RS UPLC system (Thermo Fisher Scientific, Waltham, MA, USA). The system consisted of a HPG-34000 RS binary rapid separation LC pump, a WPS-3000 TFC autosampler, a TCC-3000 RS column compartment, and a DAD-3000 (RS) diode array detector. It was controlled with Chromeleon 6.8.

5.2.1.5 Software and data analysis

The experimental data was processed and analyzed with Microsoft Excel 2016 (Microsoft, Redmond, WA, USA), Origin 2018b (OriginLab, Northampton, MA, USA), and Matlab R2017a (Mathworks, Natick, MA, USA).

5.2.2 Methods

5.2.2.1 Buffer exchange

The antibody was buffer exchanged and concentrated with Vivaspin 20 centrifgual concentrators (Sartorius, Göttingen, Germany) with PES membranes and a molecular weight cut-off (MWCO) of 10 kDa. If only small amounts of protein were required for experiments buffer exchange was carried out with PD-10 desalting columns (GE Healthcare, Little Chalfont, UK).

5.2.2.2 Column packing and storage

The fiber-based adsorbents were packed into laboratory scale Omnifit BenchMark columns (Diba Industries, Danbury, CT, USA) with an I.D. of 6.6 mm or MiniChrom columns (Repligen, Weingarten, Germany) with an I.D. of 8 mm. A fiber packing density of 0.32 g fiber per mL column volume (CV) was used. The dimensions of the columns used were 6.6 mm I.D. x 3.8 cm L and 8 mm ID x 5 cm L for the Fiber FRP S columns, and 6.6 mm I.D. x 3.6 cm L and 8 mm I.D. x 5 cm L for the Fiber SI-ATRP S columns. Packing was performed with a dry packing technique as described previously in [83]. Poros 50 HS was flow packed into Omnifit columns (6.6 mm I.D. x 4 cm L) according to the manufacturer's instructions. For the determination of dynamic binding capacities and selectivities a prepacked MiniChrom column (5 mm I.D. x 2.5 cm L) was used (Repligen, Weingarten, Germany). Sartobind S was packed into a void volume optimized flat sheet membrane holder with a flow dispenser which was obtained from Sartorius Stedim Biotech (Göttingen, Germany). 3 layers of membrane with a diameter of 3 cm and a a total bed height of 0.825 mm were packed into the holder. Within the holder 2.59 cm of the membrane are percolated, which leads to a membrane volume (MV) of 0.435 mL. For the determination of bed permeability a commercial Sartobind S nano 3 mL capsule with a bed height of 8 mm was used. Upon packing and in between experiments all columns and capsules were stored in aqueous solutions containing 20 vol% EtOH and 150 mM NaCl.

5.2.2.3 Determination of bed permeability

The permeability of the different cation exchange adsorbents was determined from pressure flow experiments in 10 mM MCB, pH 5 with different amounts of NaCl added, using a method that has been described previously [151]. Briefly, the mobile phase flow rate was varied from 0 to 25 mL/min and the resulting pressure drop over the column or membrane was calculated from measurements of the column pressure drop with and without the column or membrane. The permeability was determined from a linear regression of $\eta \cdot u \cdot L$ against Δp, where η is the dynamic viscosity of the buffer, u is the mobile phase velocity, and L is the length of the column or membrane bed. Values for the dynamic viscosity of the different buffers at 25 °C were taken from [166]. For the fiber-based adsorbents and Poros 50 HS Omnifit columns with the same I.D. (6.6 mm) and similar bed heights (3.6-4 cm) were used. For Sartobind S, a commercial Sartobind S nano 3 mL capsule with 30 membrane layers and a bed height of 8 mm was used.

5.2.2.4 Determination of dynamic binding capacities

The dynamic binding capacities of the monoclonal antibody (mAb) were determined at different mobile phase velocities by overloading the packed columns and membrane devices with antibody solution. The DBC was evaluated from the volume $V_{10\%}$ corresponding to 10% breakthrough. The retention volume of dextran $V_{ret,dextran}$ was subtracted to account for system and column dead volumes. The DBC was calculated from $V_{10\%}$, $V_{ret,dextrane}$, and the geometric column or membrane volume V as follows:

$$DBC_{10\%} = \frac{V_{10\%} - V_{ret,dextran}}{V} \tag{5.1}$$

The experiments were carried out in 10 mM MCB, pH 5.3 with different amounts of sodium chloride (0-100 mM) added. The mAb concentration in the load was 2.2 g/L. DBCs were measured at mobile phase velocities in the range of 100-1400 cm/h for the fiber-based adsorbents and Poros 50 HS, and 6-114 cm/h for Sartobind S, as higher flow rates were not possible with the instrument used.

5.2.2.5 Determination of resolution of monomer and high molecular weight aggregate species

In order to assess the resolution of monomer and high molecular weight aggregate species (HMWs) of the different adsorbents linear salt gradient elution (LGE) experiments were performed at different pH values within the range of pH 4.5-6.0. For each adsorbent 0.7 g/L CV or MV of a 4.2 g/L antibody solution in 10 mM MCB at the respective pH were injected with a sample loop. The method was composed of a 6 CV equilibration step with 10 mM MCB, followed by injection of the antibody solution, a 3-8 CV wash step until the UV signal had returned to the baseline, and a linear salt gradient from 10 mM MCB to 10 mM MCB + 1 M NaCl over 20 CV. A mobile phase velocity of 150 cm/h was used for all adsorbents except for the membrane adsorber for which the velocity was set to 10 cm/h due to flow rate limitations of the instrument that was used for the experiment. After every run the columns or membranes were stripped and cleaned with 5 CV of 1 M NaCl and 2 CV of 0.1 M NaOH. The flowthrough, wash and elution of every run was collected in constant volume fractions and analyzed via analytical SEC to determine the content of monomer and aggregate species. The relative peak areas from the analytical SEC of every fraction were used to deconvolute the UV signal of the linear gradient elution experiments into separate monomer, HMW1 and HMW2 peak profiles. Exponentially modified gaussian (EMG) functions were fit to the peak profiles of every species.

The chromatographic resolution of adjacent peaks was calculated from the statistical moments of the fitted peak functions according to

$$R_s = \frac{\mu_j - \mu_i}{2(\sigma_i + \sigma_j)} \tag{5.2}$$

where i and j stand for the compounds that elute in the peaks, and i denotes the compound that elutes first. To account for the different bed heights of the membrane device and the fiber/resin columns, the resolution was normalized to the respective bed height L according to:

$$r_s = \frac{R_s}{\sqrt{L}} \tag{5.3}$$

The normalized resolution coefficient r_s was used to calculate the ratio of column lengths that would be required to achieve the same normalized resolution.

5.2.2.6 Evaluation of performance of fiber-based adsorbents in bind-and-elute mode

In order to evaluate the performance of the fiber-based adsorbents for aggregate clearance in bind-and-elute mode the packed fiber columns were loaded with mAb to 70% of the respective $DBC_{10\%}$. The fiber columns with 8 mm I.D. and 5 cm L were used for this purpose. The experiments were performed at mobile phase velocities of 150, 300, 700 and 1060 cm/h for the FRP S fiber-based adsorbents, and 150, 300, and 480 cm/h for the SI-ATRP S fiber-based adsorbents. The columns were first equilibrated with 5 CV of 10 mM MCB + 22 mM NaCl, pH 5, and then loaded with mAb at a concentration of 2.2 g/mL in 10 mM MCB + 22 mM NaCl, pH5 to the desired load density. Subsequently the columns were washed with 5 CV of equilibration buffer, pH 5 and eluted with a gradient from 10 mM MCB + 22 mM NaCl, pH5 to 10 mM MCB + 385 mM NaCl, pH 5 in 20 CV. After every run the columns were stripped with 5 CV of 1 M NaCl and 2 CV of 0.1 M NaOH. The flowthrough from the elution steps was collected in 0.5 mL fractions and analyzed via SEC to determine the content of monomer and aggregate species. For the calculation of cumulative yield and cumulative pool volume pooling was started with the first fraction in which antibody was detected. Monomer yield, monomer purity, pool volume, pool conductivity and monomer concentration factor F_{conc} for a cumulative pool purity of 99% were calculated from the SEC analysis, the pool start and end volume, and conductivity peak area of the fractions involved.

5.2.2.7 Evaluation of performance of fiber-based adsorbents in frontal chromatography mode

In order to evaluate the performance of the fiber-based adsorbents for aggregate removal in isocratic overloaded mode the fiber columns were loaded beyond breakthrough with mAb. For this purpose the Omnifit columns with an I.D. of 6.6 mm were used. The experiments were carried out at mobile phase velocities of 150 cm/h and 1060 cm/h for the FRP S fiber-based adsorbents, and 150 cm/h and 480 cm/h for the SI-ATRP S fiber-based adsorbents. Columns were loaded to load densities of 44.5 and 28.9 g/L CV for the FRP S adsorbents, and 86.5 and 66.9 g/L CV for the SI-ATRP S adsorbents. The method consisted of a 5 CV equilibration step with 10 mM MCB + 100 mM NaCl, pH5, a loading step with mAb in 10 mM MCB + 100 mM NaCl, pH 5.3, a 5 CV wash step with 10 mM MCB + 100 mM NaCl, pH5, and a gradient from 10 mM MCB + 100 mM NaCl, pH5 to 10 mM MCB, pH5 + 375 mM NaCl over 15 CV. After each run the columns were cleaned with 5 CV of 1 M NaCl and 2 CV of 0.1 M NaOH. The flowthrough from the load and wash step was collected in 2 mL fractions, and the flowthrough from the elution step was collected in 0.5 mL fractions. The fractions were analyzed via analytical SEC to determine the respective monomer and aggregate contents. For the calculation of cumulative yield and cumulative pool volume pooling was started with the first fraction in which antibody was detected. Monomer yield, pool volume, pool conductivity and monomer concentration factor F_{conc} for a cumulative pool purity of 99% were calculated from the absorbance peak area, pool start and end volume, and conductivity peak area of the fractions involved.

5.2.2.8 Analytical size exclusion chromatography

The analytical size exclusion chromatography was carried out with a TSKgel SuperSW mAb HTP column (4.6 mm I.D x 15 cm L) at a volumetric flow rate of 0.45 mL/min. 20 μL of each sample were injected. Samples with a concentration $>$ 1 g/L were diluted accordingly with MCB.

5.3 Results and Discussion

5.3.1 Permeabilities and operating windows

As a first step we determined the permeabilites of the fiber-based adsorbents in order to calculate the operating windows of the adsorbents in terms of bed height and mobile

phase velocity. Bed height is an important factor for aggregate removal because it directly affects column resolution. In addition, knowledge about the operating windows is also important for assessing potential productivities and throughputs. For this purpose we performed pressure flow experiments under a set of buffer conditions (10 mM MCB, pH5) and salt concentrations (0 mM, 100 mM, 1000 mM NaCl) that are typically used for aggregate removal. The experiments were carried out with the fiber-based adsorbents, a commercially available membrane adsorber, Sartobind S, and a commercially available resin, Poros 50 HS, which has previously been used for aggregate removal.

For all adsorbents, linear pressure-flow profiles were obtained at all of the salt concentrations evaluated up to mobile phase velocities of 200 cm/h (Sartobind S), 4380 cm/h (Poros 50 HS), 1400 cm/h (Fibers FRP S), and 1050 cm/h (Fiber SI-ATRP S). Based on the pressure flow curves, bed permeabilities were calculated, which are summarized in Table 5.1. The permeabilities of Sartobind S ranged from 15-67 mD, while the permeabilities of Poros 50 HS varied from 788-819 mD. These values are consistent with permeabilities and pressure drops which have been reported in previous studies of Sartobind S [83] and Poros 50 HS [167]. The permeabilities of the Fiber FRP S and Fiber SI-ATRP S adsorbents were 8-14 and 27-86 times higher than the permeabilities of Sartobind S, and in the case of the Fiber FRP S adsorbent also 1.6-2.2 times higher than the permeabilities of Poros 50 HS. The permeabilities of Poros 50 HS remained nearly constant with increasing salt concentration, while the permeabilites of the fiber-based adsorbents and Sartobind S increased with increasing salt concentration. This is a consequence of the grafted hydrogel layer which is known to shrink with increasing ionic strength, i.e. increasing salt concentration. This leads to an increase in pore diameter and permeability. Poros 50 HS lacks a grafted

Table 5.1: Permeabilities of the different cation exchange adsorbents evaluated in this study in 10 mM MCB, pH5 with different amounts of NaCl added. Permeabilites were determined from linear fits of pressure flow profiles of each adsorbent and are listed with the respective 95% confidence intervals. Bed dimensions: 6.6 mm I.D. x 4 cm L (Poros 50 HS), 110 cm^2 membrane area x 8 mm L (Sartobind S nano 3 mL), 6.6 mm I.D. x 3.8 cm L (Fiber FRP S), 6.6 mm I.D. x 3.6 cm L (Fiber SI-ATRP S).

	Permeabilitiy (mD)		
	Buffer conditions		
Adsorbent	0 mM NaCl, 1.2 mS/cm	100 mM NaCl, 11.8 mS/cm	1000 mM NaCl, 87 mS/cm
Poros 50 HS	787.80 ± 3.86	804.10 ± 2.99	818.55 ± 3.74
Sartobind S	14.79 ± 0.35	40.05 ± 0.83	66.80 ± 2.62
Fibers SI-ATRP S	200.70 ± 4.71	395.84 ± 14.21	565.86 ± 28.98
Fibers FRP S	1271.38 ± 49.56	1555.06 ± 59.23	1757.84 ± 67.67

hydrogel layer, and swelling of the media upon changes in ionic strength is less than 1%, which explains that permeabilities remain nearly constant. The different extent of changes in permeability with increasing salt concentration between the fiber-based adsorbents, is a consequence of the different permeabilities and hence pore diameters at the low salt concentration, and the different hydrogel compositions. The SI-ATRP S fibers contain a controlled grafted hydrogel layer which is more uniform than the uncontrolled grafted hydrogel layer of the FRP S fibers. In addition, the hydrogel layer of FRP S is crosslinked, which limits hydrogel flexibility. For all of the grafted adsorbents the permeability was found to be logartihmically correlated to the ionic strength.

Based on the permeabilities we calculated the operating windows of the different adsorbents (cf. Fig. 5.1) for a maximum column pressure drop of 3 bar. This is a typical limit when considering a potential scale up to larger columns or devices at later stages of process development. The calculations were performed for the lowest salt concentration because under these conditions the permeabilites of all adsorbents were lowest. Under these conditions, Sartobind S had the smallest operating window. It can be operated at fast mobile phase velocities at low bed heights. In comparison to Sartobind S the fiber-based adsorbents have a larger operating window and can be operated at higher bed heights than the membrane with the same mobile phase velocities. The Fiber FRP S adsorbent could even be operated at bed heights of

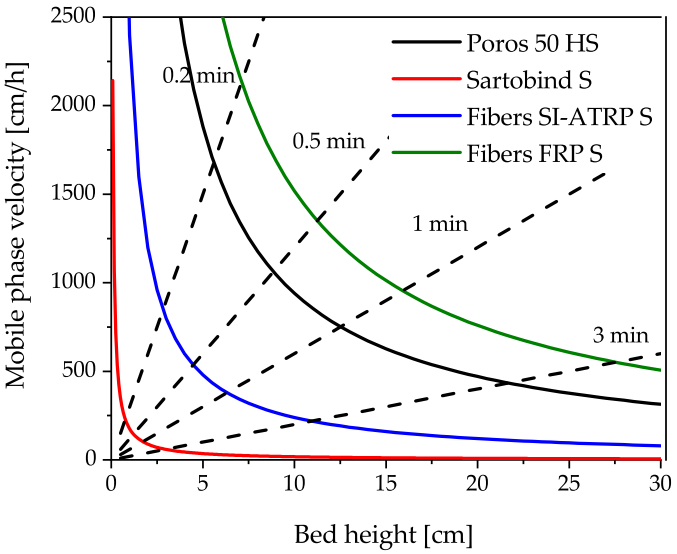

Figure 5.1: Comparison of the operating windows of the cation exchange adsorbents evaluated in this study. The solid lines were calculated from the permeability of each adsorbent and display the limits up to which each adsorbent can be operated when assuming a maximum allowable pressure drop of 3 bar. Dashed lines show bed residence times. Buffer: 10 mM MCB, pH 5, Conductivity: 1.2 mS/cm.

15-30 cm that are typically used for resins such as Poros 50 HS. Previous studies with the fiber-based adsorbents have indicated that the packing quality of the fiber-based adsorbents is sufficient for bed heights > 3-3.5 cm [83, 146]. Under these conditions the fiber-based adsorbents could be operated up to high mobile phase velocities. Depending on the effect of mobile phase velocity on dynamic binding capacity, this could be beneficial for the productivity, as long a the resolution at such short bed heights is sufficient.

5.3.2 Dynamic antibody binding capacities

Therefore, in the next step, we determined the dynamic binding capacities (DBCs) of a monoclonal antibody (mAb) on the fiber-based adsorbents and the two commercially available adsorbents. The experiments were carried out at several mobile phase velocities up to the maximum instrument flow rate or the maximum flow rate where the bed was stable, in order to investigate the impact of mobile phase velocity on DBCs. DBCs were evaluated at 10% breakthrough, and are presented in Fig. 5.2.

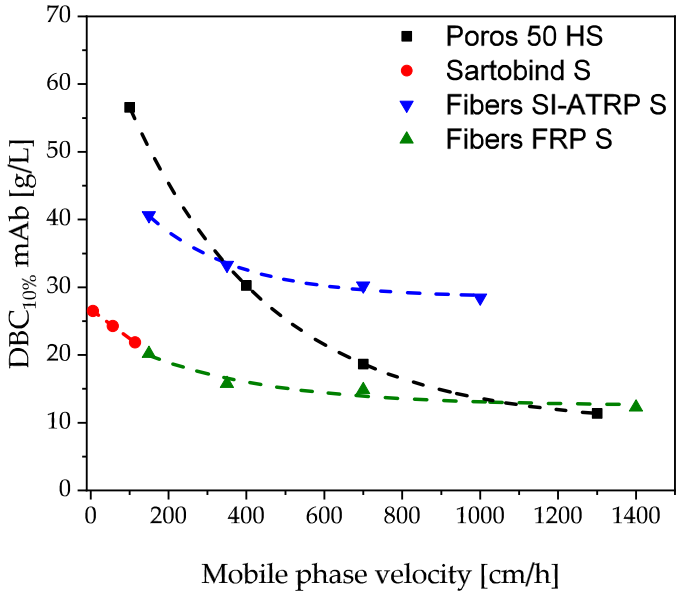

Figure 5.2: Comparison of the the dynamic mAb binding capacities (DBCs) of the two fiber-based cation exchange adsorbents evaluated in this study and different commercially available adsorbents. DBCs were evaluated at 10% breakthrough at mobile phase velocities in the range of 6-1400 cm/h in 10 mM MCB buffer, pH 5.3, with a protein concentration in the load of 2.2 g/L. Dashed lines show asymptotic exponential (Poros 50 HS, Fibers SI-ATRP S, Fibers FRP S) and linear (Sartobind S) fits to the respective data.

At slow mobile phase velocities Poros 50 HS had the highest DBC of all adsorbents with 56.6 g/L at 100 cm/h. With increasing mobile phase velocity the DBC decreased

by 80% to 11.4 g/L at 1300 cm/h. These DBCs and the change in DBCs with increasing mobile phase velocity are consistent with earlier data of other mAbs on Poros 50 HS [155, 162, 168]. The DBCs of Sartobind S were about 50% lower than the DBCs of Poros 50 HS, but decreased only slightly with increasing velocity from 26.5 g/L to 21.9 g/L. Similar DBCs have been reported in previous studies of Sartobind S [83, 155]. At the lowest mobile phase velocity the DBC of the Fiber FRP S adsorbent was similar to the DBC of Sartobind S. In comparison to Poros 50 HS, the decrease in DBC with increasing mobile phase velocity was less pronounced for the FRP S fibers. DBCs decreased by 39 % from 20.2 g/L at 150 cm/h to 12.27 g/L for 1400 cm/h. At the highest mobile phase velocity the DBC of the Fiber FRP S adsorbent was higher than the one of Poros 50 HS. The DBC of the Fiber SI-ATRP S adsorbent was about twice as high as the DBC of the Fiber FRP S adsorbent and Sartobind S. With increasing mobile phase velocity DBCs decreased by 30 % from 40.6 g/L at 150 cm/h to 28.4 g/L at 1000 cm/h, and at higher mobile phase velocities exceeded the DBCs of Poros 50 HS.

In summary, the impact of the mobile phase velocity on DBCs was less pronounced on the fiber-based adsorbents than on Poros 50 HS. This could be beneficial for the productivity. In order to utilize the higher DBCs of the fiber-based adsorbents at fast mobile phase velocities, the bed height of the fiber-based adsorbents has to be selected such that the fiber-based adsorbents can be operated at high mobile phase velocities. In order to estimate at which mobile phase velocities the DBCs of the fiber-based adsorbents exceed the DBCs of Poros 50 HS, exponential asymptotic functions where fit to the respective DBC data. For all the adsorbents the DBC data could be described reasonably well with these functions. Based on the fits, the DBC of the SI-ATRP S fibers exceeds the one of Poros 50 HS at a mobile phase velocity of 343 cm/h, while the DBC of the FRP S fibers exceeds the one of Poros 50 HS at 1059 cm/h. Such mobile phase velocities would be feasible if bed heights of the fiber-based adsorbents were selected to be smaller than 7 cm for the SI-ATRP S fibers and smaller than 14.5 cm for the FRP S fibers.

5.3.3 Resolution of monomer and high molecular weight aggregate species

In the next step, we performed linear salt gradient elution (LGE) experiments in order to investigate the resolution capabilities of the different adsorbents for the separation of monomer and high molecular weight (HMW) aggregate species. The experiments were carried out at pH 4.5, 5.0 and 6.0 with the same mAb as in the DBC experiments, which was composed of 93.97% monomer, 4.87% HMW1, and 1.16% HMW2. Bed heights were the same as in the DBC experiments, and linear salt gradients from 0-1 M NaCl over 20 CV were used for all adsorbents. The

mobile phase velocity was set to 150 cm/h, which is a typical intermediate mobile phase velocity that has been used for aggregate removal on Poros 50 HS [162]. For Sartobind S the mobile phase velocity was lowered to 10 cm/h due to instrument limitations. For the evaluation of the resolution capabilities, plots of cumulative purity versus cumulative yield and cumulative pool volume were generated. In addition for each adsorbent, the resolution of monomer and the different HMWs was calculated from the chromatograms via UV peak deconvolution and calculation of the statistical moments. Furthermore, a normalized resolution coefficient was calculated as suggested by [167] in order to account for the different bed heights of the fiber/resin columns and the membrane capsule.

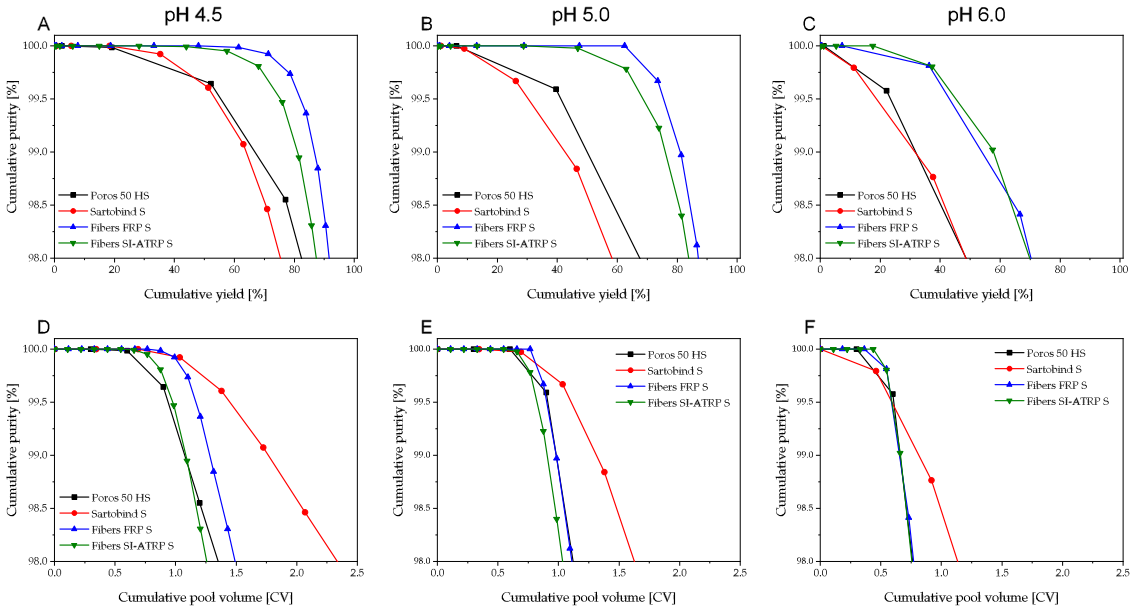

Figure 5.3: Cumulative purity versus (A-C) cumulative yield, and (E-F) cumulative pool volume for linear salt gradient elution experiments at (A, D) pH 4.5, (B, E) pH 5.0 and (C, F) pH 6.0 with the different cation exchange adsorbents used in this study. Buffer conditions: 10 mM MCB, 0 to 1 M NaCl over 20 CV. Mobile phase velocity: 150 cm/h (Poros 50 HS, Fiber SI-ATRP S, Fibers FRP S), 10 cm/h (Sartobind S). Purity of the load: 94%. Load density: 0.7 g/L CV.

Fig. 5.3 shows the cumulative purity vs. cumulative yield (cf. Fig. 5.3A-C) and cumulative pool volume (cf. Fig. 5.3D-F) plots for the different adsorbents at the 3 different pH values. The resolution capabilities of all adsorbents improved with decreasing pH, which is reflected in the shift of the respective purity versus yield plots to higher yield levels, while elution pool volumes increased with decreasing pH. At all pH values the Fiber FRP S and Fiber SI-ATRP S adsorbents showed the best resolution capabilities as indicated by the highest respective purity versus yield curves, followed by Poros 50 HS and Sartobind S. The elution pool volumes of the fiber-based adsorbents were comparable to the elution pool volumes of Poros

50 HS, while the elution pool volumes of Sartobind S were larger. This might be a consequence of the higher dead volume to bed volume ratio of the flat sheet membrane holder in comparison to the resin and fiber columns. For the fiber-based adsorbents pH 5 provided the best compromise between resolution capabilities and elution pool volume.

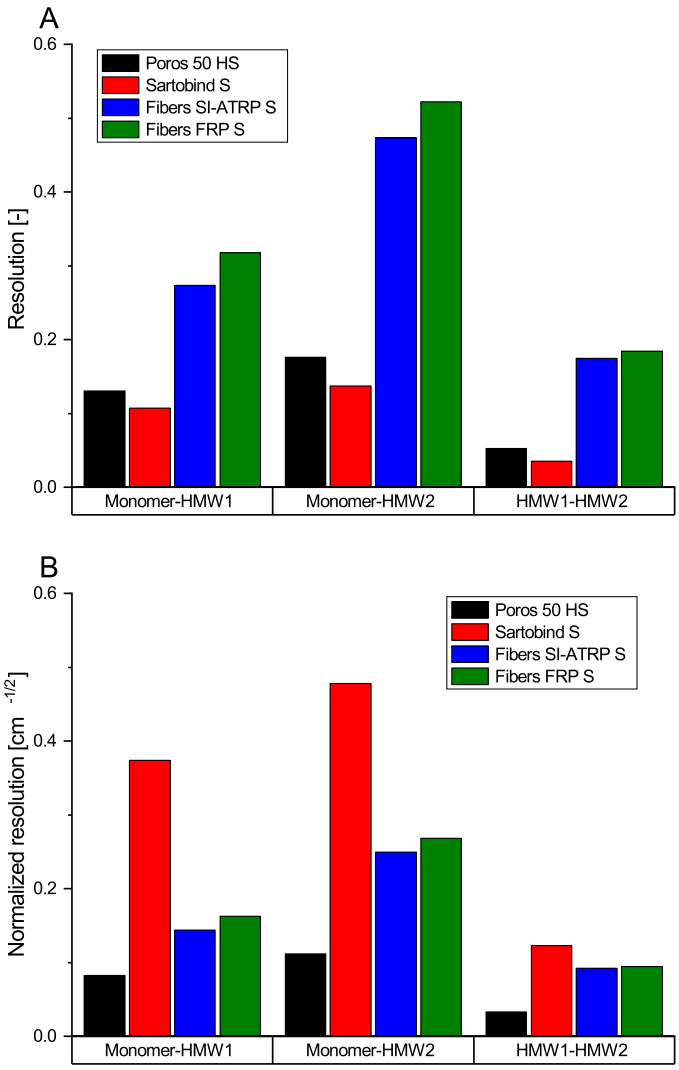

Figure 5.4: Comparison of the (A) resolution and (B) normalized resolution of monomer and HMWs of the different adsorbents evaluated in this study at pH 5.0.

Fig. 5.4 compares the resolutions (cf. Fig. 5.4A) and normalized resolutions (cf. Fig. 5.4B) of the different adsorbents at pH 5. The trend in the resolution data was consistent with the purity versus yield curves. For all separations the resolutions of the Fiber FRP S adsorbents were highest, followed by the SI-ATRP S fibers, Poros 50 HS, and Sartobind S. The normalized resolutions of the fiber-based adsorbents

ranged from 0.09 to 0.27, and were more than twice as high as the normalized resolutions of Poros 50 HS. Only Sartobind S showed better resolution capabilities per column length with normalized resolutions that ranged from 0.12-0.48. The higher normalized resolutions of the fiber-based adsorbents and Sartobind S could be a consequence of the grafted hydrogel layer which contains methacrylate. It has been shown in previous studies that methacrylate enhances the selectivity for aggregates through nonspecific hydrophobic interactions. In addition the higher resolutions might also be a consequence of better mass transfer efficiencies. For the SI-ATRP S fibers plate heights of 0.09 cm have been reported for IgG [83] at 150 cm/h, while for Poros 50 HS higher plate heights in the range of 0.13 to 0.25 cm have been reported for these conditions in previous studies [128, 168]. The high normalized resolutions of Sartobind S might be a consequence of the lower mobile phase velocity that was used for the resolution measurements.

Overall, the data from the LGE experiments indicated that the fiber-based adsorbents have good resolution capabilities for the separation of monomer and HMW aggregate species. While resolution could be further improved on any of the adsorbents, and measurements under low loading densities are only indicative for the behavior under high loading, the fiber-based adsorbents demonstrated good resolution capabilities per column length. Based on the normalized resolution coefficients, we calculated column length ratios that would be required in order to achieve the same resolution as the Fibers FRP S adsorbent (cf. Table 5.2). For instance, in order to achieve the same resolutions as a 5 cm Fibers FRP S column, a 5.3-6.4 cm long ATRP S column could be used, while the bed height of Poros 50 HS would have to be much longer, i.e. 19.5-40.7 cm. For Sartobind S a bed height of 1.0-3.0 cm would be required. While such bed heights are feasible, the range of operating velocities at such bed heights would be limited, in particular for the membrane adsorber, where the maximum bed height of current commercial devices is 8 mm.

Table 5.2: Relative column lengths for equivalent resolution. The relative columns lengths were calculated from the normalized resolution of the different adsorbents. They describe how the column length of each adsorbent would have to be set in relation to the column length of the Fiber FRP S adsorbent in order to achieve the same resolution for the separation of monomer and HMW species.

	Relative column length (-)			
Separation	Poros 50 HS	Sartobind S	Fibers SI-ATRP S	Fibers FRP S
Monomer-HMW1	3.90	0.19	1.28	1.00
Monomer-HMW2	5.77	0.31	1.15	1.00
HMW1-HMW2	8.13	0.59	1.06	1.00

5.3.4 Performance of fiber-based adsorbents in bind-and-elute mode

In the next step, we evaluated the performance of the fiber-based adsorbents under preparative loading densities in bind-and-elute mode. Bind-and-elute mode is often used for aggregate removal in mAb platform processes for robustness reasons [163]. Columns with a bed height of 5 cm were used, in order to enable an operation up to high mobile phase velocities, and investigate the impact of mobile phase velocity on separation performance. For the Fibers SI-ATRP S adsorbent mobile phase velocities of 150 cm/h up to the maximum mobile phase velocity for a column pressure drop of 3 bar, i.e. 480 cm/h (cf. Fig. 5.1) were examined. For the Fibers FRP S adsorbent mobile phase velocities were evaluated up to 1060 cm/h, which is the mobile phase velocity where the DBCs of the Fibers FRP S adsorbent and Poros 50 HS overlapped (cf. Fig. 5.2). Loading and elution conditions were further optimized, and columns were loaded to 70% of the $DBC_{10\%}$ at the respective mobile phase velocity.

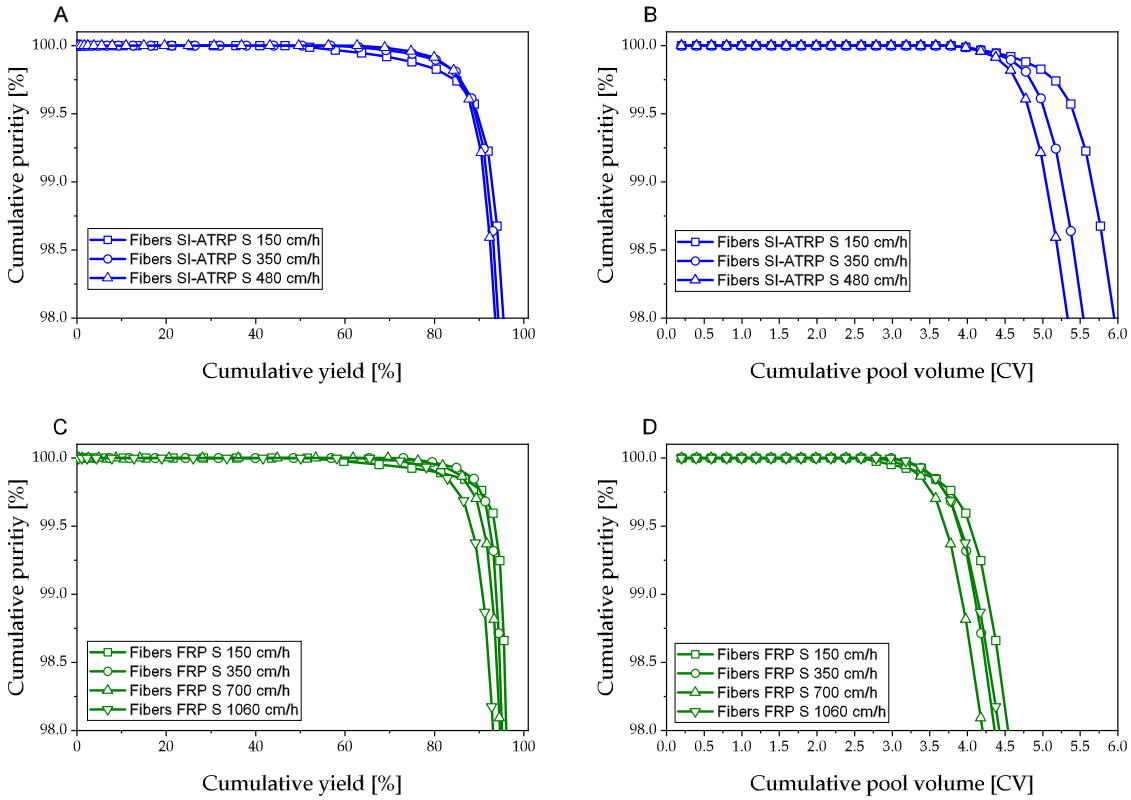

Figure 5.5: Cumulative purity versus (A, C) cumulative yield, and (B, D) cumulative pool volume for bind and elute experiments with the (A, B) Fibers SI-ATRP S, and (C, D) Fibers FRP S adsorbents evaluated in this study. Buffer conditions: 10 mM MCB, pH 5, 0 to 385 mM NaCl over 20 CV. Mobile phase velocity: 150-480 cm/h (Fiber SI-ATRP S), 150-1060 cm/h (Fiber FRP S). Purity of the load: 94%. Load density: 70% of DBC 10%.

The performance was evaluated via cumulative purity versus cumulative yield and cumulative pool volume plots which are displayed in Fig. 5.5A and B for the Fibers SI-ATRP S adsorbent, and in Fig. 5.5C and D for the Fibers FRP S adsorbent. In addition key performance indicators (KPIs) for a cumulative monomer purity target of > 99% were calculated from the experimental data. Table 5.3 lists the monomer yields, monomer purities, pool volumes, pool conductivities and monomer concentration factors for this target. Typical targets for bind-and-elute steps require yields > 80%, with monomer purities > 99% [169] at small pool volumes. Pool volume targets depend on column and tank sizes, but typically are in the range of 3-8 CV. Targets for pool conductivity and concentration factor are less clearly defined, and depend predominantly on subsequent processing steps.

The requirements with respect to purity, yield and pool volume were fulfilled by the fiber-based adsorbents under all mobile phase velocities investigated. Monomer yields ranged from 90.4-92.0% on the Fibers SI-ATRP S adsorbents and 89.2-94.6% on the Fibers FRP S adsorbents at monomer purities of 99.2% and 99.3-99.4%, and pool volumes of 5.0-5.6 and 3.8-4.2 CV (cf. Table 5.3). The higher pool volume of the SI-ATRP S in comparison to the FRP S adsorbents might be a consequence of the higher DBC and hence higher loading density. For most of the performance indicators, the impact of mobile phase velocity was limited. No change in monomer purities was observed with increasing mobile phase velocity, while yields decreased by 1.7% for the SI-ATRP S fibers and 5.7% for the FRP S fibers from the lowest to the highest mobile phase velocities. Pool volumes decreased by 10.7% and 4.8%, while pool conductivities changed by 4.2% and -0.03%. For the concentration factor a stronger decrease with increasing mobile phase velocity was observed. Concentrations factors decreased by 15% on the SI-ATRP S fibers and 36% on the FRP S adsorbents

Table 5.3: Comparison of the separation performance of the the fiber-based adsorbents in bind-and-elute mode at different mobile phase velocities for a cumulative monomer purity target of > 99% .

Mobile phase velocity	Yield (%)	Purity (%)	Pool volume (CV)	Pool conductivity (mS/cm)	F_{conc} (-)
Fibers SI-ATRP S					
150 cm/h	92.0	99.2	5.6	16.8	2.0
350 cm/h	91.0	99.2	5.2	17.3	1.8
480 cm/h	90.4	99.2	5.0	17.5	1.7
Fibers FRP S					
150 cm/h	94.6	99.3	4.2	17.8	1.4
350 cm/h	93.2	99.3	4.0	17.9	1.2
700 cm/h	91.7	99.4	3.8	18.0	1.0
1060 cm/h	89.2	99.4	4.0	17.8	0.9

for 2 fold and 7 fold increases in mobile phase velocity. This decrease is mostly a consequence of the lower loading densities at the higher mobile phase velocities, as the loading densities were adjusted based on the DBCs. However, except for the highest mobile phase velocity on the Fiber FRP S adsorbent, the product could be concentrated as indicated by concentration factors > 1. The pool conductivities would be compatible with subsequent mixed mode AEX flow-through (FT) steps. For traditional AEX FT steps, the conductivity and pH might have to be adjusted, however one could also switch the order of the CEX and AEX FT step and run the AEX step before the CEX step in order to avoid pool adjustments after the CEX step.

Overall these results indicate that the use of the fiber-based adsorbents for aggregate removal in bind-and-elute mode is feasible up to very high mobile phase velocities. This could be advantageous for achieving high productivities.

5.3.5 Performance of fiber-based adsorbents in frontal chromatography mode

Another operating mode for aggregate removal is frontal chromatography [163, 164], which has also been reported as overloaded chromatography [162]. In this operating mode the mAb feed is loaded continuously onto the adsorbent and the flowthrough (FT) is collected until a certain pool aggregate level is reached. The mobile phase conditions are selected such that both monomer and aggregates bind and emerge from the column in order of increasing interaction strength. In comparison to bind-and-elute mode the impurity binding capacity of the adsorbent can be utilized better in this operating mode, such that higher loading densities are possible, which can lead to higher productivity. Since selectivity and sufficiently fast kinetics are important for this operating mode, it has been suggested that alternative types of chromatography media might be well suited for this operating mode [163].

Therefore we evaluated the performance of the fiber-based adsorbents in this operating mode. In the first step, the impact of loading pH (5.0-5.5) and loading salt concentration (conductivity target < 15 mS/cm) on monomer and aggregate breakthrough on the fiber-based adsorbents was evaluated. The loading pH and loading salt concentration were adapted to pH 5.3 and 120 mM NaCl, where the distance between monomer and aggregate breakthrough was greatest. Subsequently the impact of mobile phase velocity was investigated. The mobile phase velocity ranges were the same as in the bind-and-elute experiments (cf. section 3.4), and for each adsorbent the lowest and the highest mobile phase velocity was evaluated, i.e. 150 cm/h and 480 cm/h for the Fibers SI-ATRP S adsorbent, and 150 cm/h and 1060 cm/h for the Fiber FRP S adsorbent. The loading densities were 3.2 times and 3.5 times as

high as in the bind-and-elute experiments and adjusted with mobile phase velocity according to the respective change in the DBCs. The elution was carried out with the same gradients as in the bind-and-elute experiments.

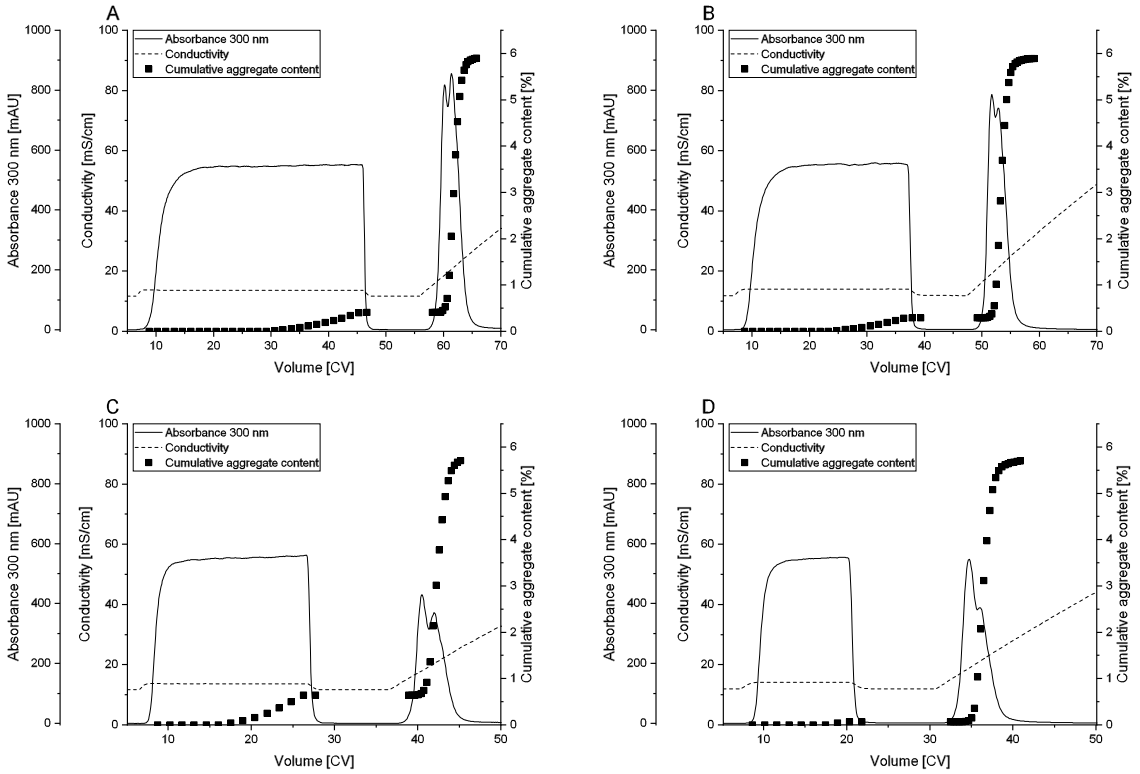

Figure 5.6: Chromatograms of frontal chromatography experiments on (A, B) Fiber SI-ATRP S, and (C, D) Fiber FRP S adsorbents. Buffer conditions: 10 mM MCB + 120 mM NaCl, pH 5.3, 13.9 mS/cm. Load concentration: 2.2 g/L. Aggregate content in the load: 6.0 %. Mobile phase velocity: (A, C) 150 cm/h, (B) 480 cm/h, (D) 1060 cm/h. Squares display the respective cumulative pool aggregate contents.

Fig. 5.6 shows the chromatograms of the experiments with the (A, B) Fibers SI-ATRP S, and (C, D) Fiber FRP S adsorbents at the (A, C) lowest and (B, D) highest mobile phase velocity, and the respective cumulative pool aggregate contents. Table 5.4 lists the KPIs for pooling of the entire FT fractions or pooling of the entire FT fractions plus the elution fractions up to a cumulative pool aggregate content of $< 1\%$. In all experiments the FT fractions consisted of pure monomer at a concentration above the load concentration, followed by a mixture of monomer and HMW1, while no breakthrough of HMW2 was observed. This pattern is consistent with a frontal chromatography mode [163, 164]. For the selected loading densities, the cumulative aggregate contents of the FT pools remained below 1% (cf. Fig 5.6 and Table 5.4), which indicates that loading could have been extended further. However, even for the selected loading densities typical yield constraints would be fulfilled. Yields ranged from 90.7-88.8 % for the Fiber SI-ATRP S adsorbent and 92.4-83.2% for

the Fibers FRP S adsorbents, for monomer purities of 99.6-99.7% and 99.4-99.9%. Yields could be further increased if the loading densities were increased or if part of the elution fractions were collected, since at all mobile phase velocities monomer and aggregates could be partly resolved in the elution gradient (cf. Fig. 5.6). If the elution fractions were collected as well, yields would increase to 95.8-94.4% for the SI-ATRP S fibers at monomer purities of a 99.3-99.5%, and 97.7-95.4% for the FRP S fibers at monomer purities of 99.1-99.6% (cf. Table 5.4). The pool volumes of the SI-ATRP S were about twice as high as the pool volumes of the FRP S fibers, while pool conductivities were similar. If the elution fractions were collected as well, pool volumes and pool conductivities would increase, while the concentration factors decrease.

The impact of mobile phase velocity on most KPIs was limited and similar to the effects in bind-and-elute mode. The KPIs that were affected most were pool volume and concentration factor which both decreased. Pool volumes decreased due to the lower loading density, and concentration factors changed accordingly as less product was collected during the FT phase. Compared to the bind-and-elute mode, similar yields and purities were attainable with the overloaded mode operation, while more product could be processed. No concentration of the product was possible with the overloaded mode operation, however this would be outweighed by the much higher loading density. Overall these results indicate that the use of the fiber-based adsorbents is also possible in overloaded mode up to high mobile phase velocities.

Table 5.4: Comparison of the separation performance of the fiber-based adsorbents in isocratic overloaded mode at different mobile phase velocities for a cumulative monomer purity target of $> 99\%$.

Mobile phase velocity	Pool	Yield (%)	Purity (%)	Pool volume (CV)	Pool conductivity (mS/cm)	F_{conc} (-)
Fibers SI-ATRP S						
150 cm/h	FT	90.7	99.6	39.4	13.6	0.9
150 cm/h	FT+Elu	95.8	99.3	42.3	13.9	0.9
480 cm/h	FT	88.8	99.7	32.1	14.0	0.8
480 cm/h	FT+Elu	95.4	99.5	35.4	14.3	0.8
Fibers FRP S						
150 cm/h	FT	92.4	99.4	20.4	13.6	0.9
150 cm/h	FT+Elu	97.7	99.1	23.0	14.0	0.9
1060 cm/h	FT	83.2	99.9	14.6	13.9	0.8
1060 cm/h	FT+Elu	95.4	99.6	17.9	14.6	0.7

5.3.6 Productivity and buffer consumption

In the last step, we calculated the productivities and buffer consumption of the two fiber-based adsorbents for the conditions investigated above, in order to assess how the mobile phase velocity affects these measures, and to compare the different operating modes and the performance of the fiber-based adsorbents. Productivity and buffer consumption are both important because they affect process economics as they define the required amount of chromatography media and buffer as well as the required processing time and associated labor costs.

Table 5.5 summarizes the productivity and buffer consumption of the two fiber-based adsorbents for the two operating modes and the different mobile phase velocities and pools. The productivities and buffer consumption are based on the full chromatographic cycles which contained a 5 CV strip/regeneration phase and a 2 CV cleaning in place (CIP) phase with a contact time of 20 min. For both fiber types and both operating modes the productivities and buffer consumption increased with increasing mobile phase velocity. In bind and elute mode the productivity of both fiber types increased by a factor of 1.9 from the lowest to the highest mobile phase velocity. The increase in productivity per increase in mobile phase velocity on the SI-ATRP S fibers was more than twice as high than on the FRP S fibers. The increase in buffer consumption with increasing mobile phase velocity was less pronounced. Buffer consumption increased by 30% on the SI-ATRP S fibers and 55% on the FRP S fibers from the lowest to the highest mobile phase velocity. The productivity and buffer consumption in bind and elute mode ranged from 13.0-24.7 g/L/h and 1.2-1.6 L/g on the SI-ATRP S fiber-based adsorbent to 7.6-14.5 g/L/h and 2.4-3.7 L/g on the FRP S adsorbent. Under the same operating conditions (same phases, same phase duration, same loading density of 70% of the $DBC_{10\%}$ at the respective mobile phase velocity) the productivity and buffer consumption of Poros 50 HS at typical bed heights (15-30 cm) and mobile phase velocities (100-300 cm/h) would range from 2.5-9.5 g/L/h and 0.8-1.3 L/g. When comparing the two types of fiber-based adsorbents, the productivity of the SI ATRP S fiber-based adsorbent is 1.7-1.8 times as high as the one of the FRP S fiber-based adsorbent with a buffer consumption that is 50-60% lower.

The impact of mobile phase velocity on productivity and buffer consumption in frontal chromatography mode was similar to the effect in bind and elute mode. Productivities increased by a factor of 1.9-2.1 from the lowest to the highest mobile phase velocity, while buffer consumption increased by 30-50%. The productivities were higher and the buffer consumption was lower if only the FT was collected. Productivities ranged from 37.3-77.7 g/L/h on the SI-ATRP S fiber-based adsorbent to 25.6-54.9 g/L/h on the FRP S fiber-based adsorbent, with a buffer consumption of 0.2-0.5 L/g and 0.5-1.0 L/g. The productivity and the buffer consumption of

Table 5.5: Comparison of the productivity and buffer consumption of the fiber-based adsorbents evaluated in this study for different operating modes and mobile phase velocities.

Operating mode	Mobile phase velocity (cm/h)	Bed height (cm)	Pool	Productivity (g/L/h)	Buffer consumption (L/g)
Fibers SI-ATRP S					
Bind/Elute	150	5	Elu	13.0	1.2
Bind/Elute	350	5	Elu	20.5	1.5
Bind/Elute	480	5	Elu	24.7	1.6
Frontal	150	4	FT	40.2	0.2
Frontal	150	4	FT+Elu	37.3	0.4
Frontal	480	4	FT	77.7	0.3
Frontal	480	4	FT+Elu	75.2	0.5
Fibers FRP S					
Bind/Elute	150	5	Elu	7.6	2.4
Bind/Elute	350	5	Elu	11.4	2.9
Bind/Elute	700	5	Elu	13.7	3.5
Bind/Elute	1060	5	Elu	14.5	3.7
Frontal	150	4	FT	28.8	0.5
Frontal	150	4	FT+Elu	25.6	0.7
Frontal	1060	4	FT	51.8	0.7
Frontal	1060	4	FT+Elu	54.9	1.0

Poros 50 HS at typical bed heights (15-30 cm) and mobile phase velocities (100-300 cm/h) under the same operating conditions depend on the load density. In previous studies load densities of up to 600 g/L have been used for Poros 50 HS [162]. For a load density of 600 g/L productivities would range from 10.3-34.5 g/L/h at a buffer consumption of 0.04-0.07 g/L, while for a lower load density of 120 g/L (similar increase in loading density from bind and elute mode to frontal mode as on the fiber-based adsorbents) productivities would range from 5.8-23.3 g/L/h for a buffer consumption of 0.17-0.27 g/L. In frontal chromatography mode the productivities of the SI-ATRP S fiber-based adsorbent were 1.4-1.5 times as high as the ones of the FRP S fibers, with a 50-60% lower buffer consumption.

When comparing the two operating modes, the productivity of the SI-ATRP S fibers in frontal chromatography mode was 2.9-3.1 times as high as in bind and elute mode, with a 70-80% lower buffer consumption. The productivity of the FRP S fibers was 3.4-4.0 times higher as in bind-and-elute mode with 70-80% lower buffer consumption. Overall the SI-ATRP S fibers had the highest productivity and the smallest buffer consumption. Thus the use of the fiber-based adsorbents in frontal chromatography mode would be advantageous, as long as the clearance of other impurities can be

ensured. Whether the implementation of frontal chromatography mode is beneficial overall also depends on the setup of the subsequent processing step. As the product can not be concentrated in frontal chromatography mode, the processing time of a subsequent step would be extended in comparison to a bind and elute mode operation. Thus, if the subsequent step was operated at a very slow flow rate, the use of bind and elute mode could still be beneficial.

Increases in the mobile phase velocity also lead to a less concentrated product (cf. Table 5.3-5.5). This could also extend the duration of a subsequent processing step. For the SI-ATRP S fiber-based adsorbents the increase in productivity outweighs the decrease in pool concentration, and an operation at higher mobile phase velocities would generally be advantageous. For the FRP S fiber, the use at faster flow rates in frontal chromatography mode is advantageous, while the use at fast mobile velocities in bind and elute mode would only be advantageous if the subsequent process step is run at a fast mobile phase velocity.

In terms of cost, the use the SI-ATRP S fiber-based adsorbents would be advantageous over the use of the FRP S fiber-based adsorbent due to the higher productivity and the lower buffer consumption. The use of the FRP S adsorbent would only be advantageous if a single use scheme is used or only a few cycles are run, and if the material cost of the FRP S fibers were lower than the material cost of the SI-ATRP S fibers. Further improvements in productivity could be achieved if fewer CIP or no CIP steps were used, as has been suggested for other types of fiber-based adsorbents [80], however it would have to be evaluated if this is feasible in the context of bioburden control. In addition, in frontal chromatography mode, productivity would increase by a factor of 1.2-1.7 and buffer consumption would drop by 50% if the bed height was reduced to 2 cm. Further improvements might be possible via adjustments in the architecture of the grafted polymer nanolayer.

5.4 Conclusions

Fiber-based adsorbents have recently been identified as promising alternative chromatography materials for preparative protein purification. However, up to now, it has not been evaluated whether, and under which conditions, the use of such adsorbents for process applications is feasible.

In the present study, the use of fiber-based cation exchange adsorbents for monoclonal antibody aggregate removal was examined. Two types of fiber-based adsorbents, which differed in the type of grafted hydrogel layer, were investigated with respect to permeability, dynamic antibody binding capacity, resolution capabilities of mAb

monomer and aggregates, and the performance in bind and elute and frontal chromatography mode in terms of key performance indicators, productivity, and buffer consumption.

The permeabilities of the fiber-based adsorbents ranged from 200-1270 mD, (providing a large enough operating window) making it possible to use the fiber-based adsorbents at intermediate bed heights with fast mobile phase velocities. Dynamic antibody binding capacities ranged from 20-41 g/L at 150 cm/h, and at higher mobile phase velocities exceeded the binding capacities of an existing resin material, Poros 50 HS, which has frequently been used for aggregate removal. Both fiber types showed good resolution capabilities of monomer and aggregates, and provided better resolution per column length than Poros 50 HS. Typical purity and yield constraints where fulfilled by both types of fiber-based adsorbents in both bind and elute and frontal chromatography mode for mobile phase velocities ranging up to 480 and 1060 cm/h.

In conclusion, the present study shows, that the use of fiber-based adsorbents for monoclonal antibody aggregate removal is feasible up to high mobile phase velocities (480-1060 cm/h) at short bed heights (4-5 cm). The overall performance of the controlled grafted fiber-based adsorbents was found to be superior to the performance of uncontrolled grafted adsorbents. While the resolution of monomer and aggregates was similar on both types of fiber-based adsorbents, the productivities were higher and buffer consumption was smaller on the controlled grafted fiber-based adsorbents. Under the conditions investigated, the performance of the fiber-based adsorbents is comparable to the performance of a conventional resin, Poros 50 HS at typical operating conditions (15-30 cm BH, 150-300 cm/h mobile phase velocity). While the buffer consumption of Poros 50 HS is smaller, the productivity of the fiber-based adsorbents is higher.

Therefore, the use of fiber-based adsorbents could a be viable alternative for process applications such as mAb aggregate removal. The use of fiber-based adsorbents could be advantageous if the adsorbents can be supplied at a fraction of the cost of current adsorbents as claimed in the literature, and/or in single use processes or process scenarios where the adsorbents are only reused for a limited number of times such as in clinical manufacturing. In the case of controlled grafted fiber-based adsorbents further performance improvements might be possible via adjustments in the grafted polymer-nanolayer architecture.

5.5 Acknowledgments

The authors gratefully acknowledge material supply by Sartorius Stedim Biotech (Jan Schwellenbach, Florian Taft, Louis Villain) and the financial support from the German Federal Ministry of Education and Research (BMBF) under the reference number 13N13322. The authors bear the complete responsibility for the content of this publication. The authors declare no conflict of interest.

6 Conclusion and Outlook

The present thesis addressed important challenges that are related to the use of fibers and fiber-based chromatography adsorbents for the preparative purification of biopharmaceuticals. The potential of fibers and fiber-based adsorbents for high-throughput and cost-efficient analytical separations has been demonstrated for different types of conventional microfiber supports with different model proteins and other model compounds in the past. For the preparative purification of biopharmaceuticals there is currently a need for more efficient and cheaper manufacturing and development processes, as the demand for biopharmaceuticals is increasing, cheaper generic versions and new classes of biopharmaceuticals are being developed, and cost constraints for biopharmaceuticals are tightening. Therefore there is a great interest in the use of alternative types of chromatography adsorbents such as fiber-based adsorbents for the preparative purification of biopharmaceuticals. However, there are several challenges that make it difficult to use fiber-based adsorbents for this purpose. These consist in the low surface area of conventional microfiber supports and hence low binding capacities of fiber-based adsorbents, which are an obstacle for preparative applications, and the packing of such adsorbents, which requires packing optimization. Moreover, there is a lack of high throughput microscale tools and mechanistic models for fiber-based adsorbents. This makes efficient material development and process development challenging. There also is a lack of knowledge whether and under which conditions the use of such adsorbents for industrial process applications is feasible.

These challenges were addressed in the present thesis by examining novel types of fiber-based adsorbents which were prepared from area enhanced surface shaped fibers via surface grafting with uncontrolled and controlled grafting techniques. First, the packing characteristics of such adsorbents were investigated in order to determine packing conditions under which such adsorbents can be used best. Subsequently it was examined whether mechanistic models and high throughput microscale tools can be developed for such adsorbents. And finally it was explored whether and under which conditions the use of such adsorbents for industrial process applications such as monoclonal antibody aggregate removal during antibody purification is feasible.

Initially, different types of surface shaped area enhanced microfibers were sourced for this thesis. Winged shaped microfibers had the highest surface area of all available surface shaped materials and were therefore examined in detail in this thesis. Both native winged shaped fibers and hydrogel grafted winged shaped fiber based adsorbents with hydrogels that were grafted either via free radical polymerization (FRP) or surface initiated atom-transfer radical polymerization (SI-ATRP) by a project partner were investigated. The grafted fibers were functionalized to either cation exchange or anion exchange fiber-based adsorbents. Other functional groups would be possible, but were not considered in this thesis. For the evaluation of the fibers and fiber-based adsorbents, tracer substances, model proteins and model nucleic acids, and feed streams from industrial antibody purification processes were used.

In the first part of this thesis, packing studies were performed in order to investigate the packing characteristics of native and grafted winged shaped fibers. For this purpose a suspension based packing technique was developed for the packing of short cut winged shaped fibers. With the use of this technique the fibers could be packed reproducibly into small laboratory scale columns with a packing reproducibility that was comparable to packing reproducibilities that have been reported for other materials and other packing techniques at similar scale. The packing quality of the winged shaped fiber beds was found to be sufficient for preparative applications. Peak asymmetries and plate heights were within typical ranges of preparative columns, and plate heights were at the lower end of those reported for other fiber supports. Multivariate packing studies revealed that both packing density and bed height impact column performance. Lower packing densities resulted in lower plate heights, while increases in bed height resulted in more symmetric peak shapes. Packing density also affected the performance of grafted fibers. Dynamic binding capacity increased with increasing packing density, while capacity utilization and resolution decreased. The results from the multivariate studies could be used in order to optimize the packing of grafted winged shaped fibers, and it could be shown that for optimized packing conditions and fast mobile phase velocities, grafted winged shaped fibers can achieve a better resolution than conventional adsorbents. Overall, the first part of this thesis provides information about the packing behavior and the packing characteristics of winged shaped fibers supports. The results indicated that the use of such area enhanced fibers for preparative applications is feasible. The results from the study enable a comparison to other fiber supports and other packing techniques, and it identifies packing conditions under which winged shaped fibers can be used most efficiently.

In the second part of this thesis, it was examined whether a mechanistic model can be developed for fiber-based adsorbents. This was assessed with the use of winged shaped anion-exchange fiber-based adsorbents. Characterization and efficiency experiments

were performed and used in conjunction with criteria for model selection in order to develop a column model for the fiber-based adsorbents. The developed model accounted well for the dispersion of non-retained molecules inside the column, and it could accurately describe the binding, breakthrough, and elution of three differently sized proteins, with molecular sizes ranging from 6 to 160 kDa. The model parameters could be identified reliably from a few experimental column runs. Model comparisons showed that both binding kinetics and lumped film and pore diffusion are relevant mechanisms on the grafted winged shaped fibers. In conclusion, the second part of this thesis demonstrated that fiber-based adsorbent can be modeled mechanistically, using grafted winged shaped fibers as an example. It showed how the required model parameters can be determined, and it could demonstrate that modeling is possible for a range of molecular sizes that would be relevant for the purification of biopharmaceuticals. The results from this study contribute to a better understanding of mass transfer properties of grafted winged shaped fibers, and the presented model enables mechanistic comparisons to other types of stationary phases. Moreover the presented model enables model based process development and optimization on fiber-based adsorbents.

In the third part of this thesis it was examined whether high-throughput microscale tools can be developed for fiber-based adsorbents. This was again assessed with the use of native and grafted winged shaped short cut microfibers. For these fibers an automated high throughput screening was established on a robotic liquid handling station in 96 well filter plates. Two techniques could be identified that enabled accurate and reproducible portioning of the fibers. The impact of several screening parameters was examined and optimized. It could be shown that the data that is obtained from the HTS correlates with data from packed fiber columns. The usefulness of the developed HTS for material and process development was demonstrated in two case studies, which showed that the developed HTS can be used to optimize the hydrogel structure of controlled grafted fiber based adsorbents, and that it can be used for the development of step elution conditions for the purification of a monoclonal antibody from product- and process-related impurities. Overall, the study that is presented in the third part of this thesis, showed that it is possible to develop high-throughput microscale tools for fiber-based adsorbents that can be utilized for material optimization and process development. The tool enables a faster and more complete characterization of fiber-based adsorbents, and it can be used for material and time efficient process development. The tool makes it easier to evaluate fiber-based adsorbents alongside other materials, and thus could make it easier to integrate fiber-based adsorbents into industrial purification processes.

In the last part of this thesis, it was evaluated if and under which conditions fiber-based adsorbents can be used for industrial purification process applications. Here, the

use of cation exchange fiber-based adsorbents for monoclonal antibody removal during antibody purification was explored. Two types of strong cation exchange fiber-based adsorbents with uncontrolled and controlled grafted hydrogel layers were examined and evaluated with respect to permeability, dynamic antibody binding capacity, resolution capabilities of mAb monomer and aggregates, and the performance in different operating modes. The study showed that due to high permeabilities, high dynamic binding capacities at fast mobile phase velocities, and good resolution capabilities of monomer and aggregates, the use of fiber-based adsorbents for mAb aggregate removal is feasible up to very high mobile phase velocities. The overall performance of the fiber-based adsorbents was found to be comparable to performance of an existing resin material, Poros 50 HS. In comparison of the two types of fiber-based adsorbents, the performance of grafted fiber-based adsorbents was found to be superior to the performance of uncontrolled grafted fiber-based adsorbents due to higher productivity and lower buffer consumption. In summary, the study that is presented in the last section, shows that the use of fiber-based adsorbents for process applications during industrial antibody manufacturing is feasible and it identifies appropriate operating conditions.

In conclusion, the present thesis contributes to a better understanding of the properties and the performance of area enhanced winged shaped fibers and fiber-based adsorbents for preparative chromatography applications. It provides information about the packing characteristics of such adsorbents, mechanistic model parameters, relevant mass transfer and binding mechanisms, and the performance for monoclonal antibody aggregate removal. This data can be used for comparisons to existing materials and other types of fiber-based adsorbents. Moreover, the present thesis provides information about how the structure of fiber-based adsorbents with respect to the packing structure and the polymer nanolayer architecture affects the performance of such adsorbents, which helps to use such adsorbents efficiently and tailor them for specific applications. In addition this thesis presents mechanistic models and high throughput screenings for fiber-based adsorbents. These models and tools will be valuable for the future design and evaluation of fiber-based adsorbents, as they enable an easier, and material and time efficient evaluation of such materials. This could make it easier to integrate such alternative adsorbents into process development workflows and processes. With respect to process applications it could be shown that the use of fiber-based adsorbents for monoclonal antibody removal is feasible and the study provides relevant processing windows for this purpose. Overall the information that is presented in this thesis could make it easier to use fiber-based adsorbents and make use of their benefits in order to address some of the current challenges in the field of downstream processing.

While the research that is presented in this thesis indicated that area enhanced fibers such as winged shaped fibers have potential for the preparative purification of

biopharmaceuticals, it also pointed at possible directions for future research. The research in this thesis centered on fiber stationary phases that were prepared from short cut winged shaped fiber supports. These fibers showed sufficient packing characteristics for preparative applications. For further improvements of the packing characteristics it would be interesting to examine ultra short cut fibers as well as other types of area enhanced surface shaped fibers which have recently been developed. In addition future studies could be directed at other fiber arrangements, other fiber packing techniques and packing at larger scales. The developed mechanistic model was set up as a lumped rate model in order to be useful for different types of fiber stationary phases. Future studies could be directed at a more detailed investigation of the fluid dynamics within the fiber columns. Moreover the presented mechanistic model could be extended to specifically incorporate the hydrogel structure and flow rate dependencies. In terms of the developed HTS tools could be built that enable automatic fiber portioning at large scale. The development of a microcolumn or microdevice format would be useful in order to also enable dynamic HT studies. If the use of the developed materials for industrial applications under reuse conditions is envisioned detailed studies of the lifecycle performance and carryover behavior should be performed. Moreover, the developed materials could be of use for other applications in biopharmaceutical purification, such as large molecule separations of vaccines, and gene therapy vectors. Other ligand systems, in particular affinity or mixed-mode chromatography, could be very interesting. In addition surface modification techniques are constantly expanding, and other surface modification techniques could be explored to further improve the properties of fiber-based adsorbents. In addition, other fiber formats could be explored as well, for instance other types of surface shaped fibers, porous fibers or porous nanofibers. Composite stationary phases that are composed of a mixture of fibers and membranes could also be of interest.

Bibliography

1. Rader, R. a.: (Re)defining biopharmaceutical. *Nature biotechnology* (2008), vol. **26**(7): 743–751 (2008) (cit. on p. 1).
2. Walsh, G.: *Biopharmaceuticals: Biochemistry and biotechnology* 2nd: 551 (J. Wiley, 2003) (cit. on pp. 1, 2).
3. Walsh, G.: *Pharmaceutical biotechnology - concepts and applications* (John Wiley & Sons, 2007) (cit. on pp. 1, 2).
4. Walsh, G.: Biopharmaceutical benchmarks 2014. *Nature Biotechnology* (2014), vol. **28**(9): 917–924 (2014) (cit. on pp. 1, 2, 132).
5. Walsh, G.: Biopharmaceutical benchmarks 2018. *Nature Biotechnology* (2018), vol. **36**(12): 1136–1145 (2018) (cit. on pp. 1, 2).
6. Kesik-Brodacka, M.: Progress in biopharmaceutical development. *Biotechnology and Applied Biochemistry* (2018), vol. **65**(3): 306–322 (2018) (cit. on p. 1).
7. Lagassé, H. D., A. Alexaki, V. L. Simhadri, N. H. Katagiri, W. Jankowski, Z. E. Sauna & C. Kimchi-Sarfaty: Recent advances in (therapeutic protein) drug development. *F1000Research* (2017), vol. **6**: 113 (2017) (cit. on pp. 2, 132).
8. Jagschies, G., E. Lindskog, K. Łacki & P. Galliher: *Biopharmaceutical Processing: Development, Design, and Implementation of Manufacturing Processes* 1–1275 (2018) (cit. on pp. 2–5, 14, 15, 20–22, 98).
9. Rathore, A. S.: *Roadmap for implementation of quality by design (QbD) for biotechnology products* 2009 (cit. on p. 4).
10. Subramanian, G.: *Continuous Biomanufacturing - Innovative Technologies and Methods* (Wiley-VCH Verlag GmbH & Co. KGaA, Weinheim, Germany, 2017) (cit. on p. 4).
11. Gronemeyer, P., R. Ditz & J. Strube: Trends in Upstream and Downstream Process Development for Antibody Manufacturing. (2014), vol.: 188–212 (2014) (cit. on p. 4).
12. Abhinav, A Shukla, B. Hubbard, T. Tressel, S. Guhan & D. Low: Downstream processing of monoclonal antibodies—Application of platform approaches. *Journal of Chromatography B* (2007), vol. **848**: 28–39 (2007) (cit. on pp. 4, 5, 14, 132).
13. Ladisch, M. R.: *Bioseparations engineering : principles, practice, and economics* 735 (Wiley, 2001) (cit. on p. 5).

14. HARRISON, R. G., P. TODD, S. R. RUDGE & D. P. PETRIDES: *Bioseparations science and engineering* 2. ed.: XXII, 547 S. (Oxford University Press, Oxford [u.a.], 2015) (cit. on p. 5).

15. LIU, H. F., J. MA, C. WINTER & R. BAYER: Recovery and purification process development for monoclonal antibody production. *mAbs* (2010), vol. **2**(5): 480–499 (2010) (cit. on p. 5).

16. PETRIDES, D., D. CARMICHAEL, C. SILETTI & A. KOULOURIS: Biopharmaceutical process optimization with simulation and scheduling tools. *Bioengineering* (2014), vol. **1**(4): 154–187 (2014) (cit. on p. 6).

17. KELLEY, B.: *Very large scale monoclonal antibody purification: The case for conventional unit operations* 2007 (cit. on p. 6).

18. HAHN, R.: Methods for characterization of biochromatography media. *Journal of separation science* (2012), vol. **35**(22): 3001–32 (2012) (cit. on pp. 6, 20–22).

19. MCNAUGHT, A. D. & A. WILKINSON: *IUPAC. Compendium of Chemical Terminology, 2nd ed. (the "Gold Book")* (1997) (cit. on p. 6).

20. CARTA, G. & A. JUNGBAUER: *Protein chromatography : process development and scale-up* 346 (Wiley-VCH, Weinheim, 2010) (cit. on pp. 6–8, 12, 20–22, 54).

21. SCHMIDT-TRAUB, H.: *Preparative Chromatography: Of Fine Chemicals and Pharmaceutical Agents* 1–458 (2005) (cit. on pp. 6–8, 12, 17, 18, 20, 21, 41, 46, 47, 59).

22. GUIOCHON, G., A. FELINGER, D. G. SHIRAZI & A. M. KATTI: *Fundamentals of Preparative and Nonlinear Chromatography* 2nd ed.: 975 (Academic Press, 2006) (cit. on pp. 7, 8, 12, 17, 69, 70).

23. Van DEEMTER, J., A. KLINKENBERG & F. J. ZUIDERWEG: Longitudinal diffusion and resistance to mass transfer as causes of nonideality in chromatography. *Chemical Engineering Science* (1956), vol. **5**(6): 271–289 (1956) (cit. on p. 11).

24. NFOR, B. K., T. AHAMED, G. W. van DEDEM, L. A. van der WIELEN, E. J. van de SANDT, M. H. EPPINK & M. OTTENS: *Design strategies for integrated protein purification processes: Challenges, progress and outlook* 2008 (cit. on p. 14).

25. NFOR, B. K., P. D. VERHAERT, L. A. van der WIELEN, J. HUBBUCH & M. OTTENS: Rational and systematic protein purification process development: the next generation. *Trends in Biotechnology* (2009), vol. **27**(12): 673–679 (2009) (cit. on p. 14).

26. HANKE, A. T. & M. OTTENS: *Purifying biopharmaceuticals: Knowledge-based chromatographic process development* 2014 (cit. on p. 14).

27. BAUMANN, P. & J. HUBBUCH: *Downstream process development strategies for effective bioprocesses: Trends, progress, and combinatorial approaches* 2017 (cit. on pp. 14, 16, 19).

28. Leser, E. & J. Asenjo: Rational design of purification processes for recombinant proteins. *Journal of Chromatography B: Biomedical Sciences and Applications* (1992), vol. **584**(1): 43–57 (1992) (cit. on p. 14).

29. Lienqueo, M. & J. A. Asenjo: Use of expert systems for the synthesis of downstream protein processes. *Computers & Chemical Engineering* (2000), vol. **24**(9-10): 2339–2350 (2000) (cit. on p. 14).

30. Hagel, L., G. Jagschies & G. Sofer: *Handbook of Process Chromatography* (2008) (cit. on p. 14).

31. Łącki, K. M.: *High throughput process development in biomanufacturing* 2014 (cit. on p. 15).

32. Łacki, K. M.: High-throughput process development of chromatography steps: Advantages and limitations of different formats used. *Biotechnology Journal* (2012), vol. **7**(10): 1192–1202 (2012) (cit. on pp. 15, 99, 111).

33. Chhatre, S. & N. J. Titchener-Hooker: Review: Microscale methods for high-throughput chromatography development in the pharmaceutical industry. *Journal of Chemical Technology & Biotechnology* (2009), vol. **84**(7): 927–940 (2009) (cit. on pp. 15, 99).

34. Bhambure, R., K. Kumar & A. S. Rathore: High-throughput process development for biopharmaceutical drug substances. *Trends in Biotechnology* (2011), vol. **29**(3): 127–135 (2011) (cit. on p. 15).

35. Huft, J., C. A. Haynes & C. L. Hansen: Microfluidic integration of parallel solid-phase liquid chromatography. *Analytical Chemistry* (2013), vol. **85**(5): 2999–3005 (2013) (cit. on pp. 15, 99, 111).

36. Rho, H., H. Gardeniers, A. Hanke & M. Ottens: A microfluidic device for the batch adsorption of a protein on adsorbent particles. *Analyst* (2017), vol.: 3656–3665 (2017) (cit. on pp. 15, 99, 111).

37. Pinto, I. F., R. R. Soares, M. R. Aires-Barros, V. Chu, J. P. Conde & A. M. Azevedo: Optimizing the Performance of Chromatographic Separations Using Microfluidics: Multiplexed and Quantitative Screening of Ligands and Target Molecules. *Biotechnology Journal* (2019), vol. **14**(10): 1800593 (2019) (cit. on pp. 15, 99).

38. Muthukumar, S. & A. S. Rathore: High throughput process development (HTPD) platform for membrane chromatography. *Journal of Membrane Science* (2013), vol. **442**: 245–253 (2013) (cit. on pp. 15, 99, 104, 112).

39. Pollard, J., P. Mcdonald & A. Hesslein: Lessons learned in building high-throughput process development capabilities. *Engineering in Life Sciences* (2016), vol. **16**(2): 93–98 (2016) (cit. on p. 16).

40. Brooks, C. A. & S. M. Cramer: Steric mass-action ion exchange: Displacement profiles and induced salt gradients. *AIChE Journal* (1992), vol. **38**(12): 1969–1978 (1992) (cit. on pp. 18, 71).

41. LADIWALA, A., K. REGE, C. M. BRENEMAN & S. M. CRAMER: A priori prediction of adsorption isotherm parameters and chromatographic behavior in ion-exchange systems. *Proceedings of the National Academy of Sciences* (2005), vol. **102**(33): 11710–11715 (2005) (cit. on p. 19).

42. WANG, G., T. BRISKOT, T. HAHN, P. BAUMANN & J. HUBBUCH: Estimation of adsorption isotherm and mass transfer parameters in protein chromatography using artificial neural networks. *Journal of Chromatography A* (2017), vol. **1487**: 211–217 (2017) (cit. on p. 19).

43. PIRRUNG, S. M., L. A. van der WIELEN, R. F. VAN BECKHOVEN, E. J. van de SANDT, M. H. EPPINK & M. OTTENS: Optimization of biopharmaceutical downstream processes supported by mechanistic models and artificial neural networks. *Biotechnology Progress* (2017), vol. (2017) (cit. on p. 19).

44. JUNGBAUER, A.: Chromatographic media for bioseparation. *Journal of Chromatography A* (2005), vol. **1065**(1): 3–12 (2005) (cit. on pp. 20, 21, 34, 55, 68).

45. MÜLLER, E.: Properties and Characterization of High Capacity Resins for Biochromatography. *Chemical Engineering & Technology* (2005), vol. **28**(11): 1295–1305 (2005) (cit. on pp. 20, 34, 55).

46. LENHOFF, A. M.: Protein adsorption and transport in polymer-functionalized ion-exchangers. *Journal of Chromatography A* (2011), vol. **1218**(49): 8748–8759 (2011) (cit. on pp. 20, 93).

47. JUNGBAUER, A. & R. HAHN: Polymethacrylate monoliths for preparative and industrial separation of biomolecular assemblies. *Journal of Chromatography A* (2008), vol. **1184**(1-2): 62–79 (2008) (cit. on pp. 21, 23).

48. GHOSH, R.: Protein separation using membrane chromatography: opportunities and challenges. *Journal of Chromatography A* (2002), vol. **952**(1-2): 13–27 (2002) (cit. on pp. 21, 23).

49. ORR, V., L. ZHONG, M. MOO-YOUNG & C. P. CHOU: Recent advances in bioprocessing application of membrane chromatography. *Biotechnology advances* (2013), vol. **31**(4): 450–65 (2013) (cit. on pp. 21, 22).

50. SCHMIDT-TRAUB, H., M. SCHULTE & A. SEIDEL-MORGENSTERN: *Preparative Chromatography: Second Edition* (2013) (cit. on p. 21).

51. ROUQUEROL, J., G. BARON, R. DENOYEL, H. GIESCHE, J. GROEN, P. KLOBES, P. LEVITZ, A. V. NEIMARK, S. RIGBY & R. SKUDAS: Recommendations for the characterization of porous solids (Technical Report). *Pure and Applied Chemistry* (1994), vol. **66**(8): 1739–1758 (1994) (cit. on p. 22).

52. ZHOU, J. X. & T. TRESSEL: Basic concepts in Q membrane chromatography for large-scale antibody production. *Biotechnology Progress* (2006), vol. **22**(2): 341–349 (2006) (cit. on pp. 22, 34).

53. Vicente, T., M. F. Sousa, C. Peixoto, J. P. Mota, P. M. Alves & M. J. Carrondo: Anion-exchange membrane chromatography for purification of rotavirus-like particles. *Journal of Membrane Science* (2008), vol. **311**(1-2): 270–283 (2008) (cit. on pp. 22, 71, 86).

54. Podgornik, A. & N. L. Krajnc: Application of monoliths for bioparticle isolation. *Journal of Separation Science* (2012), vol. **35**(22): 3059–3072 (2012) (cit. on p. 22).

55. Svec, F. & Y. Lv: Advances and recent trends in the field of monolithic columns for chromatography. *Analytical Chemistry* (2015), vol. **87**(1): 250–273 (2015) (cit. on p. 22).

56. Przybycien, T. M., N. S. Pujar & L. M. Steele: *Alternative bioseparation operations: Life beyond packed-bed chromatography* 2004 (cit. on pp. 22, 98).

57. Marcus, R. K.: Use of polymer fiber stationary phases for liquid chromatography separations: Part I – physical and chemical rationale. *Journal of Separation Science* (2008), vol. **31**(11): 1923–1935 (2008) (cit. on pp. 23–25, 34, 35, 68, 69, 99).

58. Ladisch, M. & L. Zhang: Fiber-based monolithic columns for liquid chromatography. *Analytical and Bioanalytical Chemistry* (2016), vol. **408**(25): 6871–6883 (2016) (cit. on pp. 23, 25).

59. GmbH, T. F. Y.: The Fiber Year 2019 : World Survey on Textiles & Nonwovens. (2019), vol. (19) (2019) (cit. on p. 23).

60. Gries, T., D. Veit & B. Wulfhorst: *Textile technology an introduction* (Hanser, 2015) (cit. on pp. 23, 24).

61. Zhou, F.-L. & R.-H. Gong: Manufacturing technologies of polymeric nanofibres and nanofibre yarns. *Polymer International* (2008), vol. **57**(6): 837–845 (2008) (cit. on pp. 24, 35).

62. Yeom, B. Y. & B. Pourdeyhimi: Web fabrication and characterization of unique winged shaped, area-enhanced fibers via a bicomponent spunbond process. *Journal of Materials Science* (2011), vol. **46**(10): 3252–3257 (2011) (cit. on pp. 24, 26, 35, 36, 75, 99).

63. Wang, Z. & R. K. Marcus: Determination of pore size distributions in capillary-channeled polymer fiber stationary phases by inverse size-exclusion chromatography and implications for fast protein separations. *Journal of chromatography. A* (2014), vol. **1351**: 82–9 (2014) (cit. on pp. 24, 36, 47, 59, 92).

64. Hardick, O., B. Stevens & D. G. Bracewell: Nanofibre fabrication in a temperature and humidity controlled environment for improved fibre consistency. *Journal of Materials Science* (2011), vol. **46**(11): 3890–3898 (2011) (cit. on pp. 24, 26, 35).

65. Marcus, R. K.: Use of polymer fiber stationary phases for liquid chromatography separations: Part II - Applications. *Journal of Separation Science* (2009), vol. **32**: 695–705 (2009) (cit. on pp. 24, 25, 34, 68).

66. YAVORSKY, D., J. AMARA, J. UMANA, W. CATALDO, M. KOZLOV & M. STONE: *Chromatography media and method* 2015 (cit. on pp. 24, 35, 44).

67. *Ion exchangers* (ed DORFNER, K.) Includes bibliographical references and indexIMD-Felder maschinell generiert (GBV) (de Gruyter, Berlin, 1991) (cit. on p. 25).

68. KING, J.-K. & N. G. PINTO: Short fibrous supports for preparative chromatographic separations of biomolecules. *Journal of Chromatography A* (1992), vol. **609**(1-2): 61–68 (1992) (cit. on pp. 25, 35, 69).

69. YANG, Y., A. VELAYUDHAN, C. M. LADISCH & M. R. LADISCH: Protein chromatography using a continuous stationary phase. *Journal of Chromatography A* (1992), vol. **598**(2): 169–180 (1992) (cit. on pp. 25, 35, 69, 92).

70. MARCUS, R., W. DAVIS, B. C. KNIPPEL, L. LAMOTTE, T. A. HILL, D. PERAHIA & J. JENKINS: Capillary-channeled polymer fibers as stationary phases in liquid chromatography separations. *Journal of Chromatography A* (2003), vol. **986**(1): 17–31 (2003) (cit. on pp. 25, 35, 36, 69).

71. LI, C., C. M. LADISCH, Y. YANG, R. HENDRICKSON, C. KEIM, N. MOSIER & M. R. LADISCH: Optimal packing characteristics of rolled, continuous stationary-phase columns. *Biotechnology Progress* (2002), vol. **18**(2): 309–316 (2002) (cit. on pp. 25, 36, 45, 47, 48, 52, 89).

72. WANG, Z. & R. K. MARCUS: Roles of interstitial fraction and load conditions on the dynamic binding capacity of proteins on capillary-channeled polymer fiber columns. *Biotechnology Progress* (2015), vol. **31**(1): 97–109 (2015) (cit. on pp. 25, 36, 38, 55, 89).

73. STANELLE, R. D., L. C. SANDER & R. K. MARCUS: Hydrodynamic flow in capillary-channel fiber columns for liquid chromatography. *Journal of Chromatography A* (2005), vol. **1100**(1): 68–75 (2005) (cit. on pp. 25, 36, 38, 46, 48, 52, 54, 61).

74. HAMAKER, K., J. LIU, C. LADISCH & M. LADISCH: Transport Properties of Rolled, Continuous Stationary Phase Columns. *Biotechnology Progress* (1998), vol. **14**(1): 21–30 (1998) (cit. on pp. 25, 36, 47, 89, 90, 92).

75. STANELLE, R. D., M. MIGNANELLI, P. BROWN & R. K. MARCUS: Capillary-channeled polymer (C-CP) fibers as a stationary phase in microbore high-performance liquid chromatography columns. *Analytical and Bioanalytical Chemistry* (2006), vol. **384**(1): 250–258 (2006) (cit. on pp. 25, 36, 38, 47, 48).

76. GAVARA, P. R., R. CABRERA, R. R. VENNAPUSA, M. GRASSELLI & M. FERNANDEZ-LAHORE: Preparation, characterization, and process performance of composite fibrous adsorbents as cation exchangers for high throughput and high capacity bioseparations. *Journal of Chromatography B* (2012), vol. **903**: 14–22 (2012) (cit. on pp. 26, 35, 68, 69, 99).

77. Bhut, B. V., J. Weaver, A. R. Carter, S. R. Wickramasinghe & S. M. Husson: The role of polymer nanolayer architecture on the separation performance of anion-exchange membrane adsorbers: Part II. DNA and virus separations. *Biotechnology and Bioengineering* (2011), vol. **108**(11): 2654–2660 (2011) (cit. on pp. 26, 120).

78. Gibbs, S. J. & E. N. Lightfoot: Scaling up gradient elution chromatography. *Industrial & Engineering Chemistry Fundamentals* (1986), vol. **25**(4): 490–498 (1986) (cit. on pp. 34, 68).

79. Gavara, P., N. Bibi, M. Sanchez, M. Grasselli & M. Fernandez-Lahore: Chromatographic Characterization and Process Performance of Column-Packed Anion Exchange Fibrous Adsorbents for High Throughput and High Capacity Bioseparations. en. *Processes* (2015), vol. **3**(1): 204–221 (2015) (cit. on pp. 35, 46, 47, 68, 69, 89, 90, 99, 114).

80. Hardick, O., S. Dods, B. Stevens & D. G. Bracewell: Nanofiber adsorbents for high productivity downstream processing. *Biotechnology and Bioengineering* (2013), vol. **110**(4): 1119–1128 (2013) (cit. on pp. 35, 68, 69, 99, 155).

81. Dods, S. R., O. Hardick, B. Stevens & D. G. Bracewell: Fabricating electrospun cellulose nanofibre adsorbents for ion-exchange chromatography. *Journal of chromatography. A* (2015), vol. **1376**: 74–83 (2015) (cit. on p. 35).

82. Jiang, L., Y. Jin & R. K. Marcus: Polyethylenimine modified poly(ethylene terephthalate) capillary channeled-polymer fibers for anion exchange chromatography of proteins. *Journal of Chromatography A* (2015), vol. **1410**: 200–209 (2015) (cit. on p. 35).

83. Schwellenbach, J., F. Taft, L. Villain & J. Strube: Preparation and characterization of high capacity, strong cation-exchange fiber based adsorbents. *Journal of Chromatography A* (2016), vol. **1447**: 92–106 (2016) (cit. on pp. 35, 36, 38, 68, 89, 91, 99, 101, 108, 114, 116, 118, 119, 121, 124, 133, 135, 137, 141, 143, 144, 147).

84. Czok, M. & G. Guiochon: Aligned fiber columns for size-exclusion chromatography. *Journal of Chromatography A* (1990), vol. **506**: 303–317 (1990) (cit. on pp. 35, 47, 69).

85. Nelson, D. M. & R. K. Marcus: Characterization of capillary-channeled polymer fiber stationary phases for high-performance liquid chromatography protein separations: Comparative analysis with a packed-bed column. *Analytical Chemistry* (2006), vol. **78**(24): 8462–8471 (2006) (cit. on pp. 36, 38, 45).

86. Randunu, K. M., S. Dimartino & R. K. Marcus: Dynamic evaluation of polypropylene capillary-channeled fibers as a stationary phase in high-performance liquid chromatography. *Journal of Separation Science* (2012), vol. **35**(23): 3270–3280 (2012) (cit. on pp. 36, 90).

87. STANELLE, R. D., C. M. STRAUT & R. K. MARCUS: Nylon-6 Capillary-Channeled Polymer Fibers as a Stationary Phase for the Mixed-Mode Ion Exchange / Reversed-Phase Chromatography Separation of Proteins. *Journal of Chromatographic Science* (2007), vol. **45**(August): 415–421 (2007) (cit. on pp. 38, 55, 58, 99).

88. HUUK, T. C., T. BRISKOT, T. HAHN & J. HUBBUCH: A versatile noninvasive method for adsorber quantification in batch and column chromatography based on the ionic capacity. *Biotechnology Progress* (2016), vol. **32**(3): 666–677 (2016) (cit. on pp. 38, 42).

89. MINO, G & S KAIZERMAN: A New Method for the Preparation of Graft Copolymers. Polymerization Initiated by Ceric Ion Redox Systems. *Journal of Polymer Science* (1958), vol. **31**(122): 242–243 (1958) (cit. on p. 41).

90. PAUL, S. & B. RANBY: Methyl Methacrylate (MMA)-Glycidyl Methacrylate (GMA) Copolymers. A Novel Method to Introduce Sulfonic Acid Groups on the Polymeric Chains. *Macromolecules* (1976), vol. **9**(2): 337–340 (1976) (cit. on p. 41).

91. MAHER, R. R. & R. H. WARDMAN: *The Chemistry of Textile Fibres, 2nd Edition* 439 (Royal Society of Chemistry, 2015) (cit. on p. 44).

92. SINGH, A. & N. G. PINTO: Polymeric short-fiber chromatographic supports for downstream processing of biomolecules. *Reactive Polymers* (1995), vol. **24**(3): 229–242 (1995) (cit. on pp. 44, 69).

93. KAMIŃSKI, M., J. KLAWITER & J. KOWALSCZYK: Investigation of the relationship between packing methods and efficiency of preparative columns. *Journal of Chromatography A* (1982), vol. **243**(2): 225–244 (1982) (cit. on p. 46).

94. SCHARL, T., C. JUNGREUTHMAYER, A. DÜRAUER, S. SCHWEIGER, T. SCHRÖDER & A. JUNGBAUER: Trend analysis of performance parameters of pre-packed columns for protein chromatography over a time span of ten years. *Journal of Chromatography A* (2016), vol. **1465**: 63–70 (2016) (cit. on p. 46).

95. EHRENSTEIN, G. W.: *Polymeric Materials* 1–277 (Hanser, Munich, 2001) (cit. on pp. 46, 89).

96. L. LINDA: Reviewer Guidance - Validation of chromatographic methods. *CDER. Center for Drug Evaluation and Research* (1998), vol. **22**(3): 1–30 (1998) (cit. on p. 46).

97. TYN, M. T. & T. W. GUSEK: Prediction of diffusion coefficients of plasmids. *Biotechnology and Bioengineering* (2008), vol. **99**(4): 1040–1044 (2008) (cit. on pp. 47, 74).

98. KOCH, D. L. & J. F. BRADY: Dispersion in fixed beds. *Journal of Fluid Mechanics* (1985), vol. **154**(-1): 399 (1985) (cit. on p. 47).

99. GUNN, D. J.: Axial and radial dispersion. *Chem. Eng. Sci.* (1987), vol. **42**(2): 363–373 (1987) (cit. on p. 47).

100. Wakao, N. & T. Funazkri: Effect of fluid dispersion coefficients on particle-to-fluid mass transfer coefficients in packed beds. Correlation of sherwood numbers. *Chemical Engineering Science* (1978), vol. **33**(10): 1375–1384 (1978) (cit. on p. 47).

101. Edwards, M. F. & J. F. Richardson: Gas dispersion in packed beds. *Chemical Engineering Science* (1968), vol. **23**(2): 109–23 (1968) (cit. on p. 47).

102. Eriksson, L., E. Johansson, N. Kettaneh-Wold, C. Wikström & S. Wold: *Design of Experiments: Principles and Applications* 459 (Umetrics, Umea, 2008) (cit. on p. 51).

103. Krigbaum, W. R. & F. R. Kügler: Molecular conformation of egg-white lysozyme and bovine alpha-lactalbumin in solution. *Biochemistry* (1970), vol. **9**(5): 1216–1223 (1970) (cit. on p. 55).

104. Przybycien, T. M., N. S. Pujar & L. M. Steele: Alternative bioseparation operations: life beyond packed-bed chromatography. *Current Opinion in Biotechnology* (2004), vol. **15**(5): 469–78 (2004) (cit. on p. 68).

105. Hardick, O., S. Dods, B. Stevens & D. G. Bracewell: Nanofiber adsorbents for high productivity continuous downstream processing. *Journal of Biotechnology* (2015), vol. **213**: 74–82 (2015) (cit. on pp. 68, 69, 99).

106. *Preparative Chromatography: Of Fine Chemicals and Pharmaceutical Agents* (ed Schmidt-Traub, H.) 1–458 (Wiley-VCH, 2005) (cit. on pp. 69, 78, 83, 91).

107. Kaczmarski, K., D. Antos, H. Sajonz, P. Sajonz & G. Guiochon: Comparative modeling of breakthrough curves of bovine serum albumin in anion-exchange chromatography. *Journal of Chromatography A* (2001), vol. **925**(1): 1–17 (2001) (cit. on p. 69).

108. Karlsson, D., N. Jakobsson, A. Axelsson & B. Nilsson: Model-based optimization of a preparative ion-exchange step for antibody purification. *Journal of Chromatography A* (2004), vol. **1055**(1-2): 29–39 (2004) (cit. on p. 69).

109. Kaltenbrunner, O., O. Giaverini, D. Woehle & J. A. Asenjo: Application of chromatographic theory for process characterization towards validation of an ion-exchange operation. *Biotechnology and Bioengineering* (2007), vol. **98**(1): 201–210 (2007) (cit. on p. 69).

110. Westerberg, K., E. Broberg Hansen, M. Degerman, T. Budde Hansen & B. Nilsson: Model-based process challenge of an industrial ion-exchange chromatography step. *Chemical Engineering and Technology* (2012), vol. **35**(1): 183–190 (2012) (cit. on p. 69).

111. Mollerup, J. M., T. B. Hansen, S. Kidal, L. Sejergaard & A. Staby: Development, modelling, optimisation and scale-up of chromatographic purification of a therapeutic protein. *Fluid Phase Equilibria* (2007), vol. **261**(1-2): 133–139 (2007) (cit. on p. 69).

112. GHOSH, P., M. LIN, J. H. VOGEL, D. CHOY, C. HAYNES & E. von LIERES: Zonal rate model for axial and radial flow membrane chromatography, part II: Model-based scale-up. *Biotechnology and Bioengineering* (2014), vol. **111**(8): 1587–1594 (2014) (cit. on p. 69).

113. MCCUE, J. T., G. KEMP, D. LOW & I. QUIÑONES-GARCÍA: Evaluation of protein-A chromatography media. *Journal of Chromatography A* (2003), vol. **989**(1): 139–153 (2003) (cit. on p. 69).

114. NDOCKO NDOCKO, E., R. DITZ, J.-P. JOSCH & J. STRUBE: New Material Design Strategy for Chromatographic Separation Steps in Bio-Recovery and Downstream Processing. *Chemie Ingenieur Technik* (2011), vol. **83**(1-2): 113–129 (2011) (cit. on p. 69).

115. FRANCIS, P., E. von LIERES & C. HAYNES: Zonal rate model for stacked membrane chromatography part II: Characterizing ion-exchange membrane chromatography under protein retention conditions. *Biotechnology and Bioengineering* (2012), vol. **109**: 615–629 (2012) (cit. on pp. 71, 72, 86).

116. HUUK, T. C., T. HAHN, A. OSBERGHAUS & J. HUBBUCH: Model-based integrated optimization and evaluation of a multi-step ion exchange chromatography. *Separation and Purification Technology* (2014), vol. **136**: 207–222 (2014) (cit. on p. 72).

117. Van BEIJEREN, P., P. KREIS & T. ZEINER: Development of a generic process model for membrane adsorption. *Computers & Chemical Engineering* (2013), vol. **53**: 86–101 (2013) (cit. on pp. 72, 91).

118. BOI, C.: Membrane adsorbers as purification tools for monoclonal antibody purification. *Journal of Chromatography B* (2007), vol. **848**: 19–27 (2007) (cit. on p. 72).

119. HAHN, T., T. HUUK, V. HEUVELINE & J. HUBBUCH: Simulating and Optimizing Preparative Protein Chromatography with ChromX. EN. *Journal of Chemical Education* (2015), vol. **92**(9): 1497–1502 (2015) (cit. on p. 73).

120. WALL, M.: *GAlib: A C++ Library of Genetic Algorithm Components, ver. 2.4.7* `http://lancet.mit.edu/ga/` (cit. on p. 73).

121. AGUIAR E OLIVEIRA JUNIOR, H., L. INGBER & A. PETRAGLIA. *Stochastic Global Optimization and its Applications with Fuzzy Adaptive Simulated Annealing* 33–62 (Springer, Berlin Heidelberg, 2012) (cit. on p. 73).

122. DEVERNAY, F.: *C/C++ Minpack, ver. 1.3.2* `http://devernay.free.fr/hacks/cminpack/`. 2007 (cit. on p. 73).

123. BRESTRICH, N., T. HAHN & J. HUBBUCH: Application of spectral deconvolution and inverse mechanistic modelling as a tool for root cause investigation in protein chromatography. *Journal of Chromatography A* (2016), vol. **1437**: 158–167 (2016) (cit. on p. 74).

124. Tatárová, I., R. Fáber, R. Denoyel & M. Polakovic: Characterization of pore structure of a strong anion-exchange membrane adsorbent under different buffer and salt concentration conditions. *Journal of Chromatography. A* (2009), vol. **1216**(6): 941–7 (2009) (cit. on pp. 79, 80, 89, 91).

125. Al-Bokari, M., D. Cherrak & G. Guiochon: Determination of the porosities of monolithic columns by inverse size-exclusion chromatography. *Journal of Chromatography A* (2002), vol. **975**(2): 275–284 (2002) (cit. on p. 89).

126. Staby, A., J. Nielsen, J. Krarup, M. Wiendahl, T. Hansen, S. Kidal, J. Hubbuch & J. Mollerup. *Advances in Chromatography* 193–245 (Taylor & Francis, 2009) (cit. on p. 89).

127. Staby, A. & I. H. Jensen: Comparison of chromatographic ion-exchange resins: II. More strong anion-exchange resins. *Journal of Chromatography A* (2001), vol. **908**(1): 149–161 (2001) (cit. on p. 90).

128. Wu, Y., J. Simons, S. Hooson, D. Abraham & G. Carta: Protein and virus-like particle adsorption on perfusion chromatography media. *Journal of Chromatography A* (2013), vol. **1297**: 96–105 (2013) (cit. on pp. 90, 147).

129. Detobel, F. & G. Desmet. *Monolithic Silicas in Separation Science: Concepts, Syntheses, Characterization, Modeling and Applications* (eds Unger, K. K., N. Tanaka & E. Machtejevas) 105–125 (Wiley-VCH, 2011) (cit. on p. 91).

130. Martin, C., J. Coyne & G. Carta: Properties and performance of novel high-resolution/high-permeability ion-exchange media for protein chromatography. *Journal of Chromatography A* (2005), vol. **1069**(1): 43–52 (2005) (cit. on p. 91).

131. Gebauer, K., J. Thömmes & M. Kula: Breakthrough performance of high-capacity membrane adsorbers in protein chromatography. *Chemical Engineering Science* (1997), vol. **52**(3): 405–419 (1997) (cit. on p. 91).

132. Delgado, J. M. P. Q.: A critical review of dispersion in packed beds. *Heat and Mass Transfer* (2006), vol. **42**(4): 279–310 (2006) (cit. on p. 92).

133. Wittemann, A., B. Haupt & M. Ballauff: Adsorption of proteins on spherical polyelectrolyte brushes in aqueous solution. *Physical Chemistry Chemical Physics* (2003), vol. **5**(45): 1671–1677 (2003) (cit. on p. 93).

134. Wilson, E. J. & C. J. Geankoplis: Liquid Mass Transfer at Very Low Reynolds Numbers in Packed Beds. *Industrial & Engineering Chemistry Fundamentals* (1966), vol. **5**(1): 9–14 (1966) (cit. on p. 93).

135. Thömmes, J. & M. Etzel: Alternatives to chromatographic separations. *Biotechnology progress*, vol. **23**(1): 42–5 (cit. on p. 98).

136. Yavorsky, D., J. Amara, J. Umana, W. Cataldo, M. Kozlov & M. Stone: *Chromatography media and method* 2012 (cit. on p. 99).

137. TURNBULL, J., B. WRIGHT, N. K. GREEN, R. TARRANT, I. ROBERTS, O. HARDICK & D. G. BRACEWELL: Adenovirus 5 recovery using nanofiber ion-exchange adsorbents. *Biotechnology and Bioengineering* (2019), vol. **116**(7): 1698–1709 (2019) (cit. on p. 99).

138. SCHWELLENBACH, J.: *Design, Charakterisierung und Prozessintegration nicht-partikulärer Medien für bio-chromatographische Trennaufgaben* PhD thesis (2016): 1–97 (cit. on p. 99).

139. AMARA, J, B CACACE, D YAVORSKY & J BOYLE: *Chromatography media for purifying vaccines and viruses* 2014 (cit. on p. 99).

140. RUSCIC, J., C. PERRY, T. MUKHOPADHYAY, Y. TAKEUCHI & D. G. BRACEWELL: Lentiviral Vector Purification Using Nanofiber Ion-Exchange Chromatography. *Molecular Therapy - Methods and Clinical Development* (2019), vol. **15**: 52–62 (2019) (cit. on p. 99).

141. BENSCH, M., B. SELBACH & J. HUBBUCH: High throughput screening techniques in downstream processing: Preparation, characterization and optimization of aqueous two-phase systems. *Chemical Engineering Science* (2007), vol. **62**: 2011–2021 (2007) (cit. on pp. 99, 106, 107).

142. KELLEY, B. D., M. SWITZER, P. BASTEK, J. F. KRAMARCZYK, K. MOLNAR, T. YU & J. COFFMAN: High-throughput screening of chromatographic separations: IV. Ion-exchange. *Biotechnology and Bioengineering* (2008), vol. **100**(5): 950–963 (2008) (cit. on p. 99).

143. COFFMAN, J. L., J. F. KRAMARCZYK & B. D. KELLEY: High-throughput screening of chromatographic separations: I. method development and column modeling. *Biotechnology and Bioengineering* (2008), vol. **100**(4): 605–618 (2008) (cit. on pp. 99, 104, 105, 107, 112, 113, 115, 116).

144. BERGANDER, T., K. NILSSON-VÄLIMAA, K. ÖBERG & K. M. LACKI: High-throughput process development: Determination of dynamic binding capacity using microtiter filter plates filled with chromatography resin. *Biotechnology Progress* (2008), vol. **24**(3): 632–639 (2008) (cit. on pp. 99, 106, 107, 113).

145. KRÖNER, F. & J. HUBBUCH: Systematic generation of buffer systems for pH gradient ion exchange chromatography and their application. *Journal of Chromatography A* (2013), vol. **1285**: 78–87 (2013) (cit. on pp. 100, 135).

146. WINDERL, J., T. SPIES & J. HUBBUCH: Packing characteristics of winged shaped polymer fiber supports for preparative chromatography. *Journal of Chromatography A* (2018), vol. **1553**: 67–80 (2018) (cit. on pp. 101, 108, 114, 116, 121, 135, 143).

147. SCHWELLENBACH, J., P. KOSIOL, B SÖLTER, F. TAFT & L. VILLAIN: Controlling the polymer-nanolayer architecture on anion-exchange membrane adsorbers via surface-initiated atom transfer radical polymerization. *REACT* (2016), vol. **106**: 32–42 (2016) (cit. on pp. 101, 118).

148. Herrmann, T., M. Schröder & J. Hubbuch: Generation of equally sized particle plaques using solid-liquid suspensions. *Biotechnology Progress* (2006), vol. **22**: 914–918 (2006) (cit. on pp. 104, 112).

149. Nfor, B. K., M. Noverraz, S. Chilamkurthi, P. D. Verhaert, L. A. van der Wielen & M. Ottens: High-throughput isotherm determination and thermodynamic modeling of protein adsorption on mixed mode adsorbents. *Journal of Chromatography A* (2010), vol. **1217**(44): 6829–6850 (2010) (cit. on pp. 105, 116).

150. Kramarczyk, J. F., B. D. Kelley & J. L. Coffman: High-throughput screening of chromatographic separations: II. Hydrophobic interaction. *Biotechnology and Bioengineering* (2008), vol. **100**(4): 707–720 (2008) (cit. on p. 108).

151. Winderl, J., T. Hahn & J. Hubbuch: A mechanistic model of ion-exchange chromatography on polymer fiber stationary phases. *Journal of Chromatography A* (2016), vol. **1475**: 18–30 (2016) (cit. on pp. 108, 110, 111, 115, 137).

152. McGown, E. L. & D. G. Hafeman: Multichannel pipettor performance verified by measuring pathlength of reagent dispensed into a microplate. *Analytical Biochemistry* (1998), vol. **258**(1): 155–157 (1998) (cit. on p. 110).

153. Kittelmann, J., F. Hämmerling, M. Ebeler & J. Hubbuch: Light extinction and scattering by agarose based resin beads and applications in high-throughput screening. *Journal of Chromatography A* (2015), vol. **1397**: 52–58 (2015) (cit. on p. 112).

154. Huuk, T. C., T. Briskot, T. Hahn & J. Hubbuch: A versatile noninvasive method for adsorber quantification in batch and column chromatography based on the ionic capacity. *Biotechnology Progress* (2016), vol. **32**(3): 666–677 (2016) (cit. on p. 112).

155. Knudsen, H. L., R. L. Fahrner, Y. Xu, L. A. Norling & G. S. Blank: Membrane ion-exchange chromatography for process-scale antibody purification. *Journal of Chromatography A* (2001), vol. **907**(1-2): 145–154 (2001) (cit. on pp. 119, 133, 144).

156. Kaltenbrunner, O., L. Diaz, X. Hu & M. Shearer: Continuous bind-and-elute protein A capture chromatography: Optimization under process scale column constraints and comparison to batch operation. *Biotechnology progress* (2016), vol. **32**(4): 938–948 (2016) (cit. on p. 121).

157. McDonald, P., B. Tran, C. R. Williams, M. Wong, T. Zhao, B. D. Kelley & P. Lester: The rapid identification of elution conditions for therapeutic antibodies from cation-exchange chromatography resins using high-throughput screening. *Journal of Chromatography A* (2016), vol. **1433**: 66–74 (2016) (cit. on pp. 124, 126).

158. Harinarayan, C, J Mueller, A Ljunglöf, R Fahrner, J Van Alstine & R van Reis: An exclusion mechanism in ion exchange chromatography. *Biotechnology and bioengineering* (2006), vol. **95**(5): 775–87 (2006) (cit. on p. 124).

159. VÁZQUEZ-REY, M. & D. A. LANG: Aggregates in monoclonal antibody manufacturing processes. *Biotechnology and bioengineering* (2011), vol. **108**(7): 1494–508 (2011) (cit. on pp. 132, 133).

160. ROSENBERG, A. S.: Effects of protein aggregates: An Immunologic perspective. *AAPS Journal* (2006), vol. **8**(3): 501–507 (2006) (cit. on p. 133).

161. SUDA, E. J., K. E. THOMAS, T. M. PABST, P. MENSAH, N. RAMASUBRAMANYAN, M. E. GUSTAFSON & A. K. HUNTER: Comparison of agarose and dextran-grafted agarose strong ion exchangers for the separation of protein aggregates. *Journal of Chromatography A* (2009), vol. **1216**(27): 5256–5264 (2009) (cit. on p. 133).

162. LIU, H. F., B. MCCOOEY, T. DUARTE, D. E. MYERS, T. HUDSON, A. AMANULLAH, R. van REIS & B. D. KELLEY: Exploration of overloaded cation exchange chromatography for monoclonal antibody purification. *Journal of Chromatography A* (2011), vol. **1218**(39): 6943–6952 (2011) (cit. on pp. 133, 144, 145, 150, 154).

163. RECK, J. M., T. M. PABST, A. K. HUNTER & G. CARTA: Separation of antibody monomer-dimer mixtures by frontal analysis. *Journal of Chromatography A* (2017), vol. **1500**: 96–104 (2017) (cit. on pp. 133, 148, 150, 151).

164. STONE, M. T., K. A. COTONI & J. L. STONER: Cation exchange frontal chromatography for the removal of monoclonal antibody aggregates. *Journal of Chromatography A* (2019), vol. **1599**: 152–160 (2019) (cit. on pp. 133, 150, 151).

165. ZHOU, J. X., S. DERMAWAN, F. SOLAMO, G. FLYNN, R. STENSON, T. TRESSEL & S. GUHAN: pH-conductivity hybrid gradient cation-exchange chromatography for process-scale monoclonal antibody purification. *Journal of chromatography. A* (2007), vol. **1175**(1): 69–80 (2007) (cit. on p. 133).

166. OZBEK, H., J. FAIR & S. PHILLIPS: Viscosity Of Aqueous Sodium Chloride Solutions From 0 - 150C. (1977), vol.: 18 (1977) (cit. on p. 137).

167. De NEUVILLE, B. C., A. LAMPROU, M. MORBIDELLI & M. SOOS: Perfusive ion-exchange chromatographic materials with high capacity. *Journal of Chromatography A* (2014), vol. **1374**(815): 180–188 (2014) (cit. on pp. 141, 145).

168. STABY, A., M. B. SAND, R. G. HANSEN, J. H. JACOBSEN, L. A. ANDERSEN, M. GERSTENBERG, U. K. BRUUS & I. H. JENSEN: Comparison of chromatographic ion-exchange resins: III. Strong cation-exchange resins. *Journal of Chromatography A* (2004), vol. **1034**(1-2): 85–97 (2004) (cit. on pp. 144, 147).

169. HAHN, T., T. HUUK, A. OSBERGHAUS, K. DONINGER, S. NATH, S. HEPBILDIKLER, V. HEUVELINE & J. HUBBUCH: Calibration-free inverse modeling of ion-exchange chromatography in industrial antibody purification. *Engineering in Life Sciences* (2016), vol. **16**(2): 107–113 (2016) (cit. on p. 149).